Université Fédérale
Toulouse Midi-Pyrénées

THÈSE

En vue de l'obtention du

DOCTORAT DE L'UNIVERSITÉ DE TOULOUSE

Délivré par l'Université Toulouse 3 - Paul Sabatier

Cotutelle internationale : National University

Présentée et soutenue par

Valerii BUKHANKO

Le 20 septembre 2018

Libération du monoxyde d'azote induite par deux photons à partir de complexes ruthénium-nitrosyle contenant des ligands de capacités push-pull différentes.

Ecole doctorale : **SDM - SCIENCES DE LA MATIERE - Toulouse**

Spécialité : **Chimie Organométallique et de Coordination**

Unité de recherche :
LCC - Laboratoire de Chimie de Coordination

Thèse dirigée par
Pascal LACROIX et Zoia VOITENKO

Jury

M. Jean-Pierre MALVAL, Rapporteur
M. Oleksandr ROSHAL, Rapporteur
M. Remi CHAUVIN, Examinateur
M. Yuriy SHERMOLOVICH, Examinateur
M. Pascal George LACROIX, Directeur de thèse
Mme Zoia VOITENKO, Co-directeur de thèse

PREFACE

This work has been done in collaboration between University Toulouse III – Paul Sabatier (UPS), France (Laboratory of coordination chemistry, UPR 8241 (LCC)) and Taras Shevchenko National university of Kyiv (UNTS), Ukraine (Faculty of chemistry) between 2014 and 2018. Financial support from the French government, Ukrainian government and University Paul Sabatier are gratefully acknowledged.

I am very much thankful to my supervisor Dr. Pascal George Lacroix for encouraging and fruitful scientific conversations, for his openness and readiness to help both in scientific and life questions. I also appreciate he made possible my research visits to Mexico thus opening so many opportunities to know new people, culture and establish new scientific contacts. I would like also to say thank you to Dr. Lacroix for the time he spent to teach me a brand new field of chemistry for me – DFT computations.

Many thanks to my research advisor Professor Zoia Voitenko who is one of founders of the French-Ukrainian scientific collaboration. I am thankful to her for her strong believe in me, for always being sincere and thoughtful about my needs as a researcher and a person. Never being detached from the problems she is a nice support for me.

My sincere thanks to Professor Isabelle Malfant, who made possible my work in LCC in the group under her guidance. Thank you for your critical point of view, patience and objectivity. Truly, it was a big pleasure to work in your team. I would also like to express my thanks to Dr. Isabelle Sasaki, whose pieces of advice were always helpful in the synthetic part of my work. And I also must point out a big help that Marine Tassé kindly provided every time there was a technical question in the laboratory work. My thanks to Mathilde Bocé, Hasan Mohammed and Max Roose for creating a friendly work atmosphere in the laboratory.

A big part of the work has been done with the facilities and opportunities provided by researchers from Mexico. I appreciate an invaluable help of Professor

José Norberto Farfán García at UNAM and I am very thankful to him for making possible my comfort and fruitful stay in Mexico, for providing nice conditions for work and collaboration with researchers of his group and for interesting scientific discussions. I would like also to say thank you to Dr. Rosa Luisa Santillan Baca, and Professor Farfan's big family for opening the possibilities to discover the culture of Mexico and for always being responsive and helpful.

I would like also to express many thanks to Professor Blas Flores Pérez, who has kindly provided the facilities for the research work in UNAM. I am very much thankful to PhD Alejandro Enriquez-Cabrera for his readiness to help in any question regarding research work or everyday life and for providing a valuable help in the questions of synthetic chemistry. I am also very much obliged to him and his big family for nice treatment and hosting me during my stay in Mexico. Many thanks to Margarita Romero-Ávila for her invaluable help and guidance in many complex problems in synthetic organic chemistry, for her support and sensitiveness. I would like to express my gratitude to Andrés Felipe Leon-Rojas, a student of Professor Farfan's research group, for nice collaboration and help in synthetic part of the work.

I gratefully acknowledge Dr. Gabriel Ramos-Ortiz (CIO, Leon, Mexico) for his kind attention and solicitude and for providing conditions and facilities to conduct the optical measurements. I am thankful to Rodrigo Misael Barba-Barba and PhD Jayaramakrishnan Velusamy for substantial help in measuring the two-photon absorption parameters of the complexes.

I would like also to express my thanks to my parents Olexandr and Natalia, my relatives and friends for their love and support. Thank you for understanding and empathy!

My dear Olena, thank you for your unceasing concern for me, for your believe and for being my infinite support!

Valerii Bukhanko

August, 2018

TABLE OF CONTENT

ABBREVIATIONS

AcOEt	ethylacetate
2-acpy	2-acetylpyridine
Alk	alkyl
bpy	2,2'-bipyridine
н-BuLi	*n*-butyllithium
DFT	density functional theory
dHFT	4'-(9,9-dihexyl-9*H*-fluoren-2-yl)-2,2':6',2''-terpyridine
DIPA	diisopropylamine
DIBAL-H	Diisobutylaluminum hydride
DMAFCCT	(*E*)-7-(2-([2,2':6',2''-terpyridine]-4'-yl)vinyl)-9,9-dihexyl-*N*,*N*-dimethyl-9*H*-fluoren-2-amine
DMAFT	7-([2,2':6',2''-terpyridine]-4'-yl)-9,9-dihexyl-*N*,*N*-dimethyl-9*H*-fluoren-2-amine
DMF	dimethylformamide
DMP	1,1,1-Triacetoxy-1,1-dihydro-1,2-benziodoxol-3(1*H*)-one (Dess-Martin periodinane).
DMSO	dimethylsulfoxide
EPR	electron paramagnetic resonance
equiv	equivalent
Et	ethyl
Et_3N	triethylamine
EtOH	ethanol
FCCT	(*E*)-4'-(2-(9,9-dihexyl-9*H*-fluoren-2-yl)vinyl)-2,2':6',2''-terpyridine
FCC3T	4'-((9,9-dihexyl-9*H*-fluoren-2-yl)ethynyl)-2,2':6',2''-terpyridine

FT	4'-(9*H*-fluoren-2-yl)-2,2':6',2''-terpyridine
HOMO	highest occupied molecular orbital
HPLC	high-performance liquid chromatography
HRMS	high-resolution mass-spectrometry
in vitro	in laboratory conditions
in vivo	in living organism
IR	infrared
LUMO	lowest unoccupied molecular orbital
Me	methyl
MeOH	methanol
MeO-Phtpy	4'-(4-metoxyphenyl)-2,2':6',2''-terpyridine
MGD	*N*-methyl-D-glucamine dithiocarbamate
mp.	melting point
NADP	Nicotinamide adenine dinucleotide phosphate
NLO	nonlinear optics, nonlinear optical
NMR	nuclear magnetic resonance
NONOate	1,1-R^1,R^2-2-hydroxy-2-nitrosohydrazine
OPA	linear absorption (one-photon absorption)
o-tolyl	*ortho-tolyl*
Ph	phenyl
PhMe	toluene
ppm	point per million
py	pyridine
RNS	reactive nitrogen species
ROS	reactive oxygen species
rt	room temperature
SCE	saturated calomel electrode
SNP	sodium nitroprusside
SOMO	singlyoccupied molecular orbital

TD-DFT	time-dependent density functional theory
Tf	triflate
THF	tetrahydrofuran
TLC	thin-layer chromatography
TMS	trimethylsilyl
TPA	two-photon absorption
UV	ultraviolet
Δ	heating at the boiling point
δ	chemical shift, ppm (NMR-spectroscopy)
φ	quantum yield

INTRODUCTION

Last decades, since nitric oxide was proclaimed “Molecule of the Year” by the journal “Science”, many research teams has been aiming at in-depth study of physiological role of NO. Nowadays this compound is considered one of the main constituents in biological processes. The idea of a controlled nitric oxide release has become very attractive, for instance in order to be able to cause a selective influence on malignant cells. Indeed, depending on concentration, NO can inhibit the tumour growth or lead to the cell apoptosis. Exogenous NO-donors as modifiers of NO-levels in biological tissues are one of the most promising ones. S-nitrosothiols, organic nitrates, sydnonimines are practically important nowadays.

Especially interesting group of promising potent NO-donors is metal-nitrosyl complexes, in particular ruthenium-nitrosyls. The last ones are stable in aqueous media as opposed to the majority of alternative metal-nitrosyls. But the most important advantage of ruthenium-nitrosyl complexes is their ability to release NO under irradiation exclusively, that makes them perfect candidates as prodrugs for photodynamic therapy.

One of the targets for modern photodynamic therapy is the development of photosensitization methods of prodrugs in optical therapeutic window (700-1300 nm). Beyond this range of wavelengths the activation is ineffective due to a high extinction of electromagnetic waves intensity because of their absorption by biological tissues. Most of known photoactive NO-donors nowadays are able to release NO while being activated with waves of 350-600 nm waveband. Therefore the question of photosensitization of such compounds *in vivo* is a keystone for their future implementation in medical practice.

One of approaches, opening up the possibilities for photoinitiation of Ru-N bond dissociation in ruthenium-nitrosyl complexes in optical therapeutic window is two-photon absorption (TPA). This modern method has not been widely implemented in medical practice, however it is being thoroughly studied by scientists of different fields of science and technology – from medicine and microconstruction to 3D-data storage. High spatial selectivity of electromagnetic

waves influence on organism and reduced destructive effect (when employing IR-range waves) makes the local NO-release without damage dealt to adjacent tissues possible.

Revealing of main structural elements of ruthenium-nitrosyl coordination compounds capable of participating in two-photon absorption process and understanding the mechanism of NO-release process, is thereby an actual task in designing of promising NO-donors prodrugs.

CHAPTER 1. LITRERATURE OVERVIEW

1.1 Nitric oxide: molecular structure and general chemical characteristic.

Nitric oxide (or nitrogen monoxide) is a colorless gas, which is monomeric at standard conditions; its molecules consist of an oxygen atom and a nitrogen atom connected by a multiple bond. Odd number of electrons in NO molecule makes the substance paramagnetic; in addition, it is the smallest thermally stable molecule-radical known. In terms of the molecular orbital method, it is logical to compare the structure of the compound with the structure of N_2 molecule or with one isoelectronic to it – CO (figure 1.1).

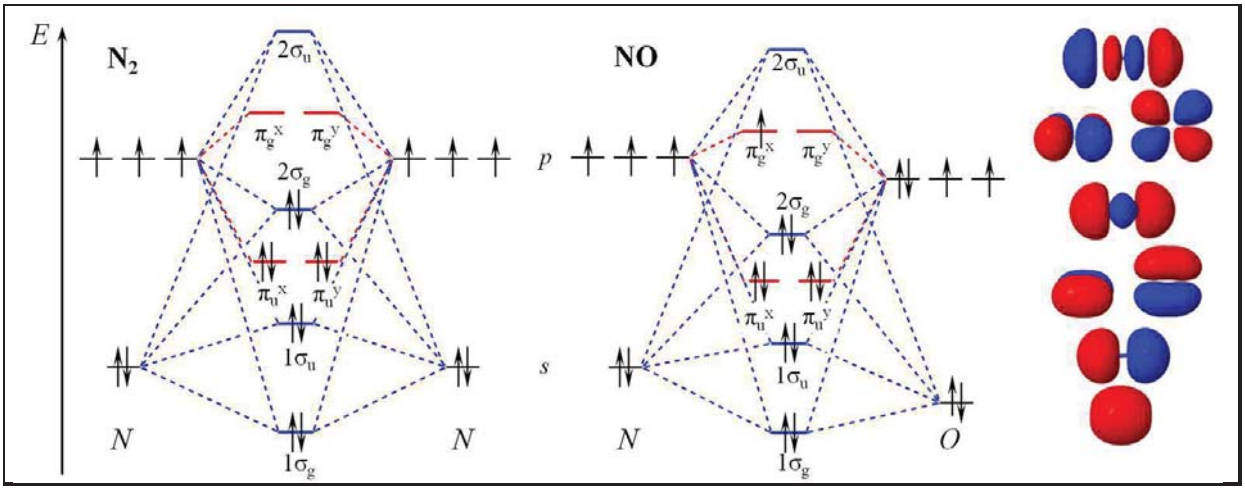

Figure 1.1. A diagram of atomic and molecular orbitals of nitrogen and nitric oxide and schematic configuration of molecular orbitals

Appearance of an additional electron (in transition from nitrogen to nitric oxide), which is located on the antibonding π_g NO orbital causes decreasing of the bond order from 3 (for N_2 molecule) to 2.5 (for NO molecule). This has a corresponding effect on the nitrogen monoxide physical and chemical properties. In particular, bond length in NO molecule is 0.115 nm. It is an intermediate value between the length of the typical double bond N-O (0.120 nm) and the interatomic distance in ionized NO^+ particle (0.106 nm), which bond order is 3.[1] And vice versa reducing the compound to NO^- increases the bond length to 0.126, which is caused by appearance of one more electron on the molecular antibonding orbital

and decrease of the bond force coefficient[2]. Nitrogen monoxide ionization potential is 9.25 eV; the value is well under the one characteristic for similar compounds which is caused by significant stabilization of the particle when losing an electron from the antibonding orbital. For comparison: ionization potentials for the following compounds: N_2, O_2, CO are 15.6 eV, 12.1 eV and 14.0 eV respectively. In practice, NO particle charge – neutral radical, cation or anion – can be distinguished by analyzing IR-spectra of the compound, which contains the particle. Thus, for nitrozonium ion (NO^+) vibration frequency is 2377 cm^{-1}, which is well over the one for nitric oxide – 1875 cm^{-1} – and, respectively, for NO^- anion – 1470 cm^{-1}. [2]

Realization of electron density distribution in nitric oxide is essential for explanation of its coordination behavior. In terms of the valence bond method, the following resonance forms could describe the structure of the compound:[3]

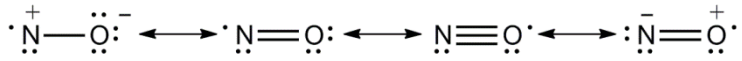

Often, however, the compound properties, in particular its low liability to dimerization, are most adequately explained in terms of Linnet's "unpaired" structures:[4]

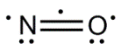

Analysis of the character of hyperfine splitting in NO EPR-spectrum indicates strong interaction between unpaired electron magnetic moment and molecule rotation; additionally, it indicates that 60% of spin density is concentrated on nitrogen atom.[3]

Due to little difference between the elements electronegativity the compound is rather slightly polar, its dipole moment is 0.15D.

Theoretical value of the dipole moment, which has been obtained in the frame of this dissertation by means of density functional theory (DFT), does not almost differ from the experimental one; it is 0.1 D.

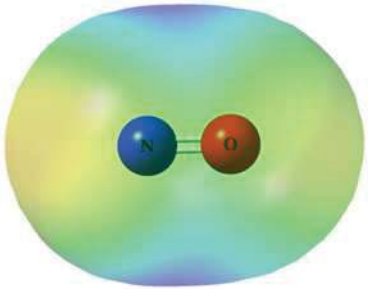

Figure 1.2. Distribution of electron density in NO molecule

Distribution of electron density in the molecule is shown on figure 1.2.

Being the simplest molecule with an odd number of electrons, nitrogen monoxide is a rather well studied compound from the point of view of its chemical properties. A great number of reactions between NO and radicals, atoms and other paramagnetic species became classical unique examples of reactions for kinetics study.

There are several number of commonly used laboratory methods of NO generation. Though the obtained nitric oxide as a rule contains impurities of other nitrogen oxides or volatile compounds. The most used method is reduction of dilute (~30%) nitric acid by copper:

$$8HNO_3 + 3Cu = 3Cu(NO_3)_2 + 4H_2O + 2NO$$

NO synthesized in this way is to be later purified in order to remove the impurity of nitrogen(IV) oxide by running the mixture of generated gases through aqueous solution of alkali. Another method of NO obtaining is reduction of alkaline metal nitrites:

$$2NaNO_2 + 2NaI + 2H_2SO_4 = I_2 + 4NaHSO_4 + 2NO$$

$$2NaNO_2 + 2FeSO_4 + 3H_2SO_4 = Fe_2(SO_4)_3 + 2NaHSO_4 + 2H_2O + 2NO$$

An up-to-date but considerably more expensive method of obtaining NO in laboratory conditions is use of so-called NONOate-compounds. The method is used when controllable NO synthesis is essential, for example, in biological studies (see section 1.3.2)

In contrast to nitrogen, nitric oxide is an endothermic compound, therefore it is less stable. Even at a temperature slightly higher than the room temperature (30-50°C), but only under high pressure, nitrogen monoxide disproportionates with generating nitrogen(I) oxide and nitrogen(IV) oxide. Decomposition to the elementary substances is happening at significantly higher temperature – close to 700^0 C in the presence of a catalyst.

Strong oxidizers can convert nitric oxide into compounds where nitrogen has higher oxidation states.[5] The most typical nitric oxide reaction is interaction with oxygen, at which the compound is oxidized to nitrogen(IV) oxide:

$$2NO + O_2 = 2NO_2$$

Whereas interaction of NO with atomic oxygen, at which chemiluminescence is observed, was used for qualitative and quantitative determination of atomic oxygen:[6]

$$NO + O = NO_2 + h\nu$$

Naturally, the presence of water in nitrogen monoxide and oxygen interaction changes the reaction path since NO_2 itself can react with water. That's why as a result of NO-oxidation by oxygen in humid condition nitrite-ions are generated. The reaction is commonly described by the following equation:[7]

$$4NO + O_2 + 2H_2O = 4H^+ + 4NO_2^-$$

NO^+ ion predicted by the theory indeed exists. Compound containing nitrosonium cation could be obtained in the reaction:

$$N_2O_3 + 3H_2SO_4 = 2NO^+ + 3HSO_4^- + H_3O^+$$

Solidity at standard conditions of nitrosylsulfate acid $NOHSO_4$ and similar compounds $NO^+ClO_4^-$, NO^+BF_4 as well as their electrolysis mechanism corroborate an ionic nature of the compounds.[5]

1.2 Nitric oxide biological role

Number of published works devoted to nitric oxide biological role is rapidly growing during last four decades. As of February 2018, number of publications found in SciFinder search system were 196712. 0.4% of them were published before 1980, 22.4% - during 1981-1999, and the major part – 77,2% appeared as late as in the 21 century.

It was the discover of the role of this small molecule as a signaling molecule in cardiovascular and nervous systems that aroused so rapidly an increasing interest to it. In 1992 the journal *Science* called nitric oxide "Molecule of the year" and in 6 years, December 10, 1998 the Nobel prize for physiology and medicine was given to three researchers from the USA – Robert F. Furchgott, Louis G. Ignarro and Ferid Murad – for investigation of nitric oxide biological functions.

Physiological effects caused by nitrogen monoxide influence onto biological

environment are often contradictory.[8] For instance, nitrogen monoxide is the best example of a substance that demonstrates at the same time both cytotoxic and cytoprotective action.

A large number of chemical reactions characteristic for NO, in industrial or laboratory routine proceed quite slowly and thus requires using high temperature and pressure being at the same time thermodynamically disadvantageous[9]. From the other side, nitric oxide chemical transformations in biological environments take time from 0.002 to 2 s.[10] These processes in NO biochemistry are usually divided into two types: direct and indirect. Direct effects caused by NO proceed quite fast and during them nitric oxide interacts directly with a biological target, whereas indirect ones are the results of NO interaction with oxygen or superoxide, that generates reactive nitrogen species (RNS), further interacting with biological objects. One of the advantages of such a differentiation is that the direct effects are caused generally by low NO concentrations (< 200 nM), while the indirect ones are the results of influence of significantly higher concentrations (> 400 nM).[9]

Nitric oxide principal biological functions are generalized on diagram 1.1.[9,10,11]

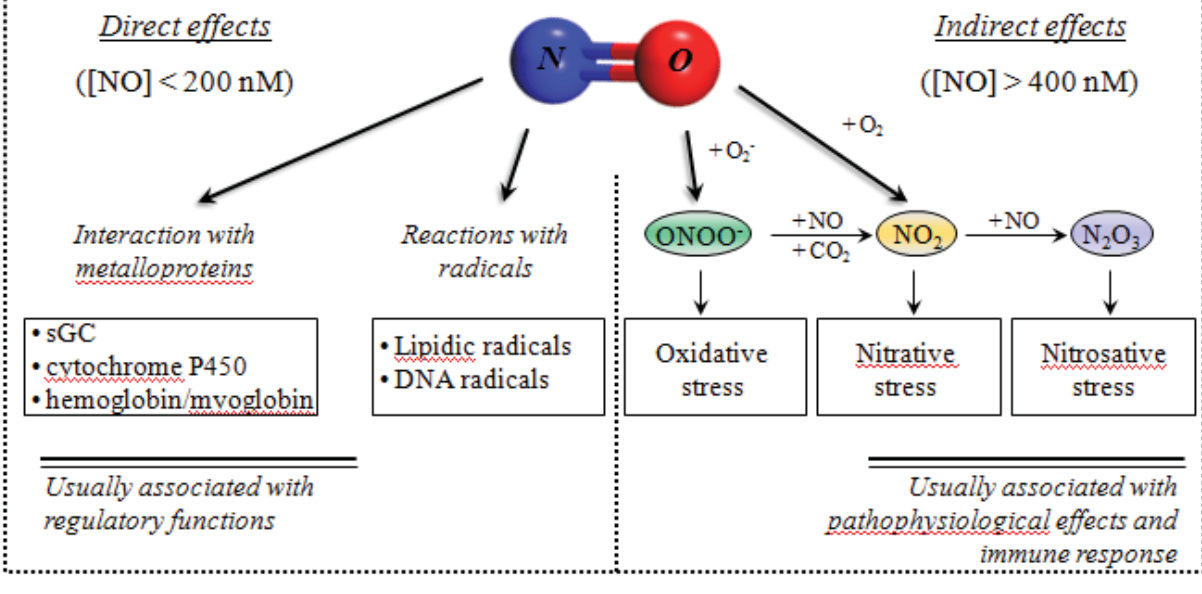

Scheme 1.1. Nitric oxide biological functions.

The main difference between direct and indirect processes is rate of its proceeding. High-speed reactions of immediate interaction between NO and biomolecules – mainly reactions with radicals or metalloproteins – are the direct processes.

A large number of NO main regulatory functions realize through its easy and rapid interaction with metalloprotein heme-prosthetic groups, such as guanylate cyclase (sGC), cytochrome P450, NO- synthase, hemoglobin etc. In such kind of processes the rate-determining step is diffusion of reacting molecules. Process of interaction between nitric oxide and Fe-S cluster protein aconitase proceeds considerably slower.[12]

Biomolecules having in their structure other metal ions, apart from Fe, are also susceptible to the influence of NO. This type of interaction could be represented by the vitamin B_{12} derivative, cobalamin, the nitrosylation of which leads to its reduced activity in the role of a cofactor of methionine synthase.

Reactions between nitric oxide and radical particles can have both positive and negative effects on cells. Lipidic and carboradicals are generated as a result of both oxidative stress and normal metabolism in a living organism. Nitrogen monoxide is able to attenuate effects caused by such reactive particles. For example, inactivation of tyrosyl radical generated in the process of ribonucleotide-reductase regular catalytic cycle by nitric oxide leads to inhibition of the mentioned enzyme.[13] DNA synthesis suppression is an example of harmful effects of NO interaction with radicals in biological environment.[12]

But it is often that the reactions of NO are of the nature of “protective” functions for cells. NO is able to interact with radicals generated in the process of lipidic peroxidation – an important component of inflammatory processes and cell death – and so terminate the chains of reactive oxygen species (ROS) radical reactions, thus protecting the lipidic membranes:[14]

$$LOO\cdot + NO\cdot = LOONO$$

$$L\cdot + NO\cdot = LNO$$

Macrophages protective functions in a living organism are also related to their ability to generate nitric oxide. Concentration of the latter in this case can considerably change depending on the "needs". Due to the ability to vary NO concentration macrophages are able to participate in a wide range of processes aimed at organism protection – phagocytosis, cancer development suppression, tissues restoration, wounds healing etc.

As for NO indirect effects, they also can be divided into two categories – nitrosation and oxidation. The subjects of nitrosation are, first of all, thiol and aminogroups while oxidation is a process that refers to quite a number of substrates – from relatively easily oxidizable catecholamines and metal centers to compounds with a high oxidation-reduction potential, such as lipids, proteins DNA. As in the case of the direct effects, oxidation and nitrosation are regular cell metabolism processes but at the same time they can influence negatively generating substances toxic for cells.

Main RNS responsible for nitrogen(II) oxide indirect effects are nitrogen(III) oxide, N_2O_3, peroxynitrite, $ONOO^-$, nitroxyl, HNO, and nitrogen(IV) oxide, NO_2. Each of the particles depending on the redox potential, electrophilicity etc. interacts with certain biological substrates. Thus, the main nitrosating agent for amines and thiols is N_2O_3, which transforms them into nitrosamines and S-nitrosothiols, respectively.[12] In turn, NO_2 participates in oxidation processes. The molecule does not possess potential high enough for DNA oxidation[15] but it can trigger lipidic peroxidation processes.[16] Among the mentioned particles, peroxynitrite anion shows the strongest oxidizing ability. Under its influence, thiols, lipids, DNA can be oxidized, this particle also participates in the processes of tyrosine, guanosine and methionine nitration.[16]

Nitric oxide has a broad spectrum of effects on cancer growth – from triggering cell mutation to destructing malignant tumours. There are several reviews devoted to nitric oxide effects on the course of cancer.[17,18] Numerous studies on the issue show that commonly nitrogen monoxide low concentrations in cancerous tumour, which is a result of permanent hypoxia, create so-called "safe

zone" and are a positive factor for cancer extension, promoting faster angiogenesis and metastasis (Figure 1.3).[19,20] If, however, NO concentration changes in the direction of decreasing or increasing this leads to transferring to the "inhibition zone" or to the "kill zone", respectively. Both concentration ranges are unfavorable for cancerous tumors and are potential targets in their treatment. Transferring to the very low concentrations range can be achieved by using NO-synthases (NOS) enzymes inhibitor compounds in therapy. The opposite approach is using nitric oxide donor compounds for NO concentration essential increasing, transferring to the "kill zone" and triggering cell death.

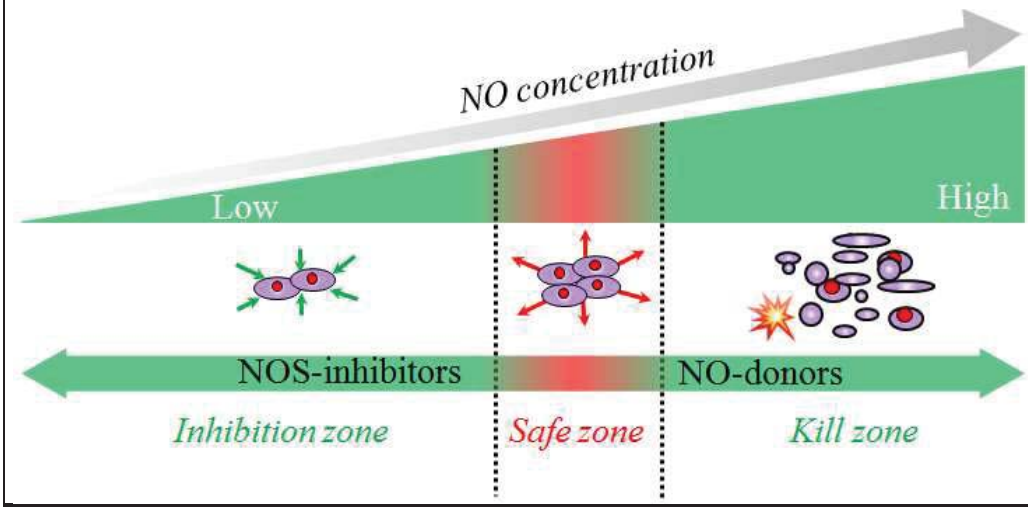

Figure 1.3. Cancerous tumour reaction to nitric oxide at its different concentrations

Generalizing the effects that NO can cause in the concentration range from 1nM to 1μM, we can say that NO low concentrations promote cells protection, their proliferation while high concentrations are responsible for blocking cell-cycle, apoptosis, aging.[9] Besides, NO plays a central role in the cardiovascular system as an endothelium-dependent relaxing factor,[21] in the central nervous system it is involved in the nerve impulses transmission and memory processes, and also performs a regulatory function in the cerebral circulation.

Having chosen nitric oxide as such a multifunctional biological regulator, nature provided living organisms with mechanisms of its biosynthesis.

1.3 NO generation from organic compounds

1.3.1 Natural pathway of nitric oxide production

Nitric oxide is one of the most universal molecular regulators of cellular metabolism. The main way of its synthesis in living organism is oxidation of the amino acid L-arginine in the presence of the NOS enzymes. The conversion occurs in two steps (Scheme 1.2).[22]

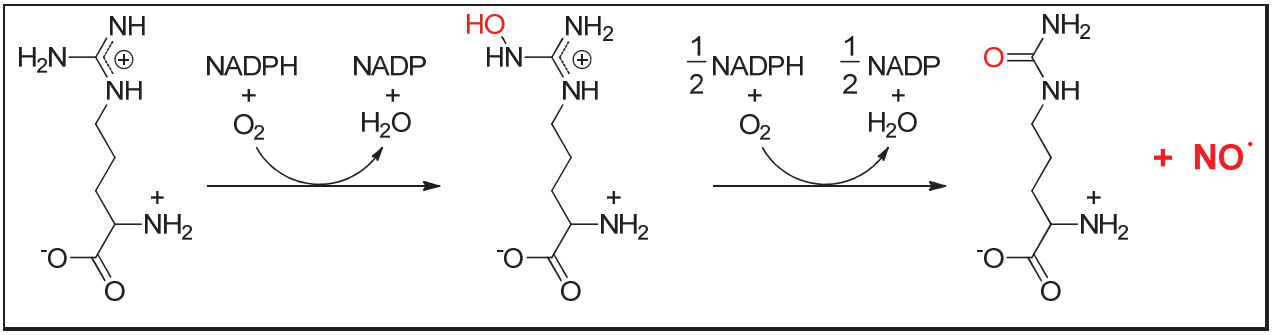

Scheme 1.2. Enzymatic transformation of L-arginine into L-citrulline with the formation of NO molecule

Initially, the 2-electron oxidation of L-arginine and its hydroxylation in the presence of oxygen and NADPH[23] leads to the formation of N^{ω}-hydroxy-L-arginine (NOHLA). Tetrahydrobiopterin accelerates the course of this step acting as a cofactor.[24] Further NOHLA oxidation (the next transformation step) leads to the formation of L-citrulline and one molecule of nitric oxide. The general scheme of the conversion of L-arginine to L-citrulline can be described by the following equation:

$$2\text{L-arginine} + 3\text{NADPH} + 3H^+ + 4O_2 = 2\text{L-citrulline} + 2NO + 4H_2O + 3NADP^+$$

Moreover there are four other cofactors, the absence of which either slows the reaction or makes it impossible to pass.[25] The NOS enzyme group includes three main enzymes - endothelial NO synthase (eNOS), neuronal NO synthase (nNOS), and inducible NO synthase (iNOS); the fourth type - mitochondrial synthase (mtNOS) is identical with the α-form of nNOS.[25] The first two enzymes are calcium-dependent and are activated in the presence of high concentration of calcium ions by calcium-calmodulin complex; typically, their activity period does not exceed few minutes after stimulation. Activated eNOS and nNOS are involved

in the conduction of nerve impulses, peristalsis regulation and instantaneous regulation of blood pressure.[26] Although all three forms of NOS require a calcium-calmodulin complex, iNOS exhibits a much higher affinity for it, which leds to longer activity period (up to days) and lower calcium-calmodulin complex concentration required.[25] iNOS activation is the response to the internal stimulation with a variety of microorganisms metabolic products, some cancer cells, cytokines etc. Activated enzymes produce millimolar amounts of NO (interacting with ROS – peroxynitrite), showing an immune-protective function by oxidizing proteins and DNA.[26] However, in the lack of oxygen (*i.e.* chronic inflammatory processes), the level of RNS can be significantly lower, and the nitric oxide provokes mutagenesis and angiogenesis instead, thus connecting directly inflammation and the initiation of cancer.[25]

Considering such a large number of biological processes in which nitric oxide is involved and which in its absence or its low concentration slow down, stop or activate undesirable chemical reactions causing a number of diseases, it seems attractive to obtain a mechanism for regulating the concentration of NO in living organism.

1.3.2 Classical donors of nitric oxide based on organic compounds.

Nitric oxide donors or NO-donors is a group of compounds or functional fragments of supramolecular systems that can release nitrogen monoxide when exogenously applied.[27] Lack of NO in a particular place of a living organism can trigger a number of pathological processes that will manifest themselves as symptoms of various diseases. Although free nitric oxide is used successfully for medical purposes (locally, for the treatment of dermatitis,[28] or in the form of inhalations in pulmonary hypertension in newborns[29]), the use of NO-donors can significantly increase the range of possible exogenous effects on the body.[28] Chemical stability and the capability of local NO elimination of NO-donors allow

the controlled delivery of nitrogen monoxide to various parts of the living organism.

NO-donors can be divided into several groups depending on the method of NO-release activation. According to the classification proposed by Philish and Stamler,[30] three major groups can be distinguished: 1) NO-donors that liberate NO spontaneously; 2) NO-donor that release NO after chemical interaction with acids, alkalis, metals, thiols; 3) NO-donors that release nitric oxide after their enzymatic oxidation (Scheme 1.3).

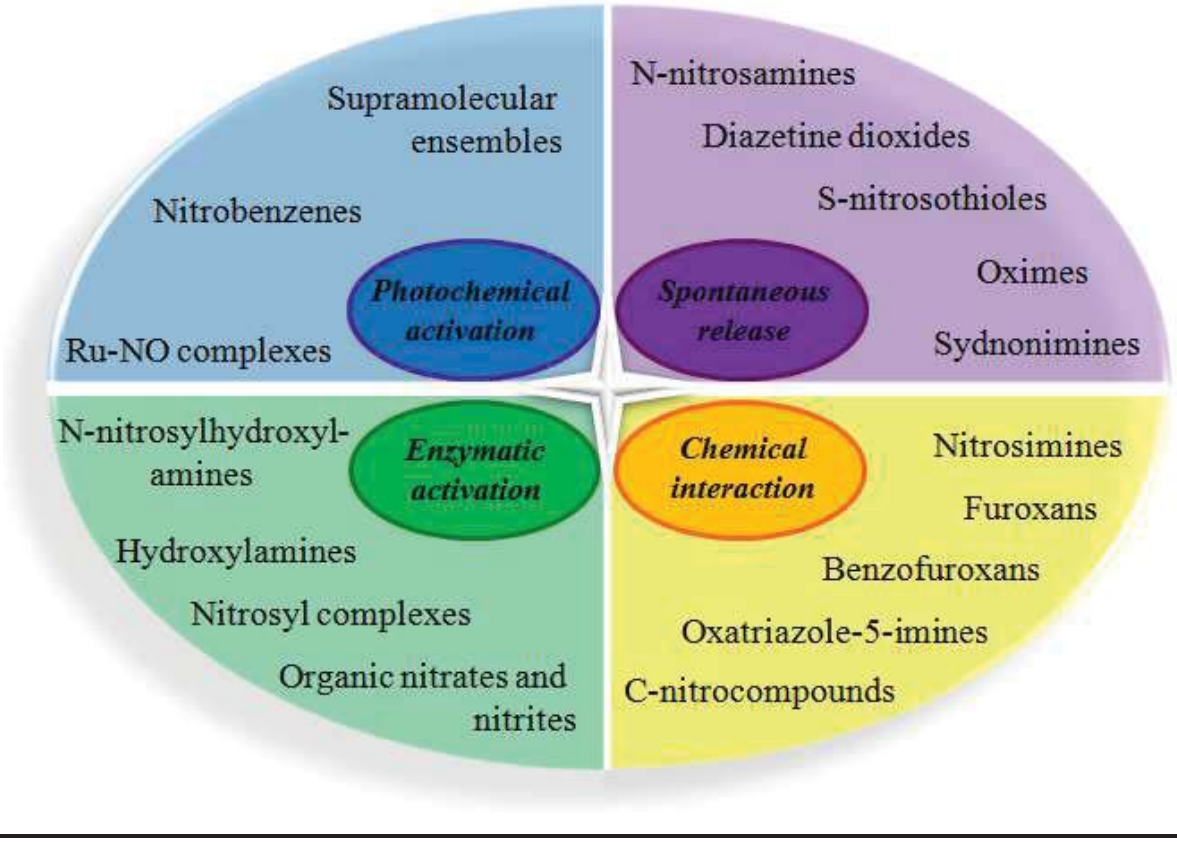

Scheme 1.3. Classification of NO-donor by the initializing of the NO release.

In this work we propose to sort out one more type of donors – compounds that are able to release NO under their photochemical activation, since many studies and research papers published recently are devoted to photoactive compounds that are amenable to NO release.

Organic nitrates are the most widespread example of NO-donors. Since they were the first approved drugs used for NO-level control they are worthy of special attention. Organic nitrates are esters of alcohols (polyols in general) and nitric acid.

Glyceryl trinitrate (GTN) is the most thoroughly studied compound of this class (Figure 1.4). Its use is not limited to vasodilating effects on the vessels. Among the pathologies for the treatment of which the use of GTN is approved, one can mention cardiac dysfunctions[31], hypotension and headaches,[32] angina and cancer.[33] Other drugs used are isosorbide dinitrate (ISDN), pentaerythril tetranitrate (PETN), isosorbide-5-mononitrate (ISMN) (Figure 1.4).[34] The mechanisms by which the nitric oxide is liberated from organic nitrates are still contradictory. However, the proposed schemes include the stage of interaction with one of the enzymes: glutathione-S-transferase, cytochrome P450, xanthine oxidoreductase, aldehyde dehydrogenase.[35]

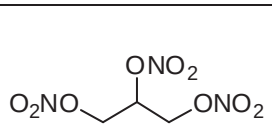

Glycerinetrinitrate (GTN)

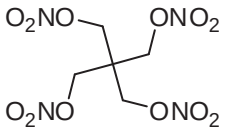

Pentaerythritol tetranitrate (PETN)

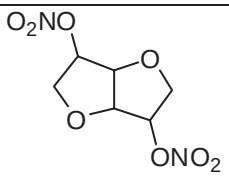

Isosorbide dinitrate (ISDN)

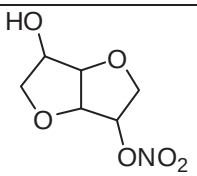

Isosorbide-5-mononitrate (ISMN)

Figure 1.4. The main representatives of the class of organic nitrates

The use of organic nitrates can lead to a number of side effects,[34] since these drugs show their effects in the body in whole, without specific localization. However, the most significant disadvantage of using organic nitrates is the tendency of the body to rapidly developed tolerance to these compounds.[36]

This feature of organic nitrates can be very useful in the treatment of cancer. The growth of cardiovascular tolerance to GTN allows its use in complex cancer therapy, along with cytostatic drugs (i.e. doxorubicin) without systematic side effects from continuous high NO levels. Research on the use of such a combination

in the treatment of mice prostate cancer shows a more effective inhibition of tumor growth than in the treatment of exclusively doxorubicin.[37]

Other commonly used compounds in cancer treatment studies are S-nitrozotioles, diazeniumdiolates (NONOate) and sydnonimines (Figure 1.5). S-nitrosothiols are compounds with a nitroso group which is directly linked to the sulfur atom. Most compounds of this class are unstable, but several of them are sufficiently stable and have already proven themselves as active drugs (*i.e.* S-nitroso-N-acetylpenicillamine (SNAP)) (Figure 1.5).[32]

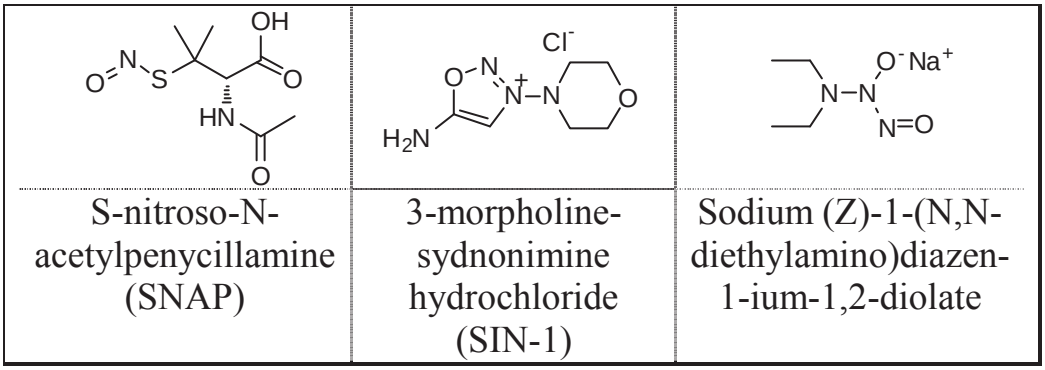

S-nitroso-N-acetylpenycillamine (SNAP)	3-morpholine-sydnonimine hydrochloride (SIN-1)	Sodium (Z)-1-(N,N-diethylamino)diazen-1-ium-1,2-diolate

Figure 1.5. Representatives of other classes of NO-donors used in oncology practice

The main advantage of S-nitrosothiols is better biocompatibility compared to other NO-donors, in particular NONOate. This conclusion comes from the fact that S-nitrosothiols are naturally present in biological systems, as for instance S-nitroso-L-cysteine (CysNO) or S-nitroso-L-glutathione (GSNO).[38] The mechanism of NO-release from S-nitrosothiols is strongly dependent on the external conditions (Scheme 1.4).

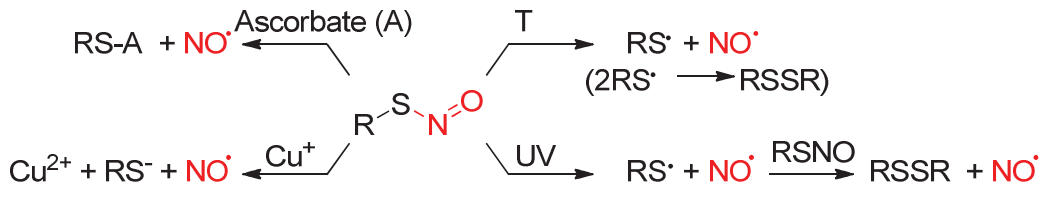

Scheme 1.4. Mechanisms for the release of nitric oxide from S-nitrosothiols

Despite the large number of publications devoted to the study of these compounds *in vivo*, they have not yet found direct application in medicine. Their ability to release NO in different environments, the ability to release it in the form of a radical or nitrosonium-cation, predictable pathway of metabolic degradation, and an almost complete absence of tolerance development with prolonged use – all these benefits make S-nitrosothioles compounds of interest as nitric oxide donors in medical practice.[39]

Another class of NO-donors is diazeniumdiolates (or NONOates). These compounds are known since the 1960s, when its first DEA/NO agent was synthesized for the first time.[40] However, they became the object of numerous studies only in the 90s of the last century,[39] after the biological role of nitric oxide had been discovered. In their structure diazoniumdiolates contain [N(O-)N=O] group. Considering the atom the group is bound to, NONOate are divided into S-linked, O-linked, N-linked, or C-linked. However, only Nitrogen-bound NONOates play significant role in biology.[38,41]

Under physiological conditions (pH 7.4 and temperatures of 37 °C), compounds of this class undergo acid hydrolysis producing 2 equivalents of nitric oxide per diazeniumdiolate group:[32,41]

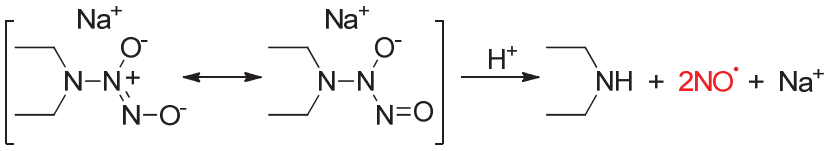

Spontaneous NO release, no need for additional activators of this process (i.e. thiols, metal complexes or enzymes), first order reaction rate moves diazeniumdiolates in one row with S-nitrosothiols and sydnonimines of promising NO-donors.

Easy predictable NO-liberation rate and its final concentration are important qualities of NONOate, due to which compounds of this class are widely used in studies aimed at desing of anticancer drugs.[27] On the other hand, the main advantage easily transforms into the serious drawback when using this compound as drug – NO-donors based on NONOate can release NO before reaching the main

target. The use of targeted drug delivery can help to overcome this disadvantage, although it significantly complicates the drug preparation process.

One of approaches of targeted delivery of this class of compounds is demonstrated in the paper of Wang and coworkers.[42] Using one of NONOates – PYRRO/NO compound as NO-donor, the researchers inactivated the compound by binding it with a certain amino acid sequence through the oxygen atom of the diolate group. The use of amino acid sequence of one segment of the substrates of prostate-specific antigen (PSA) allowed making modified PYRRO/NO compound sensitive to the presence of this enzyme. PSA is an enzyme produced by both healthy and cancerous cells of the prostate epithelium in significant amounts.[42] Increased concentration of this enzyme is observed in metastases of prostate cancer.

The resulting PYRRO / NO based drug must be inactive before hydrolysis that occurs in the presence of PSA or α-chymotrypsin. As a result, spontaneous release of NO *in vitro* from the resulting compound was observed only in the presence of one of these enzymes in solution (Scheme 1.5).[42]

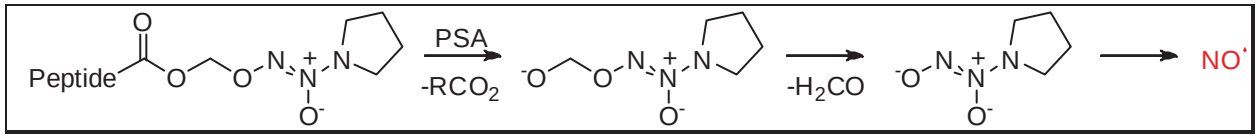

Scheme 1.5. Nitric oxide release from peptide-bound PYRRO/NO by enzyme activity PSA

Another class of NO-donors already used as medicines are sydnonimines. Sydnonimines are mesoionic heterocycles, which include the 1,2,3-oxadiazole ring and contain an imino group in the 5 position. For the first time, independently of each other, compounds of this class were synthesized in 1957 by Brooke[43] and Ohta.[44] Under normal conditions and in the absence of light sydnonimines are stable solids.

Sydnonimines release nitric oxide in an alkaline medium and the passage of this process is greatly facilitated by the presence of oxygen or under excitation with UV irradiation. The most studied example of this class is

3-morpholinosydnonimine (SIN-1, linsidomine) (Figure 1.5). The medicinal product under the brand name "Molsidomine" is based on this compound. The release of NO from this product is shown in Scheme 1.6.[45] The first step of decomposition is the enzymatic deacetylation of molsidomine in the liver with the formation of linsidomine. At physiological or alkaline pH linsidomine undergoes a non-enzymatic cycle opening. The formed product is completely stable at pH 7.4 in absence of oxidants, but even small amounts of oxygen lead to the formation of radical cation which decays producing nitric oxide and N-morpholino-aminoacetonitrile.

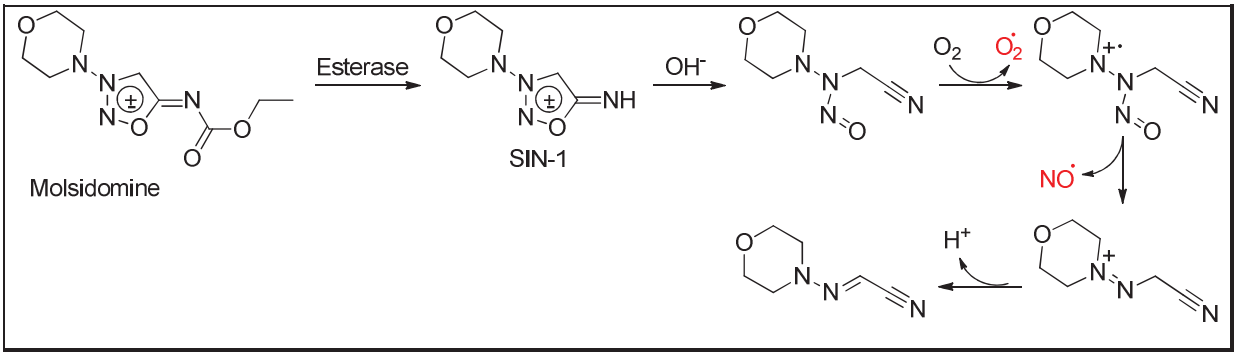

Scheme 1.6. NO-release from medicinal product "Molsidomine"

Typically sydnonimines donate NO in peroxynitrite anion form.[44] As shown on the Scheme 1.6 during the molsidomine transformation the stoichiometric amount of the superoxide radical is formed, and since the interaction of nitrogen monoxide with the superoxide radical is extremely rapid and the diffusion is the only limiting process, the formation of toxic peroxynitrite is inevitable. This feature of sydnonimines, of course, reduces the spectrum of their possible use in medicinal purposes. The advantage of these compounds is that addiction to them does not appear, and a tolerance to sydnonimines does not arise even with prolonged use.

1.3.3 Nitrobenzenes as examples of photoactive NO-donors

The ultimate goal of most studies of nitric oxide donors is the compound that is capable of controlled and predictable local NO-release. This substance would be

able to give a clear answer to the question of how different concentrations of NO affect different biological objects and to allow finding the optimal rate and the required concentration of nitrogen monoxide for a particular physiological effect.[46] The use of a controlled NO-donor will reduce the dose required for treatment and reduce the side effects associated with the release of nitric oxide beyond the immediate biological target.[47] It is clear that controlled release of NO is also extremely important for the effective treatment of cancer with the use of NO-donors, since it significantly reduces the toxic effect of RNS on healthy cells of the body.[48] Another potential use of materials capable of controlled NO-release is the creation of various devices, such as artificial blood vessels or tubes for hemodialysis.[49] One of the main ways of obtaining of such compounds is the design of photoactive NO-donors.

Among the substances that are capable of photoinduced release of NO, the most promising and studied are derivatives of nitrobenzene and metal nitrosyl complexes. However, a large number of works is also devoted to the study of supramolecular ensembles (*i.e.* liposomes, micelles), nanoparticles and polymer materials that are capable of releasing or activating the NO-donors, which in turn can produce nitric oxide locally.[27,41,50,51,52]

The investigation of aromatic nitrocompounds as NO-donors was started by Sortino and Miyata groups. In general, the functional group that directly acts as a donor of NO in these compounds is an aromatic ring with a nitrogroup and bulky substituents in the *ortho*-position (*i.e.* CH_3, CF_3, Ar etc.) (Figure 1.6a).[27] Due to the presence of closely located substituents, the nitrogroup is forced to accept the position almost perpendicular to the plane of the aromatic ring, loosing the conjugation with the benzene ring.[53] In this arrangement, the *p*-orbital of the oxygen atom considerably overlaps with the orbitals of the aromatic ring, both in the main and

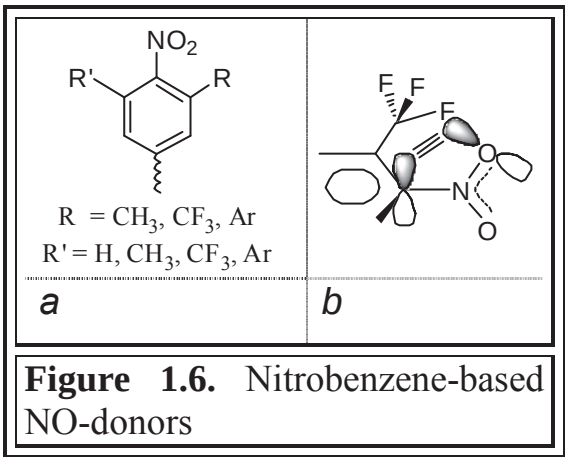

Figure 1.6. Nitrobenzene-based NO-donors

excited states. In this view the process NO-release from *o*-substituted derivatives of nitrobenzene occurs, probably, through the stage of isomerization of the nitro into the nitrite derivative and the subsequent decomposition of the latter into NO and the phenoxy radical due to O-N bond breakage (Scheme 1.7).[54] According to the authors, the key factor for the possibility of isomerization is the orthogonal arrangement of the nitrogroup and the benzene ring.[55,56]

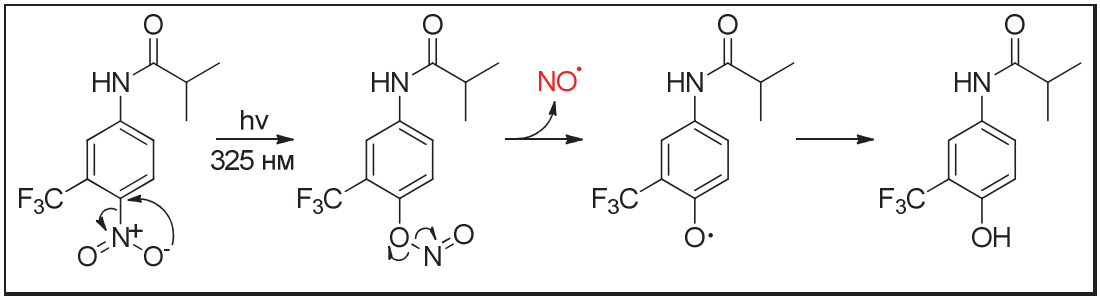

Scheme 1.7. The mechanism of nitric oxide release from an anticancer drug flutamide

Nitrobenzene-based NO-donors are thermally stable under physiological conditions, and the release of nitric oxide from these compounds can be controlled by electromagnetic irradiation. Also, the advantage of nitrobenzenes as photoactive NO donors is the absence of metal ions, the presence of which could itself provide cytotoxic properties. However, the significant disadvantage of this class of NO-donors is the need to use electromagnetic radiation of UV-region, which is significantly absorbed by biological tissues and fluids and is hazardous to healthy cells.

An example of work aimed at overcoming this lack of nitrobenzenes is the work of Naoki Miyata group.[55,57] Modification of the starting 2,6-dimethylnitrobenzene (which is responsible for the NO release) by the introduction of a compact fluorophore (such as 7-hydroxycoumarin or 7-aminocoumarin) made it possible to shift the band of absorption of compounds from UV to the visible domain of electromagnetic waves (Figure 1.7a and 1.7b).[57] An interesting fact was that in the case of a DEAMC-DNB in which there is a complete conjugation of the aminogroup with the nitrogroup through the π-chain, release of nitric oxide is not

observed under the irradiation of compound at 430-460 nm. Owing to the efficient intramolecular charge transfer, the bond order of C-N(NO2) bond increases to double, and nitro-nitrite isomerization becomes impossible. However, in the case of a compound where the π-system cross-conjugation is present (Bhc-DNB), the irradiation results in NO-release. Under excitation of the compound no significant

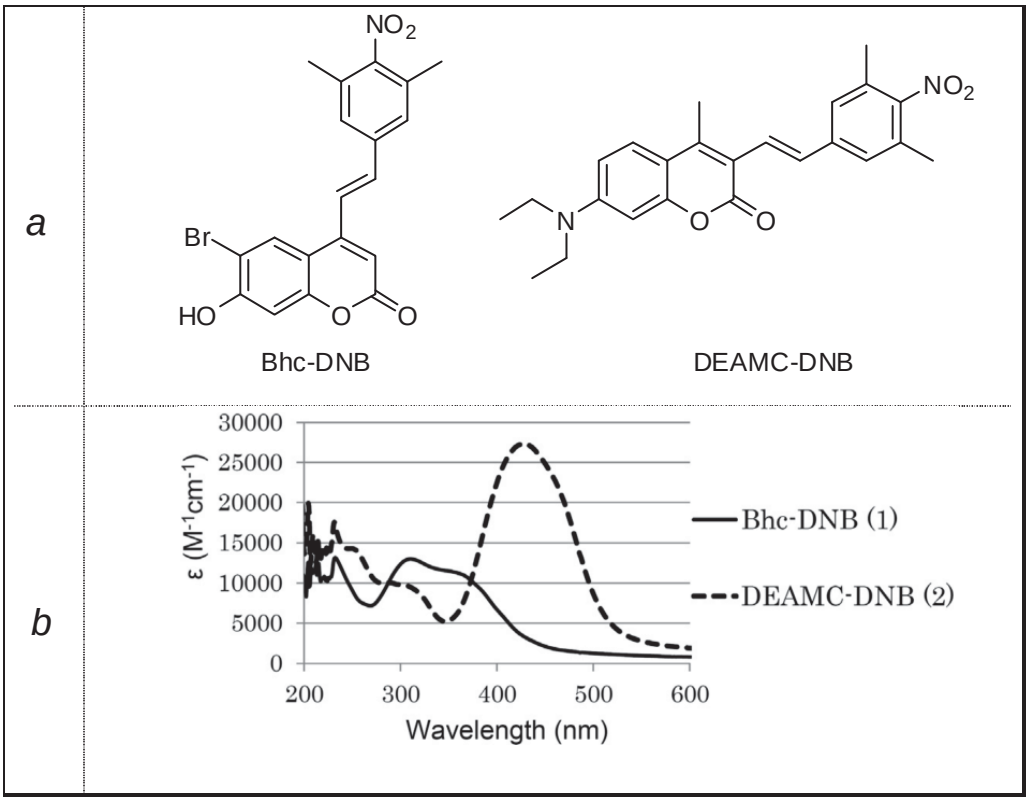

Figure 1.7. New compounds based on 2,6-dimethylnitrobenzene (a) and their electronic spectra (b).

charge transfer occurs in the molecule (as could be concluded from the absence of an intense band in the UV-visible spectrum) and the band 350-430 nm appears due to the absorption of coumarin fragment, which acts as an antenna. Thus the researchers were able to shift the excitation wavelengths required for nitrobenzene activation from UV to visible domain.[57]

Another elegant way to avoid the UV irradiation to initiate NO-release from nitrobenzenes is the use of two-photon absorption method. This approach allows shifting of the excitation wavelength up to the infrared (IR) region, which does not show a deleterious effect on the body and is more permeable for biological tissues.

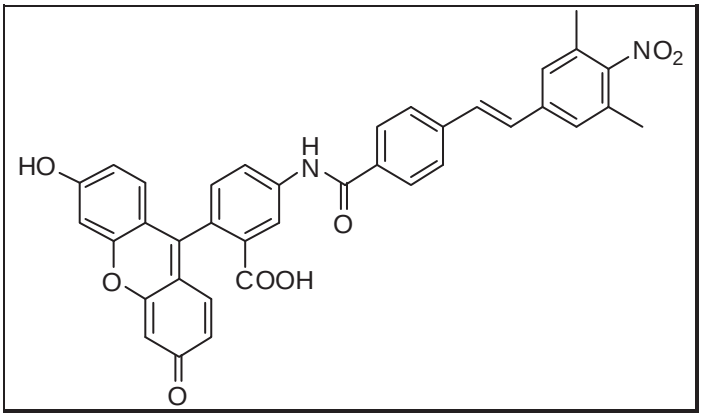

Figure 1.8. Flu-DNB is a compound capable of releasing NO by two-photon photo-excitation in wavelengths of 720-800 nm.

Binding of 2,6-dimethylnitrobenzene through a styryl and weakly conjugated amide fragment to fluorescein (which is famous for its ability to produce two-photon excited fluorescence[58]) researchers obtained a Flu-DNB compound (Figure 1.8) that released nitric oxide when irradiated with an IR pulse laser with a wavelength 720-800 nm.

1.4 NO-donors based on coordination compounds

1.4.1 General characteristics of nitrosyl complexes.

Today metal-nitrosyl complexes are considered as promising objects for targeted delivery of nitric oxide.[59] They are especially interesting as photoactive NO-donors. Before consideration of the particular examples of the NO-donor compounds one should first concentrate on several aspects of the coordination behavior of nitric oxide.

The most typical and common way of coordination of nitric oxide to metal is a monodentatable type of binding, in which the nitrogen is a donor atom. Upon such coordination, two types of geometry are possible depending on the angle M-N-O – straight and angular. The differences between them can be explained by the valence bond and orbital hybridization theories.

Considering that straight or almost straight geometry of the complex is a result of the *sp*-hybridization of nitrogen orbitals, it is assumed that the nitric oxide in such compounds is in the form of NO^+; while the angular geometry requires sp^2-hybridization, and in this case NO is in the form of NO^-. Resonance forms, whose combinations could describe the linear and angular geometry, are shown in the Scheme 1.8.[2] Those resonance structures where radicals are present can be considered as forms that possess a lone pair of electrons, and the corresponding complexes accept an intermediate geometry between the linear and angular, which is characteristic of the nitroxyl complexes.

The formation of nitrosonium-containing compounds requires the transfer of one electron from nitric oxide to a metal center, followed by σ-binding and π-backbonding interaction $d_M \rightarrow \pi^*$ (Figure 1.9), and the formation of complexes that could be described as those containing nitroxyl anion is preceded by the transition of the electron from metal to the nitric oxide (Scheme 1.8).[60]

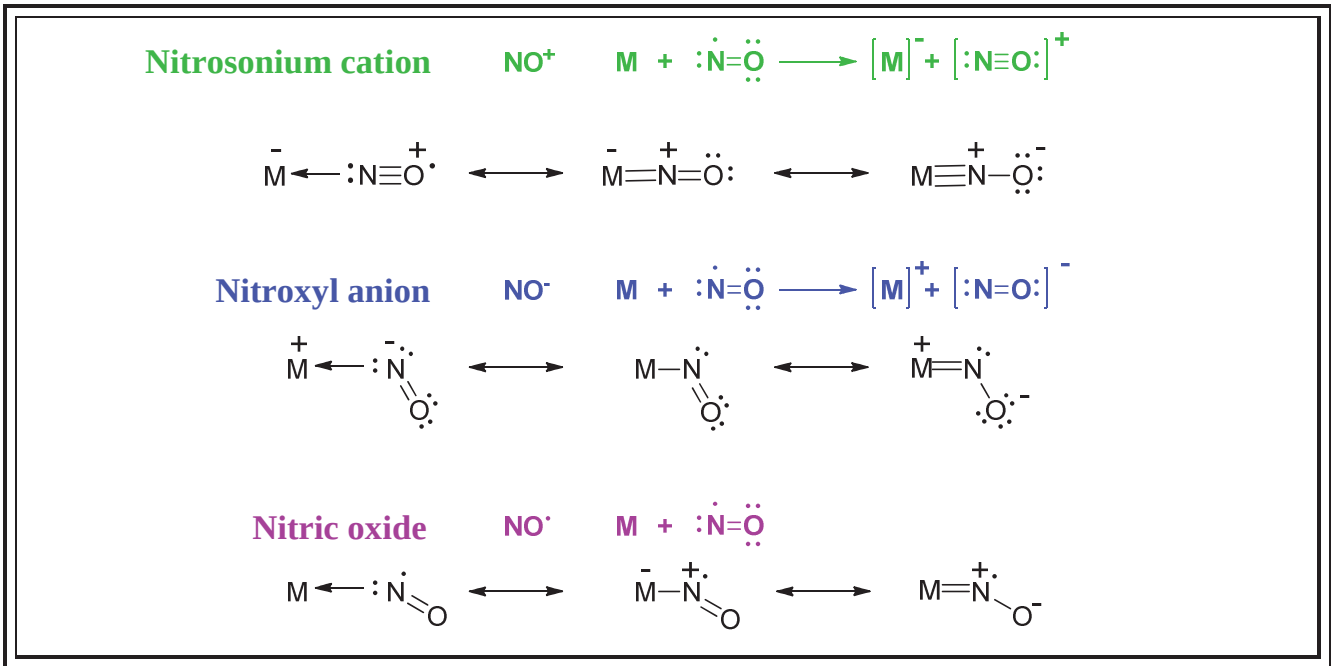

Scheme 1.8. Resonance forms of linear and angular geometry of metal-nitrosyl complexes

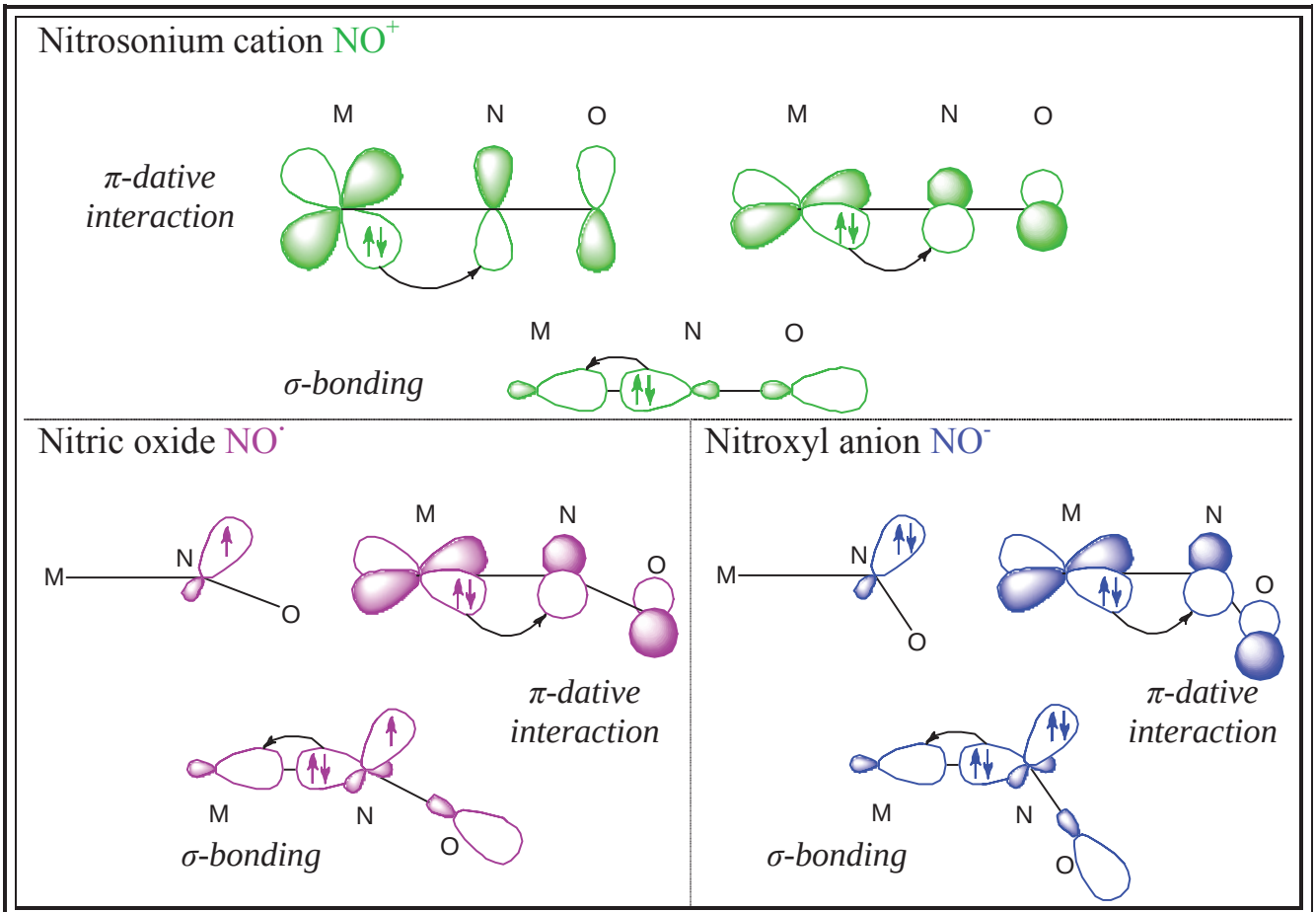

Figure 1.9. Simplified schemes of molecular orbitals for straight and bent geometries of mononitrosyl complexes

Thus, in the linear coordination form the oxide acts formally as a donor of 3 electrons, whereas in the angular form it is a donor of 1 electron. Both the method of valence bonds and the method of molecular orbitals showed that the increase in the electron density at the M-N bond due to the backdonation leads to the increase of this bond's order though by reducing the energy of N-O bond.

Due to the discovery of the biological role of nitrogen (II) oxide, the interest in the coordination compounds of this molecule with metals has exponentially increased since the 1980s. Table 1.1 presents a general information about all nitrosyl complexes found in the Cambridge Structural Database (CSD) in 2014.[60]

Angle (°)	Number of structures	Geometry	Example
180-160	2519	Linear	[Mn(NO)(CO)4][61]
160-140	121	Intermediate	[Ir(NO)2(PPh3)2][62]
140-100	115	Angular	[Co(NO)(S2CN(CH3)2)2]

Table 1.1 Generalization of metal-nitrosyl complexes from the CSD database in 2014

There are complexes (absent in the table above) that contain metal atoms bound both to oxygen and nitrogen atom of the NO group. Total number of such complexes is small; usually they are unstable and could form as a result of photoexcitation of nitrosyl complexes as transitional states. The particular example of such compounds is [Ni(NO)(η^5-Cp*)], where Cp - pentamethylcyclopentadienyl anion. The Ni-N distance in it is only 0.4 Å shorter than the Ni-O distance, and the Ni-N-O angle is 93°.[63]

Apparently, the vast majority of compounds have a linear M-N-O fragment. Complexes in which this angle is much smaller are basically the complexes of the right half of d-metals. An explanation for this lies in the presence of bigger number of electrons at the d-sublevel that reduces the ability of metals to accept three electrons from nitric oxide. But only in this case the linear geometry of the complex is possible.[1]

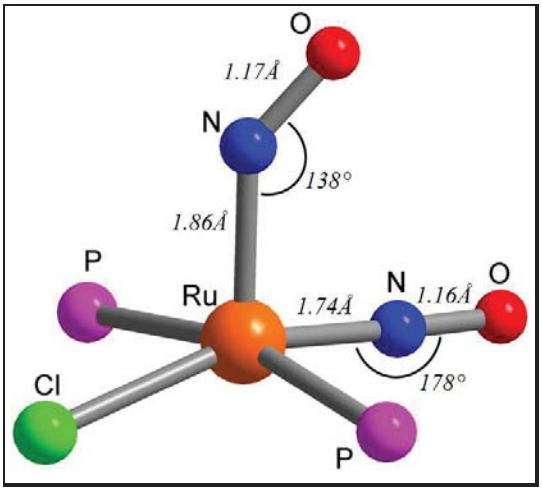

Figure 1.10. Structure of cation $[RuCl(NO)_2(PPh_3)_2]^+$ *(the phenyl fragments are omitted)*

Among the compounds found in CSD, there are also those containing from 2 to 4 NO-fragments that can assume either the same or different geometry.[64] For example, in the compound $[RuCl(NO)_2(PPh_3)_2]^+$ (Figure 1.10)[65], both atoms of one of the nitrosyl ligands and the metal atom lie on one straight line, while the other nitrosyl ligand is bound with an angle substantially less than 180°.

As shown in Figure 1.10, the lengths of the Ru-N and N-O bonds are somewhat larger in bent conformation, indicating a weakening of these bonds compared to a linear Ru-NO fragment.

Nitric oxide in linear conformation in complexes is a very strong π-acceptor. The use of photoelectron spectral methods allowed to assess the ability of NO and other ligands to withdraw electron density from metal atoms through the π-backdonating interaction.[66] Among other ligands, nitrosyl cation occupies leading positions. In particular, its π-withdrawing ability is the highest in the following series:

$$NO > CO > \eta^2\text{ - }MeC{\equiv}CMe > H_2C{=}CH_2 > SO_2 > N_2 > PMe_3 > SiCl_3 > NH_3 >$$

$$CN > H > Cl > SiMe_3 > C{\equiv}CH\ ^{66}$$

Due to the significant shift of the electron density, the M-N distance significantly decreases with increase of $d_M \rightarrow \pi^*$ dative interaction. For example, in complexes that contain both linearly coordinated nitric oxide and ammonia as ligands, the $M\text{-}N_{NO}$ bond length is less than the bond length of $M\text{-}N_{NH3}$ by 0.35-0.4 Å. The values of the M-N bond lengths in complexes indicate that these bonds are covalent for the most part. In view of this, the description of complexes as ionic compounds of nitrosonium-cation or nitroxyl anion becomes less relevant.

Another approach of describing complexes with non-innocent (redox-active) ligands (one of which is nitric oxide) is the Enemark-Feltman notation. Its advantage is the omitting of the concept of oxidation states of the central atom and ligands.

When utilizing the Enemark-Feltman formalism for complexes with nitric oxide, the latter are designated as $\{M(NO)_x\}_n$, where x is the number of NO ligands and n is the total number of electrons located on the d-orbitals of the metal atom and π* – orbitals of nitric oxide. It is assumed that the metal atom is in its formal oxidation state, and nitric oxide is neutral.[64] Examples of the use of the Enemark-Feltman notation for coordination compounds nitric oxide are shown below:

$[Co(NH_3)_5NO]^{2+}$	Co^{II}	d^7	$\{Co(NO)\}^8$
$[Fe(SR)_2(NO)_2]^-$	Fe^{I}	d^7	$\{Fe(NO)_2\}^9$
$[RuCl_2(terpy)(NO)]^+$	Ru^{III}	d^5	$\{Ru(NO)\}^6$
$[Mn(CN)_5NO]^{3-}$	Mn^{II}	d^5	$\{Mn(NO)\}^6$

(terpy – terpyridine*)*

Although the description of NO-complexes in this way eliminates ambiguity in determining the oxidation state of central atom and ligands, in some cases assigning a charge to them helps in understanding of electronic and magnetic properties of compounds.

To complete a picture of the coordination capabilities of NO, its ability to act as a bridging ligand should be considered as well. Similarly to the coordination behavior of carbon monoxide, nitric oxide is capable of binding two, three, and in some cases four metal atoms, stabilizing metal cluster complexes (Figure 1.11). An example of such a cluster is homobimetallic nitrosyl copper complex $[(Cu_2(XYL\text{-}O^-)(\mu\text{-}NO)](PF_6)_2$, where XYL-O is 2,6-bis(bis(2-pirydyletyl)-aminomethyl)phenolate) (Figure 1.11a). This compound is interesting because of the fact that ineracting with

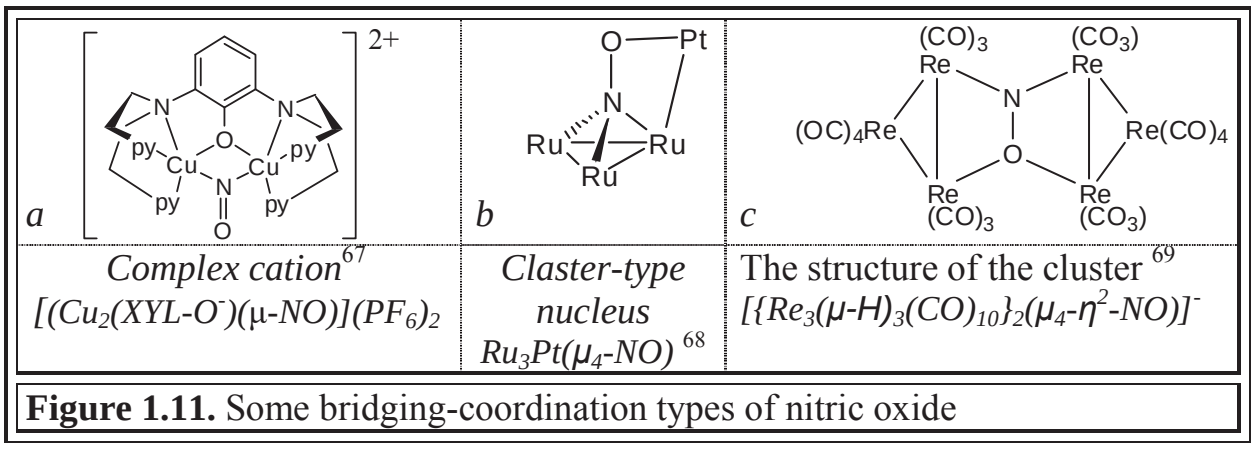

Complex cation[67] *$[(Cu_2(XYL\text{-}O^-)(\mu\text{-}NO)](PF_6)_2$*	*Claster-type nucleus $Ru_3Pt(\mu_4\text{-}NO)$* [68]	The structure of the cluster [69] *$[\{Re_3(\mu\text{-}H)_3(CO)_{10}\}_2(\mu_4\text{-}\eta^2\text{-}NO)]^-$*

Figure 1.11. Some bridging-coordination types of nitric oxide

nitrite anion and transforming into $[(Cu_2(XYL\text{-}O^-)(\mu\text{-}O)]^+$ it emulates the nitrite reductase activity (an enzyme consisting of diatomic copper cluster). Indeed, it is known that the main mechanism of this transformation includes the copper-nitrosyl complex as an intermediate stage.[70]

1.4.2 Study of metal-nitrosyl complexes by means of IR spectroscopy

Modern physicochemical methods allow an accurate characterization of metal-nitrosyl complexes; in particular, it is possible to determine the binding parameters and electronic structure of the M-N-O fragment without X-ray diffraction analysis. However, the interpretation of the obtained spectral data should be carried out with extreme caution and captiousness. In cases of possible ambiguity in the interpretation of certain results, methods of quantum chemistry serve as an auxiliary tool and enable a deeper understanding of the electronic structure of the complex.

The most important and frequently used spectral methods in the study of nitrosyl complexes are IR, EPR, UV and NMR spectroscopy. Less commonly used and more specific methods are the Mössbauer spectroscopy, X-ray (XAS) spectroscopy, magnetic circular dichroism, and the study of magnetic susceptibility.[71]

The use of vibrational spectroscopy for the study of nitrosyl complexes has become widely used. In fact, the dependence of the characteristic vibrations of NO on the donor-acceptor properties of the environment can serve as a tool for understanding the nature of the interaction of metal atom with nitric oxide. As indicated in section 1.1, the valence vibrations of free NO radical have a frequency of 1875 cm^{-1}. After coordination of NO to the metal atom, the value may either increase or decrease depending on different parameters such as the nature of other ligands in the coordination sphere, the electronic configuration of the central atom, the total charge of the complex and its geometry. For metal-nitrosyl complexes there is a general tendency for the increase of vibrations frequency with the increase of the positive charge of nitrosyl ligand from 1300 cm^{-1} to 1950 cm^{-1}.[2] In addition, for compounds with linearly coordinated nitric oxide this value lies within the limits of 1950-1450 cm^{-1}, and for those in which the M-N-O angle is considerably less than

180° vibrations in the region of 1720-1400 cm^{-1} are more typical; for bridging nitric oxide – from 1650 cm^{-1} to 1300 cm^{-1} (Figure 1.12).

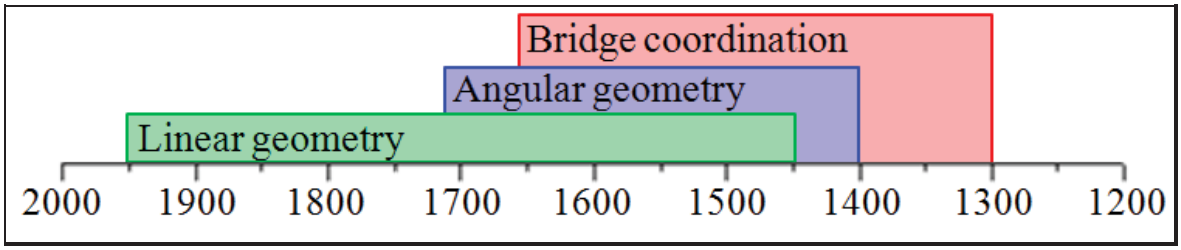

Figure 1.12. Frequency ranges of valence vibrations of the N-O bond depending on the type of nitric oxide coordination

As shown, these ranges strongly overlap and an unambiguous determination of the coordination type on the basis on the value of the frequency is not possible. Nevertheless, if the frequency value is higher than 1750 cm^{-1}, the linear geometry can be accurately established.

More correct and reliable correlation can be considered for the complexes similar in their electronic structure. For example, if the central atom is represented by one of the transition elements of 8th group (Fe, Ru, Os), and the complex have the following structure $\{M(NO)\}^{6-8}$ (by the Enemark-Felthman notation) (Table 1.2).[71]

Complex	Frequency
$\{M(NO)\}^8$	1270-1500
$\{M(NO)\}^7$	1600-1700
$\{M(NO)\}^6$	1800-1960

Table 1.2. Valence vibrations of N-O in complexes of metals of the 8th group metals.

As it was mentioned, the frequency of the valence vibrations of nitric oxide in complexes depends on many factors (in particular, on the nature of other ligands present in the complex). In the work of De La Cruz and Sheppard, authors made an attempt to summarize the effects of other ligands on the variation of the frequency of the vibration of the N-O bond.[72] A brief summation is presented in Table 1.3.

Charge and ligands	$\Delta\nu$(NO) (cm^{-1})
A. Ionic charges	
Unit of positive charge	+100
Unit of negative charge	-145
B. Electron-withdrawing ligands	
Linear cyanide	+50
Linear halogens	+30
Bridging halogens	<+15
C. Linear or bridging CO ligand	≈ 0
D. Electron-donating ligands	
PF_3	+10
$P(OPh)_3$	-30
$PAlk_3$ (Alk – alkyl)	-70
η^5-C_5H_5	-60
η^5-C_5H_4Me	-70
η^5-C_5Me_5	-80

Table 1.3. The influence of ligands of different nature and charges on the vibrational frequency of nitric oxide in complexes.

1.4.3. Ruthenium-nitrosyl complexes as NO donors

The idea of utilizing of metal complexes as NO-donors falls in line with the fact that the primary goal for the attack of NO in the human body is iron-containing enzymes.[32] Among the coordination compounds with nitric oxide donating ability sodium nitroprusside (SNP) is the most studied and well known one. More than for 90 years SNP is used for medical purposes as a hypotensive drug of the class of vasodilators. In the solid state $Na_2[Fe(CN)_5NO]\cdot 2H_2O$ can be stored for years in the absence of light and moisture, but in the solution the compound becomes extremely photosensitive and reactive to oxygen.[44]

The mechanism of NO release from SNP *in vivo* is not yet fully understood, but this process is thought to be initiated by photoexcitation or one-electron reduction, and the presence of thiols accelerates it (Scheme 1.9).[44]

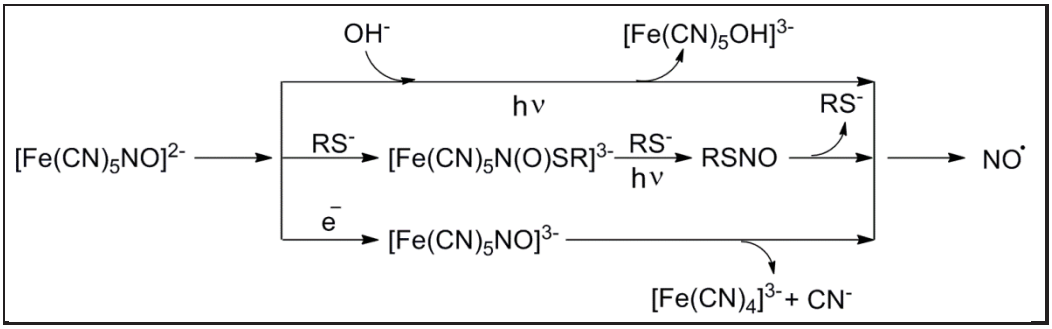

Scheme 1.9 Possible mechanisms for the release of nitric oxide from SNP

As can be seen from the scheme, the process of reduction and subsequent decomposition of SNP is accompanied by the release of cyanide anion (sometimes up to 5 equivalents in biological conditions)[44]; this can lead to significant toxic effects on the whole body if significant amount of SNP was used. Also, the spontaneous decomposition of the compound increases the local concentration of the cytotoxic peroxynitrite anion. But, although SNP has some deleterious effects, its use as a vasodilating agent is justified, since the use of even small amounts of the drug is often enough to provoke biological effects. However, the use of this compound is very limited, and the search for new cooordination compounds that would be devoid of these shortcomings is a topical issue.

Among other metals, ruthenium attracts attention due to its ability to emulate the coordination features of iron.[2] Unlike the latter, the ruthenium complexes are always low-spin ones, both in the oxidation states +3 or +2, which contributes to their higher stability compared to iron complexes, as well as the lower lability of the ligands (including nitric oxide) in its coordination environment;[59,73] this is a prerequisite for their biological application. Confirmation of this can be a found in comparison of SNP with its Ruthenium analogue $[Ru(CN)_5NO]^{2-}$. Like sodium nitroprusside, $[Ru(CN)_5NO]^{2-}$ is capable of being excited with electromagnetic waves, but unlike SNP, this compound does not release toxic cyanide ions in solution.[70]

Ruthenium-nitrosyl complexes also have several advantages, which are often not typical for coordination compounds of other metals - good water solubility,

resistance to air oxidation and low cytotoxicity.[74] The kinetics of ruthenium interaction with bioligands is often compared to the effects caused by platinum on the body;[75] however, numerous studies indicate a significantly lower toxic effect of ruthenium, which may be due to its close to iron coordination behavior and its ability to bind albumin molecules and iron-transporting transferrin proteins.[76]

Depending on the type of ligands in the coordination sphere, ruthenium can exhibit several basic oxidation levels that can exist in the biological environment – Ru(II), Ru(III) and Ru(IV). In the presence of reducing agents as glutathione or ascorbate Ru(III) could easily be reduced to Ru(II). Coordination compounds in which ruthenium is in the oxidation state +2 are more susceptible to ligand exchange and readily interact with N-donor or S-donor biomolecules.[44] By changing the donor-acceptor properties of the ligands (*i.e.* their ability to π-binding) the energy and strength of the bond Ru-N_{NO} in the ruthenium-nitrosyl complexes can be varied affecting the efficiency and rate of nitric oxide release.[44]

An important advantage of ruthenium (along with Mn and Fe) in comparison with other metals is the photoactivity of its nitrosyl complexes. Despite the high stability of the coordination compounds of ruthenium with nitrogen monoxide, they are capable of releasing NO under irradiation by electromagnetic waves of a certain length.[48] Due to this feature ruthenium-nitrosyl complexes are intensively studied for the purpose of obtaining the NO-donor capable of local, time-controlled, photosensitive release of nitric oxide.

The first studies of NO-release from ruthenium-nitrosyl complexes under the influence of light were carried out on $\{Ru(NO)\}^6$ compounds with monodentate ligands – mainly amines and halogens (Figure 1.13).

The investigation of nitric oxide photorelease and the nature of corresponding photoproduct was carried out in 1983 by Sinitsyn and his collaborators; in this case the compound $K_2[RuCl_5(NO)]$ was chosen as NO-donor. The signal observed in EPR spectroscopy during the experiment of photorelease having g-factor equal to 2.34 denoted the presence of paramagnetic low-spin d^5-Ru(III) particles in the solution.[77]

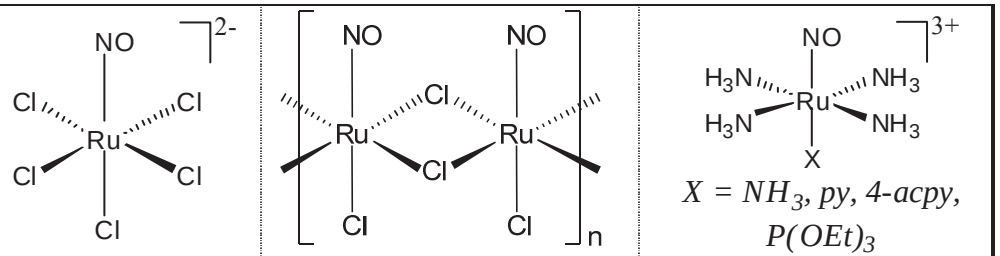

The anion of $K_2[RuCl_5(NO)]$	$RuNOCl_3$	Cation of *trans*-$[Ru(NH_3)_4(X)(NO)]^{3+}$

Figure 1.13. Examples of the photoactive $\{Ru(NO)\}^6$ complexes with monodentate ligands

The stoichiometric ratios confirmed the previously proposed NO-release mechanism:

$$Ru\text{-}(NO) + solv \rightarrow Ru^{III}\text{-}(solv) + NO$$

The quantum yields (φ) found for compounds $K_2[RuCl_5(NO)]$ and $RuNOCl_3$ are 0.06 and 0.012 respectively.[78] This difference in the values for two quite similar compounds arises from the fact that the presence of a greater number of negatively charged ligands (5 chlorine atoms per ruthenium atom in the first compound against 3 chlorine atoms in the second) facilitates the process of NO-photorelease. Today these compounds are well studied and are commercially available.[77]

Studies of analogous compounds in which chlorine atoms in the equatorial plane are replaced with ammonia molecules – *trans*-$[Ru(NH_3)_4(X)(NO)]^{3+}$ – have shown that the ligand that is in the *trans*-position to nitric oxide has a significant effect on the rate and efficiency of NO-release. Thus, in the case of the phosphite $P(OEt)_3$ ligand the quantum yield of NO-release was φ = 0.3, while for the compound with the imidazole ligand in the *trans*-position to NO this value was only 0.04.[77]

Giving preference to polydentane ligands over monodentate ones in the study of compounds for the purpose of their further use for medical purposes is determined by a greater stability of chelating complexes and complexes with macrocyclic ligands.[77] The necessity of using complexes with high stability constants becomes clear if we take into account the infinite number of biomolecules in the body that can strongly bind metal atoms, competing with monodentate ligands. Thus, polydentane

ligands make it impossible to bind metals with bioligands, thus reducing or eliminating the harmful effects of the former;[77] and also, which is important for photoactive compounds, polydentate ligands provide the stability of complexes, and therefore thir photochemical characteristics.

Since prosthetic groups of heme proteins (hemoglobin, sGC, cytochromes) are the primary targets for nitric oxide attack in the body (see section 1.2), one of the first attempts to receive NO-donor based on coordination compounds of ruthenium with polydentane ligands was made precisely with the use of porphyrins.[73] The resulting compounds of the general formula [(P)Ru(NO)Cl], where P is porphyrin, were thermally more stable and less susceptible to oxidation by oxygen in the absence of irradtiation than similar iron complexes. However, the reverse recombination of released NO molecule was too fast ($k \approx 1*10^8$ $M^{-1}s^{-1}$), that made these compounds unsuitable for targeted NO delivery.[48,73,79]

More promising from a practical point of view are non-porphyrin-type ligands – Schiff's bases, thiolates, polypyridyl and other polydentane ligands. Examples of some typical ligands of these classes are shown in Figure 1.14.

Schiff's bases are the classic example of the podand ligands. In 2002 Ford and coworkers synthesized several $\{RuNO\}^6$ complexes using N,N'-bis(salicylidene)ethylenediamine (H_2salen) as a ligand (Figure 1.14). Like the porphyrin ligand, compounds of this type contain four donor atoms, two nitrogen atoms in imine group and two phenolic oxygen atoms occupying four positions in the equatorial plane of the ruthenium polyhedron (Figure 1.15).

The study of the NO-release from these compounds under irradiation (λ = 365 nm) showed a certain dependence on the nature of the solvent in which the process took place. Donor solvents such as acetonitrile have been shown to be able to stabilize the generated photoproduct, and the reverse process of the released NO-molecule coordination is relatively slow ($k \approx 10^{-2}$-10^{-4} $M^{-1}s^{-1}$).[77] If tetrahydrofuran (THF) or toluene (PhMe) is used instead of acetonitrile the process of photo-release is immediately followed by a very rapid recombination.[80]

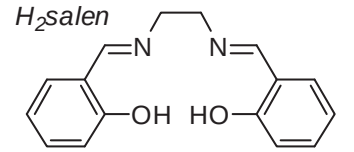

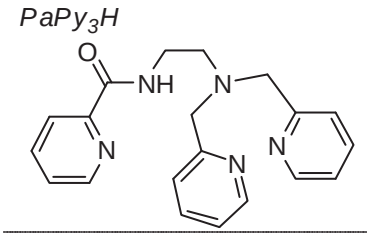

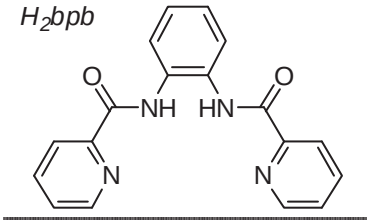

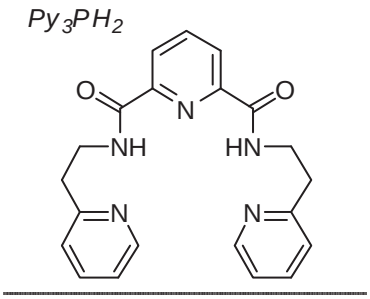

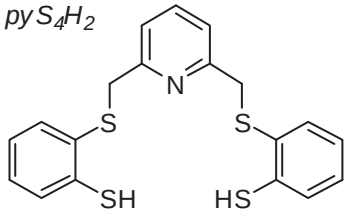

Figure 1.14. Ligands for the synthesis of ruthenium-nitrosil complexes

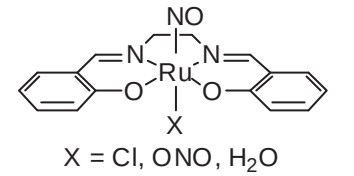

Figure 1.15. Cation of ruthenium nitrosyl complexes with *salen* ligand

In this work it was also found the dependence of the photochemical activity of complexes on the ligand donor strength (Figure 1.15): with decreasing of σ-donating activity moving from Cl to H_2O in the series Cl^- – ONO^- – H_2O quantum yield decreases as follows 0.13 - 0.067 - 0.005 respectively,.

Deep investigation of ruthenium-nitrosyl complexes with $PaPy_3H$ type ligands (Figure 1.14) were performed by Mascharak's group. The principal feature of the structure of these ligands is the presence of the carboxamide nitrogen atom in its structure. The idea of using such a fragment was suggested by the structure of the enzyme nitrile hydratase.[81] Two of the six donor atoms in the iron coordination polyhedron in active cite of this enzyme are carboxamide Nitrogen atoms, and its activity is regulated by the coordination of nitric oxide to the central iron atom.

Formation of the complex $[(PaPy_3)Ru(NO)]^{2+}$ with this ligand (Figure 1.16) occurs with deprotonation of the nitrogen atom of the carboxamide group. Thus, in the formed complex the negatively charged nitrogen atom acts as σ-donor in the *trans*-position to the nitrosyl ligand. Such an important nuance in the structure of the complex makes the compound stable in an aqueous medium at pH ranging from 5 to 9, despite the fact, that vast majority of ruthenium-nitrosyl coordination compounds undergo the transformation into nitrite form at pH>5:[77]

$$Ru–NO + H_2O \rightarrow Ru–NO_2 + 2H^+$$

The absence of this transformation even in the

presence of hydroxide anions indicates that a strong σ-donor ligand in the *trans*-position to nitric oxide in the $\{RuNO\}^6$ complex protects the NO-group from the nucleophilic attack. Along with the high stability of $[(PaPy_3)Ru(NO)]^{2+}$ in solution, the compound also exhibits good photochemical properties. Nitric oxide is easily released from the compound ($\varphi = 0.05$), and the process of reverse recombination is not observed.[77] These parameters (stability and NO-release ability) make the compound interesting in terms of its direct use in biological research. Successful attempts to use $[(PaPy_3)Ru(NO)]^{2+}$ for the transport of NO to myoglobin and cytochrome oxidase are described by Mascharak group.[82]

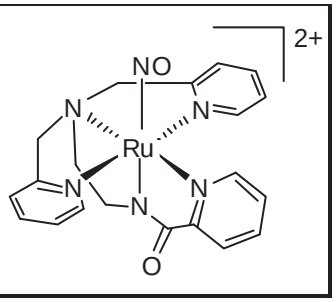

Figure 1.16. Complex structure $[(PaPy_3)Ru(NO)]^{2+}$

Many works have recently been aimed at finding ways to sensitize ruthenium-nitrosyl complexes in the visible and infrared domains of light. For the purpose of the bathochromic shift of the transition $d_\pi(Ru) - \pi^*(NO)$, Mascharak group attempted to attach the ruthenium-nitrosyl complex to a molecule of a dye that absorbs light in the visible domain. Resorufin (Resf) and fluorescein derivatives (FlEt) were used as such molecules (Figure 1.17).

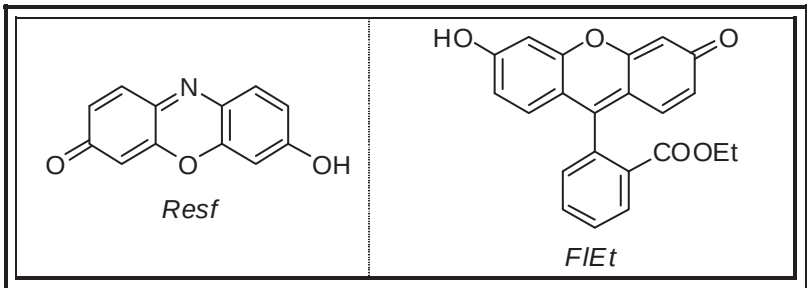

Figure 1.17. Dyes resorufin Resf (left) and fluorescein ethyl ester *FlEt* (right)

Using the ruthenium complex containing the dimethyl derivative H_2bpb (Figure 1.14) as the basic platform, the researchers replaced the chlorine atom in the *trans*-position to the nitrosyl group with the molecule of a dye (Dye) that was bound to ruthenium atom through a covalent bond with hydroxyl group:[83,84]

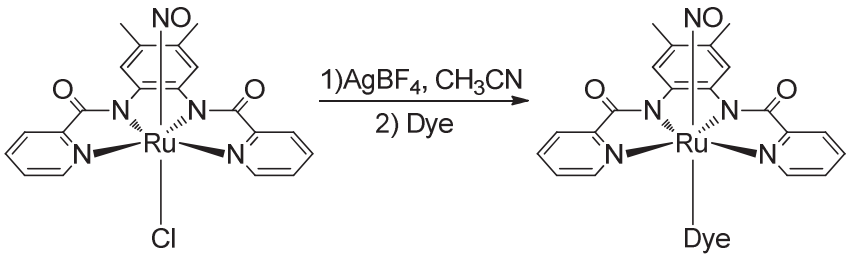

The absorption maxima (λ_{max}) of the lowest energy transitions in the electronic spectra of the obtained complexes [Ru(Resf)(Me_2bpb)NO] (abbreviated 1-Resf) and [Ru(FlEt)(Me_2bpb)NO] (abbreviated 1-FlEt) lie in visible part of the spectrum (Figure 1.18). Compared to the starting complex with chloro-ligand [RuCl(Me_2bpb)NO] (abbreviated as 1-Cl), for which λ_{max} lies in the near-UV region

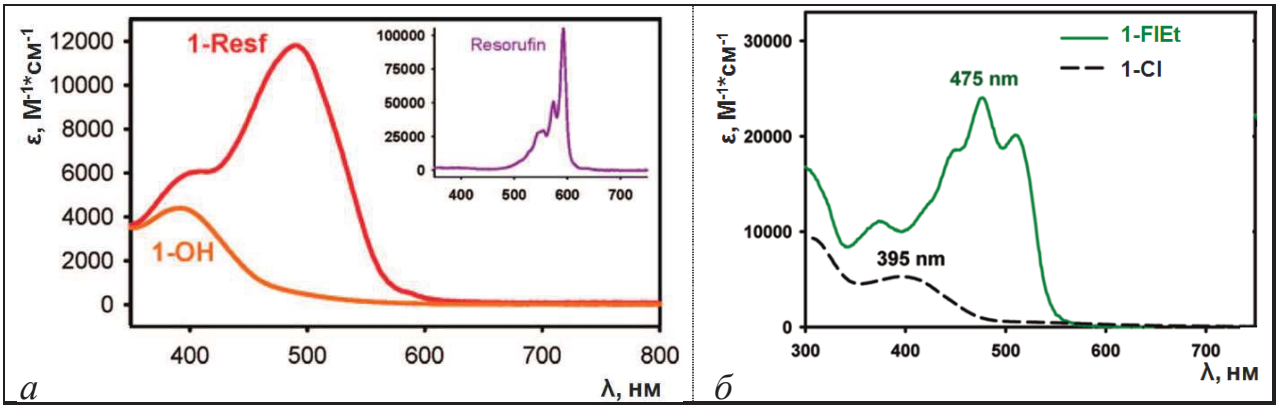

Fig. 1.18 Electronic spectra of ruthenium nitrosyl complexes with dyes: a) comparison of the free resorufin spectrum with the spectrum of the 1-Resf complex and the 1-OH complex; 2) comparison of the spectrum of the 1-FlEt complex with the spectrum of the 1-Cl complex

(390-400 nm), for compounds 1-Resf and 1-FlEt these values are 500 nm and 475 nm respectively. At the same time, the alteration of the donor atom exclusively – substitution of chlorine atom with the oxygen atom (in the comlex [Ru(OH)(Me_2bpb)NO] (abbreviated 1-OH)) - does not significantly affect the shift of λ_{max}.[83]

The release of NO from these compounds under irradiation showed not only their ability to be effectively sensitized in the visible region, but also revealed the unique ability of these complexes. The presence of molecules capable of luminescence in their structure, provided a tool for the NO-release control. Interestingly, the compound 1-Resf is fluorescent, in contrast to 1-FlEt.[83,84]

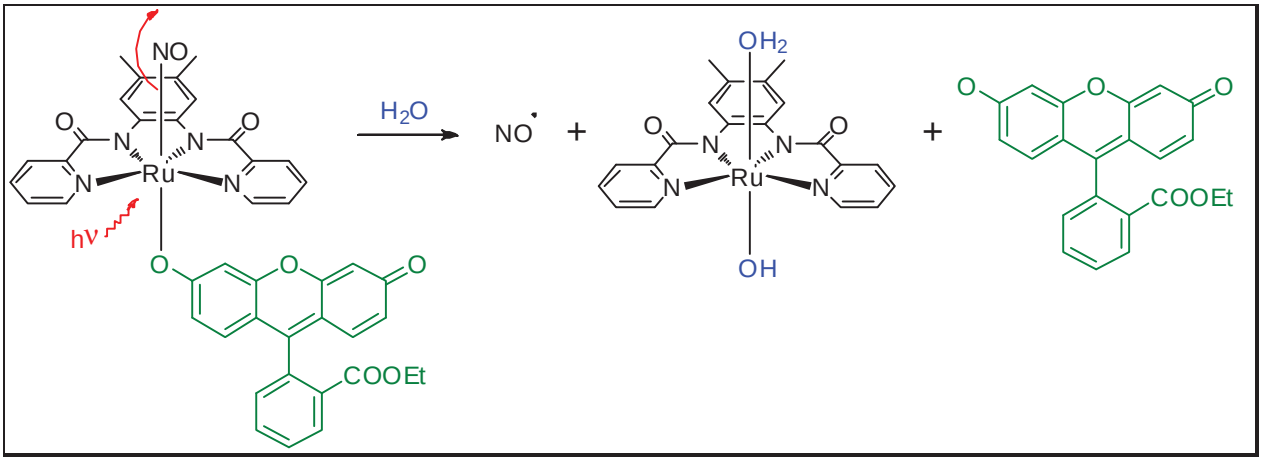

Fig. 1.19 The process for the release of nitric oxide with the simultaneous liberation of the dye molecule from 1-FlEt

But the situation changes to the opposite at the moment of NO-release. The photoproduct produced from compound 1-Resf does not show fluorescence, that caused by the presence of a paramagnetic d^5-Ru(III)-center.[84] In the case of 1-FlEt irradiation of the compound is accompanied with a liberation of a nitric oxide molecule and a molecule of a dye (Fig. 1.19), that restores its intense emission in a free state. These studies indicate the possibility of shifting the absorption band of ruthenium-nitrosyl complexes into visible region and exemplify the release of NO when these compounds are irradiated with waves of this domain.

Another widely used ligand for synthesis of ruthenium-nitrosyl complexes is terpyridine. As with other polypyridyl complexes, ruthenium compounds with terpyridine exhibit high stability. In addition to the chelate effect of terpyridine, the high stability of these complexes is supported by a significant d-π* backdonating interaction.[85] An intensive study of ruthenium-nitrosyl complexes with these ligands was performed by Roberto Santana da Silva and Isabelle Malfant groups.

The use of terpyridine ligand in ruthenium nitrosyl complexes leaves two of the coordinating positions in the polyhedra of ruthenium free. Consequently, these positions may be occupied by either two monodentate ligands (amines, ammonia, halogens, etc.) or bidentate ligand.

In the year 2014 the group of I. Malfant obtained ruthenium-nitrosyl complexes with terpyridine ligand and two chloro-ligands (Figure 1.20).[86]

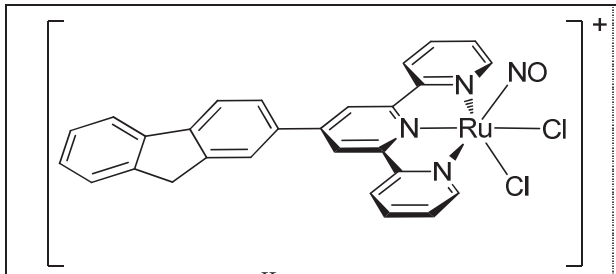

cis-(Cl,Cl)-[Ru^{II}(FT)(Cl)$_2$(NO)]$^+$ *trans-(Cl,Cl)-[Ru^{II}(FT)(Cl)$_2$(NO)]$^+$*

Figure 1.20. The structure of complexes with terpyridine ligand and two monodentate chloro-ligands

Synthesis was carried out in full accordance with the method described by Nagao et al. in which $K_2[RuCl_5(NO)]$ reacts with an unsubstituted terpyridine.[87] However, unlike in the published method the use of terpyridine with the fluorenyl substituent (9*H*-fluorenyl) in the 4th position results in the formation of a mixture of compounds. In addition to the two isomers shown in Figure 1.20, the so-called homoleptic $[Ru(FT)_2]^{2+}$ complex (Figure 1.21) is formed as well.[86]

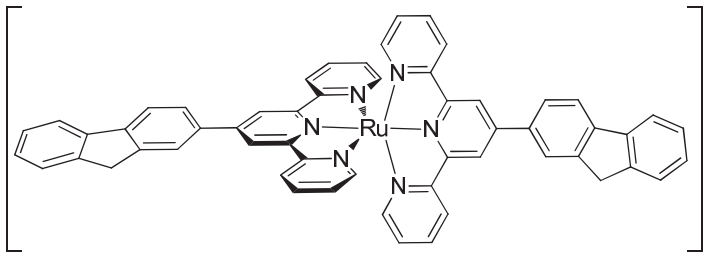

Figure 1.21. The structure of homoleptic complex $[Ru(FT)_2]^{2+}$

The separation of these complexes was carried out using the method of high-performance liquid reverse-phase chromatography (HPLC). The frequency of the NO vibrations in IR spectroscopy was proposed for the distinction of isomers: for the *trans*-isomer (the nitrosyl moiety is in the *trans*-position to the pyridine ring of terpyridine) this value is 1901 cm^{-1}, and for the *cis*-isomer (nitrosyl in *trans*-position to chloro-ligand) – 1894 cm^{-1}.[86]

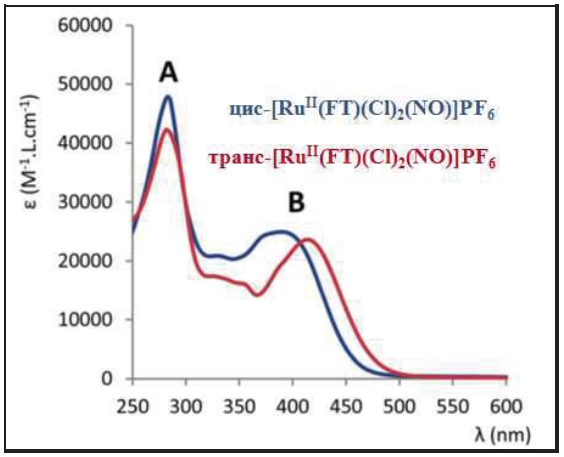

Figure 1.22. Electronic absorption spectra of *cis*- and *trans*-[Ru^{II}(FT)$(Cl)_2$(NO)](PF_6)

The electronic spectra of the two complexes are similar, although for the *trans*-isomer (λ_{max} = 414 nm), the lowest transition is shifted by an energy of 0.2 eV into the visible region (for the *cis*-isomer λ_{max} = 389 nm). Quantum-chemical calculations with the use of the density functional theory (DFT) show that the electronic transition responsible for the appearance of the band B (Figure 1.22) is mainly the transition between the highest occupied molecular orbital (HOMO) and the lowest unoccupied molecular orbital (LUMO) (Fig. 1.23). In both complexes, HOMO is a binding orbital located on an electron-donating 9,9-hexyl-9*H*-fluorenyl moiety. At the same time the transition from HOMO to LUMO is essentially the transfer of the electronic density from the terpyridine ligand to the antibonding $d_{Ru} - \pi^*$(NO) bond.

Taking into account that the electronic transition corresponding to the band B leads to a weakening of Ru-N(NO) bond the study of the release of nitric oxide from both isomers was carried out under the irradiation with λ = 405 nm – the wavelength at which both complexes show a significant absorption coefficient. Quantum yields for *cis*-[Ru^{II}(FT)$(Cl)_2$(NO)](PF_6) and *trans*-[Ru^{II}(FT)$(Cl)_2$(NO)](PF_6) are 0.106 and 0.307 respectively.[86] Despite the fact that these compounds show good photochemical characteristics, the authors emphasize that their practical use is limited because of the need to irradiate the complexes with electromagnetic irradiation

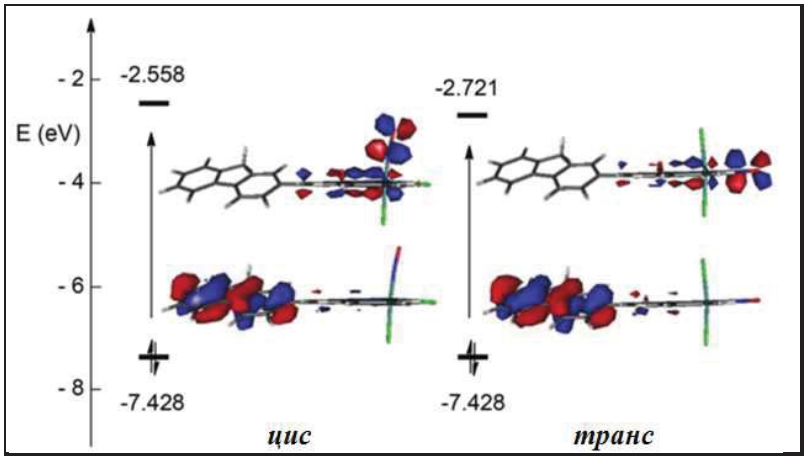

Fig. 1.23 HOMO and LUMO for *cis*- and *trans*-[Ru^{II}(FT)$(Cl)_2$(NO)]$^+$, calculated with DFT

that is poorly permeable into biological objects.

The confirmation of nitrogen monoxide release in this work was done with the use of indirect method – the Griess test, which consists in the photometric determination of pink diazo-dye (λ_{max} = 548 nm), which is formed as a result of the reaction of nitrite anions (formed as a result of oxidation of NO in solution) with sulfanilic acid.[88] Another, more reliable direct method for the determination of nitric oxide is the use of iron-N-methyl-D-glucamine dithiocarbamate ($Fe(MGD)_2$) as a specific spin trap for nitric oxide with further determination of the $Fe(MGD)_2$-NO complex by EPR spectroscopy.[89]

As an example of terpyridine ruthenium-nitrosyl complexes, the coordination sphere of which is complemented with the bidentate ligand, we can also cite the compounds synthesized by Liu's group.

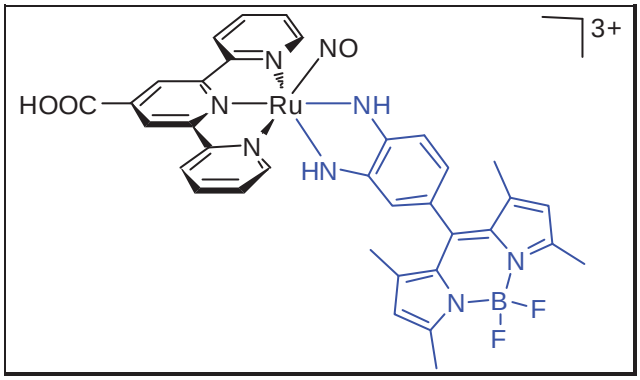

Figure 1.24. Complex cation $[Ru(tpy^{COOH})(DAMBO)NO](PF_6)_3$

In order to integrate the ruthenium-nitrosyl complex into nanoparticles for subsequent NO targeted delivery into biological objects, the terpyridine ligand has been functionalized with the carboxyl group, which will enable covalent binding of the NO donor to "nano-carriers", in particular TiO_2. The photosensitization of the obtained compound in the visible region of the spectrum was done by attachment of the DAMBO dye (8-(3,4-diaminophenyl)-4,4-difluoro-1,3,5,7-tetramethyl-4-boron-3*a*, 4*a*-diaza-s-indacene) directly to the metal center. The resulting complex $[Ru(tpy^{COOH})(DAMBO)NO](PF_6)_3$ integrated on the TiO_2 surface was stable in the absence of light and was capable of releasing nitric oxide when irradiated.[48,90] An interesting feature of this complex is the ability to generate both NO and singlet oxygen $^1O_2$ when irradiated with visible light; this is the first example of compounds capable of releasing both particles that play a key role in photodynamic therapy.[90] Thus, the use of terpyridine for the strong binding of

ruthenium ion may be promising in the design of ruthenium-nitrosyl complexes as NO donors.

1.4.4 Mechanism of nitric oxide release from ruthenium-nitrosyl complexes: theoretical studies

A detailed theoretical study of the release of NO from ruthenium-nitrosyl polypyridyl complexes was carried out by Juan Sanz Garcia.[91]

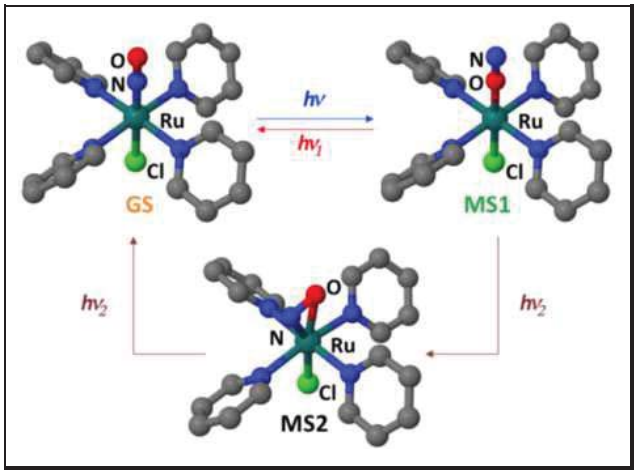

Figure 1.25. Three main isomeric forms of $[RuCl(py)_4NO]^{2+}$ - GS, MS1 та MS2.

The theory developed by J. Garcia and co-authors shows that the process of NO-release is not one-step mechanism, but rather occurs in several steps, which include the transition between several geometric forms conjugated with different electronic states of cationic ruthenium-nitrosyl complexes. The main (stationary) forms in this process are three isomeric structures of the ruthenium-nitrosyl complexes: the ground state, GS (*ground state*), metastable state-1, MS1 (*metastable state*), and metastable state-2, MS2 (Figure 1.25). In essence, they are linkage isomers: GS -ruthenium nitrosyl complex, MS1 - ruthenium isonitrosyl complex, MS2 - complex containing bridged NO ligand [Ru(η^2-NO)]. The possibility of obtaining of all three isomers was shown for the compound $[RuCl(py)_4NO]^{2+}$ (Figure 1.25).

In the solid state, the transition from one of them to another occurs when the complex is irradiated by electromagnetic waves of different lengths (Fig.1.26).[92] According to the results of theoretical studies, the release of nitric oxide from ruthenium-nitrosyl complexes is preceded by isomerization of the latter.

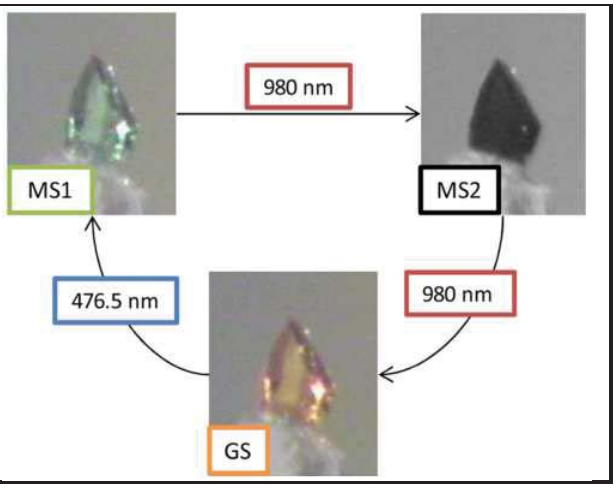

Figure 1.26. Color change of the $[RuCl(py)_4NO](PF_6)_2$ crystal under irradiation by 476.5 and 980 nm waves at 180 K.

Therefore, a detailed study of the processes underlying the isomerization of the {Ru-NO} complexes can reveal the key structural and electronic features of the ligands that affect the process of NO-release.

All the processes occurring during the isomerization of the ruthenium-nitrosyl complex from GS to MS1 are schematically depicted in the scheme 1.10. The principal feature of this sequence of transformations is the presence of two cases of photon absorption - process "a" and process "g". The initial absorption of one photon (process a) excites a molecule being in the ground state. Further intersystem crossing leads to the population of the triplet excited state T_n (process b), which through internal conversion, transforms into the main ^{3}GS triplet state (process c). The transition to the main electronic state of the isomer [Ru(η^2-NO)] - MS2 can pass by two ways. Given that the Ru-NO angle considerably changes with this transition (from 134.2° in ^{3}GS to 84.7° at MS2), the transition from the lower vibrational level to ^{3}GS requires

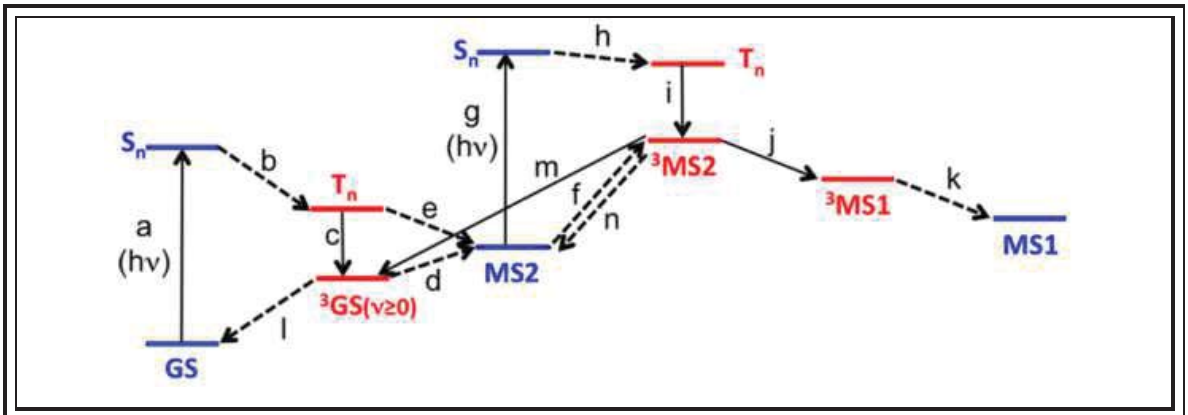

Scheme 1.10 Schematic representation of all electronic transitions involved in the GS-MS1 isomerization process according to Garcia's theory. Transitions between states with the same multiplicity are represented by solid arrows, between different - dotted. Singlet states are depicted in blue, triplets - in red.

an overcoming of the energy barrier of 0.67 eV, which in principle is the limit of the possible vibrational activation of the molecule at ^{3}GS-level (process d); an alternative to this transition can be a direct intersystem crossing from the excited triplet state T_n (transition e). Further isomerization requires a transition to the triplet state ^{3}MS2, from which, through j and k transitions that do not require additional activation, the molecule could isomerize to the isonitrosyl complex (MS1). The presence of a deep potential hole (an energy barrier of 0.73 eV) in the state MS2 makes it impossible to switch to a triplet state by thermal activation. Therefore, the most probable mechanism for overcoming such a barrier is photoexcitation.

The absorption of a photon transfers the molecule into a singlet excited state (process g), from which the ^{3}MS2 triplet level population occurs as a result of intersystem crossing (process h) and subsequent internal conversion (process i).[93]

It should be noted that the magnitudes of the energies corresponding to the phototransitions a and g are very close. Calculated electronic spectra using a time-dependent density function theory (TDDFT) for all three isomers are shown in Figure 1.27.

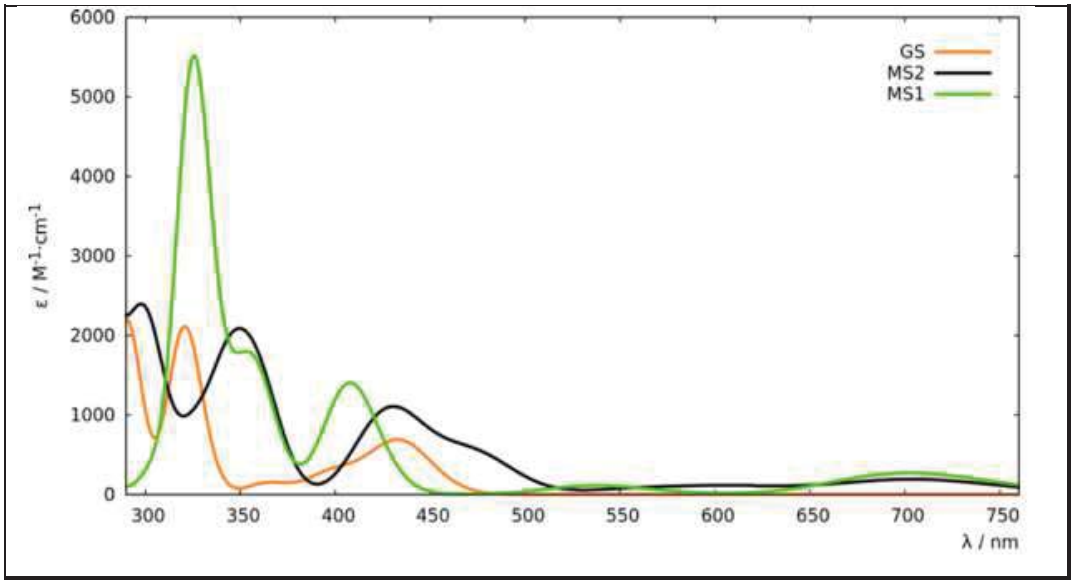

Fig. 1.27 Electronic spectra of all three GS, MS1 and MS2 isomers calculated using TDDFT

As can be seen from the compounds spectra, electromagnetic irradiation with a 473 nm wavelength is absorbed by both GS and MS2 isomer. In this case, the

isonitrosile complex (MS1) is not excited by the light of such energy ($\varepsilon \approx 0$). From experimental studies it is known that isomerization of the nitrosyl complex $[RuCl(NO)(py)_4]^{2+}$ occurs when it is irradiated with wavelength $\lambda = 473$ nm. In view of the isomerization mechanism, we can say that the use of light for this process leads to the absorption of two photons instead of only one that eventually leads to the population of an unstable ^{3}MS, from which the molecule transforms into isonitrosyl complex. At the same time the photons of this energy are not absorbed by the MS1 complex. However, under irradiation with the red light the resulting isonitrosyl complex isomerizes into the starting ruthenium complex, which does not absorb light of this wavelength domain.

According to the study, reaching of the ^{3}MS2 level is important not only for the isomerization process, but also for the release of nitric oxide from the complex. In previous works (Bitterwolf et al.[94], Woike et al.[95]) attention has already been paid to the importance of linkage isomers in the process of NO-release from ruthenium-nitrosyl complexes.

An attempt to explain the inclinations of the ruthenium-nitrosylcomplexes either to isomerization or the release of NO based on the structure of complexes was made in the work of García et al.[91] It is noteworthy that the proposed mechanism and the explanation for different values of quantum yield for NO-release is consistent with experimental data obtained in various scientific groups. When the compound transit to the ^{3}MS2 triplet state its further transformation can take place in two ways: isomerization with the formation of the MS1-isomer or the release of NO. The competition between them is determined by the kinetics of both processes or rather by the difference between the energy of the dissociation D_{e2} and the energy barrier that must be overcome for isomerization (Figure 1.11).

Thus, when $D_{e2} <^3$B2, the release of nitric oxide occurs easier, otherwise the complexes are more prone to isomerization.

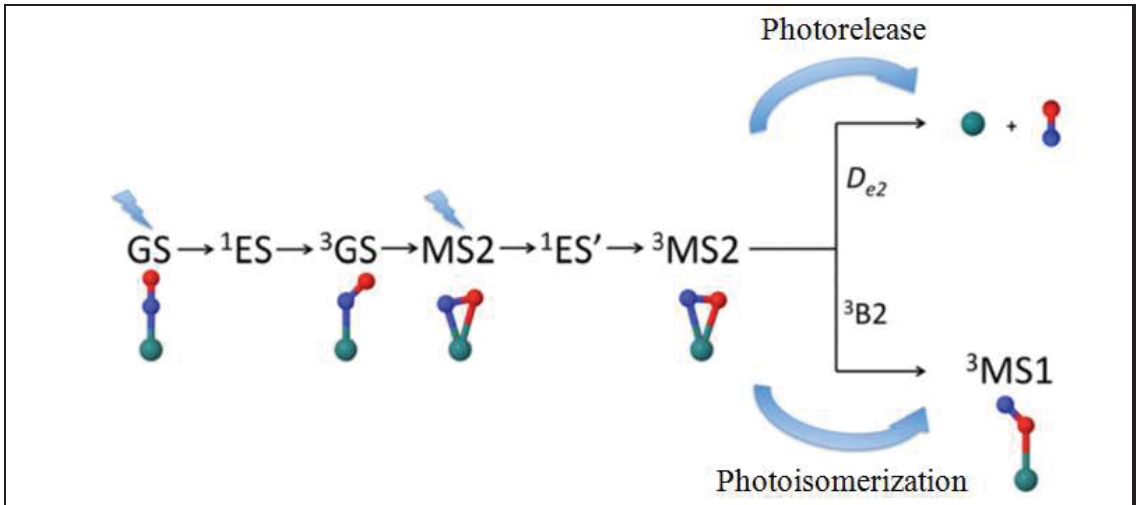

Scheme 1.11 Competition between the release of nitric oxide and isomerization in ruthenium-nitrosyl complexes.

In summary, we can say that, like the process of isomerization, the process of NO-release from ruthenium-nitrosyl complexes occurs as a result of absorption of two photons. In this case, as a result of several electronic transitions, the molecule transits to a triplet state, and then, depending on the relation between the dissociation energy and the isomerization energy, both the NO-release and the isomerization with the formation of the isonitrosyl complex can take place.

1.5 Two-photon absorption as a method of photosensitization of compounds within the therapeutic window

The two-photon absorption phenomenon was predicted by Maria Göppert-Mayer[96] in 1931, although it was practically observed for the first time only 30 years later by Kaiser and Garrett.[97] The TPA process is the excitation of a molecule, which occurs when absorbing not one, as in the case of linear absorption, but two photons (must not be confused with the mechanism described in 1.4.4, which includes two separate steps of absorption of photons). The process of absorption of two photons occurs simultaneously, but it is still considered that the transition to a "stable" excited state is preceded by the transition to the so-called "virtual level" when molecule absorbed one of two photon (Scheme 1.12).

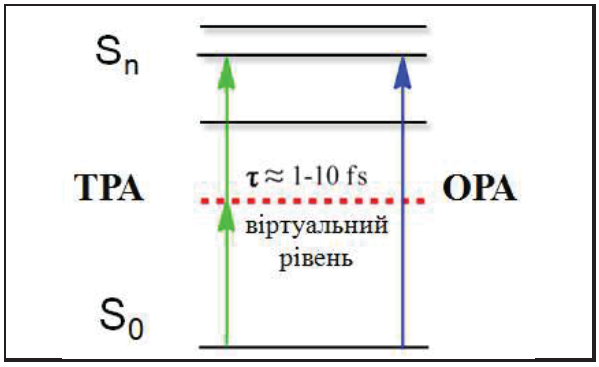

Scheme 1.12 Schematic comparison of one- (OPA) and two-photon (TPA) absorption processes .

The lifetime of this virtual state is of the order of several femtoseconds, and the very phenomenon of TPA will be possible only if the second photon is absorbed up to the moment of the reverse transition of the molecule to the ground state. And, unlike single-photon absorption, the probability of which is linearly proportional to the intensity of light, the possibility of two-photon absorption depends on the temporal and spatial availability of two photons, and quadratically depends on the intensity of the exciting radiation.[98]

Two-photon absorption (TPA) is a third ofder nonlinear optical phenomenon.[99] It is possible to describe the response of a substance on the action of light using the dependence of the macroscopic polarization P on the intensity of the electric field E:

$$P = P^{(1)} + P^{(2)} + P^{(3)} + \ldots = \varepsilon_0(\chi^{(1)}E + \chi^{(2)}E + \chi^{(3)}E + \ldots),$$

where ε_0 is the dielectric constant in a vacuum, $P^{(n)}$ is the polarization of the n^{th} order, $\chi^{(n)}$ is the optical susceptibility of the n^{th} order; while $\chi^{(1)}$ describes the linear properties of the materials, $\chi^{(2)}$ is an important parameter for the phenomena of the second harmonic generation, sum-frequency generation etc. The third-order susceptibility $\chi^{(3)}$ is associated with such phenomena as generation of the third harmonic, nonlinear refraction, two-photon absorption and others.

When light passes through substances capable of one- (OPA) and two-photon absorption (TPA), its intensity I(z) change as follows:

$$\frac{dI(z)}{dz} = -\alpha I(z) - \beta I^2(z) - \ldots,$$

where α and β are the coefficients of one- and two-photon absorption of the medium, respectively. The index z indicates the propagation of light along the conventional axis z in the medium. In the case when the substance does not exhibit linear absorption of the light, and only two-photon absorption is present, the expression simplifies to the next form:[100]

$$\frac{dI(z)}{dz} = -\beta I^2(z)$$

The physical interpretation of this expression is that the magnitude of the two-photon absorption is proportional to the square of the intensity of light. The solution of this differential equation is:

$$I(z,\lambda) = \frac{I_0(\lambda)}{1 + \beta(\lambda) I_0(\lambda) z}$$

In this expression, I_0 is the initial intensity of the exciting radiation, z is the thickness of the medium layer in which light propagation occurs. β(λ) is a macroscopic parameter, which depends on the concentration of molecules capable of two-photon absorption, and can be represented in the following form: [100]

$$\beta = \frac{\sigma N_A c}{\hbar \nu},$$

where c is the concentration of the photoactive substance, N_A is Avogadro number, h is Planck's constant, ν is the frequency of the light, and σ is the two-photon absorption cross-section. σ is a parameter that characterizes the intensity of the absorption of two photons by a molecule. As a unit of measure for σ it is common to use $cm^4 \cdot s$. But since the values of σ in practice vary within 10^{-51} - 10^{-46} $cm^4 \cdot s$, a special unit of measurement GM (from the name of Maria Göper-Meyer) was introduced for convenience:

$$1\ GM = 10^{-50}\ cm^4 \cdot c$$

Two-photon absorption is a modern, promising tool for *in vivo* photoactivation of biologically active substances, in particular recent researches are devoted to the design of nitric oxide donors with high TPA cross-sections.[101] The reason for such an interest in this method of activation is the benefits of the TPA. The main advantage of using the TPA approach is the possibility to activate the compounds with electromagnetic radiation in the "therapeutic window" area. Most donors of nitric oxide known today have an absorption maximum in the visible or near UV region.[48,55] Waves of such lengths are poorly permeable in the biological environment and, in the case of UV radiation, can cause significant negative effects. An effective extinction coefficient of biological tissues against the wavelength is shown in figure

1.28 in a pink color. The range of wavelengths of 700-1100 (1300) nm[102] is called "therapeutic window"; waves of this region are the most permeable in the biological environment. According to the scheme 1.12, in the case of TPA, the transition energy $S_0 \rightarrow S_n$ is divided into two photons, for example, if the excitation of a molecule in a single-photon process requires the use of a wave with $\lambda = 400$ nm, in the case of TPA the wavelength will be twice as large as 800 nm. Thus, the activation of the compound becomes possible under irradiation with electromagnetic waves of therapeutic window.

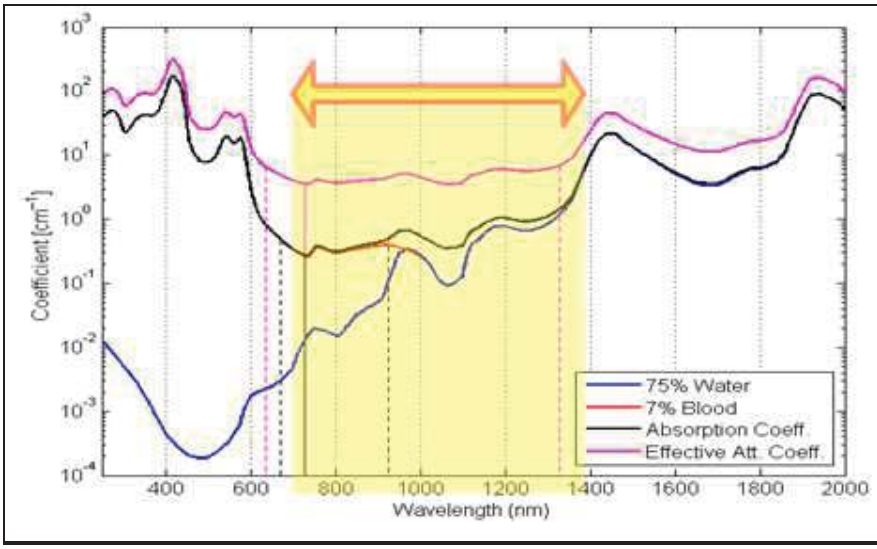

Figure 1.28. Absorption of electromagnetic irradiation by biological tissues and fluids. The area of the therapeutic window (700-1300 nm).

Another important advantage of using TPA is the accurate localization of the effect on the biological object, which is the result of the quadratic dependence of the two-photon absorption on the intensity of the applied irradiation. From figure 1.29 it is clear that in the case of TPA, the excitation of a photoactive substance takes place in a small volume around the focus of the laser radiation source – this is where the necessary "concentration" of photons is attained, and where the phenomenon of TPA becomes possible.

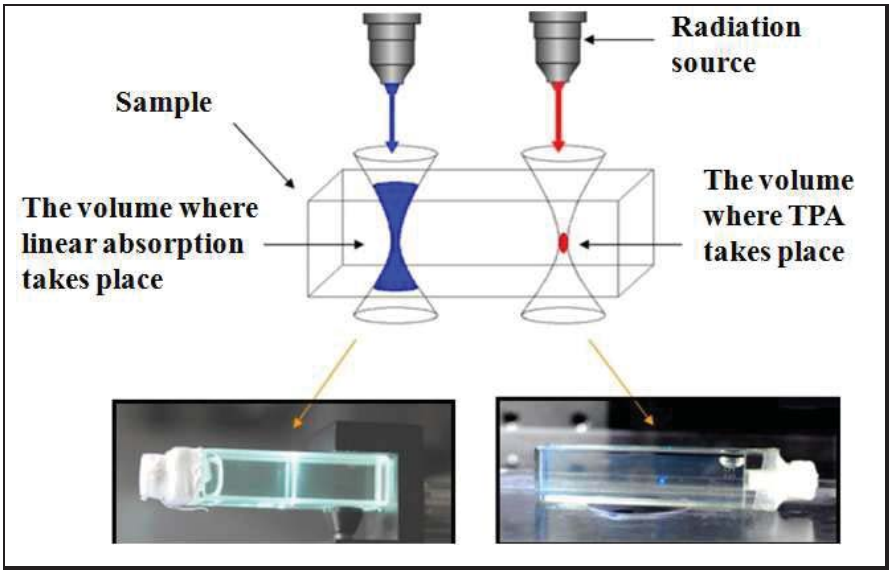

Fig. 1.29 Comparison of sample volumes in which one- and two-photon absorption take place.[103]

Many organic compounds such as polymeric and small-size molecules containing π-conjugated chains exhibit nonlinear optical properties. The highest values of the TPA cross-section (σ) to date are 10^4 GM.[104] The application of photoactive compounds for the treatment or *in vivo* imaging of objects requires the development of substances with high σ values. Two basic approaches for obtaining of such compounds are: the design of the linear and the two-dimensional structures. Increasing TPA efficiency in linear molecules (which, in particular, are studied in this work) can be achieved by forming structures D-π-A (D-donor, A-acceptor), D-π-A-π-D, A-π-D-π-A. Donor-acceptor molecule character increases the TPA due to the increased difference between the dipole moment in its ground and excited state.[104] The most common donor groups in the design of compounds with high σ are dyphenilamino-, diethyl- and dimethylaminogroups. Phenyl, fluorenyl, thiophene and other linkers often play a role of the bridges with long conjugation chain; they can form planar structures that improve the interaction of the π-systems of the molecule fragments. Also some studies indicate that the triple bond can play the role of an effective π-bridge as well.[104]

CHAPTER 2. THE REPLACEMENT OF CHLORO-LIGANDS WITH 2,2'-BIPYRIDINE IN {Ru-NO} COMPLEXES AND ITS EFFECT ON TPA OF COMPOUNDS

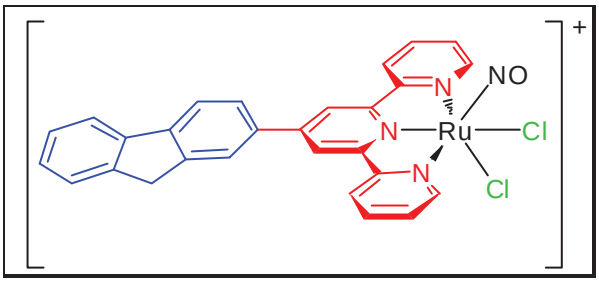

Figure 2.1. The structure of cation of *cis*-[Ru^{II}(FT)Cl_2(NO)](PF_6) (*cis1*).

The basis for the structures of compounds studied in this dissertation were the complex ions of ruthenium-nitrosyl complexes obtained by I. Malfant research group in 2014,[86] - *cis*- and *trans*-[Ru^{II}(FT)Cl_2(NO)](PF_6). These are cationic complexes that according to Enemark-Feltman notation are the complexes {RuNO}^{6}. This is evidenced by the data of NMR and IR spectroscopy. In particular, the frequency of the valence oscillations of the N-O bond in cis- and trans- isomers is 1894 cm^{-1} and 1901 cm^{-1}, respectively, which is typical for compounds with a formal charge distribution {Ru^{II}-$(NO)^+$}. The octahedral environment of the central ruthenium atom is formed by the nitrosyl moiety NO, two chlorine atoms which may be in the cis- or trans- position, and by the three nitrogen atoms of the pyridine rings of the terpyridine ligand (Figure 2.1).

Terpyridine provides high stability of the complex with ruthenium due to the formation of two five-membered chelate cycles and π-backdonation. At the same time the two positions remaining unoccupied in the coordination polyhedron (without considering nitric oxide) leave the possibility for altering the redistribution of electronic density in the complex through variation of the ligands nature there. The relative position of the three monodentate ligands (Cl, Cl, NO) has a significant effect on the photochemical behavior of the compounds. The complex cis(Cl,Cl)-[Ru^{II}(FT)Cl_2(NO)](PF_6) where the chloro-ligand is located in the *trans*-position to the nitrosyl ligand, releases nitric oxide with quantum yield of 0.31 under irradiation λ_{max} = 405 nm, whereas the quantum yield of NO-release from the *trans*-isomer, in which the nitrogen of the central pyridine ring is located in the *trans*-position to NO, is 0.11 under the same conditions.[86,105]

As in the studies of ruthenium-nitrosyl complexes with other ligands (see 1.4.3), the authors emphasize the decisive influence of the ligand in the *trans* position to NO on photochemical properties of the complex. For the sake of simplification the compound cis(Cl, Cl) – $[Ru^{II}(FT)Cl_2(NO)](PF_6)$ is designated as cis1, trans(Cl, Cl) – $[Ru^{II}(FT)Cl_2(NO)](PF_6)$ as trans1.

As noted in Chapter 1, the presence of monodentate ligands in the complexes is generally undesirable when designing drugs. The alternative proposed in this work for chloro-ligands is 2,2'-bipyridine. The choice of this ligand is justified by several factors: (i) higher stability of such complex in the biological environment due to increased thermodynamic stability of the {Ru(tpy)bpyNO} complex compared to $\{RuCl_2(tpy)NO\}$; (ii) eliminating the need for a painstaking and complex process of separating the mixture of *cis*- and *trans-isomers* when monodentate ligands are present; (iii) the potentially higher ability of the compound with 2,2'-bipyridine to participate in two-photon absorption process (TPA). The last statement needs a more detailed explanation.

First, the very presence of an additional fragment with a long chain of conjugation in the compound can lead to an increase of its ability to undergo two-photon absorption. Another argument favoring the idea of increasing the TPA cross section (σ) when introducing 2,2'-bipyridine into the complex is the results of the quantum-chemical calculations performed for these compounds, in particular the calculated angles between the mean plane of the fluorenyl fragment and the mean plane of terpyridine. According to the DFT calculations in a row of trans1-cis1-bpy1 (where bpy1 is a complex in which two chloro-ligands are replaced by a 2,2'-bipyridine molecule) the angle between the planes decreases (Table 2.1). This could be explained from the point of view that removing of two negatively charged chloro-ligands will necessarily increase the withdrawing effect of {Ru(tpy)NO} moiety. Moreover, inserting of π-accepting fragment (2,2'-bipyridine) will increase this withdrawing effect, thus the fluorene moiety will be more effectively conjugated with terpyridine fragment.

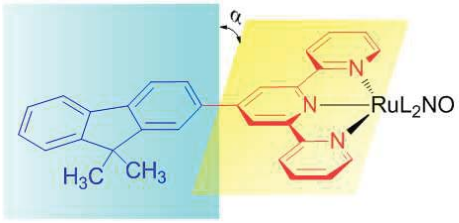

trans1'	α = 34.19°	(cos α = 0.83)
cis1'	α = 34.12°	(cos α = 0.83)
bpy1'	α = 31.99°	(cos α = 0.85)

Table 2.1. The angles between the mean planes of fluorene and terpyridine fragments, calculated from DFT-optimized structures of dimethyl-derivatives trans1', cis1' та bpy1'.

As is known, the efficiency of orbitals overlap is directly proportional to the cosine of the angle between them.[106] Although the difference in the cos α values of these three compounds is not significant (Table 2.1), the greater value of this parameter may increase the efficiency of the compound bpy1 in TPA due to an increase in the efficiency of the intramolecular charge transfer.

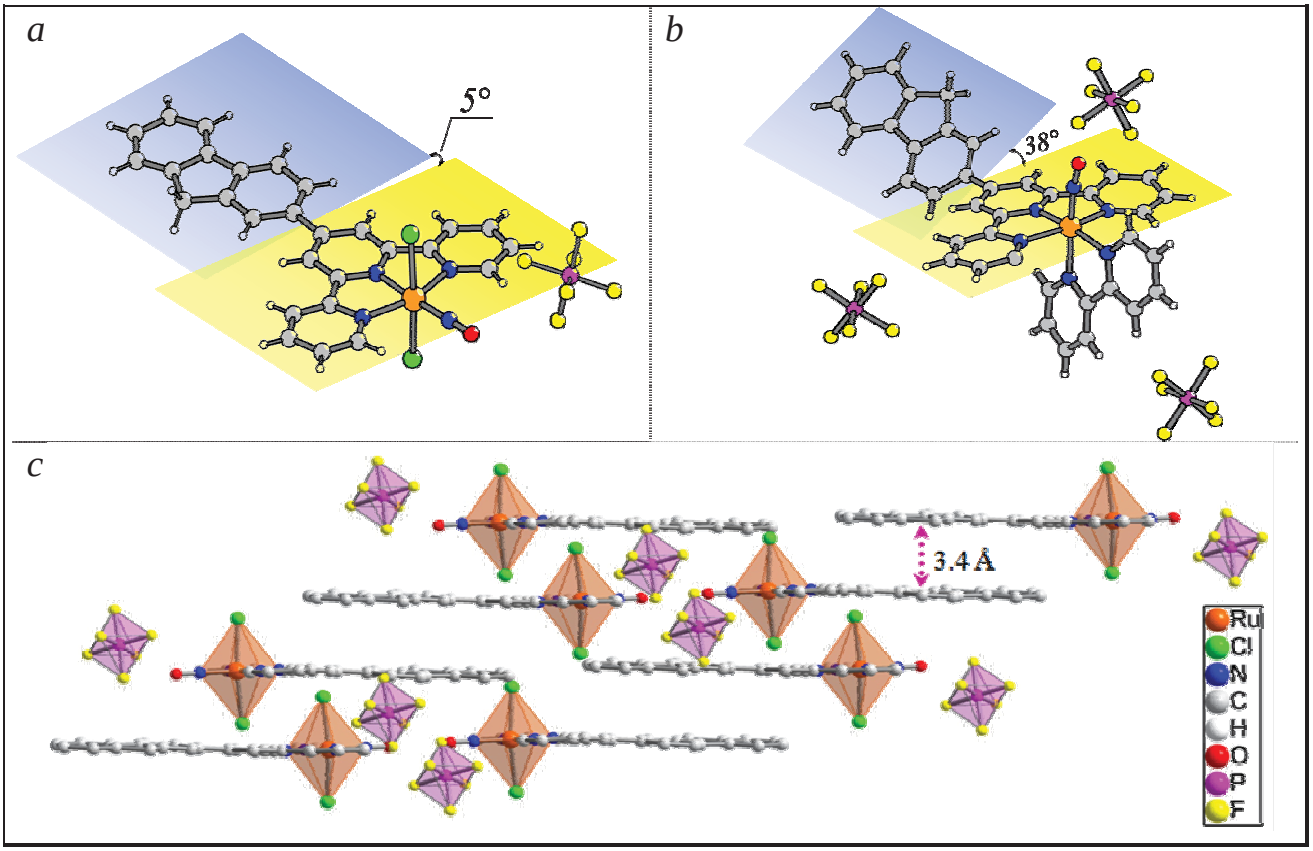

Figure 2.2. Crystal structures of trans1 (a,c) та bpy1 (b).

The compound bpy1 of the formula $[Ru(FT)(bpy)NO](PF_6)_3$ was synthesized by us, and its structure was proved by NMR, IR spectroscopy and elemental analysis. A

single crystal of the complex was also obtained and the structure was confirmed by X-ray diffraction analysis.[107]

Interestingly, there is no correlation between the values of the torsion angles fluorene-terpiridine in complexes in solutions obtained by DFT computations and torsion angles observed for compounds in the crystalline state. The torsion angles in cis1 and trans1 in the solid state are approaching 180 °, while the corresponding angle in the compound bpy1 is 38.08 ° (Figure 2.2a, b). Such a significant difference is probably due to the peculiarities of the interaction in the crystalline state of the compounds: π-π stacking becomes possible between the molecular ions of the complexes cis1 and trans1 owing to the close (≈ 3.4 Å) arrangement of the layers of the molecules (Figure 2.2c), whereas the presence of significantly larger 2,2'-bipyridyl ligand and the three bulky PF_6^--anions makes such interaction impossible in the solid state of the compound bpy1, and the geometry of the molecule is closer to that in the solution.

2.1 Comparison of electronic spectra of compounds bpy1, cis1 and trans1.

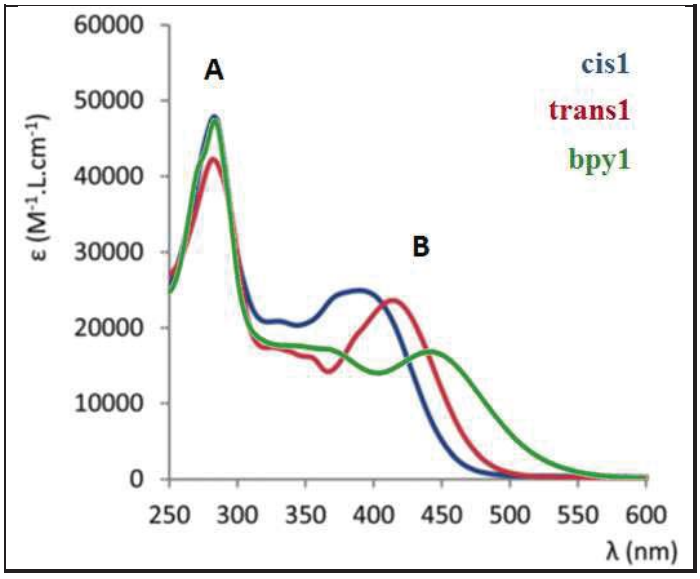

Figure 2.3. Electronic spectra of cis1, trans1 bpy1 solutions in CH_3CN.

Electronic spectra of acetonitrile solutions of all three compounds are shown in Figure 2.3. The main absorption band B is at the boundary of the visible spectral region, but for the bpy1 compound there is a bathochromic shift of this band compared to complexes containing chloro ligands. In this case, the molar extinction coefficient for the band B of the compound bpy1 is slightly lower.

The values of λ_{max} obtained theoretically using the time-dependent theory of density functional (TD-DFT) do not differ significantly from the experimental data: the experimental values of energies are shifted by less than 3000 cm^{-1}. Nevertheless,

in both cases, there is a tendency toward a bathochromic shift and a decrease in the absorption rate in a series of cis1-trans1-bpy1 (Table 2.2).

Compound	Experimental data		TD-DFT computations	
	λ_{max}	ε	λ_{max}	f
cis1	389	24950	355	0.724
trans1	414	23600	370	0.665
bpy1	440	16700	428	0.331

Table 2.2. Comparison of experimental and theoretical parameters of band B in electronic spectra of compounds

A detailed analysis of the electron excitations responsible for the appearance of the band B in the spectra shows that for all three compounds, the most intense transitions are mostly the HOMO-LUMO transitions, with some contribution of HOMO-LUMO + 2 excitation. HOMO concentrates mainly on the fluorenyl moiety that is a donor substituent in the complexes, while the main contribution to the LUMO makes ruthenium nitrosyl fragment in which the interaction d_{Ru}-π*(NO) has an antibonding character (Figure 2.4).

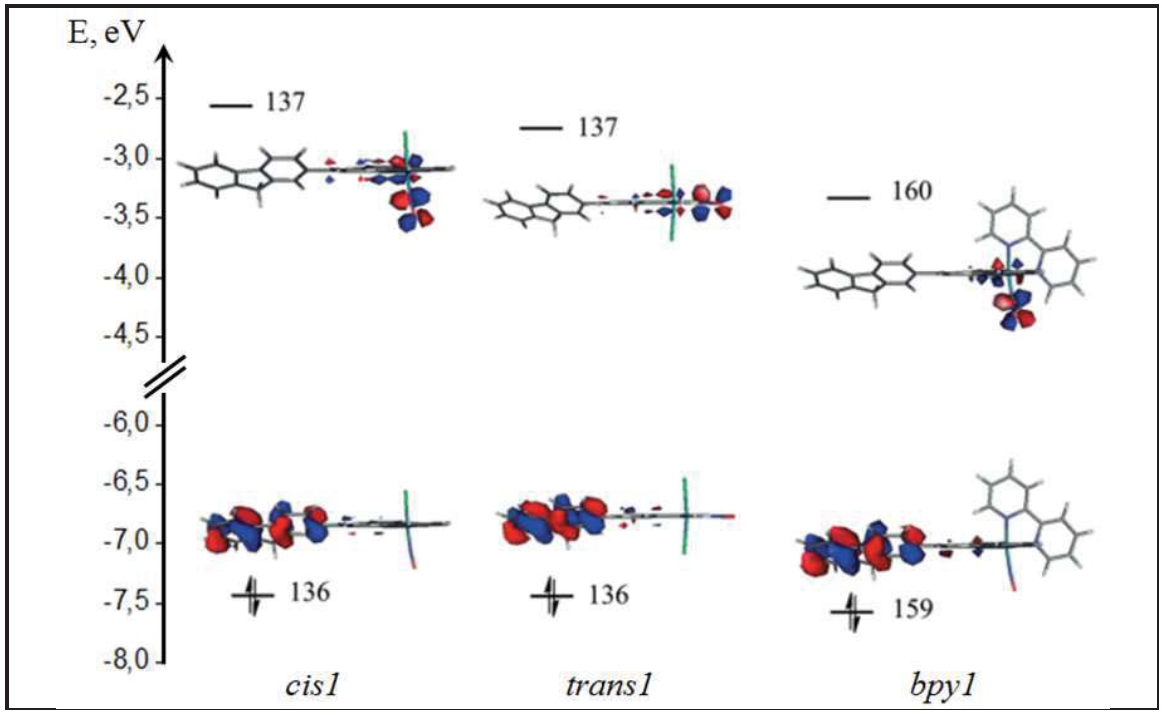

Figure 2.4. HOMO(136 for cis1 and trans1, 159 for bpy1) and LUMO (137 for cis1 and trans1, 160 for bpy1) visualization for cis1, trans1, bpy1.

Expectedly, the energy of these transitions decreases in a row cis1-trans1-bpy1, which is antibate to the change of λ_{max} in experimental UV-visible spectra of compounds. A more detailed description of electronic transitions with the electron density transfer toward {Ru-NO} fragment calculated by TD-DFT methods is presented in Table 2.3.

Compound	transition	λ_{max}	f	$\Delta\mu$	Main excitations contributions
cis1	$g_0 \rightarrow e_6$	355	0.724	18.96	$\chi_{136\rightarrow137}$(50.8 %) + $\chi_{136\rightarrow139}$ (19.7 %)
trans1	$g_0 \rightarrow e_6$	370	0.665	22.77	$\chi_{136\rightarrow137}$(69.2 %) + $\chi_{136\rightarrow139}$ (10.8 %)
bpy1	$g_0 \rightarrow e_1$	428	0.331	30.07	$\chi_{159\rightarrow160}$(80.6 %) + $\chi_{159\rightarrow162}$ (4.8 %)

Table 2.3. TD-DFT-computed parameters of electron transitions with electron charge transfer onto {Ru-NO}. (Orbitals 136 are HOMO, orbitals 137 – LUMO for compounds cis1 and trans1; orbital 159 is HOMO, orbital 160 – LUMO for bpy1. g_0 – ground state, e_n – n^{th} excited state.)

Neither of the terpiridine {Ru-NO} complexes obtained in this work nor of the similar complexes obtained in the group of I. Malfant exhibits luminescence. None of coordination compounds obtained at intermediate stages of the synthesis of final {Ru-NO} complexes exhibits luminescence either. Moreover, as noted in chapter 1, the introduction of typical fluorescent dyes in the nitrosyl complexes completely quenches the fluorescence of the first ones, or at least sharply decreases its intensity as in the case of complexes with resorufin and fluorescein derivatives (paragraph 1.4.3).[83,84]

An explanation for such a phenomenon can be found in the structure of the energy levels of polypyridyl ruthenium complexes. Let's consider the main transitions that occur in the complex upon its excitation using as an example the substance $[RuCl(py)_4NO]^{2+}$ investigated theoretically by J. Garcia.[108] The absorption of a certain energy photon excites the compound to one of the excited singlet energy levels, which, undergoing the internal conversion, passes to the lowest excited level S_1 (Figure 2.5). Formally the process boils down to the transition $S_0 \rightarrow S_1$. For a molecular ion $[RuCl(py)_4NO]^{2+}$ this transition corresponds, in fact, to the electron

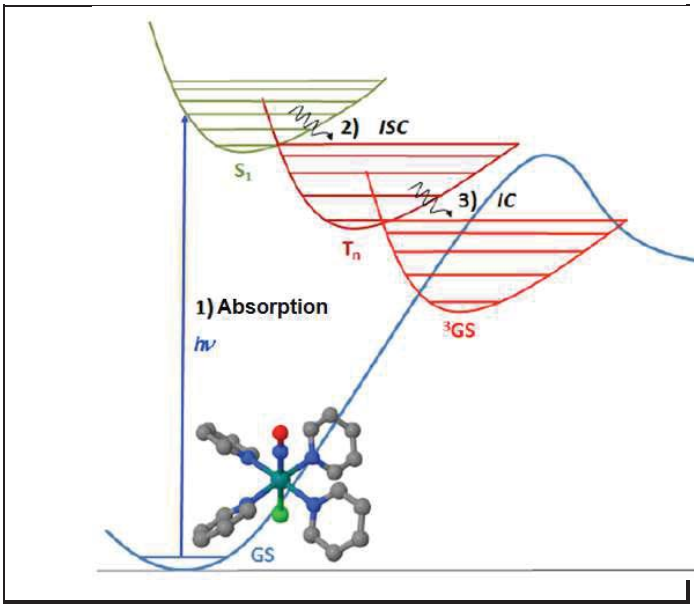

Figure 2.5. Some electron transitions in complex $[RuCl(py)_4NO]^{2+}$ happening when its photoactivation takes place.

transition from the Ru(d_{xy}) orbital to an antibonding Ru(dπ)NO(π*) orbital. After absorption of the photon, an ultra-fast intersystem crossing (ISC) takes place

and subsequent internal conversion (IC) results in the population of a triplet ^{3}GS state. The presence of a massive ruthenium atom in the complex furthers the rapid ISC from the state S_1 to T_n, so the fluorescence from the state S1 becomes impossible. The phosphorescence from ^{3}GS does not occur due to the fast "barrier-free" ISC between the ^{3}GS and GS states. Another transition from the ^{3}GS level may lead to the MS2 population which can finally result in nitrosyl-isonitrosyl isomerization or release of nitric oxide. This case was discussed in paragraph 1.4.4. In the case of ruthenium-nitrosyl complexes with a terpyridine ligand containing a fluorenyl substituent, such as cis1, trans1 or bpy1, the electron transition of a lowest energy corresponds to the transfer of electron density from a donating fluorenyl moiety to LUMO located at a strongly withdrawing ruthenium-nitrosyl group. Thus, the electron density is shifted from the potentially fluorescent fluorenyl moiety: the population of the lower-energy triplet state with an electron localized on the Ru-NO fragment occurs very rapidly and the fluorescence becomes impossible.[109]

2.2 Study of the release of nitric oxide from the complex bpy1.

As noted above, a study of the release of nitric oxide from the compounds cis1 and trans1 published by the research group of I. Malfant revealed quite good quantum yields for these complexes,[86] which are of the same order with those of the terpyridine complexes with similar structure obtained in the group of da Silva.[110]

The release of nitric oxide is followed by the formation of a solvent-bound ruthenium(III) photoproduct, according to the following equation:

$$(L)Ru^{II}\text{-}NO + solvent \xrightarrow{h\nu} (L)Ru^{III} - solvent + NO\cdot$$

The presence of a photoproduct containing a paramagnetic ruthenium atom in the oxidation state Ru^{+3} is confirmed by EPR spectroscopy and voltammetric methods.[86] An interesting fact is that the photoproduct formed by the photolysis of trans1 is also formed when compound cis1 is irradiated that was confirmed by the X-ray diffraction analysis of the obtained single crystals of photoproducts. [101] In both reactions trans(Cl,Cl)-$[Ru^{III}(FT)Cl_2(CH_3CN)]^+$ is formed. The structure is similar to the trans1 compound, in which the nitrosyl ligand is replaced by a molecule of acetonitrile.

The cis isomer cis1 shows better quantum yield of photorelease of nitrogen monoxide, which is 0.31, while for trans isomer this value is approximately 3 times

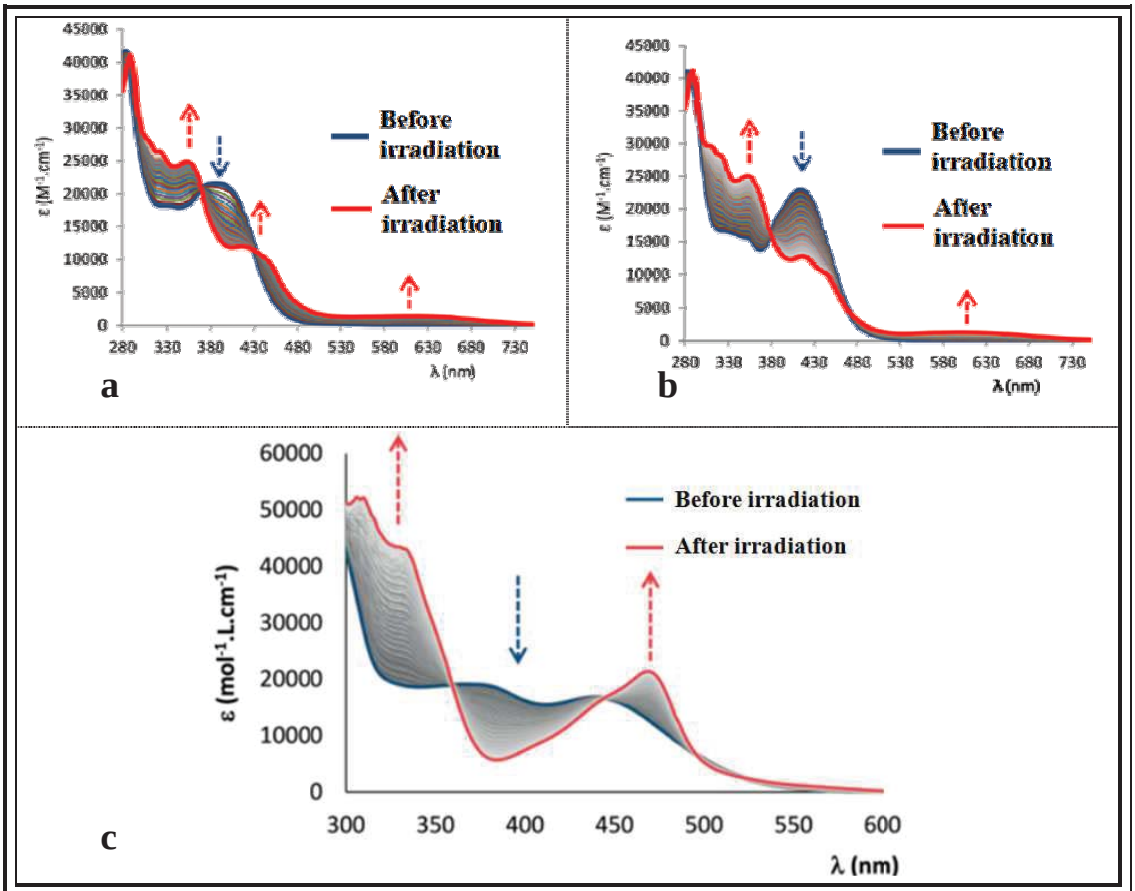

Figure 2.6. Changes in UV-vis spectra of cis1, trans1 and bpy1 acetonitrile solutions during irradiation with electromagnetic waves with λ_{max} = 405 nm.

lower – 0.11. The compound bpy1 shows a slightly reduced quantum yield compared to trans1 - 0.06. The changes in electronic spectra of all three compounds solutions in CH_3CN during irradiation are depicted in figure 2.6.

It is interesting that the quantum yields for trans1 and bpy1 are similar to each other and at the same time differ significantly from the value of the quantum yield for the compound cis1, although formally, in terms of the structure of compounds, bpy1 is closer to cis1. The values of quantum yields of NO-release are dependent on the nature of the ligand in the *trans*-position to the nitrosyl group: the presence of a pyridyl ring *trans* to NO instead of a chloro-ligand reduces the quantum yield of nitric oxide photorelease.[111]

2.3 Determination of the oxidation state of ruthenium in photoproduct through the analysis of its electronic spectrum.

A characteristic feature of UV-visible spectra of photoproducts solutions formed after irradiation of cis1 and trans1 compounds is the presence of a wide absorption band in the region of 530-680 nm (Figure 2.6 a, b). It is important to notice that such a band is absent in the spectrum of the photoproduct solution formed as a result of irradiation of the bpy1 complex. Similar electronic transitions responsible for the appearance of this band are absent in the initial complexes, as evidenced by the absence of any significant absorption in their spectra in the region $\lambda > 500$ nm. The reason for the appearance of this band could be the transition with the electron density transfer to the SOMO that appears due to the formation of the paramagnetic complex Ru^{III}. To confirm this theory, we carried out TD-DFT calculations for the photoproduct *trans*(Cl, Cl)- $[Ru^{III}(FT)Cl_2(CH_3CN)]^+$. The spectrum calculated with the use of a hybrid functional taking into account the long-range correlation (long-range corrected) CAM-B3LYP (Figure 2.7) was the closest to the experimentally obtained UV-visible spectrum of the compound. The lowest energy transition which causes the appearance of a band in the UV-visible spectrum is, according to calculations, a transition with energy of 2.41 eV. The difference in energy with a

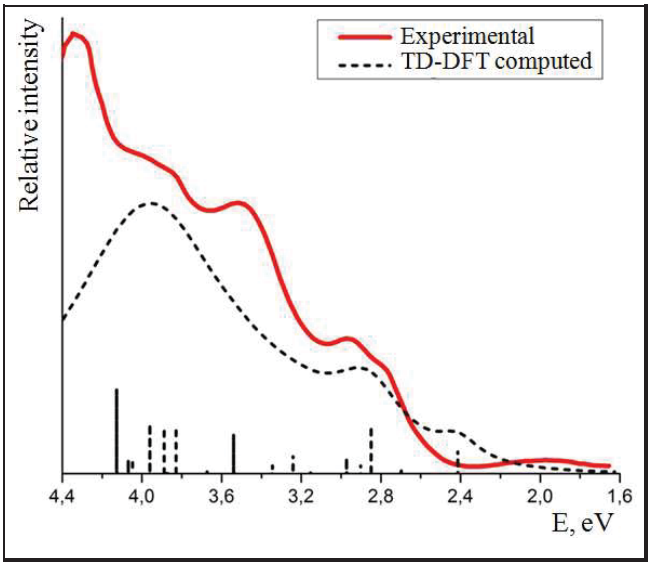

Figure 2.7. Experimental and DFT-computed spectra of photoproduct $[Ru^{III}(FT)Cl_2(CH_3CN)]^+$.

similar absorption band in the experimental spectrum (≈2 eV) is 0.4 eV. This is an acceptable deviation, but rather high.

The analysis of the orbitals involved in this electron transition shows that it occurs exclusively within the fluorenyl moiety, and represents the transfer of the electron density to the SOMO (Figure 2.8).

The spectra calculated using other functionalities, in particular B3LYP, PBE0, B3PW91 etc., exhibit worse correlation with the experimentally obtained electronic spectrum. However, the lowest energy transition computed with B3LYP functional has the energy of 2.17 eV, and the difference with the corresponding band of the experimental spectrum is only 0.17 eV. But unlike the transition at 2.41 eV, obtained using CAM-B3LYP, the main contribution to this transition is made by the electron density transfer excitation from the d-orbitals of the metal to the π-system of the fluorenyl moiety (Figure 2.8). Such calculations are consistent with the data obtained earlier in theoretical studies.[112]

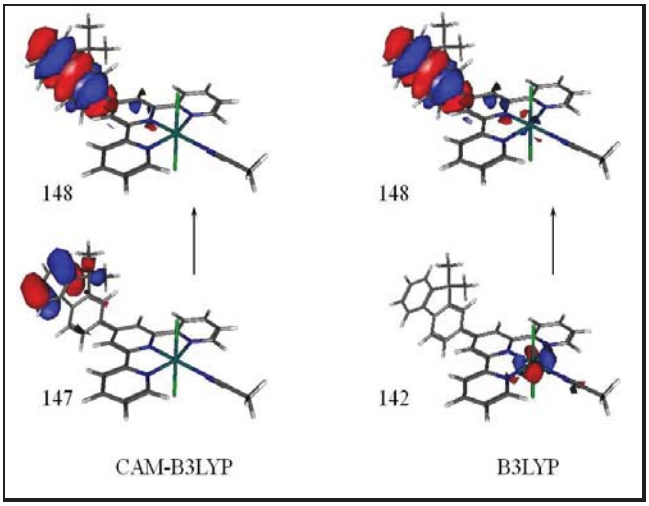

Figure 2.8. Orbitals that participate in low-energy transitions of compound $[Ru^{III}(FT)Cl_2(CH_3CN)]^+$ computed using the functionals CAM-B3LYP (on the left) and B3LYP (on the right).

The absence of such transitions in the spectrum of the photoproduct obtained by photolysis of bpy1 may indicate the formation of a diamagnetic complex – Ru^{II}-complex.[107] Perhaps, the photoproduct formed after NO-release, containing Ru^{III}, is instantaneously reduced in solution, and the only compound observed as a

photoproduct is $[Ru^{II}(FT)bpy(CH_3CN)]^{2+}$. The presence of distinct isosbestic points in a series of spectra obtained during the process of nitric oxide photorelease (Figure 2.6c) speaks in support of such a theory.

2.4 Investigation of two-photon absorption of cis2, trans2 and bpy2 compounds.

The first attempt to measure the two-photon absorption of cis1 and trans1 compounds was unsuccessful due to insufficient solubility of both complexes in CH_3CN (the required concentration for investigation of TPA of compounds by means of z-scan experiment is 10^{-2} M), therefore we have obtained analogues of these complexes, in which the position 9 of the fluorenyl fragment of FT ligand is substituted with two *n*-hexyl chains. The presence of long alkyl chains in the structure of the dHFT (4'-(9,9-dihexyl-9*H*-fluoren-2-yl)-2,2':6',2''-terpyridine) significantly increased the solubility of the complexes, leaving π-π* electronic transitions in compounds almost unchanged. Thus, we obtained the cis(Cl,Cl)-$[Ru^{II}(dHFT)Cl_2(NO)](PF_6)$ – cis2, trans(Cl,Cl)-$[Ru^{II}(dHFT)Cl_2(NO)](PF_6)$ – trans2, and $[Ru^{II}(dHFT)(bpy)(NO)](PF_6)_3$ – bpy2 (Figure 2.8).[107]

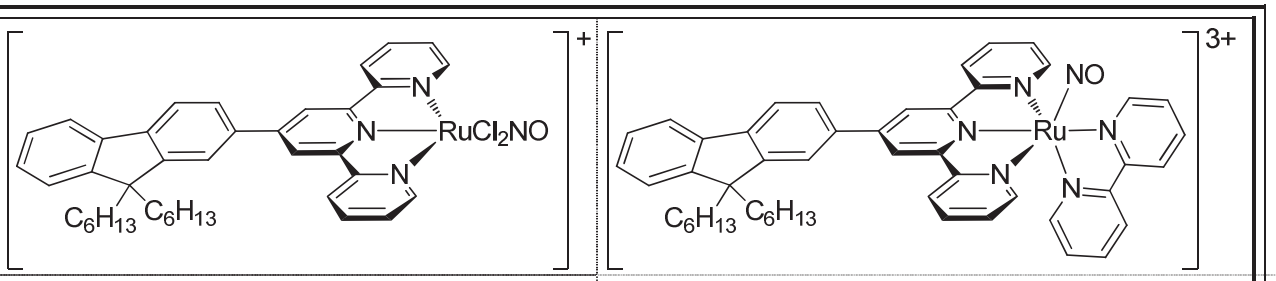

a – cis(Cl,Cl), b – trans(Cl,Cl) *c*

Figure 2.8. The structure of obtained complexes: a) cis2, b) trans2, c) bpy2.

Today, there are two main methods for determining the TPA cross-section σ: z-scan and the two-photon-excited fluorescence (TPEF) method yet there are others, for example the method of thermal lens and photo-acoustic methods.[104] Although the most sensitive among them is TPEF, its use is limited to cases of fluorescence compounds. Z-scan is a direct method to determine the nonlinear absorption in bulk

materials consists in monitoring the transmittance of the sample under test as a function of the incident intensity of a laser beam. In the practice this is achieved by changing the position (Z coordinates) of the sample in the vicinity of a focal plane of the radiation source. A more detailed description of the z-scan method is given in the experimental part.

The study of two-photon absorption of compounds was carried out using a femtosecond laser radiation source. The use of short-pulse radiation excludes other nonlinear optical phenomena that can significantly overestimate the value of the cross-section σ_{TPA}. In particular moving from femtosecond to nanosecond lasers in the TPA study may increase the measured σ hundreds of times due to undesirable additional absorption of excited levels.[100,104,107]

As noted above, from absorption spectra of cis1 and trans1 and TDDFT analysis of their excited states it can be seen that the electronic transition that initiates the transfer of the electron density from the fluorenyl substituent onto {Ru-NO} fragment has an energy of about 3 eV corresponding to the energy of electromagnetic radiation with a wavelength of about 400 nm (Figure 2.3). The use of two-photon absorption reduces the energy of exciting radiation and makes possible switching from 400 nm to 800 nm.

In spite of the fact that the corresponding band in the UV-visible spectrum of the bpy1 compound is shifted bathochromically to 450 nm (corresponding to 900 nm in TPA process) compared with derivatives with chloro-ligands, the study of TPA of its analog bpy2 was also carried out at a wavelength of 800 nm. The reason for such a choice is the practical aspects of the use of TPA. In the biophotonics the most promising is the use of wavelengths of 700-900 nm,[107] but obtaining radiation with a wavelength of 800 nm is much simpler and cheaper. In fact, the TPA study requires the use of a Ti-Sapphire laser (Ti:Sa), and the peak intensity of such an oscillator is just at 800 nm.

For comparison we still carried out a TPA study at 900 nm for bpy2, but as will be shown below there was no significant difference between the values of σ_{900} and σ_{800}.

The research was conducted at different laser irradiation intensities. The energy of electromagnetic radiation pulses varied from 30 nJ to 95 nJ. For the three investigated compounds at different intensities of irradiation symmetric z-scan curves were observed, that is an important characteristic as it confirms the absence of other potential nonlinear optical phenomena that often appear at higher energy of light pulses and significantly distort typical transmission curves. The asymmetry of the curves in the study of compounds capable of photoinitiated chemical transformations may also indicate the formation of new compounds – photoproducts. Since the formation of new compounds in the z-scan experiment is inevitable, their ability to change sample absorption should be taken into account. The good reproducibility of the experiment and the absence of artifacts on the transmission curve indicate a poor change in the concentration of the studied complexes and photoproducts.

The TPA curves obtained for the compounds cis2, trans2 and bpy2 are shown in Figure 2.9(a, b, c).

For each of the studied complexes, at least 20 scans were performed at different light-pulse energies, and, as expected, an increase in the intensity of the light beam resulted in a decrease in the transmittance (T (z)) of the studied sample in the focal plane (z = 0). In all cases, irrespective of the compound and energy of irradiation, the approximation of data was in accordance of high accuracy with the law that corresponds to the change in absorption intensity at TPA.

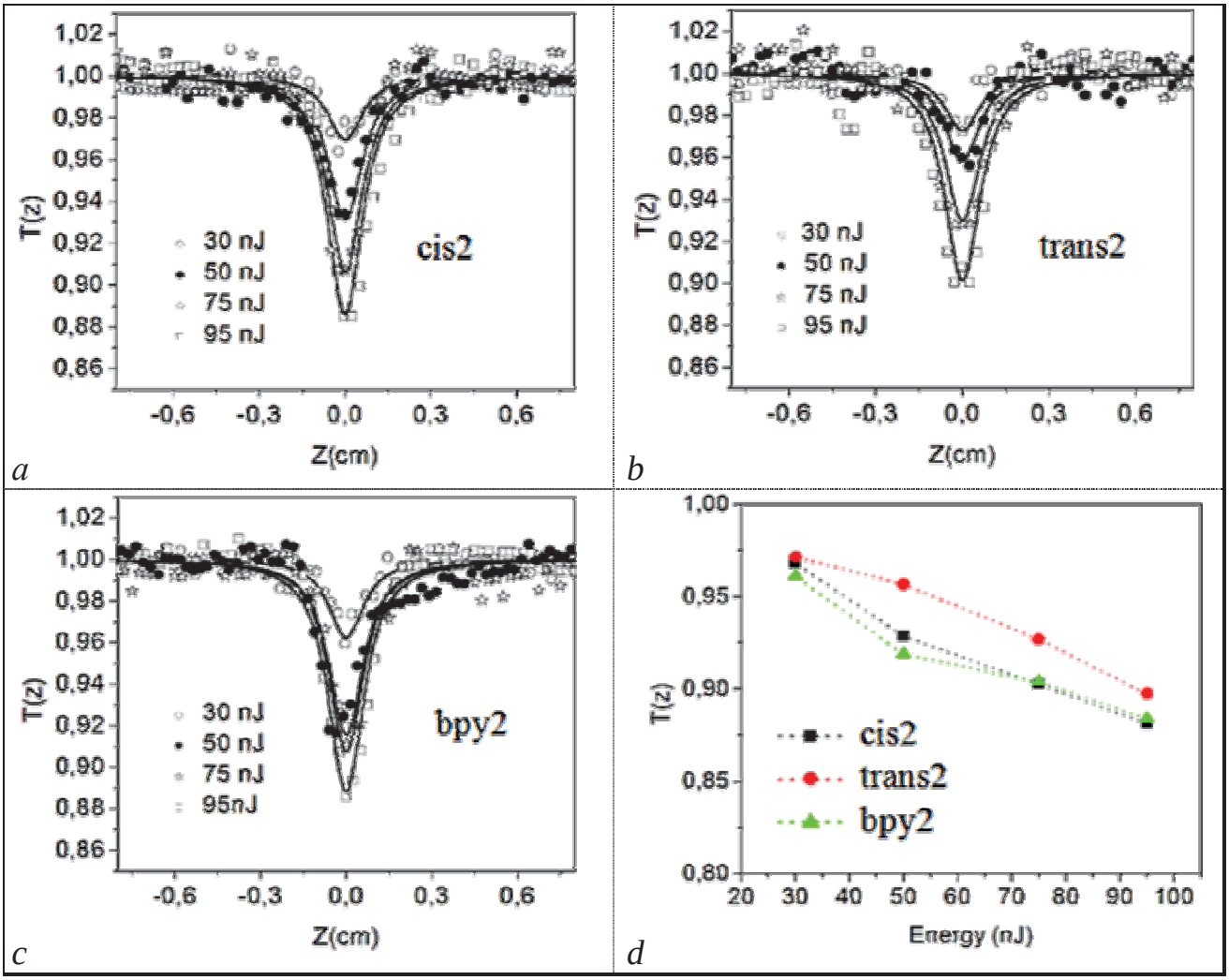

Figure. 2.9. Curves of laser irradiation (λ = 800 nm) transmission for acetonitrile solutions of a) cis2, b) trans2, c) bpy2. Decrease of transmission with the increase of irradiation intesity (d).

The obtained two-photon absorption coefficients (β) and the calculated two-photon absorption cross-sections (σ) calculated from β are gathered in Table 2.4.

Compound	$\beta \cdot 10^{11}$ cm/W		σ, GM	
	800 nm	900 nm	800 nm	900 nm
cis2	2.43 ± 0.32		100.2 ± 13	
trans2	2.12 ± 0.34		87.3 ± 14	
bpy2	2.63 ± 0.43	2.17 ± 0.43	108 ± 18	89.3 ±20

Table 2.4. Two-photon absorption coefficients and cross-sections values for compounds cis2, trans2, bpy2.

Taking into account the measurement error, we can say that the obtained values of σ have the same order and fall in the region of 100 GM, with some tendency to increase the efficiency of the TPA in the series trans2 <cis2 <bpy2.

Investigation of the compound bpy2, however, requires some additional explanation. Since the absorption band in the electronic spectrum of this compound is shifted by about 2500 cm^{-1} bathochromically and is at 450 nm, it seems more logical to undertake TPA studies at 900 nm. But it is important to keep in mind that the spectrum of two-photon absorption of compounds can differ significantly from the spectrum of single-photon absorption, although for compounds with a strictly linear structure it's less common. In this regard, moving to 900 nm for TPA does not necessarily have to increase the absorption cross-section σ. And, as noted above, another advantage of using a laser irradiation of 800 nm is its low cost and ease of obtaining. Nevertheless, we analyzed the ability of the compound bpy2 to the TPA upon the excitation with 900 nm waves. However, there was no significant change in the σ-value (Table 2.4).

The obtained values of nonlinear optical parameters for compounds cis2, trans2 and bpy2 are close to those published in literature where the donating fragment is represented by fluorene fragment.[107] These values are also close to the nonlinear parameters of typical push-pull molecules, in particular, 4-dialkylamino-4'-nitrostilben (DANS, σ = 88 GM), disperse red (σ = 110 GM). However the obtained complexes possess a considerably lower capability of participating in TPA regarding to the highest known σ among the ruthenium complexes. In particular, for one of the ruthenium coordination compounds – tris(bipyridyl) complex, in which the ligands contain donating dibutylaminophenylvinyl substituents – this value is 2200 GM. But the comparison of the complexes cis2, trans2 and bpy2 with this type of compounds may be somewhat incorrect because of their substantially different structure. Thus, the high value of σ for the described tris(bipyridyl) ruthenium complex is likely to be due to its octupolar structure and to the presence of strong donating substituents in bipyridyl ligands.[113]

Thus, we have proposed a new nitric oxide donor – $[Ru^{II}(FT)(bpy)(NO)]$ $(PF_6)_3$, which has several advantages over previously known $[Ru^{II}(FT)Cl_2(NO)](PF_6)$. Those are: a simpler method for obtaining a compound, its higher stability (as a result of replacing of labile chloro-ligands with chelate 2,2'-bipyridine) that will definitely increase its stability in the biological environment. The quantum yield of NO release from the new complex is 0.06 and is close to trans1, which is likely to be due to the trans-effect of pyridine rings in complexes. The TPA cross-sections for all three compounds cis2, trans2 and bpy2 have been investigated and are within 80-120 GM at the wavelength $\lambda = 800$ nm.

CHAPTER 3. PYRIDOISOINDOLE AND ISOMERIC HETEROCYCLES AS DONATING FRAGMENTS IN {Ru-NO} COMPLEXES: THEORETICAL INVESTIGATION.

The fluorenyl substituent acting as a donor fragment in the studied ruthenium-nitrosyl complexes cis1, trans1, bpy1 and their analogs containing alkyl substituents in the 9th position of fluorene plays the role of a source of electron density transmitted to the {Ru-NO} withdrawing group upon excitation of the compound with electromagnetic radiation of 405 nm wavelength in single-photon activation, or 800-900 nm in two-photon absorption. In addition, fluorene plays the role of an antenna for the absorption of two photons in TPA. The high efficiency of this polycyclic fragment in TPA is confirmed by numerous studies and an increasing interest in its application in the design of compounds with nonlinear optical (NLO) properties.[114,115]

The mechanism of the nitric oxide photorelease from ruthenium-nitrosyl compounds remains a controversial issue. And its investigation by methods of theoretical chemistry is an urgent question. However, the first step in obtaining NO from its coordination compounds is believed to be the transfer of electron density toward a strongly withdraing group {Ru-NO}. It was therefore assumed that the enhancement of the push-pull nature of the complex can increase the efficiency of this transition. Given that this electronic transcription should also be active in the TPA, further work was aimed at finding potential donor fragments that being introduced into complexes with already available acceptor group {Ru-NO} would enable the design of effective one-dimensional push-pull systems highly active in TPA.[116]

In the case of long range delocalized push-pull effects, the expression of σ_{TPA} can be tentatively approached by a simple two-level model involving the current $g \rightarrow e$ transition as follows:[117]

$$\sigma_{TPA} \approx \frac{16\pi^2 f\left(\mu_{ee} - \mu_{gg}\right)^2}{5\hbar^2 c^2 \Gamma E_{ge}} \qquad 3.1$$

In this equation, E_{ge} is the energy of the transition, f its oscillator strength, μ_{gg} and μ_{ee} the dipole moments in the ground and excited states, respectively. It is interesting to point out that equation 3.1 is reminiscent of the simplified but widely used "two-level" description of the first hyperpolarizability (β in equation 3.2), which relates the property to the sum of the contribution of each of the g → e_i transitions as follows:[118]

$$\beta_{2l} \approx \sum_i \frac{3e^2\hbar f_i\left(\mu_{ee}-\mu_{gg}\right)_i}{2m(E_{ge})_i^3} \times \frac{(E_{ge})_i^4}{\left[(E_{ge})_i^2-(2\hbar\omega)^2\right]\left[(E_{ge})_i^2-(\hbar\omega)^2\right]}, \qquad 3.2$$

an expression in which *m* is the mass of the electron.

In the case of species exhibiting strong push-pull charge transfer capabilities, the summation is usually restricted to the contribution of a single and low-lying HOMO → LUMO based (g → e) transition. Furthermore, the second term of the right part of equation (3.2) is a dimensionless coefficient accounting for β dispersion by resonance effect, when the incident ($\hbar\omega$) or frequency doubled ($2\hbar\omega$) energy of the laser is getting close to the transition energy (E_{ge}). It is therefore more relevant to use the intrinsic hyperpolarizability (β_0), independent of the laser frequency:

$$\beta_0 \approx \frac{3e^2\hbar f\left(\mu_{ee} - \mu_{gg}\right)}{2m(E_{ge})^3} \qquad 3.3.$$

It is noteworthy that expressions (3.1) and (3.3) involve the same parameters ($\mu_{ee} - \mu_{gg}$, f, and E_{ge}). These similarities imply that a promising strategy in the search for molecules with high σ_{TPA} values should be to target molecules designed for high β values for which the two-level model (β_0) has long been applied successfully.[119]

3.1. Pyridoisoindoles and isomeric heterocycles as potentially more effective fluorene analogues

In the compound trans1that was taken as the reference for this study the fluorenyl substituent A (Figure 3.1), as noted, plays the role of a donor of electron density. However, the donating properties of fluorene are quite moderate. The introduction of an electron rich center delocalized within the polycyclic structure should be a means of guaranteeing an enhancement of the donating capabilities of the substituent. For instance, the introduction of pyrrole-type nitrogen atom in the central node leads to the pyrido[2,1-*a*]isoindole species, in which a 14-π-electrons path of delocalization can provide a sizeable push-pull effect either towards position 6 or 4 (B and C respectively, Figure 3.1).

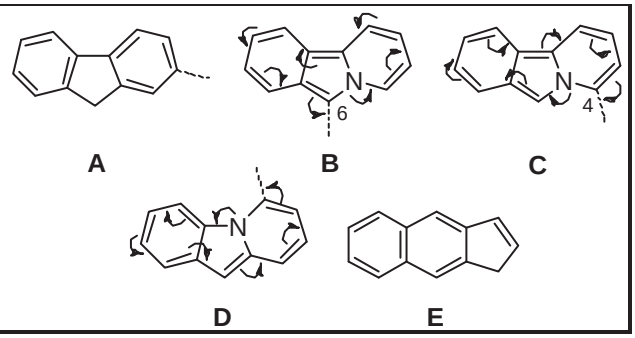

Figure. 3.1. Several polycyclic systems with donating capabilities.

In the studies of Kovtunenko and Voitenko it was previously shown by theoretical calculations using several approaches and then proved with X-ray diffraction analysis and mass spectrometry that the nitrogen atom of the isoindole is strongly involved in the π-delocalized structure.[120,121] Owing to an electron-rich o-quinonic structure, isoindole can act as an efficient electron-donating moiety. Joining an additional pyridine ring to the isoindole core evolves 10 π-electron system to 14 π-system along with conservation of a conjugation over the entire extend of the rings.[121] Pyrido[1,2-*a*]indole (compound D, Figure 3.1) could theoretically also act as a donor, and the joining of the terpyridine-ruthenium-nitrosyl moiety exactly at position 6 of such a system will potentially involve all double bonds in the π-system conjugation.

In the present work, various $[Ru^{II}(R\text{-terpy})(Cl)_2(NO)]^+$ complexes bearing R donating substituents (isomeric to pyrido[2,1-*a*]isoindolyl residue) are investigated computationally in a research effort aimed at targeting suitable candidates for high β values, and therefore potentially enhanced TPA response.

For more thorough analysis of formally similar tricyclic systems with one nitrogen atom, we extended the spectrum of compounds and systems with those constructed from skeleton E (Fig. 3.1), varying the position of the nitrogen atom in the compound. Altogether, this approach leads to a total of 107 potential isomers. Owing to the large number of isomers, the only ones selected here were those having the whole 14 π-electrons potentially involved in the path of conjugation from the nitrogen atom to the linkage towards the terpyridine, for a better comparison of their induced push-pull capabilities. The different structures can be gathered in two groups depending on the position of the 5-membered ring either on the side (6-6-5) or in the center (6-5-6) of the moiety (Scheme 3.1).

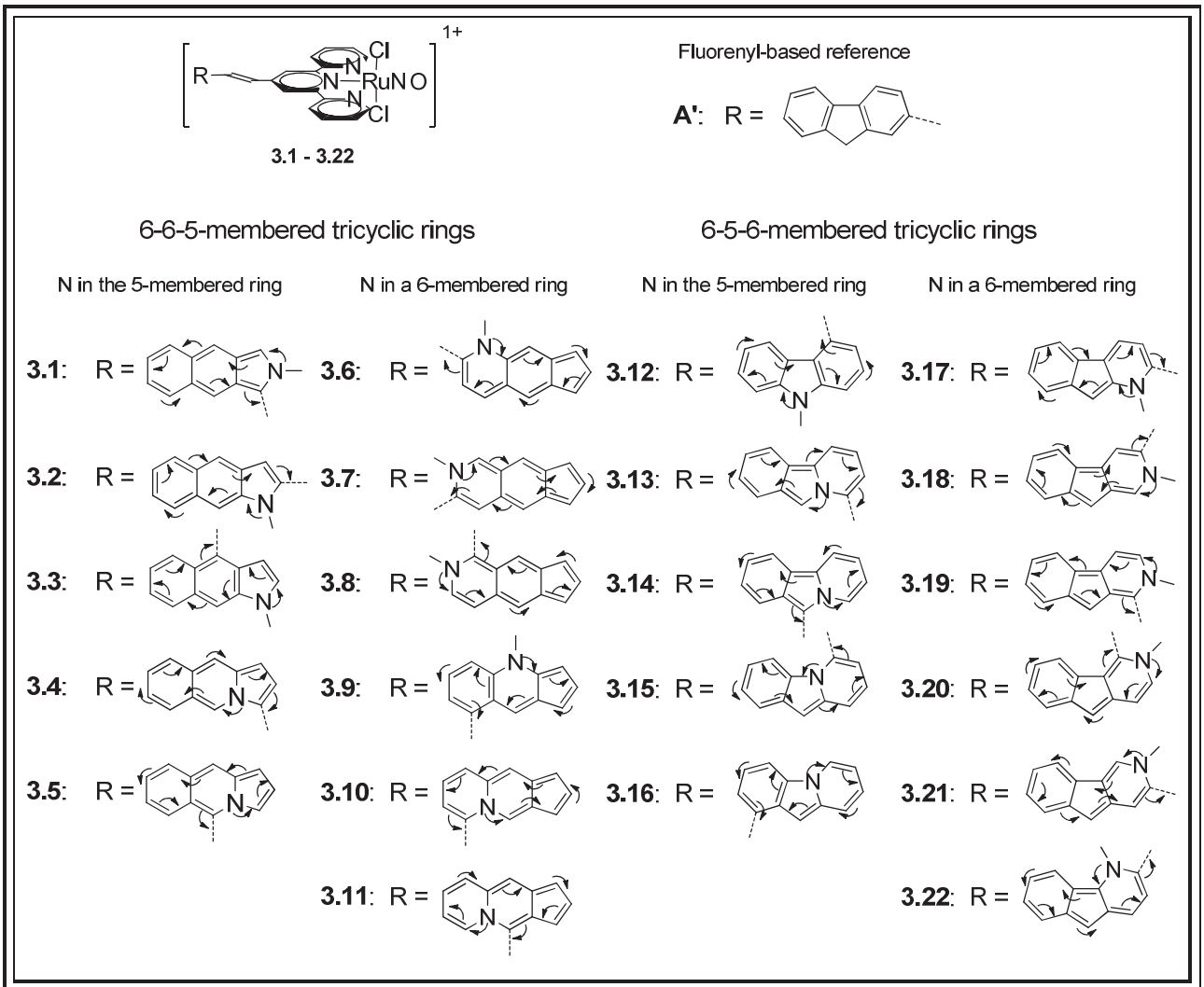

Scheme 3.1. Isomeric ruthenium-nitrosyl complexes with donating tricyclic substituents 6-6-5 *(3.1-3.11)* and 6-5-6 *(3.12-3.22)*and a reference compound A' .

Note that, for the sake of simplification, the 3-fused rings systems (acenaphtylene derivatives) or bent structures (like an analog of linear 2-methyl-2*H*-benzo[*f*]isoindole (compound 3.1) – 2*H*-benzo[*e*]isoindole) were discarded from the selection.

Each system is further identified by the position of the nitrogen atom, and by that of the linkage. Depending on the place of the nitrogen in the rings, and to ensure that a tertiary amine is present in any case, any –NH group is replaced by –NMe. Finally, an ethenyl (-CH=CH-) unit is inserted between the polyaromatic system and the terpyridine moiety to reduce the steric hindrance in the molecules. This modification is achieved in order to decrease undesirable torsion angles and to enhance the conjugation of π-bonds. Such alteration allows us to compare the real influence of the isomeric heterocycles on optical and electronic properties of the complexes. The compound with a fluorenyl donor substituent A' (Scheme 3.1) is a reference for comparing the nonlinear-optical properties of the studied complexes.

The ruthenium complexes were optimized in gas phase using the Gaussian-09 program package within the framework of the DFT. The details for the computed coordination spheres of the 23 complexes under investigations are provided in Table 3.1.

The details of computational methods used are presented in experimental part of the work (Chapter 6).

In the table 3.1 the parameters of cordination sphere of 23 complexes are compared to that of the previously reported complex trans1. The computed coordination spheres appear similar in any case, with largest relative bond lengths difference of 0.6 % observed at the Ru-N (central pyridine) between **3.7** (1.993 Å) and **3.12** (2.006 Å). The agreement with the experimental data available is found satisfactory, with a general shortening of bond lengths in the X-ray geometries, from those computed by DFT.

Compound	Ru-N_{NO}	Ru-N (central py)	Ru-N (lateral py)	Ru-Cl	Cl-Ru-Cl
3.1	1.760	1.994	2.087	2.405	172.5
3.2	1.759	2.002	2.087	2.401	171.8
3.3	1.758	2.001	2.088	2.401	171.9
3.4	1.759	1.995	2.087	2.404	172.4
3.5	1.759	1.998	2.087	2.403	172.1
3.6	1.763	1.994	2.086	2.405	172.5
3.7	1.761	1.993	2.086	2.406	172.6
3.8	1.764	1.998	2.085	2.404	172.1
3.9	1.758	2.005	2.087	2.400	171.4
3.10	1.760	1.999	2.087	2.402	172.0
3.11	1.760	2.000	2.087	2.402	171.9
3.12	1.758	2.006	2.088	2.399	171.4
3.13	1.759	2.000	2.087	2.402	171.9
3.14	1.759	1.996	2.087	2.404	172.5
3.15	1.759	2.003	2.087	2.401	171.6
3.16	1.758	2.001	2.087	2.402	171.9
3.17	1.759	2.003	2.087	2.400	171.6
3.18	1.760	1.994	2.086	2.405	172.6
3.19	1.760	1.996	2.086	2.404	172.3
3.20	1.759	2.005	2.087	2.400	171.4
3.21	1.760	1.998	2.087	2.402	172.1
3.22	1.760	1.996	2.087	2.404	172.4
A'	1.760	2.004	2.088	2.400	171.6
trans1	1.759	2.001(5)	2.081(6) 2.073(6)	2.348(2) 2.364(2)	172.58(6)

Table 3.1. Main bond lengths (in Å) and angles (in °) in the computed coordination spheres of compounds 3.1-3.22. The values for B are experimental X-ray data, provided as references.

3.2. Quantum-chemical calculations of nonlinear optical parameters of complexes.

The relevant NLO parameters (β, β_0, and σ_{TPA}) of the 22 selected isomers are gathered in Table 3.2. It is important to note that, while β corresponds to the quadratic NLO response of the entire molecule (equation 3.2), β_0, and σ_{TPA} refer to response of an individual transition from the (g) ground to a given (e) excited state. The excited states given in the table correspond to the only ones providing significant

Compound	β (10^{-30} cm^5 esu^{-1})	# excited state	relative β_0 value	relative σ value
3.1	487.2	i=1	0.83	0.24
3.2	732.3	i=1	0.96	0.56
		i=5	0.63	0.57
3.3	450.4	i=1	1.32	1.01
3.4	475.8	i=1	0.90	0.30
3.5	502.3	i=1	1.34	0.48
3.6	2709.9	i=1	0.58	< 0.01
3.7	1539.5	i=1	2.82	0.57
3.8	2751.7	i=1	3.34	0.09
3.9	301.4	i=1	0.29	0.15
3.10	1130.0	i=1	0.96	0.10
3.11	733.2	i=1	1.37	0.03
3.12	233.1	i=3	0.48	0.52
		i=5	0.15	0.21
3.13	754.2	i=1	1.43	0.48
3.14	376.1	i=1	0.74	0.24
3.15	540.4	i=1	0.85	0.28
3.16	553.3	i=1	1.04	0.53
3.17	975.3	i=1	0.97	0.28
3.18	855.1	i=1	1.30	0.27
3.19	782.8	i=1	0.94	0.08
		i=8	0.19	0.10
3.20	328.8	i=1	0.21	0.03
		i=7	0.21	0.11
3.21	1289.8	i=1	1.48	0.34
3.22	1041.2	i=1	1.11	0.25
		i=8	0.54	0.43
A'	463.2	i=4	1	1

Table 3.2. NLO quadratic (β and relative β_0 related to the i^{th} transition) and cubic (relative σ_{TPA} cross-section related to the i^{th} transition) for **3.1**-**3.22**, and **A'** for which β_0 and σ_{TPA} are set at 1, and used as references.

β_0 values. To further simplify the understanding, β_0, and σ_{TPA} are expressed as relative values, those of the A' reference system being taken as 1.

The first thing to observe in the Table 3.2 is that the β values of compounds **3.1**-**3.22** are generally larger than that of the reference compound A'. This confirms the donating capabilities of the electron-rich heterocyclic amines. Nevertheless, this tendency is not observed in compounds **3.3**, **3.9**, **3.12**, **3.14**, and **3.20**, which

emphasizes the role of the conjugation path, although the delocalization over the whole extent of the π-system is present in any case.

More generally, what strikes from the examination of Table 3.2 is the magnitude of the computed values, for isomeric species containing the same acceptor (NO), conjugated path length (arylethenyl-substituted terpyridine) and closely related donors. Indeed, β ranges from 233.1 (**3.12**) to 2751.7 (**3.8**) × 10^{-30} cm^5 esu^{-1}, β_0 from 0.21 (**3.20**) to 3.34 (**3.8**), and σ_{TPA} from <0.01 (**3.6**) to 1.01 (**3.3**).

3.3 Push-pull effects in studied complexes

Computed β values around $100 \cdot 10^{-30}$ cm^5 esu^{-1} are rather common in conjugated organic species.[122] Values larger than $1000 \cdot 10^{-30}$ cm^5 esu^{-1} have occasionally been found in the case of donor-acceptor effects extended over a path of conjugation in the range of 20 bonds.[123] Few experimental data have been reported in which the withdrawing core is based on a Ru^{II} center. Representative examples are provided in Figure 3.2.

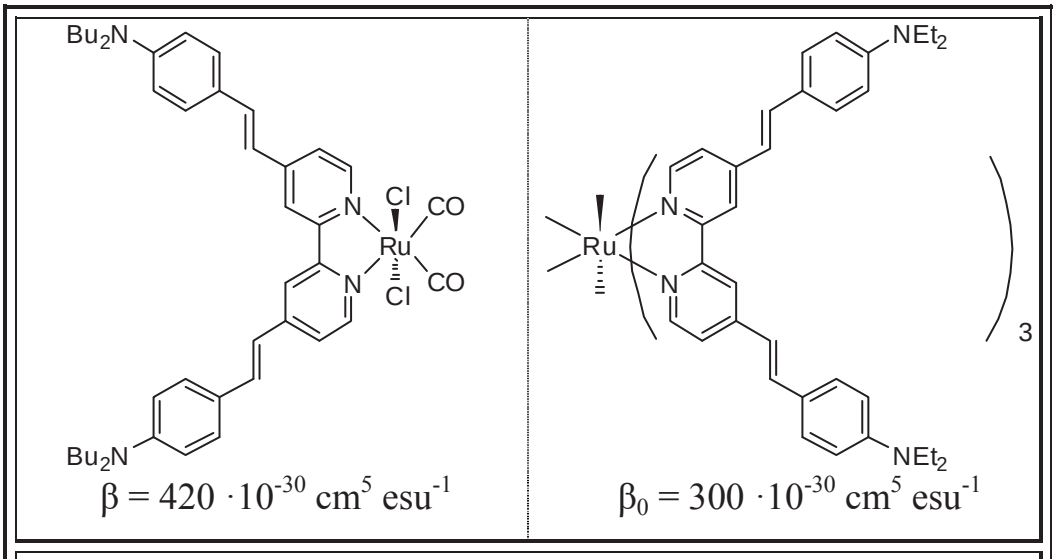

Figure 3.2. Ruthenium-organic chromophores with sizeable experimental quadratic NLO response in dipolar (left) and octupolar (right) geometries.

They are associated with typical β values around $300\text{-}500 \cdot 10^{-30} \cdot cm^5$ esu^{-1}. Therefore, the large values computed here (β = 2709.9 and $2751.7 \cdot 10^{-30}$ cm^5 esu^{-1} for **3.6** and **3.8**, respectively) may be accurate and therefore deserve further analyses.

Following the conventional picture of donor-acceptor chromophores, increasing β would imply increasing the push-pull effect from the heterocyclic amine towards the Ru(NO) core. This should normally lead to an increase of the electron transfer to an antibonding π* orbital of the nitrosyl ligand, with the outcomes of an increase of the electron density (Mulliken population) on NO, and a decrease of the ν(NO) stretching frequency. This is illustrated in Figure 3.3.

It is worth pointing out that the computed ν(NO) frequencies appear larger than experimental data,[92] a discrepancy which has to be related to the modest accuracy of the computational method. Nevertheless, comparing the differences in frequencies instead of the absolute values is more reliable in this case.

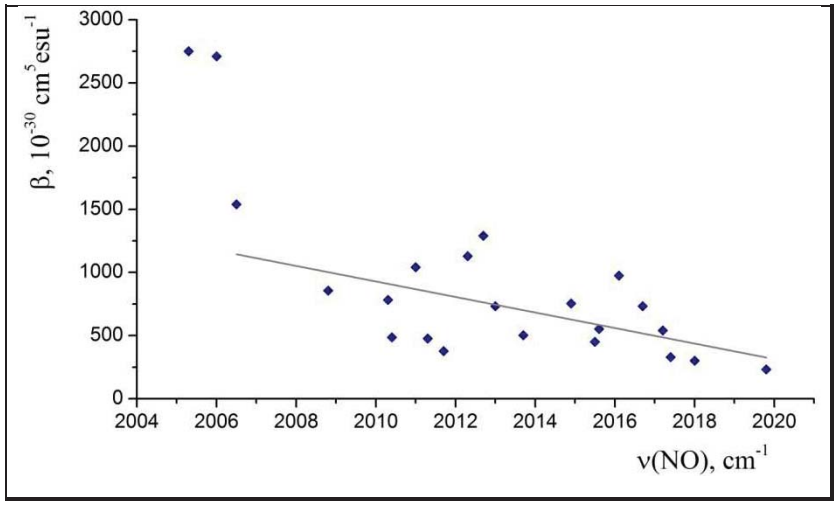

Figure 3.3. β values against ν(NO) frequencies for the series of 3.1-3.22 derivatives. 3.6 and 3.8 are excluded for the computation of the trend line.

Owing to the crude tendency observed in the Figure 3.3, the β values of compounds 6 and 8 should lie in the $1000 - 2000 \cdot 10^{-30}$ cm^5 esu^{-1} range. Therefore, the large computed values ($> 2500 \cdot 10^{-30}$ cm^5 esu^{-1}) strongly suggest that the properties cannot be fully understood within the framework of the simplified two-level model in these species.

The possible explanation for the observed β values could be the following statement: the larger the shortest conjugation path, the higher the hyperpolarizability. In other words, the most efficient of them are those in which the 14 π-electrons are necessarily involved in the path of delocalization. This is exemplified in Scheme 3.2 for complexes **3.10** ($\beta = 1130 \times 10^{-30}$ cm^5 esu^{-1}), and **3.11** ($\beta = 732 \times 10^{-30}$ cm^5 esu^{-1}), which contain the same R isomer, and accepting (A) moieties, but differ in the

position of the linkage. While the only path of delocalization involves the 14 π-electrons in **3.10**, a shorter possibility occurs in **3.11** in which only 10 π-electrons contribute to the mesomeric equilibrium (bottom of Scheme 3.2).

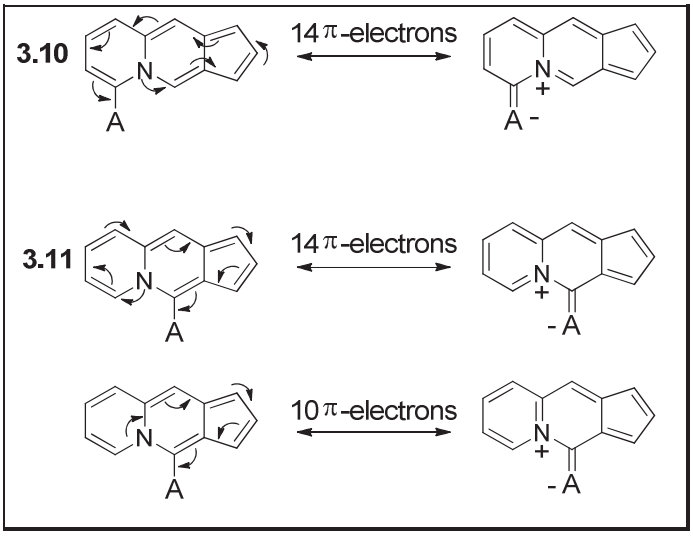

Scheme 3.2. Possibilities for mesomeric equilibrium between the nitrogen rich donor and the accepting (A) moieties in 3.10 and 3.11.

In support of such theory it is worth mentioning that all compounds, in which the shortest conjugation path is represented by 6π-electons chain (**3.1**, **3.3**, **3.4**, **3.14**, **3.16**) don't display hyperpolarizability values higher than 553.3 (for compound **3.16**).

Interestingly, the only complexes in which the whole π-electrons of R are necessarily involved in the path of delocalization are **3.6**, **3.7**, **3.8**, and **3.10**. They correspond to the species associated to the highest β values, which suggests that this is probably a key electronic parameter to account for their enhanced capabilities.

Additionally, the β_0 values associated to the contribution of the dominant transitions of **3.1**-**3.22** are gathered in Table 1. In most cases, a single and low-lying HOMO → LUMO based transition leads to a significant β_0, as anticipated in most push-pull organic chromophores.[119] Nevertheless, a second transition is involved in complexes **3.2**, **3.12**, **3.19**, **3.20**, and **3.22**, however with a reduced weight, except in the case of **3.20**, where two transitions (0 → 1 and 0 → 7) lead to the same β_0 value.

At this stage, the issue of a correlation between β and the dominant β_0 arises naturally, in an attempt to provide a simple picture of the quadratic NLO response. β is drawn against β_0 in Figure 3.4.

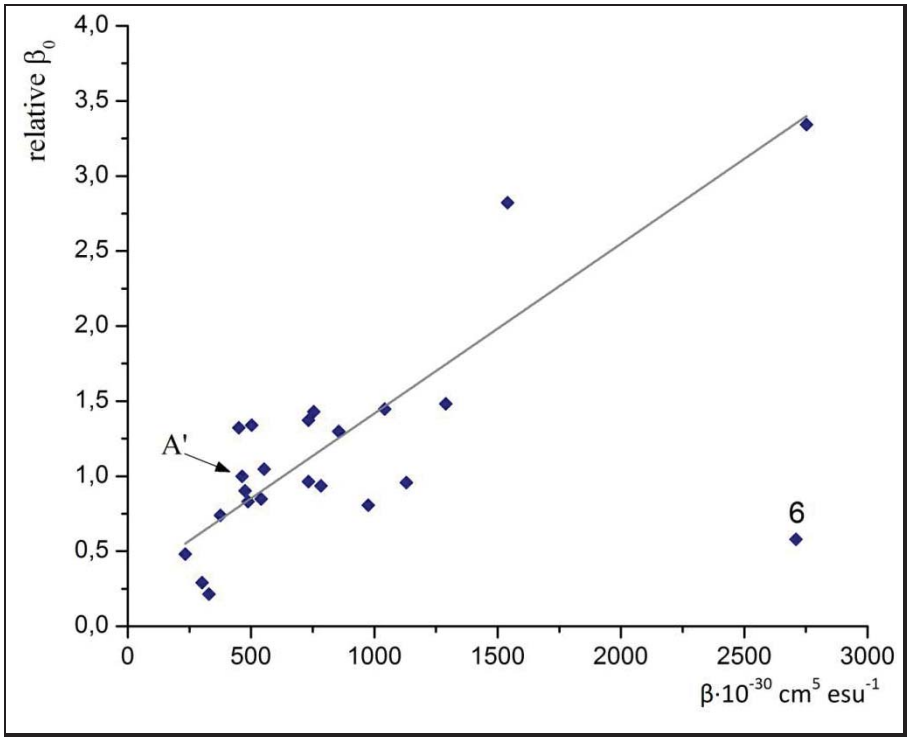

Figure 3.4. Relative β_0 against β for 3.1-3.22 and A'.

Asserting that β_0 scales like β would far be excessive. Nevertheless, there is a rough tendency, for larger β_0 values in the case of larger β value, except in compound **3.6**. The parameters used in the computation of β_0 (equation 3.3) are gathered in Table 3.3. Finding λ_{max} values in the 500 – 1 000 nm range is fully acceptable in push-pull molecules with delocalization over the whole extent of a chain containing more than 20 π-electrons. Nevertheless, λ_{max} values larger than 2 000 nm (**3.6** and **3.8**) are rather surprising. The fact that they are associated with transitions of unusually weak intensity (**3.8**) or unusually reduced $\mu_{ee} - \mu_{gg}$ value (**3.6**) makes these species definitely unconventional. And understanding of the nature of these compounds requires both more profound theoretical and experimental analyses that, by-turn, raises the issue of the synthetic feasibility of such complexes.

Compound	transition	λ_{max}	f	$\mu_{ee} - \mu_{gg}$	composition
3.1	0 → 1	581	1.14	8.22	HOMO → LUMO (87 %)
3.2	0 → 1	623	0.46	19.2	HOMO → LUMO (83 %)
3.3	0 → 1	578	0.70	21.7	HOMO → LUMO (82 %)
3.4	0 → 1	569	1.18	9.17	HOMO → LUMO (85 %)
3.5	0 → 1	662	0.76	13.5	HOMO → LUMO (76 %)
3.6	0 → 1	2183	0.12	1.07	HOMO → LUMO (59 %)
3.7	0 → 1	824	0.96	11.7	HOMO → LUMO (84 %)
3.8	0 → 1	2236	0.06	10.9	HOMO → LUMO (85 %)
3.9	0 → 1	727	0.07	22.9	HOMO → LUMO (77 %)
3.10	0 → 1	881	0.45	6.84	HOMO → LUMO (83 %)
3.11	0 → 1	896	0.32	13.3	HOMO → LUMO (67 %)
3.12	0 → 3	496	0.39	22.7	HOMO → LUMO (80 %)
3.13	0 → 1	699	0.67	13.9	HOMO → LUMO (80 %)
3.14	0 → 1	555	1.14	8.43	HOMO → LUMO (87 %)
3.15	0 → 1	709	0.38	13.9	HOMO → LUMO (80 %)
3.16	0 → 1	603	0.68	15.6	HOMO → LUMO (80 %)
3.17	0 → 1	920	0.13	20.8	HOMO → LUMO (74 %)
3.18	0 → 1	656	1.34	7.60	HOMO → LUMO (92 %)
3.19	0 → 1	919	0.41	6.50	HOMO → LUMO (67 %)
3.20	0 → 1	999	0.03	13.9	HOMO → LUMO (78 %)
	0 → 7	514	0.30	11.8	HOMO-1 → LUMO (73 %)
3.21	0 → 1	756	0.68	11.1	HOMO → LUMO (87 %)
3.22	0 → 1	822	0.59	9.77	HOMO → LUMO (65 %)
A'	0 → 4	464	1.21	18.4	HOMO → LUMO (79 %)

Table 3.3. Dominant transition for β_0: absorption maxima (λ_{max}) in nm, intensity (f), $\mu_{ee} - \mu_{gg}$ in D, and composition of the configuration interaction.

3.4 Quadratic (β) against cubic (σ_{TPA}) properties of complexes.

The capability of the complexes **3.1**-**3.22** for TPA is estimated by the relative σ values (σ for the reference compound A' taken as 1), calculated by formula 3.1. The experimental value is known only for the complex with the fluorenyl substituent A (Figure 3.1), which is 100 ± 13 GM.[107]

The examination of the data leads to the first conclusion that, in spite of their donating capabilities, the heterocyclic amines do not enhance the σ_{TPA} values with respect to that of the fluorenyl-based A' reference. More generally, there is no correlation between σ_{TPA} and β_0. Additionally, it can be observed in Table 3.2 that, when two low-lying intense transitions are present (compounds **3.2**, **3.12**, **3.19**, **3.20**,

3.22), the lowest energy transition is associated with the highest β_0 value. This is not the case for σ_{TPA} where the highest energy transition appears to be that of larger cross-section, except in **3.12**. This difference points out the versatility of the energy as a key parameter in the prediction of the NLO properties.

In push-pull species, the fact that β varies as $1/E^3$ leads to the expectation of efficient NLO effects restricted to the contribution of the 1st (HOMO/LUMO-based) excited state. In the $[R\text{-}T\text{-}Ru^{II}(Cl)_2(NO)]^+$ complexes built up from R-donor substituted terpyridines, the electron densities at the LUMO level are mostly located on the Ru(NO) moieties and therefore, are rather unaffected by the presence of the substituent.[86] By contrast, R provides the main contribution to the HOMO level. This is illustrated in Figure 3.5.

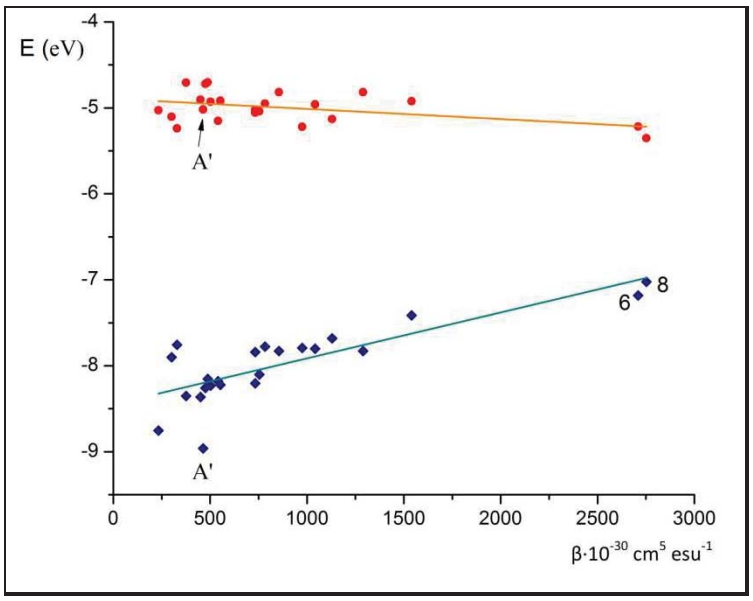

Figure 3.5. HOMO (blue) and LUMO (red) energies of compounds 3.1-3.22 against β.

The HOMO energy level appears to be the ultimate microscopic parameter to account for β, along the **3.1**-**3.22** series: the highest the HOMO energy, the lowest the transition energy, and hence the highest the β value.

By contrast, the requirement for low-energy transition appears much less pressing in σ_{TPA}. Indeed, in the case of compounds **3.2**, **3.12**, **3.19**, **3.20**, and **3.22**, where two low-lying intense transitions are present, the trend is that the second transition leads to higher σ_{TPA} value. In Table 2, the only parameter which varies as σ_{TPA} within a given molecule is the oscillator strength f, which leads to the conclusion that, in push-pull species, the two-photon absorption spectrum should be reminiscent of the one-photon absorption. Nevertheless, determining

precisely the full extent of σ_{TPA} within a series of related molecules (e.g. **3.1-3.22**) remains a very challenging issue.

The prediction of extremely large β values in some of the isomers under investigation within the **3.1-3.22** series raises the issue of their synthetic feasibility. This should likely depend on the availability of the heterocyclic amine system (R) and the possibility of its modification for further coupling with the terpyridine moiety. To reach these target species, several strategies are currently being the subject of intense investigation, notably indenopyridines (**3.17-3.22**),[124] isoindoles (**3.1)** and pyridoisoindoles (**3.13-3.14**).[125] A literature survey reveals that the cyclopentaquinolines species precursors of molecules **3.6-3.8** were never approached, either theoretically or experimentally that could be related to their potential instability. In order to evaluate the stability of the complexes in the first approximation, we compared their free Gibbs energies (ΔG) obtained by quantum-chemical calculations.

To be relevant, the comparison has to be carried out on molecules having the same formula, which are here the molecules in which –NH was replaced by –NMe. It appears that, while the carbazole-based compound **3.12** is the stablest one, the most efficient materials (**3.8**, **3.6**, and **3.7**) correspond to the most unstable species (Figure 3.6). In order to find a simple rationale to account for the relative instability of molecules such as **3.6**, **3.7**, **3.8**, the examination of Scheme 3.1 shows that they

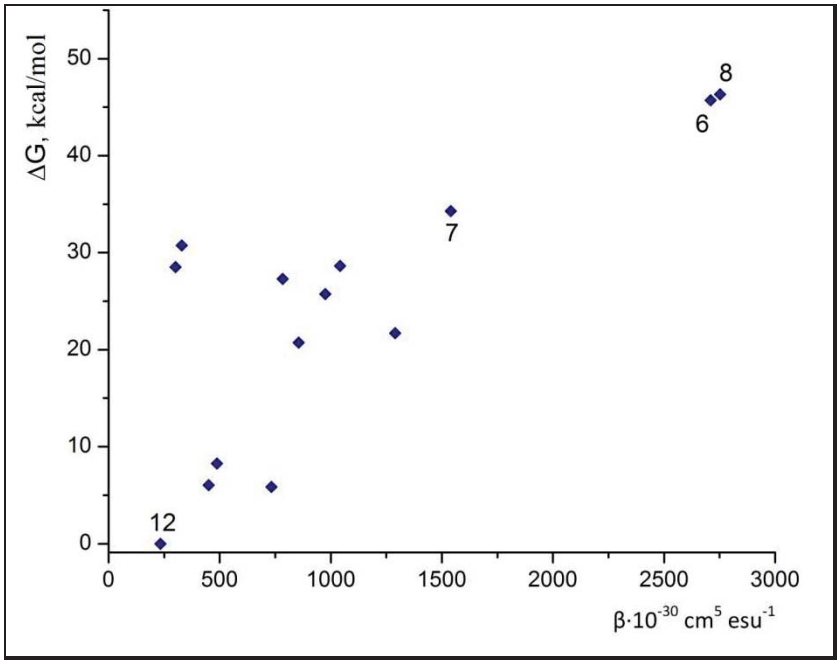

Figure 3.6. Gibbs free energy of isomers with N-methylheterocyclic substituents drawn against β. The energy of the carbazole-based 3.12 is set at zero.

possess no aromatic sextets, by contrast to the stable species **12**, which possesses 2 of them.

Thus in this theoretical study, for the complexes **3.1**-**3.22**, the nonlinear optical parameters of the second order (β) and the third order (σ) vary in wide range. The values of the TPA cross-section σ are generally lower than those of the reference compound A'. But the values of their hyperpolarizability in some cases are several times higher than that for A '. Nevertheless, the most promising systems correspond to the isomers of higher free Gibbs energy, thus pointing out the challenging issue of their synthetic availability.

CHAPTER 4. ENHANCEMENT OF THE EFFICIENCY OF RUTHENIUM-NITROSYL COMPLEXES IN TPA

Replacing two chloro-ligands with the 2,2'-bipyridine molecule, as shown in chapter 2, leads to a decrease in the quantum yield of nitric oxide photorelease, but somewhat increases the efficiency of the complex in two-photon absorption (TPA). The overall efficiency of NO-donor can be estimated from its ability to release NO when the compound is activated by two photons. For this purpose it is convenient to use a parameter similar to brightness for fluorescent compounds, which is the product of the molar extinction coefficient of luminescent material (ε) and the quantum yield of the luminescence (φ). For ruthenium-nitrosyl compounds that release nitric oxide when irradiated with UV light this parameter will be the product of the molar extinction coefficient of the complex and the NO-release quantum yield (φ) - ε·φ. By replacing the molar extinction coefficient with its corresponding parameter for two-photon absorption, the TPA cross-section σ, we obtain the expression σ·φ, which can serve as a parameter for comparing two ruthenium-nitrosyl complexes in their ability to act as NO-donors under two-photon activation.

The strategy of the search for the optimal NO-donor should be based on an increase of both parameters, while we give preference to the enhancement of σ. This choice is primarily due to the fact that an increase in the quantum yield of a photorelease up to several times can significantly complicate the process of obtaining and further work with ruthenium-nitrosyl complex, since even a momentary exposition of the compound to the radiation of UV-visible frequency range of the spectrum will initiate the decomposition of the complex.

This chapter is devoted to the attempts made to increase the value of the cross-section of TPA by chemical modification of the structure of organic ligands present in ruthenium-nitrosyl complexes. In particular, there will be discussed the effect of improvement of the conjugation between the donor group and the ruthenium-terpyridine fragment on the ability of the complexes to two-photon absorption, as

well as the correlation between the donating ability of the substituents in the structure of the complex and their nonlinear optical property.

4.1. Influence of the efficiency of conjugation between fluorenyl and terpyridine-ruthenium nitrosyl fragments on the ability of complexes to TPA

The efficiency of the electron density transfer from a donor to an acceptor in an organic fluorenyl-terpyridine ligand of ruthenium-nitrosyl complexes depends on the angle between the terpyridine plane and the donating fragment plane. As it was noted, the overlap of orbital is stronger, the greater the cosine of the angle between them.

The compounds described in the Chapter 3 contain a double bond between the tricyclic system and terpyridine. In this way, the energy of the steric interaction of the hydrogen atoms belonging to these two parts of the ligand is reduced, which makes possible the flattenning of the ligand. A smaller angle between the mean planes of the donor and acceptor fragments makes the conjugation more efficient, and increases the ability of the molecules to display nonlinear optical properties.

We adopted this idea to obtain ruthenium-nitrosyl complexes potentially more effective in TPA. The compound bpy1 was taken as a base for them (Figure 2.2). As a donor fragment, it was decided to use a fluorenyl substituent, which showed one of the highest values of the σ_{TPA} in the theoretical study comparing to heterocyclic 14 π-electronic aromatic systems.[116]

Thus, in order to find out how the diminution of the torsion angle will affect the efficacy of the compounds in TPA, we sought to obtain the compounds shown in Figure 4.1 – [Ru(FCCT)(bpy)NO](PF$_6$)$_3$ and [(FCC3T)(bpy)NO](PF$_6$)$_3$, wherein the organic ligands FCCT and FCC3T are the compounds (*E*)-4'-(2-(9,9-dihexyl-9*H*-fluoren-2-yl)vinyl)-2,2':6',2''-terpyridine and 4'-((9,9-dihexyl-9*H*-fluoren-2-yl)ethynyl)-2,2'6',2''- terpyridine respectively . Besides, inserting the multiple bond between two fragments will not only improve the conjugation but also enlarge the π-system of the molecule. Along with the decreasing of the angle, this effect would improve the polarizability of the system and consequently its ability to TPA.

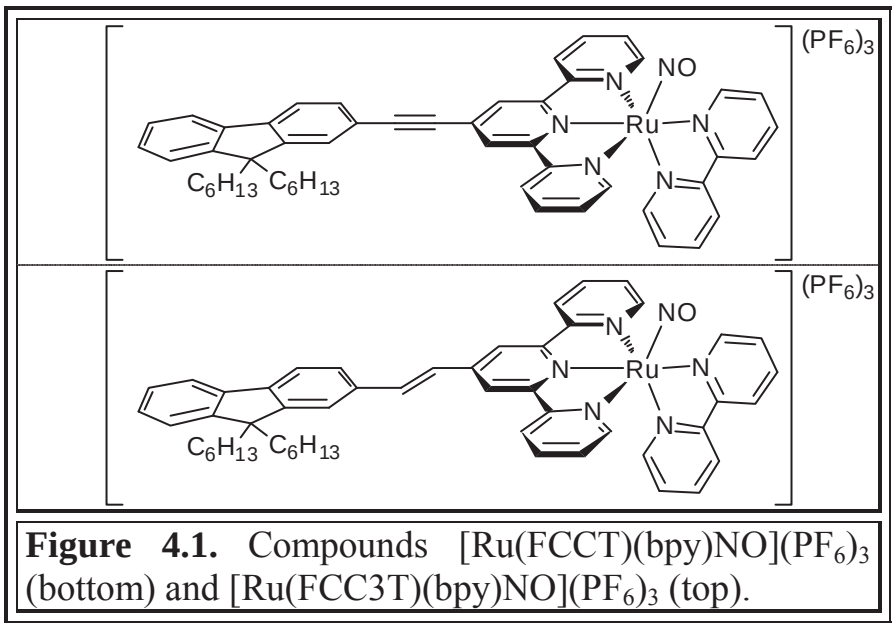

Figure 4.1. Compounds [Ru(FCCT)(bpy)NO](PF$_6$)$_3$ (bottom) and [Ru(FCC3T)(bpy)NO](PF$_6$)$_3$ (top).

According to the DFT calculations on these complexes, the angle between the terpyridine and fluorenyl mean planes indeed diminishes with the introduction of a multiple bond for the spatial separation of the two fragments. It acquires a lesser value in complex with a ligand containing a double bond, but the values of the cosine almost do not differ for both compounds, and are approximately equal to 1 (Table 4.1).

L =	FT	$\alpha = 31.99°$ ($\cos\alpha = 0.85$)
	FCCT	$\alpha = 1.56°$ ($\cos\alpha \approx 1$)
	FCC3T	$\alpha = 3.35°$ ($\cos\alpha \approx 1$)

Table 4.1. The values ot the angles between the mean plane of fluorenyl and terpyridine fragments in [Ru(L)(bpy)NO]$^{3+}$ and the corresponding cosine values.

4.1.1 The synthesis of FCCT and FCC3T ligands

An attempt to obtain the ligand FCCT containing a double bond between terpyridine and fluorene through a convergent synthesis method made it possible to obtain the compound in a very low overall yield. Given the fact that the final step of synthesis occurs with a yield of about 4%, the total yield made 0.3%. The scheme of synthesis followed is shown in Scheme 4.1.

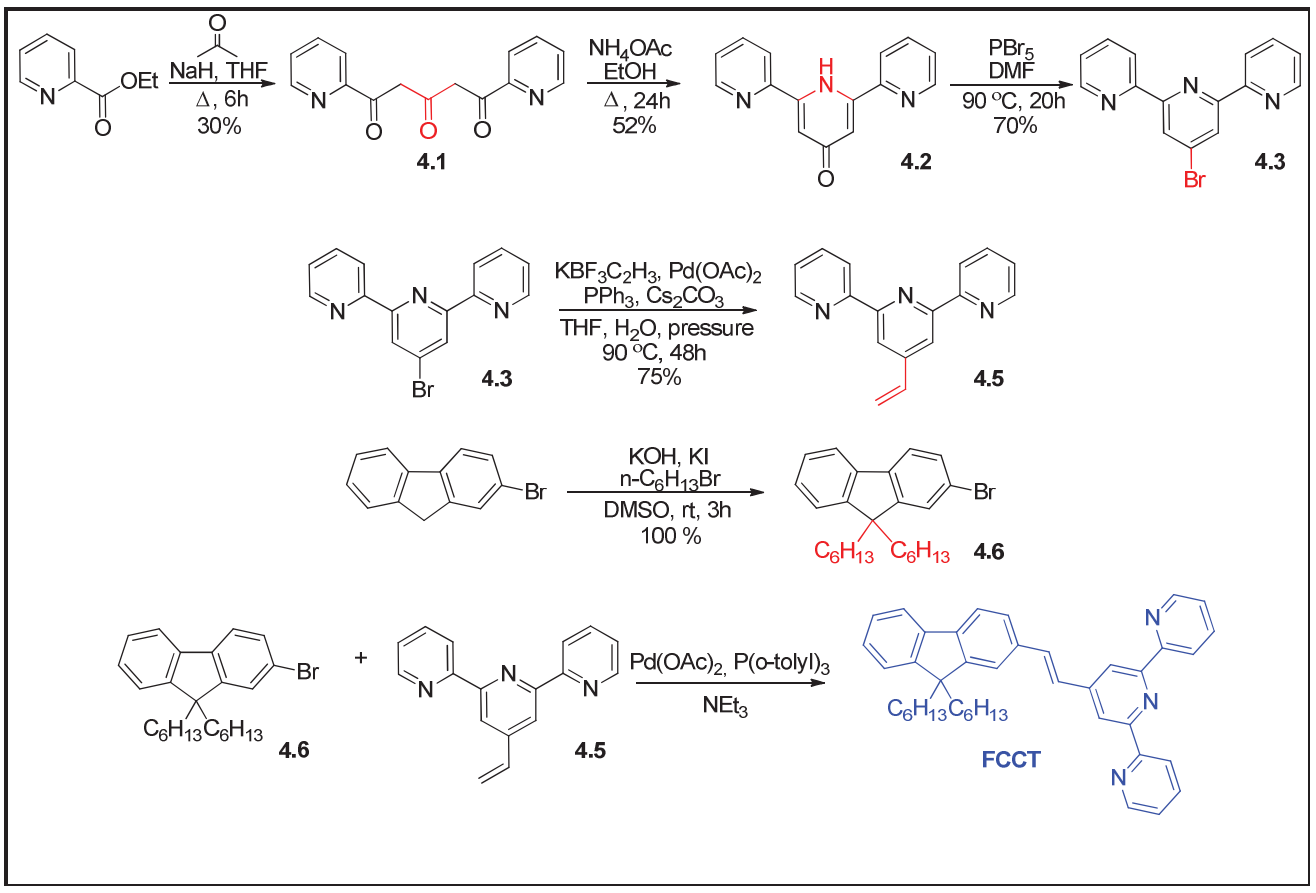

Scheme 4.1. Ligand FCCT synthesis by a convergent approach.

The terpyridine core was formed in two stages according to the approach previously utilized by Constable and Ward.[126] According to this method, at the first stage the Claisen condensation between 2-acetylpyridine and acetone leads to the obtaining of 1,5-di(pyridine-2-yl)pentane-1,3,5-trione **4.1**, and subsequent cyclization with ammonia makes possible the formation of the terpyridine central ring substituted at the 4th position (**4.2**). Depending on how carefully the compound **4.2** was purified, the peak around 11 ppm in the ^{1}H-NMR spectrum (DMSO-d6) may appear. This signal belongs to acetic acid, which according to the literature, forms a stable adduct 1:1 with ketone **4.2**.[127] This, however, does not have a significant influence on the proceeding of the next step. The conversion of **4.2** to the bromo derivative is usually carried out using $POBr_3$ as a solvent.[128] We've replaced the latter with a cheaper N,N-dimethylformamide that almost did not affect the yield of the reaction. Compound **4.5** was prepared according to the method described in the literature.[129]

In order to improve the solubility of the ruthenium-nitrosyl complexes up to that required for the TPA (10^{-2} M), we introduced two n-hexyl chains in the 9th position of the fluorenyl system, that was done at the first stage of the modification of the fluorene component. The last step of obtaining of FCCT ligand, namely the coupling reaction, occurs with a low yield, as noted above. Unfortunately, we were not able to identify the by-products of this reaction. Nevertheless, we have tried to increase the yield of the final stage of synthesis by modifying the conditions of the reaction and the catalyst.

In particular, we tried to change the position of the vinyl group. In this reaction modification, the aryl halide component of the Heck reaction was terpyridine triflate, while the vinyl moiety was attached to the fluorene. This alternative approach is shown in scheme 4.2.

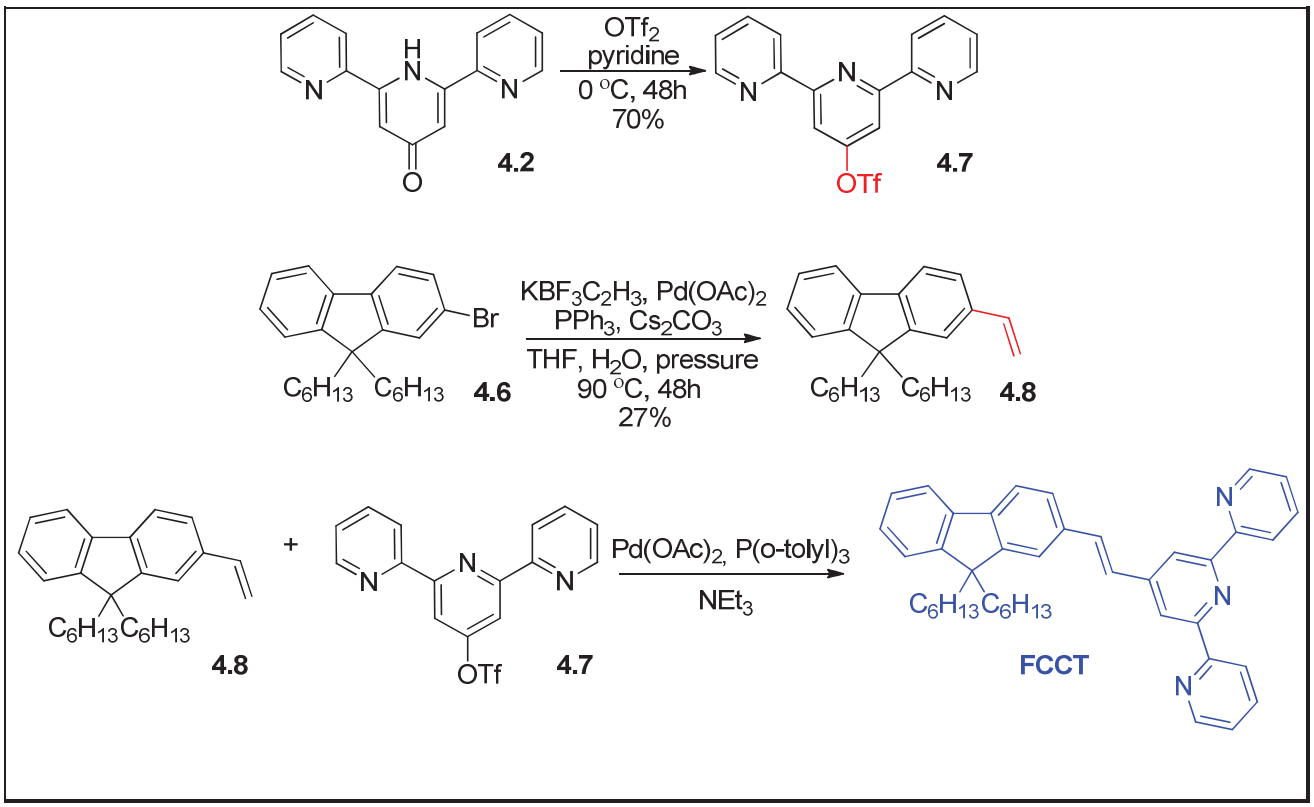

Scheme 4.2. An alternative way of FCCT synthesis.

The presence of a better leaving triflate group could facilitate the first stage of the reaction - the oxidative addition of terpyridine triflate to the catalyst. Such an

approach, however, did not lead to an increase of the yield of the last step of synthesis.

In order to try to improve the yield of FCCT synthesis, we varied the solvent used (Et_3N, dioxane, DMF) and the catalyst ($Pd(OAc)_2/PPh_3$, $Pd(OAc)_2/P(o\text{-}tolyl)_3$, $[Pd(PPh_3)_4]$). Either potash or Et_3N were used as bases. None of the studied variations of the reaction conditions resulted in a significant increase of the total yield of the ligand synthesis.

So far as previous attempts to obtain the compound were not effective, we decided to substantially change the approach of obtaining of FCCT ligand. Unlike the original convergent variant, the new path involves a linear transformation of the parent compound (Scheme 4.3).

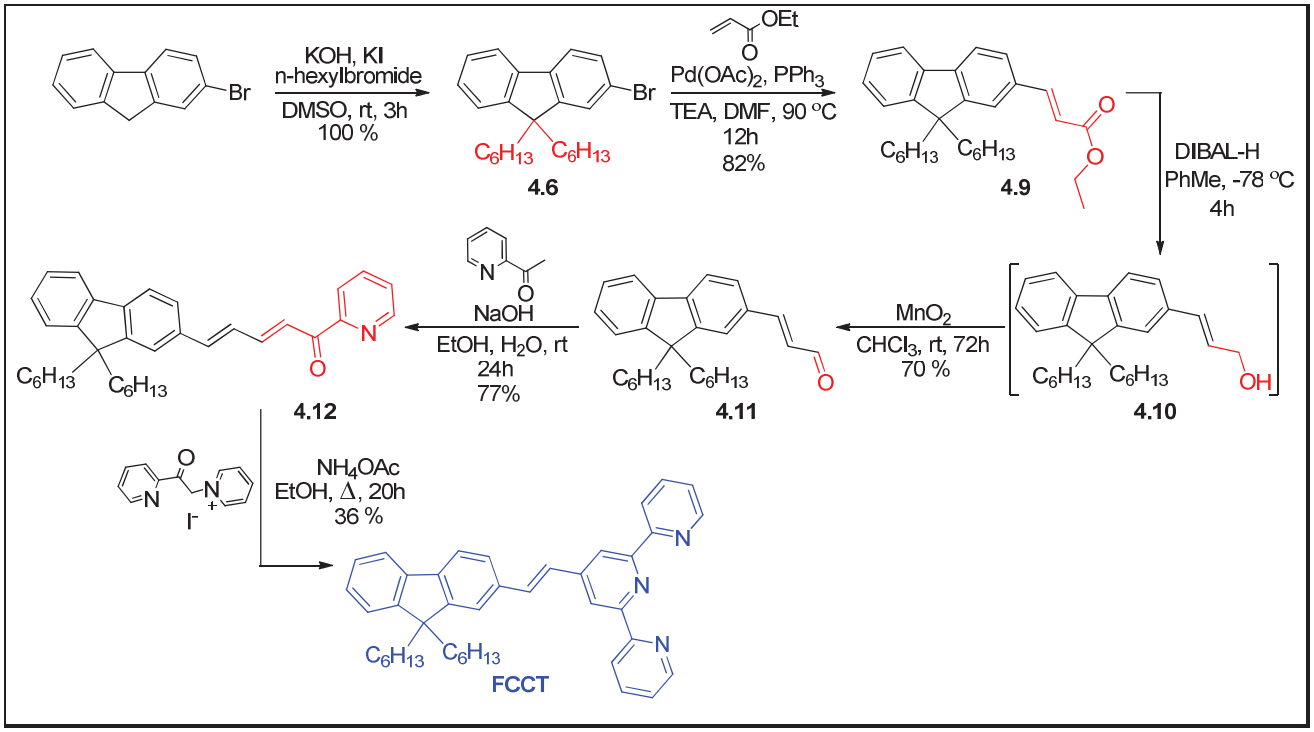

Scheme 4.3. The synthesis of FCCT ligand by a linear approach.

This method is based on the introduction of a double bond, already functionalized, through the Heck reaction between the alkylated bromofluorene **4.6** and ethyl acrylate. The further possibility of a direct transformation of the ester group into the terpyridine core eliminates the necessity for another coupling reaction. The cross-coupling stage was carried out according to an optimized technique described

in the literature for similar compounds.[130] The reduction of the ester **4.9** followed by the oxidation of the resulting allyl alcohol leads to the formation of the aldehyde **4.11**. As the reference for this step we took the procedure of the reduction of substituted acylates, well-described in the literature.[131] Then following the typical method of obtaining of terpyridines based on the Claisen condensation of corresponding aldehyde we received a chalcone **4.12**. A further Michael reaction between the compound **4.12** and the Kröhnke salt followed by heterocyclicization allowed obtaining of FCCT with the total yield of 11%. The mechanism of the reaction is given in scheme **4.4**.

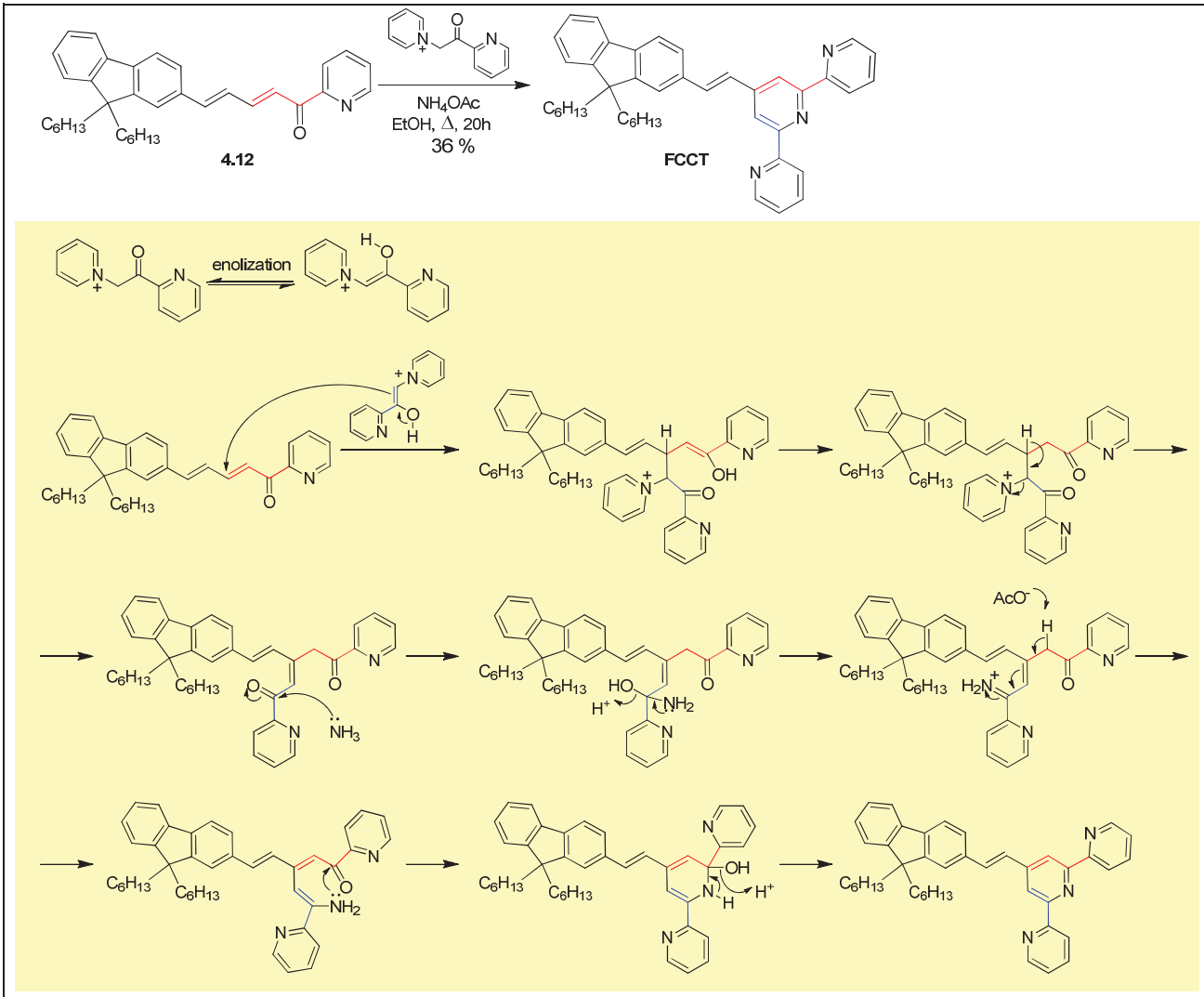

Scheme 4.4. Mechanism of Michael reaction between aldehyde 4.12 and the Kröhnke salt followed by heterocyclicization.

The structure of the FCCT molecule was confirmed by NMR (^{1}H, ^{13}C), 2D-NMR spectroscopy and high resolution mass spectrometry (HRMS).

The Kröhnke salt, 1-(2-oxo-2-(pyridin-2-yl)ethyl)pyridine-1-ium iodide was obtained according to the known methodology of the Ortoleva-King reaction, according to which 2-acetylpyridine interacts with pyridine solution of iodine (scheme 4.5).[132]

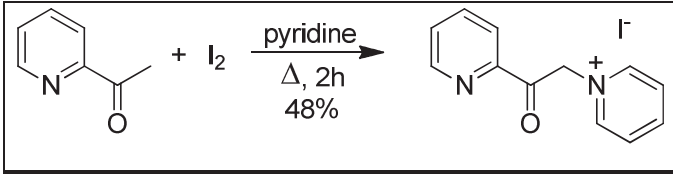

Scheme 4.5. The synthesis of the salt 1-(2-oxo-2-(pyridin-2-yl)ethyl)pyridine-1-ium iodide.

The ligand containing the triple bond between the donor and acceptor fragments of the complex was synthesized according to a convergent scheme in 7 steps (Scheme 4.6).

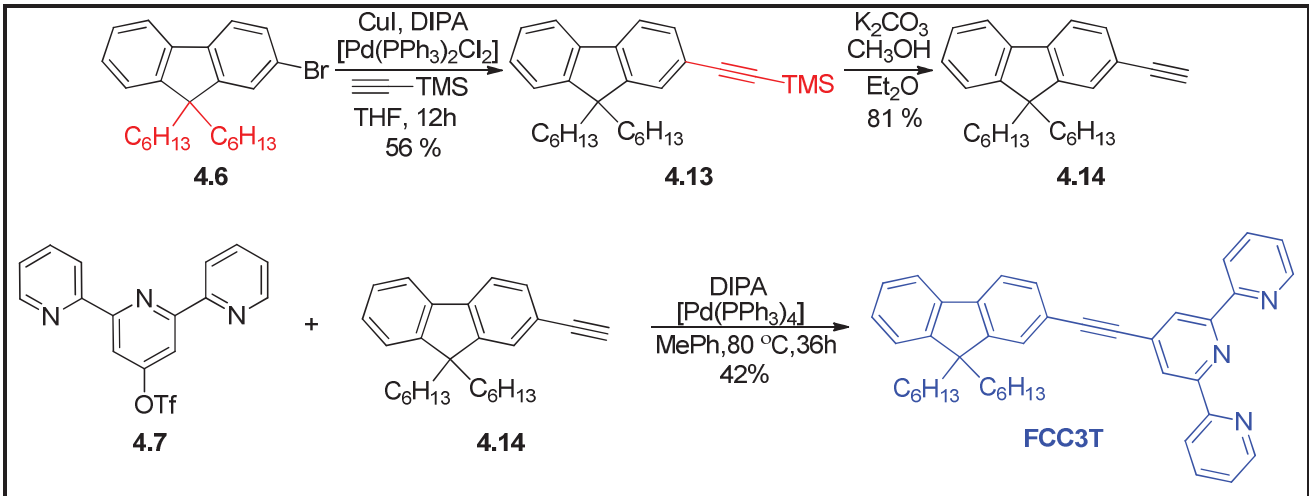

Scheme 4.6. The synthesis of FCC3T ligand.

The reaction of terpyridone **4.2** with triflate anhydride proceeds to give a good yield of terpyridine triflate **4.7**, which was confirmed by the appearance of the signal at -72.9 ppm in the ^{19}F-NMR spectrum.

The alkylated fluorene derivative **4.6** reacts with ethynyltrimethylsilane through Sonogashira cross-coupling giving the compound **4.13**; the trimethylsilyl group was subsequently removed under basic conditions with the formation of ethynylfluorene **4.14**.

The final step in the synthesis of the ligand is the reaction of cross-coupling of 2-ethynyl-9,9-di-hexyl-9*H*-fluorene **4.14** with (2,2':6',2"-terpyridin-4'-yl) trifluoromethylsulfonate **4.7** giving FCC3T with a yield of 42%. The total yield of ligand synthesis was 4.6%. The structure of the compound was confirmed by NMR (^{1}H, ^{13}C) and elemental analysis.

4.1.2 Synthesis of ruthenium-nitrosyl complexes with FCCT and FCC3T ligands

The first step of the synthesis of ruthenium-nitrosyl complexes with terpyridine ligands FCCT and FCC3T is the interaction of the latter with ruthenium (III) chloride (Scheme 4.7).

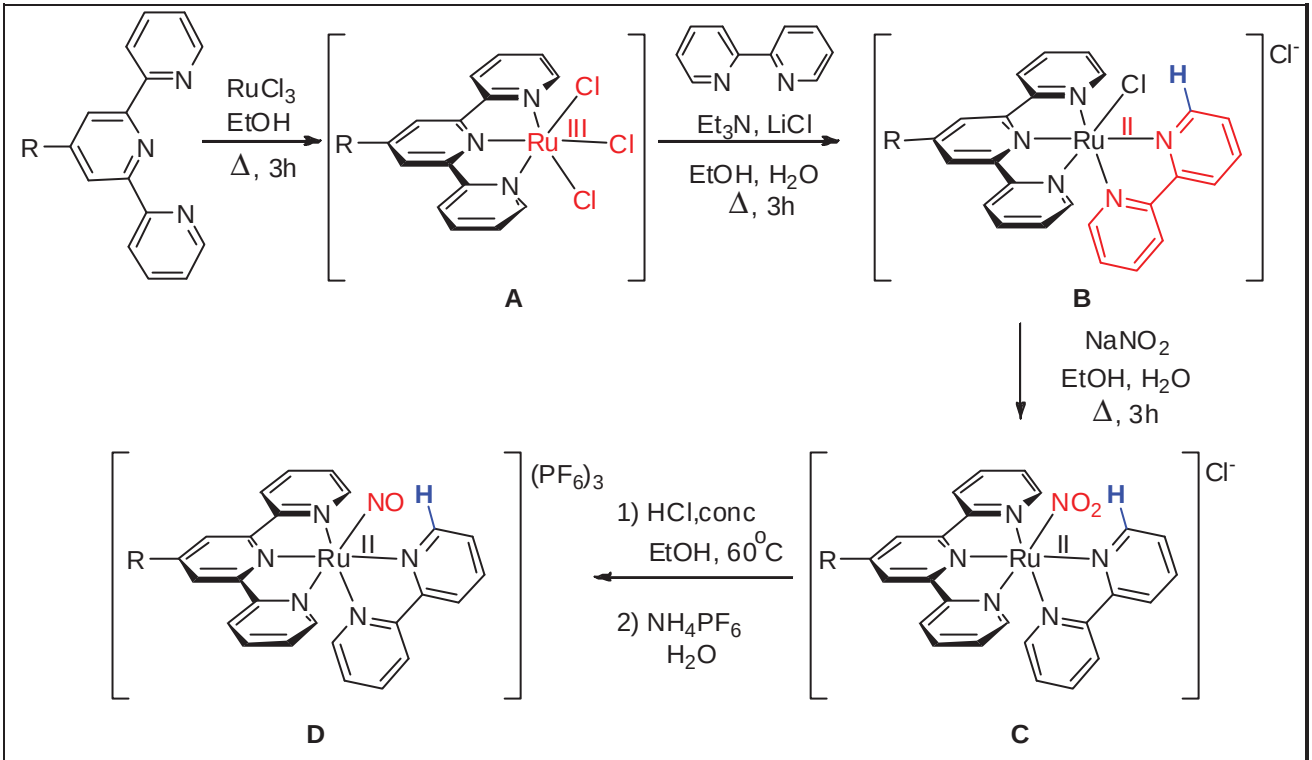

Scheme 4.7. The general scheme of the synthesis of ruthenium-nitrosyl complexes with terpyridine ligands FCCT and FCC3T and 2,2'-bipyridine. The chemical shift of the proton highlighted in blue is the most senstitive to the substitution of monodentate ligand.

The method of synthesis chosen differs from that used to obtain cis1 and trans1 compounds, in which the ruthenium-nitrosyl moiety is introduced into the structure of the complex in one step by the interaction of $K_2[RuCl_5(NO)]$ with a ligand.[86] The main advantage of a new approach is the reduced formation of undesirable homoleptic complexes $[Ru(tpy)_2]^{2+}$.

Thus the first stage of complex synthesis is the interaction of FCCT or FCC3T compounds with $RuCl_3$, which results in the formation of a paramagnetic complex A (Scheme 4.7). In the second step, A interacts with 2,2'-bipyridine in the presence of triethylamine to form a diamagnetic complex B. Use of triethylamine facilitates the reduction of Ru^{III} to Ru^{II}. A possible mechanism of this process is presented in Scheme 4.8.

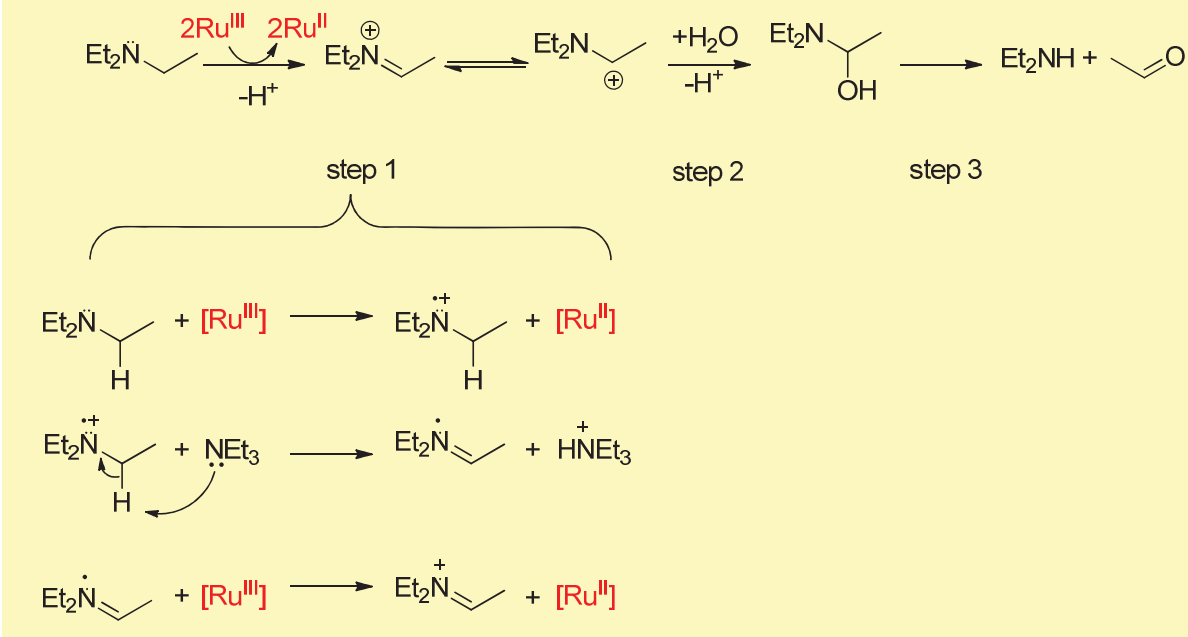

Scheme 4.8. The possible mechanism of Ru^{III} reduction

The assumption of the mechanism is based on previously proposed mechanisms for the reduction of transition metal complexes with amines.[133,134] These mechanisms involve the coordination of amines to metal atoms, with the subsequent inclusion of the latter in the adjacent C-H bond, which is accompanied by its breakage. The process ends up with the reduction of the metal center and the dissociation with the

proton elimination. A similar mechanism of the first stage of the process was published for a series of transition metal complexes (Pd, Rh, Fe, Ru, Au).[134,135,136] However, in the case of complexes assuming the octahedral geometry ($[Fe(CN)_6]^{3-}$, $[Ru(bpy)_3]^{3+}$) that apparently are not capable of coordinating an additional triethylamine molecule through an associative mechanism, the process of electron transfer from triethylamine molecule is likely to occur without direct bidning (step 1, scheme 4.8). Complex B is more likely to be attributed to this case.

An iminium cation formed as a result of the oxidation of triethylamine undergoes hydrolysis to carbinolamine (step 2, scheme 4.8) that breaks down to form diethylamine and acetaldehyde (step 3).

The use of lithium chloride in the second step of the synthesis prevents the formation of a significant amount of homoleptic complex due to the decreasing of the dissociation of chloro-ligands in the complex B.

The formation of complexes C and D can be easily monitored by NMR spectroscopy. The proton H(1) in position 6 of bipyridine (depicted in blue in scheme 4.7) is spatially approached to a single monodentate ligand present in the complex. Its chemical shift in the ^{1}H-NMR spectra strongly depends on the nature of this ligand (Cl, NO_2, NO). In fact, according to the crystallographic data for the analogous complex that will be described in Chapter 5 containing substituted terpyridine and 2,2'-bipyridine ligands ($[Ru^{II}(MeO\text{-}Phtpy)(bpy)(NO)](PF_6)_3$), the distance between proton H(1) and atoms of nitrosyl ligand N(1) and O(1) in the complex D are 2.595(1) and 2.719(1) Å respectively. Therefore the replacement of the ligand Cl^- with NO_2^- and finally with NO^+ leads to a gradual move of the peak of atom H(1) upfield. This effect is shown in Figure 4.2 for the FCC3T-based complex. When in addition to the terpyridine ligand and 2,2'-bipyridine the coordination polyhedron contains the Cl-atom, the chemical shift of the proton H(1) is 10.23 ppm (in CD3OD), whereas for its nitroanalogue the peak of the proton H(1) is at 9.90 ppm (in CD3OD). In the final ruthenium-nitrosyl complex the peak of the corresponding proton is located at 9.31 ppm (in CD3CN).

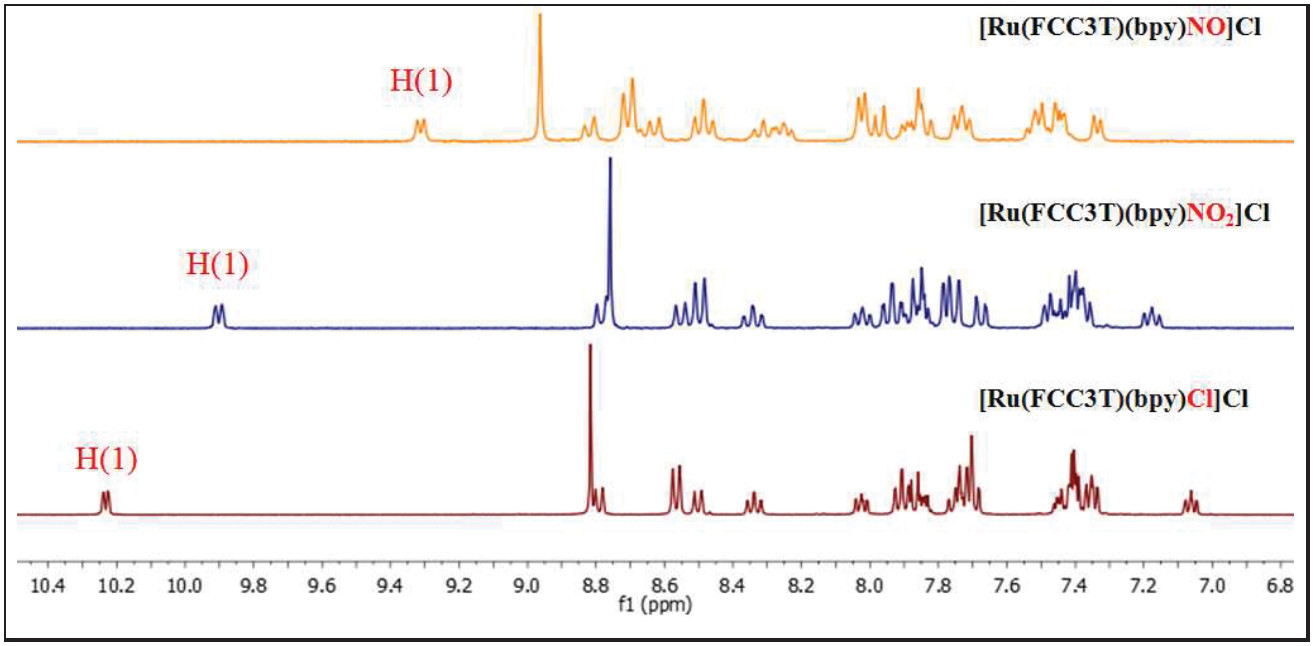

Figure 4.2. The changes in ^{1}H-NMR spectra when replacing the monodentate ligand in the structure of complex. Spectra of compounds [Ru(FCC3T)(bpy)Cl]Cl and [Ru(FCC3T)(bpy)NO_2]Cl are obtained from the solutions in CD_3OD, [Ru(FCC3T)(bpy)NO]Cl – from the solution in CD_3CN.

4.1.3 Electronic spectra of [Ru(FCCT)(bpy)NO]$(PF_6)_3$ and [Ru(FCC3T)(bpy)NO]$(PF_6)_3$.

Experimental electronic spectra of both complexes and spectra obtained from quantum-chemical computations are presented in Figure 4.3.

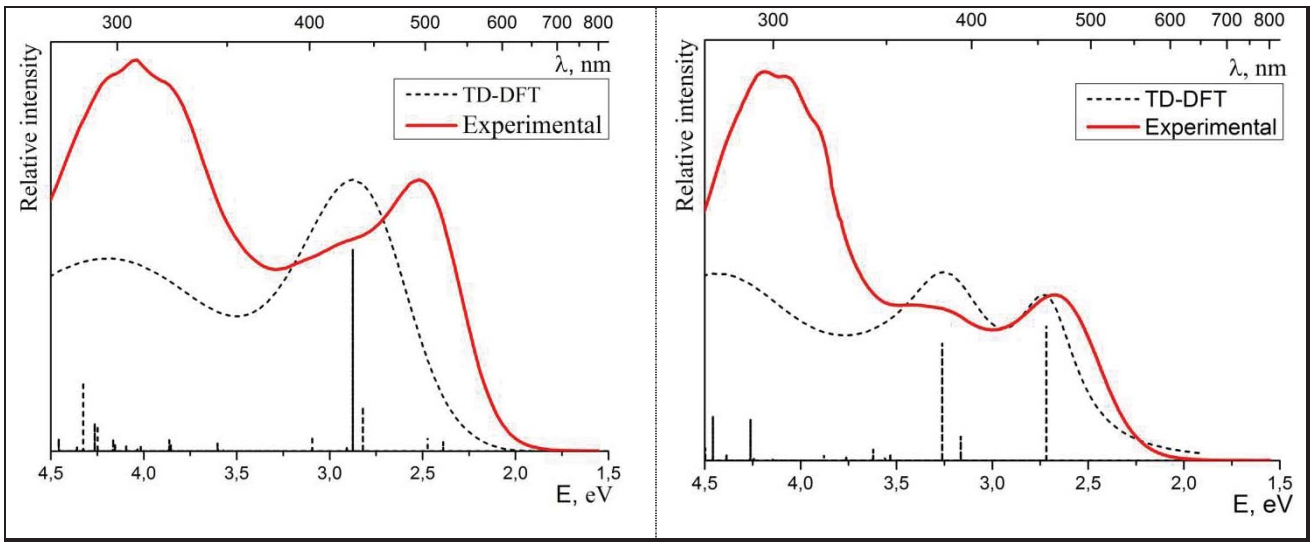

Figure 4.3. Experimental and computed electronic spectra of compounds [Ru(FCCT)(bpy)NO]$(PF_6)_3$ (left) and [Ru(FCC3T)(bpy)NO]$(PF_6)_3$ (right).

To facilitate the process of optimization of the geometries of molecular ions the quantum-chemical calculations were carried out on complexes containing methyl groups in the 9th position of the fluorenyl moiety instead of n-hexyls. This however doesn't affect significantly the distribution of electron density in the ion.

The most obvious difference of spectrum of the complex with FCC3T ligand from the one of the complex with FCCT ligand is the presence of two absorption bands in the region 350-500 nm, while the electronic spectrum of the compound $[Ru(FCCT)(bpy)NO](PF_6)_3$ shows only one absorption band at these wavelength. The spectra calculated by the TD-DFT method are in an acceptable agreement with the experimental results. The largest deviation of 0.35 eV can be observed for the low-energy band of the complex $[Ru(FCCT)(bpy)NO](PF_6)_3$.

The parameters of the absorption bands in the experimental and computed electronic spectra of the complexes $[Ru(FCCT)(bpy)NO](PF_6)$ and $[Ru(FCC3T)(bpy)NO](PF_6)_3$ are presented in Table 4.2 and Table 4.3, respectively.

	Experimental spectrum		Computed spectrum	
	λ_{max} (nm)	ε ($M^{-1}\cdot cm^{-1}$)	λ_{max} (nm)	f
Band 1	308	36 215	291	0.8189
Band 2	493	25 103	432	1.6337

Table 4.2. Absorption bands in experimental electronic spectrum of the compound $[Ru(FCCT)(bpy)NO](PF_6)_3$ compared to those of electronic spectrum for the ion $[Ru(FCCT)(bpy)NO]^{3+}$ computed by TD-DFT at CAM-B3LYP/6-31G* level of theory.

	Experimental spectrum		Computed spectrum	
	λ_{max} (nm)	ε ($M^{-1}\cdot cm^{-1}$)	λ_{max} (nm)	f
Band 1	296	47 386	279	0.8010
Band 2	375	18 729	381	0.8425
Band 3	465	20 200	457	0.8027

Table 4.3. Absorption bands in experimental electronic spectrum of the compound $[Ru(FCC3T)(bpy)NO](PF_6)_3$ compared to those of electronic spectrum for the ion $[Ru(FCC3T)(bpy)NO]^{3+}$ computed by TD-DFT at CAM-B3LYP/6-31G* level of theory.

Detailed descriptions of electronic transitions responsible for the appearance of bands in the UV-visible spectra of compounds [Ru(FCCT)(bpy)NO](PF$_6$)$_3$ and [Ru(FCC3T)(bpy)NO](PF$_6$)$_3$ are presented in Tables 4.4 and 4.5, respectively.

Transition	λ_{max}	f	Dominant contribution	Character
Band 1				
0 → 25	293	0.1725	16% $\chi_{160} \rightarrow \chi_{175}$ + 8% $\chi_{171} \rightarrow \chi_{176}$ + 7% $\chi_{173} \rightarrow \chi_{176}$	bpy → bpy + NO
0 → 26	291	0.1857	21% $\chi_{168} \rightarrow \chi_{177}$ + 16% $\chi_{167} \rightarrow \chi_{183}$	tpy +bpy → tpy
0 → 27	287	0.4607	53% $\chi_{174} \rightarrow \chi_{182}$	fluorene → tpy + -C=C-
Band 2				
0 → 6	441	0.2951	34% $\chi_{169} \rightarrow \chi_{175}$ + 22% $\chi_{167} \rightarrow \chi_{175}$ + 22% $\chi_{170} \rightarrow \chi_{175}$	Ru(bpy)NO → Ru(bpy)NO
0 → 7	432	1.3386	64% $\chi_{174} \rightarrow \chi_{177}$	fluorene + -C=C- → tpy + -C=C-

Table 4.4. TD-DFT computed absorption maxima, oscillator strengths and configurations of electronic transitions of the cation[Ru(FCCT)(bpy)(NO)]$^{3+}$. Orbital 174 is HOMO, orbital 175 – LUMO.

Transition	λ_{max}	f	Dominant contributions	Character
Band 1				
$0 \rightarrow 18$	292	0.2466	66% $\chi_{169} \rightarrow \chi_{176}$	tpy → Ru(tpy)NO
$0 \rightarrow 21$	279	0.2632	35% $\chi_{166} \rightarrow \chi_{174}$ + 17% $\chi_{173} \rightarrow \chi_{180}$	tpy + fluorene → Ru(tpy)NO
$0 \rightarrow 26$	270	0.2912	85% $\chi_{168} \rightarrow \chi_{177}$	bpy → bpy
Band 2				
$0 \rightarrow 4$	393	0.1439	67% $\chi_{165} \rightarrow \chi_{175}$	Ru(bpy) → Ru(NO)
$0 \rightarrow 6$	381	0.6986	55% $\chi_{173} \rightarrow \chi_{176}$	fluorene → Ru(tpy)NO
Band 3				
$0 \rightarrow 1$	457	0.8027	76% $\chi_{173} \rightarrow \chi_{174}$	fluorene → Ru(NO)

Table 4.5. TD-DFT computed absorption maxima, oscillator strengths and configurations of electronic transitions of the cation$[Ru(FCC3T)(bpy)(NO)]^{3+}$. Orbital 173 is HOMO, orbital 174 – LUMO.

The analysis of orbitals involved in the electronic transitions in the cation $[Ru(FCCT)(bpy)(NO)]^{3+}$ shows that none of the possible excitations of a molecule results in an activation of the transfer of electron density directly from fluorenyl fragment to the {RuNO} center, and the least energetic intense transition (0 → 7) occurs purely within the fluorenyl-terpyridine ligand.

A completely different picture is observed for the ion $[Ru(FCC3T)(bpy)(NO)]^{3+}$. Both low-energy absorption bands (λ = 465 nm, λ = 375 nm) appear due to the presence of transitions in which the electron density moves from fluorene to the strongly accepting ruthenium-nitrosyl fragment (Table 4.5).

Although similar transitions are still present in the compound $[Ru(FCCT)(bpy)(NO)](PF_6)_3$ their intensity is very small. In particular, the transition to the second excited state (λ = 559 nm) is basically a HOMO-LUMO (71%) transition and this excitation causes the electron transfer from fluorene to {Ru(bpy)NO}, however, we do not observe such an absorption neither in the theoretical computed spectrum nor in the experimental because of its low intensity (f = 0.0009). An explanation for this may be the orthogonality of the HOMO (π of fluorene-terpyridine) and the LUMO (dπ* of RuNO) orbitals (Figure 4.4), and therefore the impossibility of the efficient transfer of the electron from the donor to the acceptor.

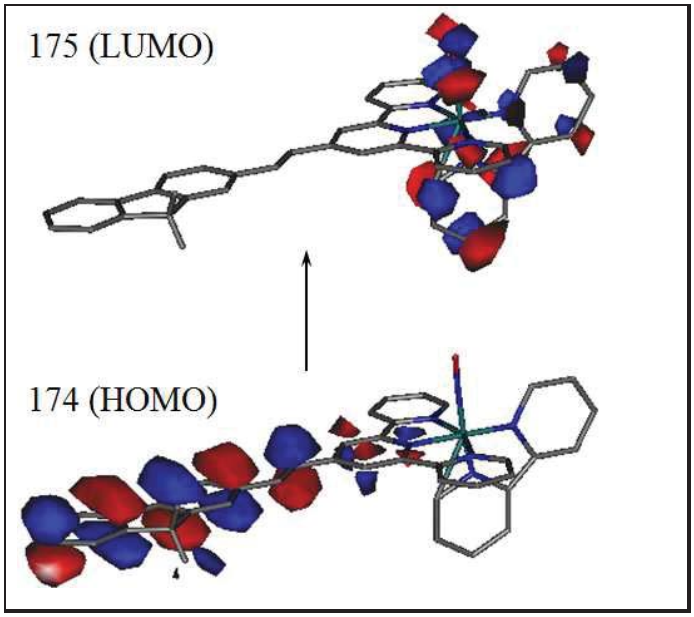

Figure 4.4. HOMO and LUMO orbitals of the cation $[Ru(FCCT)(bpy)(NO)]^{3+}$.

Another transition, which, according to calculations, involves the contribution of the electronic density transfer from fluorene to the ruthenium-nitrosyl fragment, is the transition 0 → 6 at λ = 441 nm. According to Table 4.4, this excitation doesn't imply the charge transfer from fluorene to ruthenium-nitrosyl moiety, but as little as 4% of contribution to 0 → 6 is still made by the excitation $\chi_{174} \rightarrow \chi_{176}$, where 174 - HOMO,

and 176 is an orbital located on the {RuNO}-fragment and rotated by an angle of 90° around the axis Ru-N relative to the orbital 175 (LUMO), shown in Figure 4.4. This arrangement of the orbitals 174 and 176 makes it possible the electron transfer from fluorene to the ruthenium-nitrosyl fragment, but its small contribution to the transition 0 → 6 makes it ineffective.

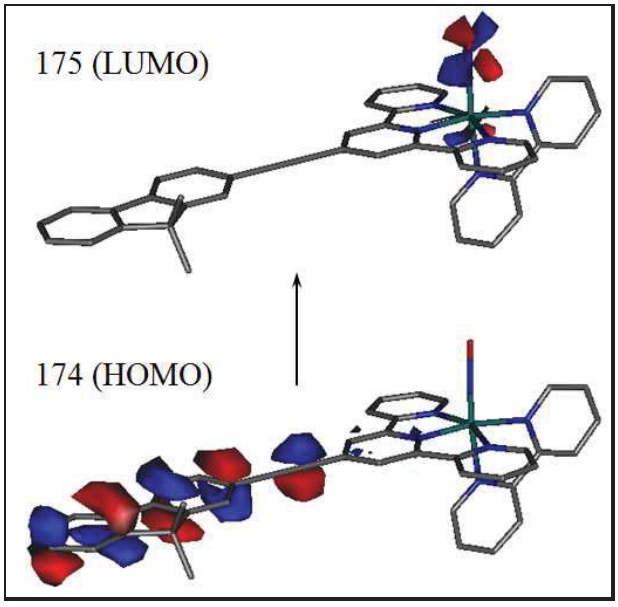

Figure 4.5. HOMO and LUMO orbitals of the cation $[Ru(FCC3T)(bpy)(NO)]^{3+}$.

As opposed to the compound $[Ru(FCCT)(bpy)(NO)](PF_6)_3$, all transitions in the complex with FCC3T ligand implying fluorene → {RuNO} contribution have significant intensity, and in particular, the HOMO and LUMO orbitals involved in the least energetic electron transition 0 → 1 and inducing the appearance of the band 3, are not orthogonal (Fig. 4.5).

Taking into account the results of the theoretical study, we assumed that the release of nitric oxide under irradiation of the complex with triple bond would be much more effective than in the case of the complex with the ligand FCCT.

4.1.4. The study of NO-release from complexes $[Ru(FCCT)(bpy)NO](PF_6)_3$ and $[Ru(FCC3T)(bpy)NO](PF_6)_3$

The investigation of the process of nitric oxide photorelease from complexes was carried out on their solutions in acetonitrile. The excitation occurred at a wavelength λ = 436 nm. This wavelength corresponds to the transition 0 → 7 in the compound with double bond and lies between transitions 0 → 1 and 0 → 6 in the compound with triple bond. Thus both exciations provide very different charge transfer character: ligand-to-ligand in $[Ru(FCCT)(bpy)NO](PF_6)_3$ and ligand to RuNO in $[Ru(FCC3T)(bpy)NO](PF_6)_3$. The change in the electronic spectra of

acetonitrile solutions of compounds observed during the experiment is presented in Figure 4.6.

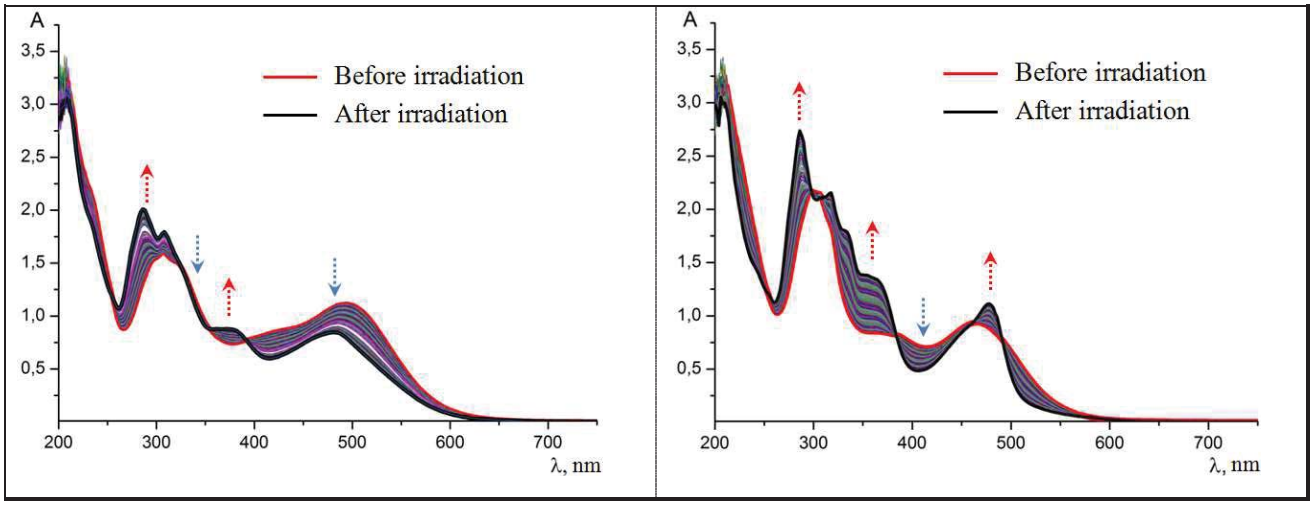

Figure 4.6. The changes in electronic spectra of acetonitrile solutions of compounds $[Ru(FCCT)(bpy)(NO)](PF_6)_3$ (left) and $[Ru(FCC3T)(bpy)(NO)](PF_6)_3$ (right) observed under irradiation with electromagnetic waves $\lambda = 436$ nm.

The presence of sharp isosbestic points in both cases (393, 354, 327, 255 nm – compound $[Ru(FCCT)(bpy)(NO)](PF_6)_3$; 491, 461, 383, 253 – compound $[Ru(FCC3T)(bpy)(NO)](PF_6)_3$) indicates the direct transformation of the starting complexes into final photoproduct without the formation of intermediates. The back-reaction was not observed when the irradiation of the solutions was suspended. Interestingly, the quantum yield of the photoreaction of the nitric oxide release for both compounds was the same – 0.03. This contradicts the assumption that a compound in which the excitation results in the transfer of electron density from the fluorene to ruthenium nitrosyl fragment – $[Ru(FCC3T)(bpy)(NO)](PF_6)_3$ – should display an enhanced value of NO-release quantum yield. Obviously, the transition of the electron density from the donating moiety of the complex to the antibonding orbital located on the fragment {RuNO} is not the only factor that influences the efficiency of the photoactivation of NO-release.

It should be noted that, as in the case of bpy1, the absence of a wide absorption band in the spectra of photoproducts in the region of 500-700 nm may indicate the

formation of the complex with ruthenium in oxidation state +2 – $[Ru(FCCT)(bpy)(CH_3CN)]^{2+}$ and $[Ru(FCC3T)(bpy)(CH_3CN)]^{2+}$.

4.1.5 The study of two-photon absorption of compounds $[Ru(FCCT)(bpy)(NO)](PF_6)_3$ and $[Ru(FCC3T)(bpy)(NO)](PF_6)_3$

Investigation of two-photon absorption of both complexes was carried out at different values of the intensity of laser radiation. The increase in the energy of laser pulses (which corresponds to an increase in the intensity of the exciting light) leads to an almost linear decrease in the transmission of radiation by a sample (Figure 4.7). This fact, as well as the absence of significant distortion of the background transmission line, suggests that other effects, other than two-photon absorption, do not occur during the experiment. The transmission curves are shown in Figure 4.7.

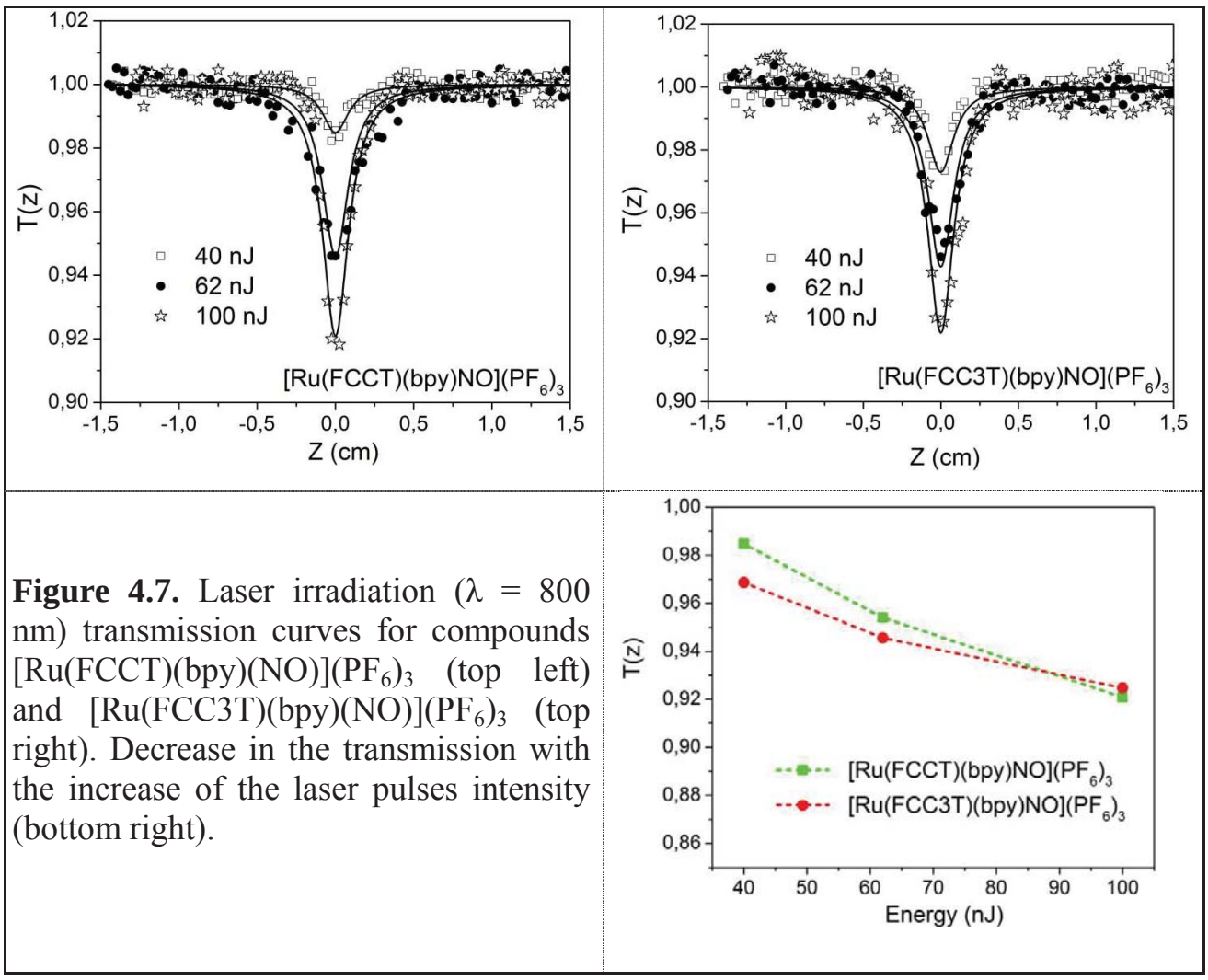

Figure 4.7. Laser irradiation (λ = 800 nm) transmission curves for compounds $[Ru(FCCT)(bpy)(NO)](PF_6)_3$ (top left) and $[Ru(FCC3T)(bpy)(NO)](PF_6)_3$ (top right). Decrease in the transmission with the increase of the laser pulses intensity (bottom right).

The obtained values of the two-photon absorption coefficients and the corresponding values of the TPA cross-sections are summarized in Table 4.6.

Compound	$\beta \cdot 10^{11}$ cm/W	σ, GM
$[Ru(FCCT)(bpy)(NO)](PF_6)_3$	3.17	131
$[Ru(FCC3T)(bpy)(NO)](PF_6)_3$	3.63	150

Table 4.6. Two-photon absorption coefficients β and the corresponding values of the TPA cross-sections σ for compounds cis2, trans2, bpy2.

Thus, the introduction of a multiple bond between the donor group and the acceptor terpyridine ruthenium-nitrosyl fragment in the organic ligand reduces the steric interaction between two moieties and increases the polarizability of the compound. This leads to a more efficient interaction of the π-systems of both parts of the ligand and facilitates the process of intramolecular charge transfer. This effect manifests itself in the bathochromic shift of low-energy electronic transitions in the compounds and the increase of their efficiency in two-photon absorption. The compound $[Ru(FCCT)(bpy)(NO)](PF_6)_3$ exhibits a slightly lower capacity for two-photon absorption at wavelength λ = 800 nm compared to the $[Ru(FCC3T)(bpy)(NO)](PF_6)_3$ complex. The introduction of the triple bond leads to an increase in the TPA cross-section by 40%, while the double bond causes an increase of σ only by 21%. An explanation for such a difference could be the configuration of the electronic transitions of both compounds, namely: none of the electronic transitions in the molecular ion $[Ru(FCCT)(bpy)(NO)]^{3+}$ by its nature is the transfer of the electronic density from fluorene to {RuNO}-moiety, thus there is no possibility of an intense transition with a significant change in the dipole moment of the molecule.

4.2. Influence of the donating ability of the substituents in terpyridine ligands on the efficiency of ruthenium-nitrosyl complexes in TPA.

The capacity of compounds for TPA depends on many factors. One of the key parameters of a molecule which determines its ability to absorb two photons of a

given energy is the symmetry of a molecule. In particular, it is known that the selection rules for transitions in centrosymmetric molecules differ from those for noncentrosymmetric molecules, and the spectra of two-photon and single-photon absorption are often very different.[104] Ruthenium-nitrosyl complexes studied within the scope of the work refer to noncentrosymmetric dipolar compounds. As indicated in Chapter 3, an approximate two-level model can be used to estimate the TPA cross-section of polar molecules, in which the excitation results in an intense transfer of electronic density. According to this model, σ can be described by formula 3.1 (see chapter 3):

$$\boldsymbol{\sigma_{TPA} \approx \frac{16\pi^2 f(\mu_{ee} - \mu_{gg})^2}{5\hbar^2 c^2 \Gamma E_{ge}}}$$

Enhancement of conjugation in the chain of π-bonds between a donor and an acceptor in a molecule results in a decrease of the energy gap between HOMO and LUMO, which reduces the E_{ge} value, and increases the intensity of the transition (f). These changes eventually lead to some growth of σ. Another factor that has a significant effect on the absorption cross section is the change in the dipole moment ($\Delta\mu = \mu_{ee} - \mu_{gg}$) of the molecule during excitation, and σ depends on this parameter quadratically.

The increase in the Δμ-parameter can be achieved by increasing the polarity of the molecule. In this case, in the presence of a highly withdrawing ruthenium-nitrosyl site, the introduction of an electron-rich donating group into the structure could provide a significant increase in the dipole. Fluorene partially plays the role of such a group, but an additional increase in its donating ability will allow us to understand how the increase in the polarity and push-pull nature of the molecule will affect its capacity for TPA. Therefore, we attempted to introduce a donor substituent in the fluorenyl fragment of terpyridine ligand. The dimethylaminogroup (DMA) was chosen as such a substituent. The target ligands thus were DMAFT and DMAFCCT (Figure 4.8).

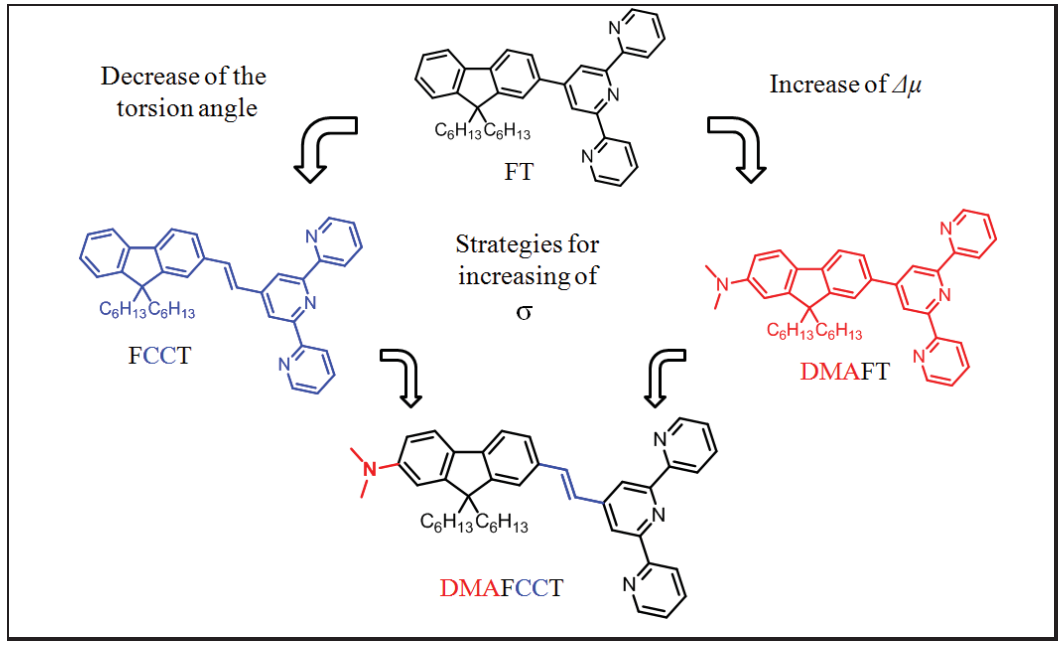

Figure 4.8. Strategies for increasing of TPA cross-section through modification of the terpyridine ligand structure.

4.2.1. Syntheses of the ligands DMAFT, DMAFCCT and ruthenium-nitrosyl complexes based on them.

At the first attempt the DMAFT ligand was obtained in 7 steps (Scheme 4.9).

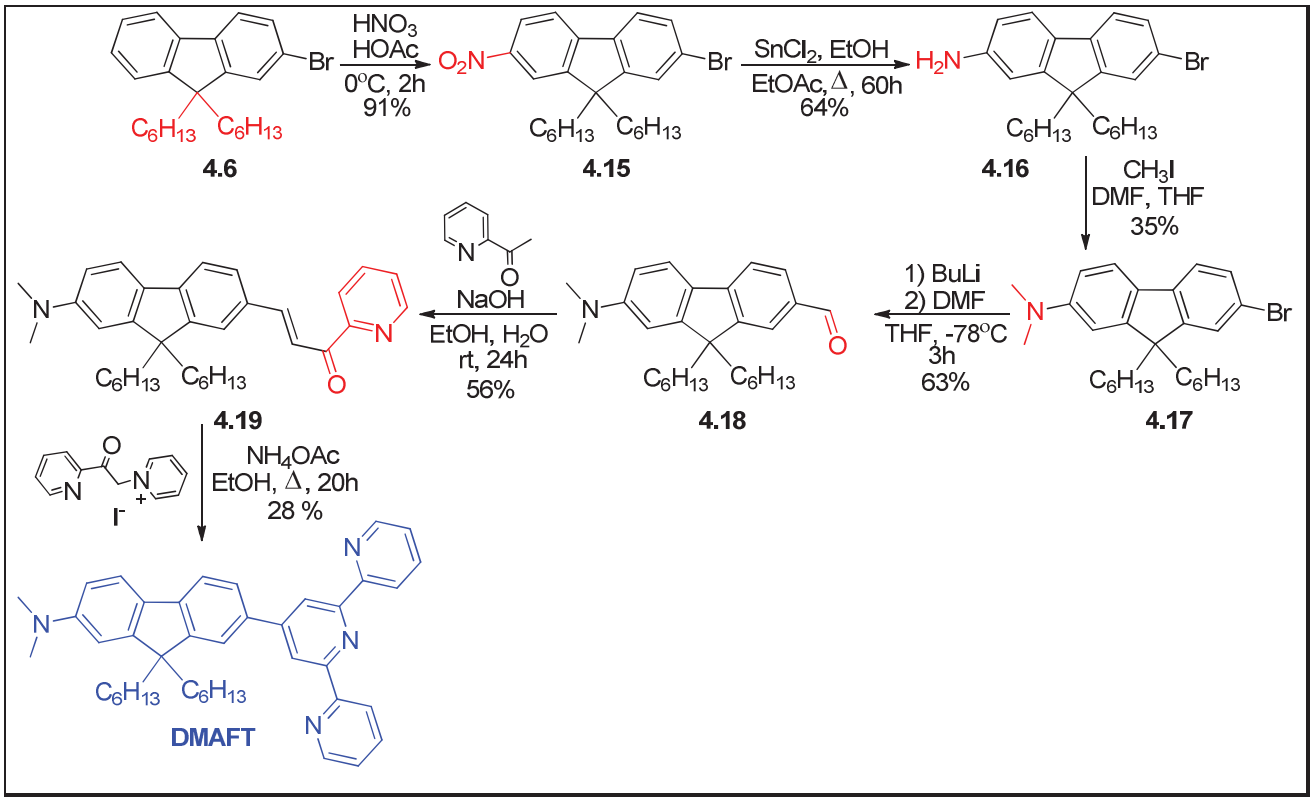

Scheme 4.9. The scheme of DMAFT synthesis.

The first four of them are the modification of the fluorenyl moiety – the introduction of n-hexyl substituents to form compound **4.6**, its nitration (compound **4.15**), the reduction of the nitrogroup in the position 7 to the amino-function (compound **4.16**), and subsequent methylation of the latter to form 7-bromo-9,9-dihexyl-N, N-dimethyl-9*H*-fluorene-2-amine (**4.17**). The modification was carried out by a slightly modified approach, described in the literature.[137] The last two steps of synthesis – condensation with 2-acetylpyridine and the Michael reaction followed by heterocyclicization – were carried out similarly to the reactions used to synthesize the FCCT compound, although with somewhat lower yields. Thus, the total yield of the DMAFT compound synthesis made 2%.

An attempt to optimize the synthesis path made it possible to increase the total yield of the product to 6%. The lowest yield among all the steps of synthesis was observed for methylation of aminogroup process. Along with the formation of a desired product in the reaction mixture there was a monomethylated derivative and the starting material, while the use of larger quantities of methyl iodide did not allow the production of exclusively dimethylaminofluorenyl derivative; though all three compounds could be isolated by column chromatography and re-introduced to the reaction.

In the year 2014, another method for the obtaining of dimethylamino derivatives of aromatic compounds was published. The starting compounds for these amines according to the approach are corresponding nitro compounds (Scheme 4.10).[138,139]

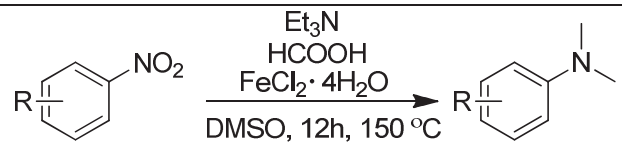

Схема 4.10. Obtention of aromatic tertiary amines in one step from corresponding nitro derivative.

This method is not yet widely used, but allows to obtain a dimethylamino derivative in one step without the use of toxic methylating reagents, such as methyl iodide or dimethyl sulfate. The transformation occurs in one step, in the presence of

Fe^{2+} ions playing the role of catalyst. The methylating agent in the reaction is dimethyl sulfoxide. The mechanism of the reaction involves the primary reduction of nitrofluorene to the corresponding amine. This is the point where, according to the studies of Beller and colleagues, iron ions play the role of a catalyst, and formic acid acts as a donor of hydrogen atoms.[140] The acylation of DMSO leads to the formation of an intermediate, which, by the Pummerer rearrangement transforms into methylene sulphonium cation **4.20** (Scheme 4.11).

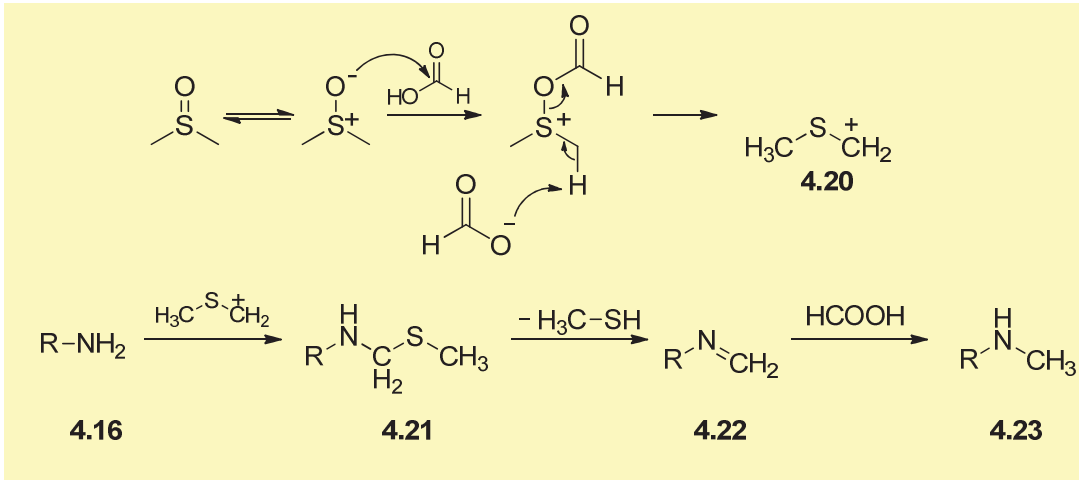

Scheme 4.11. The mechanism of methylation fo aromatic aminogroup by DMSO in the presense of formic acid (R = 7-bromo-9,9-dihexy.-9*H*-fluoren-2-yl).

The subsequent nucleophilic attack of amine leads to the formation of compound **4.21**, and elimination of methylthiol from **4.21** leads to the imine **4.22**, which by-turn being reduced with formic acid produces a monomethyl derivative. Acting as a nucleophile the intermediate product **4.23** attacks the cation **4.20** once again that results in the formation of a dimethylaminogroup.

The yield of the methylation reaction in such conditions is 63%, while the approach involving the transformation of nitro compound in dimethylamine derivative in two steps through the reduction step in total makes 22%. Thus we increased the yield of the synthesis of DMAFT ligand almost three times, which eventually made 6%.

An attempt to obtain DMAFCCT by a convergent synthesis method (8 steps) similar to those shown in Schemes 4.1 and 4.2 for compound FCCT was ineffective.

The total yield was 0.2%. As in the case of the FCCT synthesis, the last stage, namely the Heck coupling between compounds **4.17** and **4.5**, proceeds with a very low yield of 3%.Therefore, the DMAFCCT synthesis was carried out according to a linear scheme, which is a combination of methods for obtaining of FCCT and DMAFT. The first three steps are analogous to the first stages of the synthesis of DMAFT (Scheme 4.9), the last five steps – are similar to the conversion of compound **4.6** to the final FCCT ligand (Scheme 4.3), with the only difference that the fluorene in this case contained a dimethylaminogroup.

However, the introduction of the donor function into the fluorene structure substantially changed the passage of the step of coupling with ethyl acrylate and the subsequent transformation of the ester group. In particular, the yield of Heck reaction between ethyl acrylate and compound **4.17** was almost 4 times lower than for a similar reaction of compound **4.6**, which proceeded under the same conditions (Scheme 4.12).

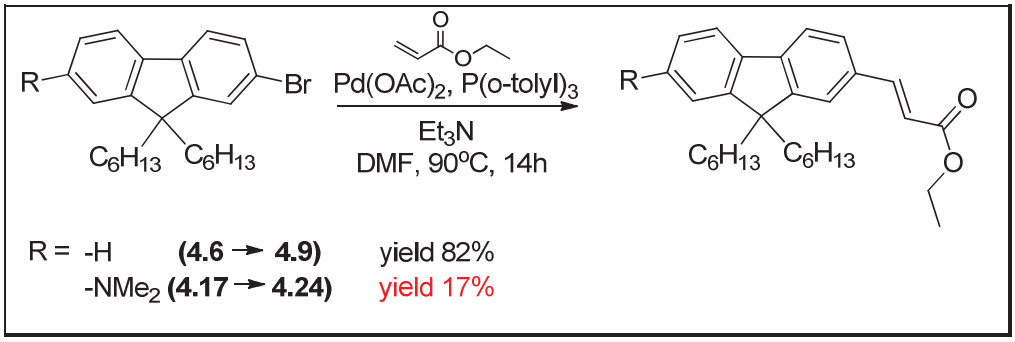

Scheme 4.12. Comparison of the yields of coupling reaction of ethyl acrylate with 2-bromofluorene (**4.6**) and its dimethylamino analogue (**4.17**) before the optimization.

An attempt to replace the catalytic system $Pd(OAc)_2/P(o\text{-tolyl})_3$ with another palladium catalyst -$[Pd(PPh_3)_4]$ increased the yield by only 2%. However, in the case when both catalysts were introduced into the reaction mixture the yield of compound **4.24** made 77%.

The following transformations performed to obtain the DMAFCCT compound are shown in Scheme 4.13.

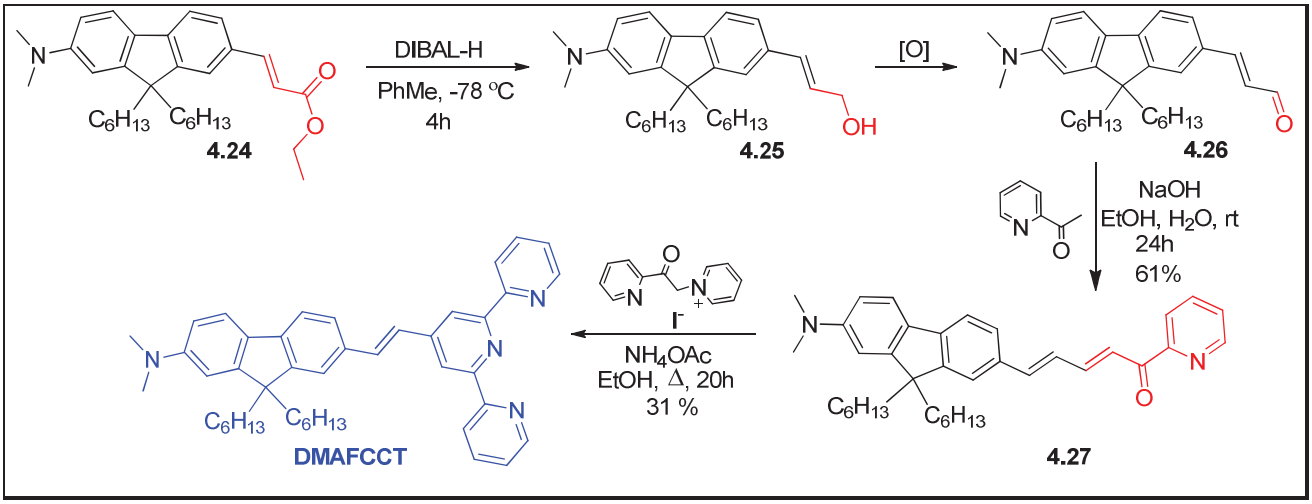

Scheme 4.13. The synthesis of DMAFCCT.

The reduction of the ester **4.24** with diisobutylaluminum hydride leads to the formation of an alcohol **4.25**, which under oxidation converts to aldehyde **4.26**. A similar transformation for compound **4.9** (analogue of compound **4.24** without dimethylamino) readily occurs. However, the reduction and further oxidation of compound **4.24** is not so easy to perform.

According to the methodology compound **4.25** is not to be purified and after being isolated from the reaction mixture, it is introduced in the next step with possible impurities present therein. This procedure reduces the possibility of side reactions of this allyl alcohol possible when it is exposed to the air. In the analogous case of the synthesis of the FCCT compound, an allyl alcohol obtained by the reduction of the corresponding ester was dissolved in $CHCl_3$ and oxidized with a manganese(IV) oxide that resulted in the formation of a desired aldehyde with a good yield. However, even during a short-term exposure of the compound **4.25** to the air, it undergoes certain transformations that are easy to observe with the help of thin-layer chromatography (TLC). Quickly, instead of one pale yellow with blue fluorescence spot, corresponding to the alcohol **4.25** another one appears, having a slightly lower value of R_f. The subsequent oxidation of the mixture of these two products leads to the formation of the desired aldehyde **4.26** and another product. Moreover, the ratio

between the values of R_f for these two components of the mixture is the same as for the compounds in the previous step.

Unfortunately, we were not able to identify the structure of by-products. One of the possible unwanted reactions that occur with compound **4.25** may be an allyl rearrangement. As has been shown in the studies of Jin Qu,[141] allyl alcohols are capable of undergoing rearrangement in the presence of water, albeit at elevated temperatures. Thus heating of their aqueous solutions to 40-100 °C leads to isomerisation of allyl alcohols with yields from 56% to 99%, while water plays the role of acid catalyst. It was also found that the presence of donor groups conjugated with π-bond of allylic alcohol facilitates the process of isomerisation. In view of this, we assume that the following reaction could take place in the process of isolation of an alcohol **4.25** from the reaction mixture and its exposure to the air:

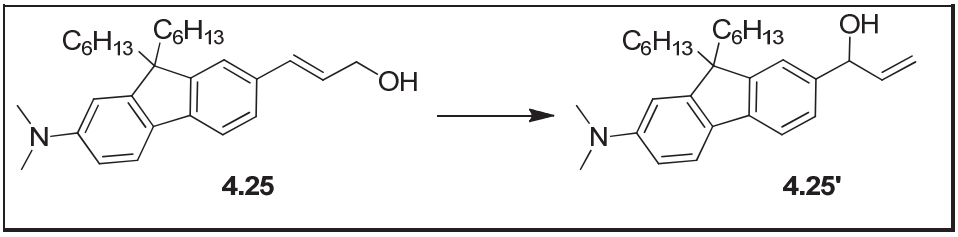

Scheme 4.14. Isomerisation of allyl alcohol **4.25** in the presence of water.

This step of the synthesis and the subsequent oxidation process significantly reduce the overall yield of the DMAFCCT ligand. In contrast to the oxidation reaction of compound **4.10** with MnO_2 which ends in two days, the oxidation of allyl alcohol **4.25** does not occur at all, while long-term staying of the compound in the solution results in the formation of an even greater amount of the by-product. Additional air passage through the solution contributes to partial oxidation with the formation of aldehyde **4.26**, but rapid alcohol degradation does not allow using this approach as preparative.

In the search of an appropriate oxidant the experiments on oxidation of alcohol with pure oxygen, 2 iodoxybenzoic acid (IBX) were conducted as well. The most effective method was the oxidation of alcohol with Dess-Martin reagent. The

maximum yield observed for this reaction was 79%. The following condensation and Michael reaction worked with fairly good yields.

Syntheses of coordination compounds based on DMAFT and DMAFCCT ligands were conducted similarly to the general scheme 4.7. However, the attempts to obtain ruthenium-nitrosyl complexes were not successful with any of them. At the second step of the reaction – obtaining of complex B – where it becomes possible to study the product by NMR (the complex becomes diamagnetic), we observed a decrease in the integral intensity of methyl protons of dimethylamino group, and the ratio between the peak intensities of protons of n-hexyl substituents and protons of the group -NMe_2 increased. In an utmost case we observed a loss of one of methyl radicals of dimethylamino group with the formation of monomethylamine derivative. A possible explanation for this phenomenon could be the probable oxidation of the -NMe_2 group with the participation of Ru^{III}, which occurs similarly to the triethylamine oxidation process at the second step of the synthesis of the complex described in paragraph 4.1.2. Thus the reduction of Ru^{III} and the addition of the 2,2'-bipyridine molecule leads to the formation of a monomethylamine derivative (Scheme 4.15).

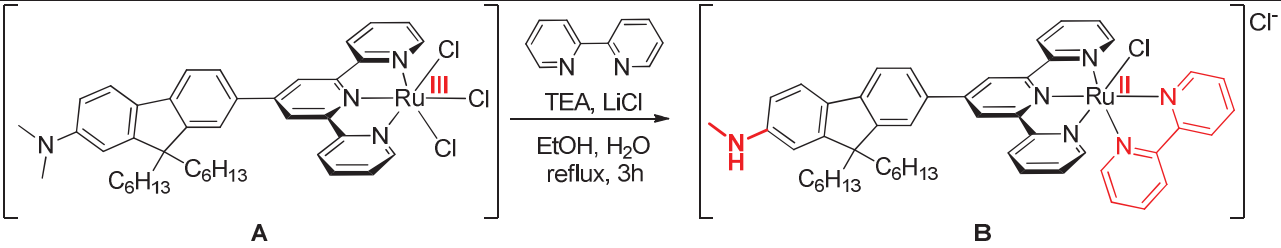

Scheme 4.15. A possible demethylation of [Ru(DMAFT)(bpy)Cl]Cl during the second step of the complex synthesis.

This process is unexpected for us, since unlike in triethylamine the lone pair of electrons of the nitrogen atom of the amino group in the DMAFT ligand is strongly conjugated with the π-system of the complex, which is evidenced by the flat structure of the ligand obtained during the DFT-optimization of the ion geometry. Therefore, the reducing properties of the -NMe_2-group in the complex are probably weaker. As a result, the reaction mixture contained several compounds that are, unfortunately,

difficult to separate. Nevertheless, obtaining of the complexes with these ligands may be possible with the modification of the approach used in this work.

4.2.2. Dependence of the TPA cross-section on the donor strength of the substituent in a row of ruthenium-nitrosyl complexes with substituted phenylterpyridines

Proceeding from the complexity of the process of obtaining of substituted fluorenyl-terpyridines, we have synthesized a series of ruthenium-nitrosyl complexes containing phenylterpyridines as ligands. In these compounds, the position 4 of benzene ring is substituted with groups of different electron-donating abilities: -NO_2, -H, -Br, -OMe, -NEt_2. The coordination polyhedra of the complexes is supplemented with two chloro-ligands, and thus the synthesized compounds are analogs of the compounds cis1 and trans1. The first stage of their preparation, as in the case of other complexes described in this work, is the interaction of ruthenium(III) chloride with the corresponding phenylperpyridine; the second step involves passing of gaseous NO through the solution of the complex in DMF that leads to the formation of cis- and trans- isomers of the complex $[Ru(RPh\text{-}tpy)Cl_2NO]^+$. The process of nitric oxide photorelease from the obtained compounds was also investigated. The data are presented in Table 4.7.

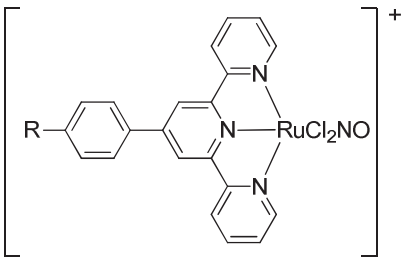

R	φ(NO)	
	cis-	trans-
-NO_2	0.24	0.05
-H	0.39	0.12
-Br	0.32	0.11
-OMe	0.28	0.07
-NEt_2	0.23	0.13

Table 4.7. The structure of the complexes $[Ru(RPh\text{-}tpy)Cl_2NO]^+$, and the quantum yields of NO-release from them.

A detailed discussion on the ability of these complexes to release nitric oxide and the dependence of their quantum yields on the structure is given in the

corresponding publication.[102] An exception is the compounds with the group -NEt_2: the data on these two isomers are not published at the time of the defense of the thesis, the values were obtained by M. Tasse, P. G. Lacroix and I. Malfant.

The study of the efficiency of these compounds in two-photon absorption by z-scan method was carried out on their acetonitrile solutions at a concentration of 10^{-2} M. The curves of laser radiation (800 nm) transmission by the complexes solutions are shown in Figure 4.9.

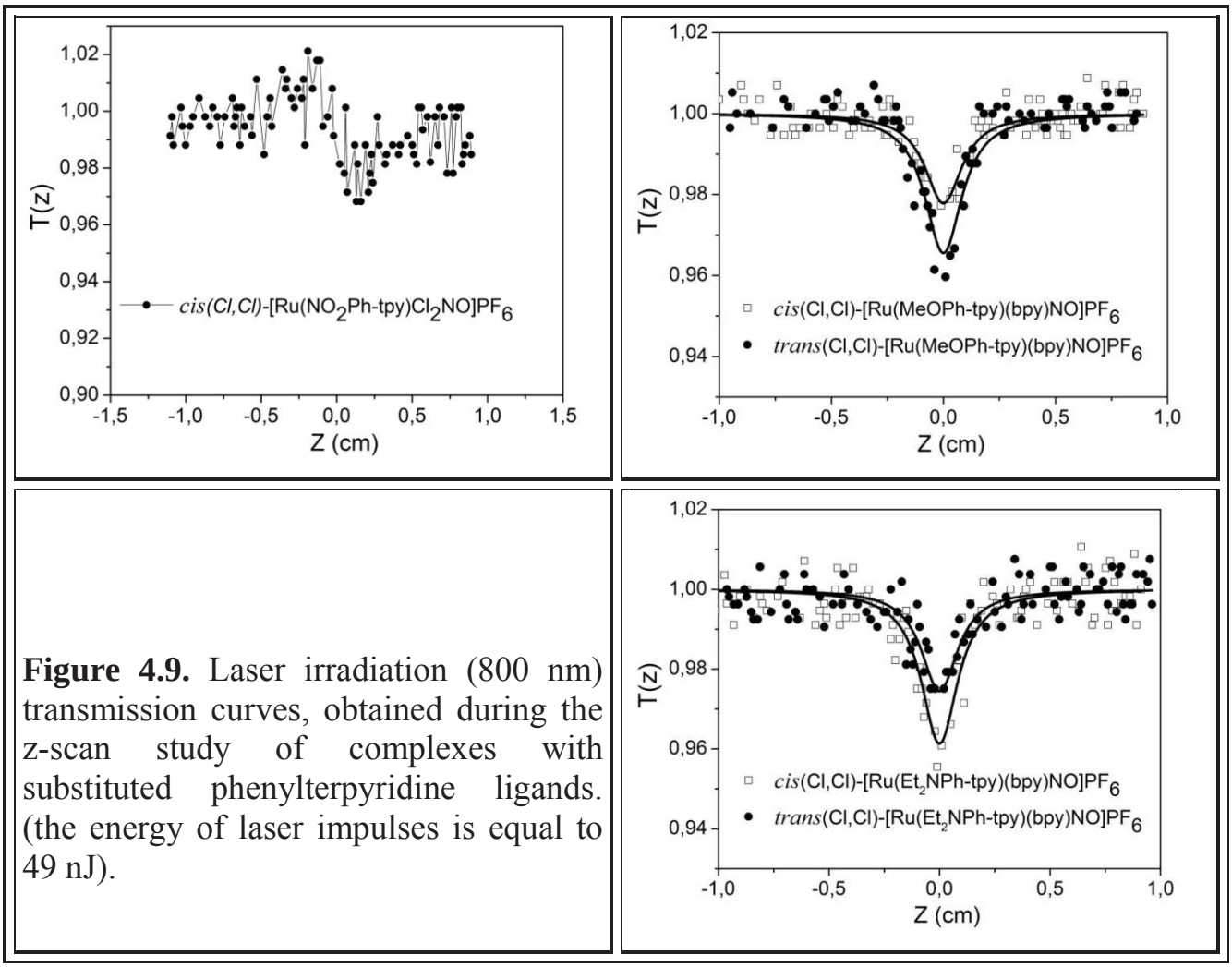

Figure 4.9. Laser irradiation (800 nm) transmission curves, obtained during the z-scan study of complexes with substituted phenylterpyridine ligands. (the energy of laser impulses is equal to 49 nJ).

Among 10 complexes studied only 4 exhibited two-photon absorption, which could be registered in the experimental conditions. Obviously, 6 other complexes exhibit very low ability for TPA. As expected, those of them that contain a donating group, either methoxyl or dimethylamino groups, have the highest absorption cross-sections. Compounds bearing nitrogroup, an atom of bromine or hydrogen atom, most of the time gave a characteristic curve similar to that shown in figure 4.9 for the

compound cis(Cl, Cl)-[Ru(NO_2-Phtpy)Cl_2NO]PF_6. A characteristic sinusoidal form indicates that there is a thermal effect that reduces the sensitivity of the measurement. However, even when it was possible to obtain a curve without displaying a thermal effect, the signal corresponding to the minimum transmittance in the focus of the laser radiation source was commensurable to the background oscillations, which made it impossible to determine the TPA cross-sections for these compounds.

Complexes [Ru(MeOPh-tpy)Cl_2NO]PF_6 and [Ru(Et_2NPh-tpy)Cl_2NO]PF_6, both cis- and trans- isomers, gave typical z-scan curves shown in Figure 4.9. The study of all four complexes was carried out at different values of the intensity of the exciting radiation; and with the increase of the intensity a linear decreasing of the transmittance was observed.

The values of the two-photon absorption coefficients (β) and TPA cross-sections for compounds are shown in Table 4.8.

	[Ru(MeOPh-tpy)Cl_2NO]PF_6		[Ru(Et_2NPh-tpy)Cl_2NO]PF_6	
	cis-	trans-	cis-	trans-
$\beta \cdot 10^{11}$ cm/W	3.22	3.73	3.44	2.73
σ, GM	133	154	142	113

Table 4.8. TPA coefficients and cross-sections for cis- and trans- isomers of compounds [Ru(MeOPh-tpy)Cl_2NO]PF_6 and [Ru(Et_2NPh-tpy)Cl_2NO]PF_6.

All values fall in the same range of about 110-150 GM. In general, compounds with methoxyl substituent appear to be more efficient in TPA, in contrast to our expectation that the introduction of dimethylamino-function will increase the difference in the dipole moments between the main and the excited state more strongly and thus will lead to higher values of σ. Therefore more detailed theoretical studies of compounds are required to deeply understand the key factors that play a role in the two-photon absorption of ruthenium nitrosyl complexes with electron-donating substituents.

Thus, we have synthesized new ruthenium-nitrosyl complexes $[Ru(FCCT)(bpy)NO](PF_6)_3$ and $[Ru(FCC3T)(bpy)NO](PF_6)_3$, where the torsion angle between fluorenyl and terpyridine fragments is reduced in comparison with bpy1. This effect along with the elongation of the π-system enhances the interaction between fragments and the polarizability of the compound. A more effective transfer of electronic density in a complex with a FCC3T ligand does not lead to a higher value of the quantum yield of NO-release, but it probably contributes to an increase in the TPA cross-section by 40% compared with bpy1, whereas for the compound $[Ru(FCCT)(bpy)NO](PF_6)_3$ this value is higher by only 21%.

It was shown that the acceptor groups in the terpyridine ligand do not lead to the increase in the value of σ for ruthenium-nitrosyl complexes, in contrast to the electron donating substituents.

From the point of view of the ability of the compounds to release nitric oxide upon the two-photon activation, compounds with chloro-ligands are more effective comparing to their analogs with 2,2'-bipyridine. This conclusion can be made based on the values of the product of the quantum yield of NO-release and the TPA cross-section (Table 4.9).

	φ(NO)	σ, GM	φ(NO)·σ
cis1	0.31	100	31.0
trans1	0.11	87	9.57
bpy1	0.06	108	6.48
$[Ru(FCCT)(bpy)NO](PF_6)_3$	0.03	131	3.93
$[Ru(FCC3T)(bpy)NO](PF_6)_3$	0.03	150	4.50
cis(Cl,Cl)-$Ru(MeOPh\text{-}tpy)Cl_2NO]PF_6$	0.28	133	37.2
trans(Cl,Cl)-$Ru(MeOPh\text{-}tpy)Cl_2NO]PF_6$	0.07	154	10.8
cis(Cl,Cl)-$Ru(Et_2NPh\text{-}tpy)Cl_2NO]PF_6$	0.23	142	32.7
trans(Cl,Cl)-$Ru(Et_2NPh\text{-}tpy)Cl_2NO]PF_6$	0.13	113	14.7

Table 4.9. The values of quantum yields, TPA cross-sections and the products of these two parameters for ruthenium-nitrosyl complexes, studied within the scope of this thesis.

The main effect on the product $\varphi(NO)\cdot\sigma$ is made by the quantum yield of NO-release, since these values vary considerably more broadly – the maximum value (0.31) is 10 times larger than the smallest (0.03), whereas the difference between the largest value of σ (154 GM) and the smallest (87 GM) one is only 77%.

CHAPTER 5. INVESTIGATION OF THE MECHANISM OF NO-PHOTORELEASE FROM RUTHENIUM-NITROSYL COMPLEX WITH THE LIGAND 4'-(4-METOXYPHENYL)-2,2':6',2''-TERPYRIDIN

The nitric oxide release from terpyridine ruthenium-nitrosyl complexes is not a one-stage process, it is quite complex to be descibed in a simplified model of electronic density transfer from a donor to an acceptor. As shown in Section 4, the introduction of donor groups leads to an increase in the TPA efficiency of the compound. However, an obvious correlation between the donor ability of the substituent and the quantum yield of nitric oxide release was not observed. This chapter is devoted to the study of some aspects of the release of nitrogen monoxide - the dependence of NO-release on the energy of exciting radiation, the structure of the photoproduct and the transformation of the released nitric oxide in vitro.

Taking into account that the highest value of the TPA cross-section was observed for the compound with the terpyridine ligand containing donating 4-methoxyphenyl substituent, this ligand was selected for the synthesis of the complex with 2,2'-bipyridine and the study of the nitric oxide photorelease was conducted on this complex.

5.1 Synthesis and characterisation of the complex $[Ru^{II}$(MeO-Phtpy)(bpy)(NO)$](PF_6)_3$

The ligand 4 '- (4-methoxyphenyl)-2,2':6', 2''- terpyridine (MeO-Phtpy) was synthesized according to the method described previously[142], which involves carrying out the aldol condensation followed by the Michael addition. Following the procedure, 2 equivalents of 2-acetylpyridine are introduced in the reaction with 4-methoxybenzaldehyde in a water-ethanol solution in the presence of KOH followed by addition of ammonium acetate. Equation of reaction and its mechanism are shown in scheme 5.1.

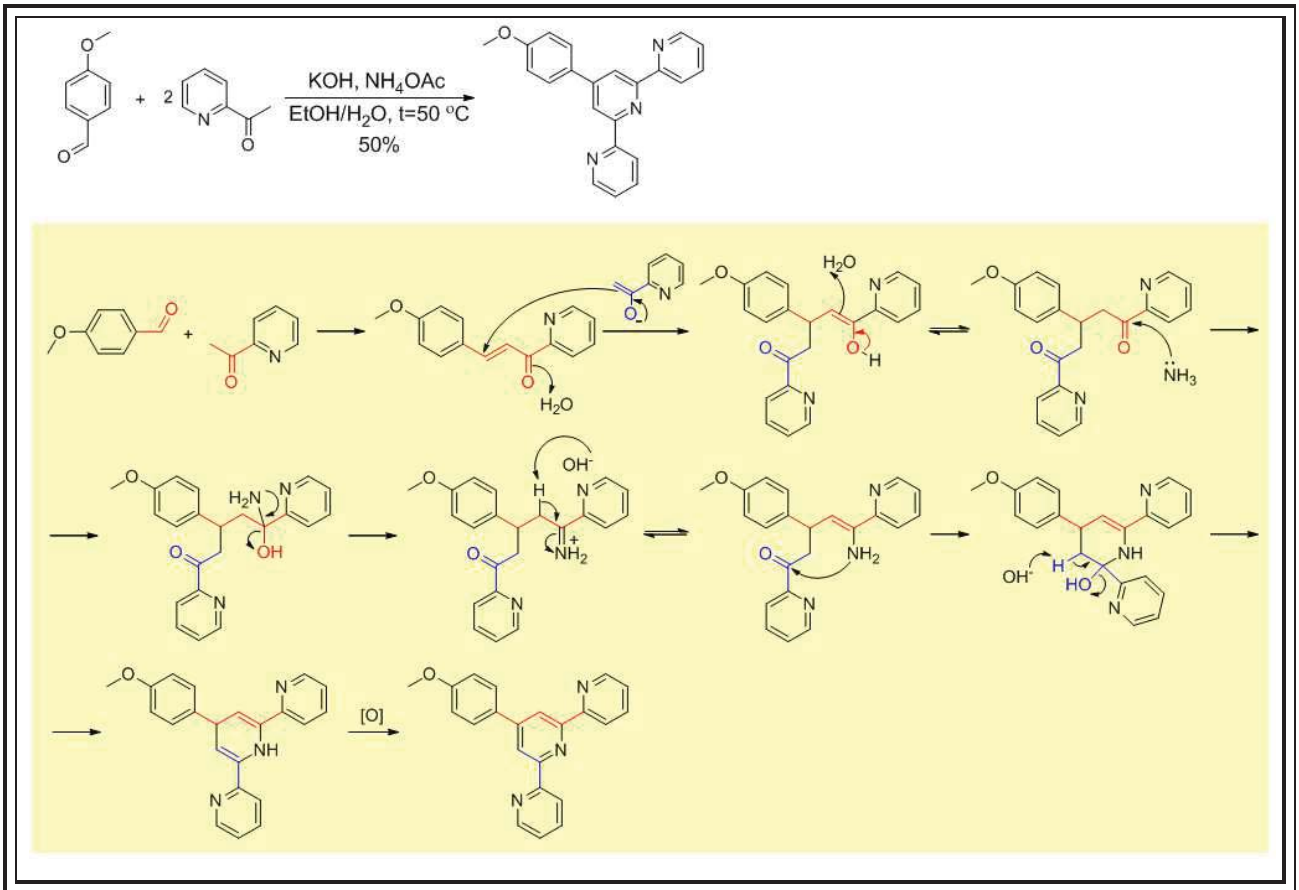

Scheme 5.1. The synthesis of the ligand 4'-(4-metoxyphenyl)-2,2':6'2"-terpyridine and the mechanism of the reaction.

The complex $[Ru^{II}(MeO\text{-}Phtpy)(bpy)(NO)](PF_6)_3$ was obtained in 4 steps, similar to the complexes with FCCT and FCC3T ligands, the synthesis of which is described in section 4 (scheme 4.7). The use of 2D-NMR spectroscopy techniques, in

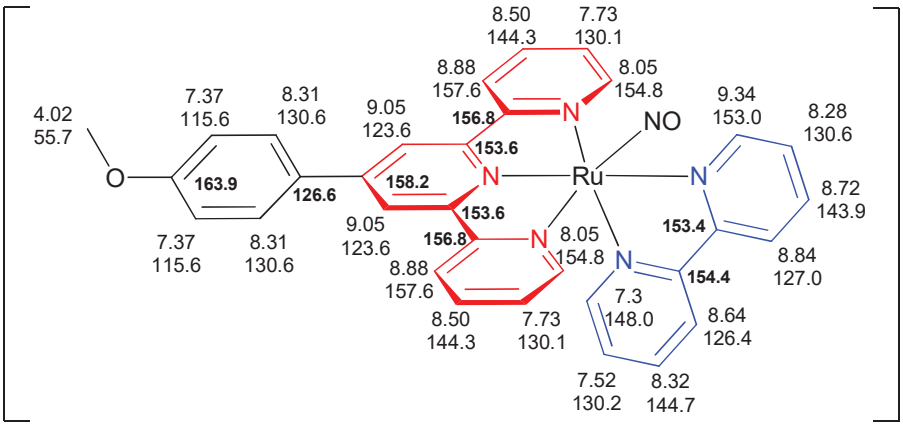

Figure 5.1. Chemical shifts of ^{1}H and ^{13}C in the NMR spectra of acetonitrile solutions of the complex $[Ru^{II}(MeO\text{-}Phtpy)(bpy)(NO)](PF_6)_3$, correlated with the help of COSY, HMQC, HMBC techniques.

particular homonuclear COSY and heteronuclear HMQC and HMBC, allowed to confirm the structure of the resulting complex and correlate signals in NMR spectra of ^{1}H and ^{13}C (Figure 5.1).

The frequency of the valence vibrations of the N-O bond is 1940 cm^{-1}. The value is very close to the frequency ν(NO) in the bpy1 complex – 1942 cm^{-1} – in which 2,2'-bipyridine and terpyridine ligand substituted with a donating fluorenyl substituent play the role of ligands.[107] However, it is much larger than the frequency of the valence vibrations of this bond in complexes, where the coordination sphere of ruthenium contain two chloro-ligands instead of bidentate 2,2'-bipyridine[86,102]. The difference between these values of 40-50 cm^{-1} is likely to arise as a result of the π-backdonating interaction between 2,2'-bipyridine and the ruthenium atom and the decrease in the population of the antibonding orbitals of the nitrosyl ligand.

The structure of the complex was confirmed by X-ray diffraction analysis. An assymetric unit of the elementary cell consists of one cation $[Ru^{II}$(MeO-Phtpy)(bpy)(NO)$]^{3+}$, three anions PF_6^- and a molecule of acetonitrile (Figure 5.2).

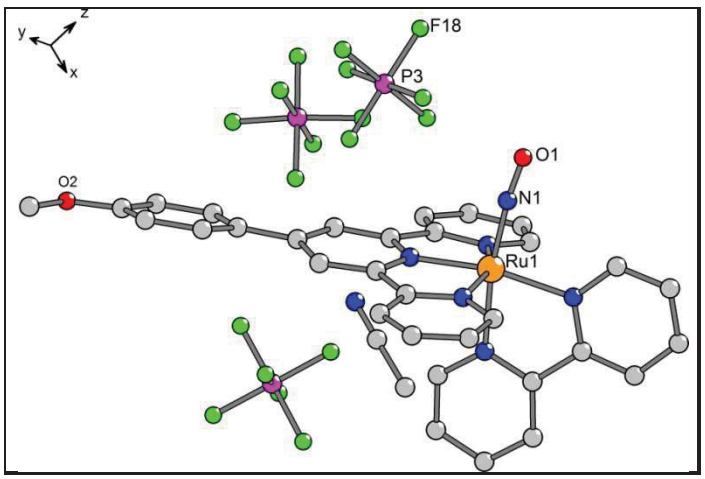

Figure 5.2. The structure of the asymmetric unit of the elementary cell of the complex $[Ru^{II}$(MeO-Phtpy)(bpy)(NO)$](PF_6)_3$.

No π-interaction was observed between the ligands – either between 2,2'-bipyridine fragments of two adjacent complex ions, or between terpyridine ligands. There is a weak interaction between the nitrosyl ligand and the anion PF_6^- (O(1) – F(14) = 2.767(10) Å, O(1) - F(8) = 2.873(7)).

The terpyridine fragment is almost planar with the largest deviation from the mean plane (18 atoms) of 0.154 Å (C14 atom). The bipyridine ligand is more flat with the greatest deviation from the mean plane of 0.043 Å (C9 atom). The terpyridine and bipyridine planes are almost orthogonal with a torsion angle of 87.88 °. An important parameter of the structure is the torsion angle between

the phenyl ring and the terpyridine ligand plane – 6.59° – indicating a potentially effective transfer of the electron density from donating methoxyphenyl to accepting ruthenium-nitrosyl fragments.

As mentioned in chapter 1, the ambiguity in the distribution of the electronic density between the metal atom and the NO ligand ($Ru^{II}(NO^{+})$ or $Ru^{III}(NO\cdot)$ form) is eliminated by the use of the Enemark-Feltman notation, according to which the complex $[Ru^{II}(MeO\text{-}Phtpy)(bpy)(NO)](PF_6)_3$ should be attributed to $\{Ru(NO)\}^6$. Nevertheless, the definition of the most typical resonance form in each case for ruthenium-nitrosyl complexes makes possible deeper inderstanding of the electronic and magnetic properties of the compounds. In this case, the linear fragment Ru-NO (the angle Ru-N-O is 172.93 °) indicates the proximity of the complex to the structure $Ru^{II}(NO^{+})$. An alternative parameter that could indicate the oxidation state of ruthenium atom could be the length of the Ru-N_{py} bonds. However, it has previously been shown that the Ru-N bonds are almost the same in the compounds $[Ru(bpy)_3]^{2+}$ and $[Ru(bpy)_3]^{3+}$, and have the length 2.053(2) Å and 2.057(3) Å [143], therefore this parameter can not be used to estimate the oxidation state of ruthenium.

Other important interatomic distances and angles in the coordination sphere of the complex are presented in Table 5.1.

Nitrosyl		*Terpyridine*		*Bipyridine*	
Ru(1) – N(1)	1.7668(9)	Ru(1) – N(4)	2.0888(8)	Ru(1) – N(2)	2.1002(8)
N(1) – O(1)	1.1313(11)	Ru(1) – N(5)	1.9880(8)	Ru(1) – N(3)	2.0881(8)
Ru(1)-N(1)-O(1)	172.94(8)	Ru(1) – N(6)	2.0840(8)		

Table 5.1. The main interatomic distances (Å) and angles (°) in coordination sphere of the complex $[Ru^{II}(MeO\text{-}Phtpy)(bpy)(NO)](PF_6)_3$.

5.2 Electronic spectrum and basic electronic transitions in the compound $[Ru^{II}(MeO\text{-}Phtpy)(bpy)(NO)](PF_6)_3$

The UV-visible spectra of $[Ru^{II}(MeO\text{-}Phtpy)(bpy)(NO)](PF_6)_3$ and that of the related MeO-Phtpy ligand recorded in acetonitrile are compared in figure 5.3. The ligand exhibits a single and very intense band with an absorption maximum (λ_{max}) at 284 nm (ε = 37 700 mol^{-1} L cm^{-1}). By contrast, $[Ru^{II}(MeO\text{-}Phtpy)(bpy)(NO)](PF_6)_3$

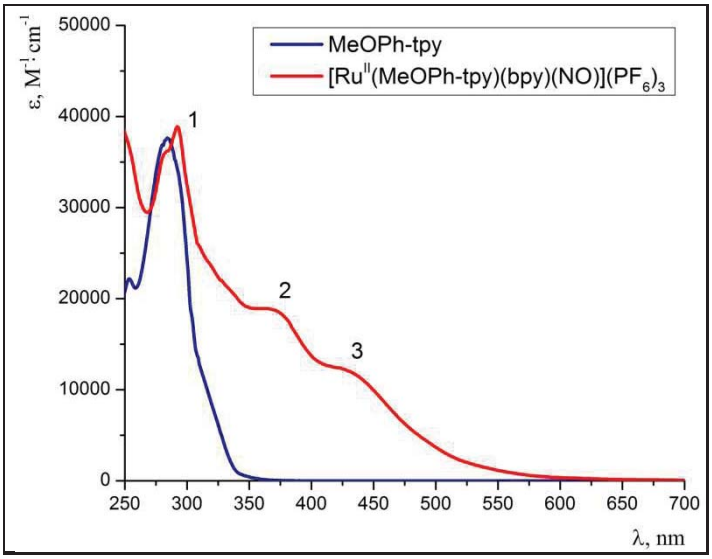

Figure 5.3. UV/vis spectra of the ligand MeO-Phtpy (blue) and the complex $[Ru^{II}(MeO\text{-}Phtpy)(bpy)(NO)](PF_6)_3$ (red) in acetonitrile showing the three (*1-3*) bands of interest present in the ruthenium(II) complex.

exhibits a more complex spectrum. While the high energy band is present (λ_{max} = 292 nm, ε = 38 900 $M^{-1}\cdot cm^{-1}$) and slightly red-shifted, two additional features appear at 375 nm (band ***2***) and 420 nm (band ***3***) with intensities of 18 900 mol^{-1} L cm^{-1} and 12 400 mol^{-1} L cm^{-1}, respectively. The differences observed between ligand and metal complex strongly suggests that the contributions of the ruthenium nitrosyl withdrawing fragment are important in the low energy bands ***2*** and ***3***. Therefore, it encourages a computational analysis of the related electronic transitions. complex is, of course, more complicated.

The comparison of the experimental and computed electron spectra of the complex is presented in the table 5.2.

	Experimental spectra		Computed spectra	
	λ_{max} (nm)	ε ($M^{-1}\cdot см^{-1}$)	λ_{max} (nm)	f
Band 1	292	38 900	265	0.628
Band 2	375	18 900	342	0.632
Band 3	420	12 400	417	0.227

Таблиця 5.2. Absorption bands in the electronic spectrum of the complex $[Ru^{II}(MeO\text{-}Phtpy)(bpy)(NO)](PF_6)_3$, and corresponding absorption bands for the ion $[Ru^{II}(MeO\text{-}Phtpy)(bpy)(NO)]^{3+}$, computed by means of TD-DFT on the CAM-B3LYP/6-31G* level of theory.

The comparison between the experimental (UV-visible) and computed (TD-DFT) data are provided in Table 5.3. Although the computed wavelengths are slightly blue-shifted, the agreement is found satisfactory, thus making the interpretation at the orbital level fully reliable.

Transition	λ_{max}	f	Dominant contribution	Character
Band 1				
$0 \rightarrow 20$	270	0.266	87% $\chi_{141} \rightarrow \chi_{148}$	bpy → bpy
$0 \rightarrow 23$	258	0.362	53% $\chi_{142} \rightarrow \chi_{149}$ + 20% $\chi_{140} \rightarrow \chi_{147}$	tpy → tpy
Band 2				
$0 \rightarrow 6$	355	0.265	30% $\chi_{142} \rightarrow \chi_{146}$ + 19% $\chi_{144} \rightarrow \chi_{147}$ + 15% $\chi_{137} \rightarrow \chi_{146}$	MeOPhtpy → tpyRu(NO)
$0 \rightarrow 9$	335	0.176	42% $\chi_{142} \rightarrow \chi_{146}$ + 40% $\chi_{144} \rightarrow \chi_{147}$	MeOPhtpy → tpyRu(NO)
$0 \rightarrow 10$	327	0.191	22% $\chi_{144} \rightarrow \chi_{147}$ + 18% χ_{142} χ_{146} + 17% $\chi_{141} \rightarrow \chi_{146}$	MeOPhtpy + bpy → tpyRu(NO)
Band 3				
$0 \rightarrow 2$	417	0.227	76% $\chi_{144} \rightarrow \chi_{145}$	MeOPh → Ru(NO)

Table 5.3. TD-DFT-computed maxima of absorption, oscillator strength and configurations of the transitions of the complex $[Ru^{II}(MeO\text{-}Phtpy)(bpy)(NO)](PF_6)_3$. The orbital 144 is HOMO, the orbital 145 – LUMO.

Band ***1*** exhibits a $\pi \rightarrow \pi^*$ character, and involves the contribution of two $0 \rightarrow 20$ and $0 \rightarrow 23$ transitions centered on the bipyridine and the terpyridine, respectively. As anticipated, both low-energy bands ***2*** and ***3*** possess a strong charge transfer character towards the Ru(NO) fragment. This is further illustrated in Figure 4, where the main orbitals of interest contributing to bands ***2*** and ***3*** are drawn, with their relative energy levels.

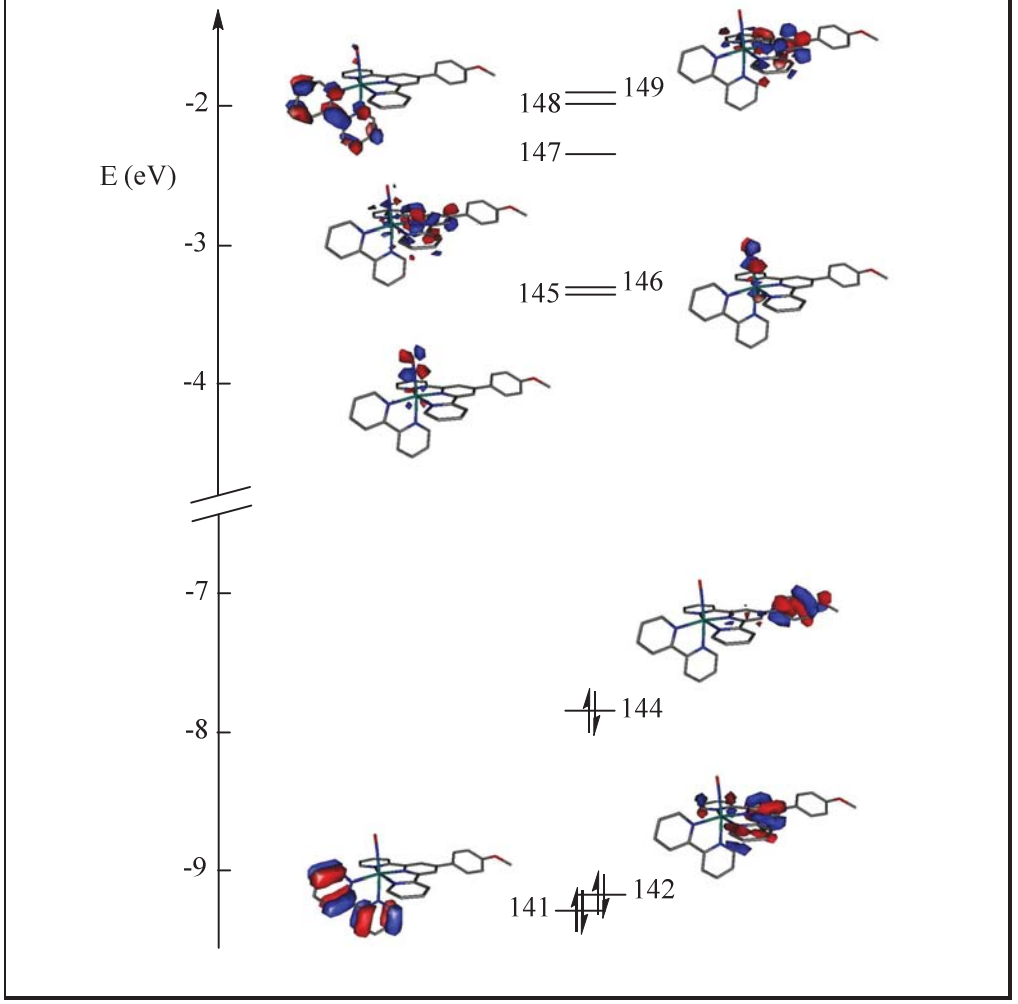

Figure 5.4. Orbitals involved in electronic transitions of bands 2 and 3 in UV-visible spectra of the compound $[Ru^{II}(MeO\text{-}Phtpy)(bpy)(NO)](PF_6)_3$.

Band ***3*** is readily described as a HOMO → LUMO based charge transfer with the excited state electron density being totally located on the Ru(NO) fragment. Therefore, this transition should induce an efficient $NO^{\cdot}$ release process. By contrast, band ***2*** involves the contribution of three ($0 \rightarrow 6$, $0 \rightarrow 9$, and $0 \rightarrow 10$) transitions in

which the dominant charge transfer occurs towards the LUMO+1 level. Interestingly, the electronic features of the LUMO+1 are closely related to those of the LUMO, with a rotation of 90° around the Ru-NO axis, and hence with the same expected effect in term of NO release capabilities. Nevertheless, the transitions involved in band ***2*** also involve a charge transfer towards the orbital 147 which is strongly located on the terpyridine fragment (Figure 4). Based on the assumption that the NO· release process implies a single charge transfer transition towards the nitrosyl fragment, it should readily be concluded that an irradiation will be less efficient on band ***2*** than on band ***3***.

5.3 NO-release from the complex $[Ru^{II}(MeO\text{-}Phtpy)(bpy)(NO)](PF_6)_3$

As previously shown, the release of nitric oxide from ruthenium-nitrosyl complexes results in the formation of a photoproduct in which the ruthenium is in the oxidation state +3, and the coordination position previously occupied by the nitrosyl ligand is occupied by the molecule of the solvent molecule:[86]

$$[Ru^{II}(NO)^{+}] + solvent \rightarrow [Ru^{III}(solvent)] + NO^{\cdot}$$

However, as discussed in chapter 2 in the case of bpy1, the photoproduct that we observe when the photoreaction finished may be different from the expected one. Owing to the presence of two bands in the UV-visible spectrum having absorption maxima located at 375 nm (band *2*) and 420 nm (band *3*), the irradiations were performed at 365 nm and 436 nm using a set of available filters, in order to determine the NO· release efficiencies for bands *2* and *3*, respectively.

The changes in the electronic absorption spectrum of $[Ru^{II}(MeO\text{-}Phtpy)(bpy)(NO)](PF_6)_3$ exposed to 365 nm light in acetonitrile are shown in figure 5.5 at the top. The presence of isosbestic points at 268, 344 and 434 nm indicates a clean conversion of the $Ru^{II}(NO^{+})$ complexes to related photolysed species. No back-reaction is observed when the light is turned off. In the photolysed species, new bands located at 286, 308,434 and 470 nm arise. The fact that the photoproduct does not absorb significantly at 365 nm leads to a fast photoreaction process, completed

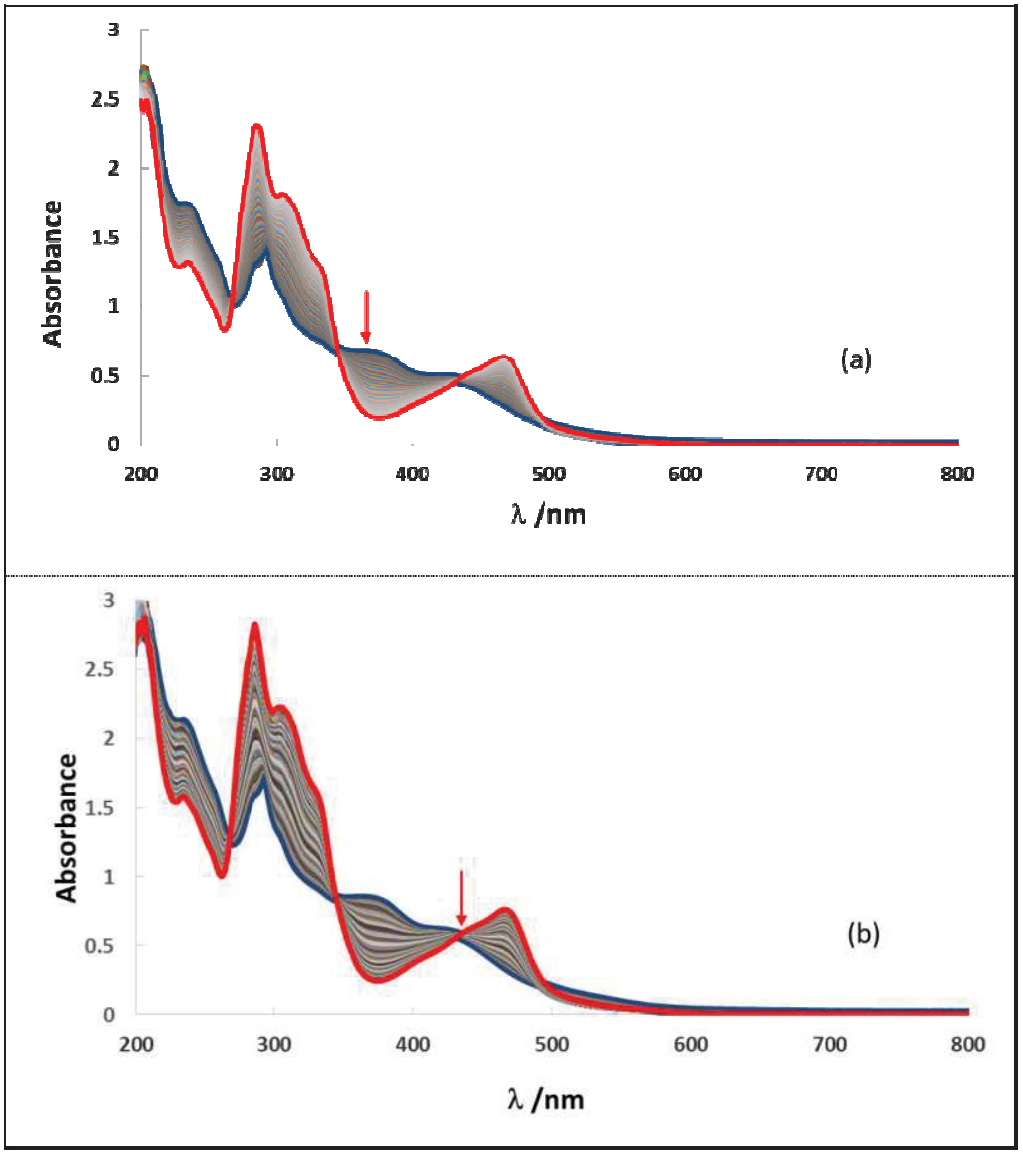

Figure 5.5. Evolution in the absorption spectra of $[Ru^{II}(MeO\text{-}Phtpy)(bpy)(NO)](PF_6)_3$ in acetonitrile under irradiation at λ = 365nm (a) and at λ = 436nm (b). Blue line: before irradiation; red line: after completeness of the photo-chemical process.

after 80 minutes without further evolution. The changes in the electronic absorption spectrum of $[Ru^{II}(MeO\text{-}Phtpy)(bpy)(NO)](PF_6)_3$ exposed to 436 nm light in acetonitrile are shown in figure 5.5 bottom. The presence of isosbestic points at 266, 346 and 436 nm indicates a clean conversion of the $Ru^{II}(NO^+)$ complexes to related photolysed species. No back-reaction is observed when the light is turned off neither. In the photolysed species, new bands located at 286, 308,434 and 470 nm arise. Due to a significant absorption of the photoproduct at 436 nm, the release takes

7 hours to reach completeness. Nevertheless, both experiments leading to the same photoproduct, the two figures 5.5a and 5.5b appear nearly identical.

The quantum yield of NO· release (φ) observed for $[Ru^{II}(MeO\text{-}Phtpy)(bpy)(NO)](PF_6)_3$ is equal to 0.08 and 0.03 under light irradiation at 365 nm (band *2*) and 436 nm (band *3*), respectively. These values are in complete disagreement with the expectation of a more efficient NO· release when the charge transfer towards the Ru(NO) fragment appears more significant. Within these experimental features, the issue of the real mechanism involved in the NO· release process is naturally addressed. Clearly, an explanation based on the analysis of a single charge transfer transition appears to be an oversimplified picture of a mechanism, which seems to be more complex. As described in section 1.4.4, a recent theoretical investigation has suggested that the NO· release could require more than one photon, with the contribution of an intermediate triplet state.[91] Moreover, the investigation of the ultrafast dynamics of the photoinduced NO· release in a ruthenium-nitrosyl complex with terpyridine has also provided experimental evidences for a secondary photochemical process within a few ps, although it was not possible to determine the nature of the intermediate state.[144]

Additionally, it is interesting to observe that the shape of the photoproduct UV-spectrum (red line in figure 5.5) corresponds to a Ru^{II} complex, because of the lack of band at 600 nm characteristic of Ru^{III} species (see section 2.3). A similar situation was observed in the case of bpy1 compound: replacing of the chloro-ligands in terpyridine ruthenium-nitrosyl complexes with 2,2'-bipyridine led to the disappearance of such absorption in the spectrum of photoproduct.[107]

In view of the presence of distinct isosbestic points in experiments with spectrophotometric monitoring of the NO-release process (Figure 5.5, Figure 2.6c), we assume that in the case when in addition to terpyridine a molecule of 2,2'-bipyridine is present in the coordination environment of ruthenium in the ruthenium-nitrosyl complex the photoproduct with a ruthenium atom in oxidation +3, formed in photoreaction

$$\{Ru^{II}(tpy)(bpy)\text{-}NO\}^{3+} + CH_3CN \xrightarrow{h\nu} \{Ru^{III}(tpy)(bpy)\text{-}CH_3CN\}^{3+} + NO,$$

is instantly reduced to $\{Ru^{II}(tpy)(bpy)CH_3CN\}^{2+}$, and this photoproduct is the final one. Thus, according to our theory the cation of the complex $[Ru^{II}(MeO\text{-}Phtpy)(bpy)(NO)](PF_6)_3$ is converted to $[Ru^{II}(MeO\text{-}Phtpy)(bpy)(CH_3CN)]^{2+}$. Additional studies to confirm this theory have been carried out.

5.4. Oxidation state of ruthenium within the release process

The study we conducted is based on a series of spectroscopic methods for analyzing the photoproducts and the very process of release of NO-radical – electronic spectra, NMR, ESR and X-ray structural studies[145].

If the reduction process is indeed occurs in photoproduce, then it passes very quickly, since formation of the intermediate Ru^{III} compound is not observed in UV-visible spectra. The absence of paramagnetic particles was confirmed by NMR spectroscopy.

In view of the fact that the back reaction is not observed under the suspension of complex irradiation, we conducted an experiment to monitor the release of nitric oxide by NMR. Deuterated acetonitrile was taken as the solvent for the $[Ru^{II}(MeO\text{-}Phtpy)(bpy)(NO)](PF_6)_3$ complex and the irradiation of the compound occurred directly in the ampoule for NMR studies. As a source of radiation a simpler and cheaper (in comparison with the Hg-lamp used for kinetics of NO-release studies), homemade device based on LEDs with a light wavelength range of 350-450 nm was used (see Experimental part). After 5 minutes of irradiation, the sample was studied by ^{1}H-NMR spectroscopy, and then the irradiation continued for another 5 min etc. The evolution of the ^{1}H-NMR spectrum of $[Ru^{II}(MeO\text{-}Phtpy)(bpy)(NO)](PF_6)_3$ under irradiation in the 350-450 nm range is presented in figure 5.6.

The gradual transformation of the complex into a diamagnetic photoproduct is apparent in the figure (*e.g.* the singlet of methyl group protons at 4.00 ppm decreases while the corresponding signal of photoproduct at 3.95 ppm rises). In general several

peaks show some broadening, but it's small and it confirms the absence of any paramagnetic Ru^{III} complex.

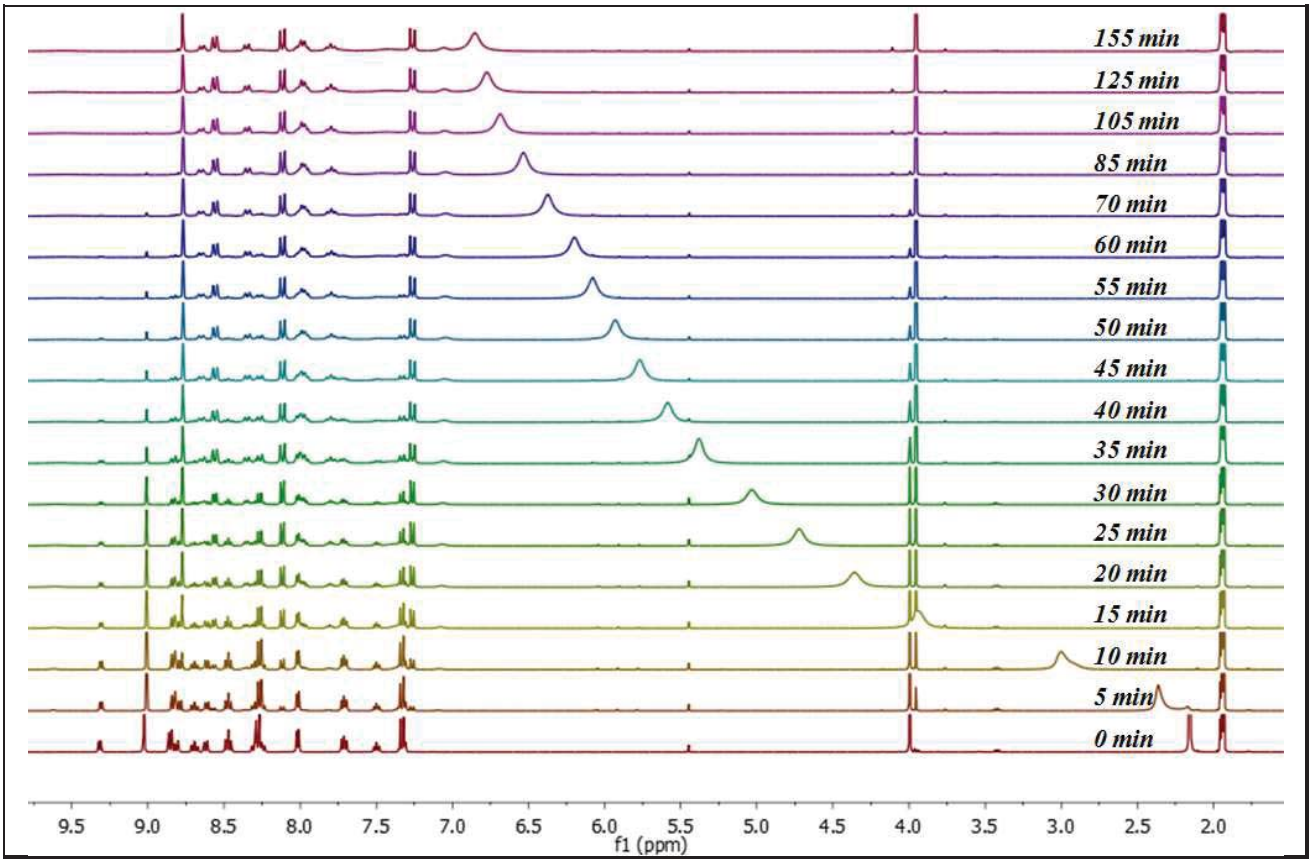

Figure 5.6. ^{1}H-NMR-tracking of NO· release from [Ru^{II}(MeO-Phtpy)(bpy)(NO)]$(PF_6)_3$ irradiated with continuous light in the 350-450 nm range, in CD_3CN.

The most noticeable evolution in Figure 1 is the shift of a peak tentatively attributed to traces of water from 2.13 ppm in the initial solution to 6.85 ppm after 155 minutes of irradiation. An explanation for such a change may be the change of the acidity of the solution, which is probably caused by the formation of derivatives of nitrogen in higher oxidation stages (in particular nitrite and nitrate anions), as a result of the oxidation of nitrogen monoxide by the air and the interaction with water traces which are inevitably present in the solvent.

No attempts were made to deoxygenate and to dry the solvent. As an example of possible transformations, the following chemical reactions could be proposed:

$$4NO\cdot + O_2 + 2H_2O \rightarrow 4NO_2^- + 4H^+,$$

$$4NO\cdot + 3O_2 + 2H_2O \rightarrow 4NO_3^- + 4H^+$$

An attempt to recreate the NO-photorelease experiment in the absence of oxygen and water was carried out using DMSO-d6 as a solvent. The initial spectrum of the $[Ru^{II}(MeO\text{-}Phtpy)(bpy)(NO)](PF_6)_3$ complex and the spectrum of the resulting photoproduct are shown in Figure 5.7.

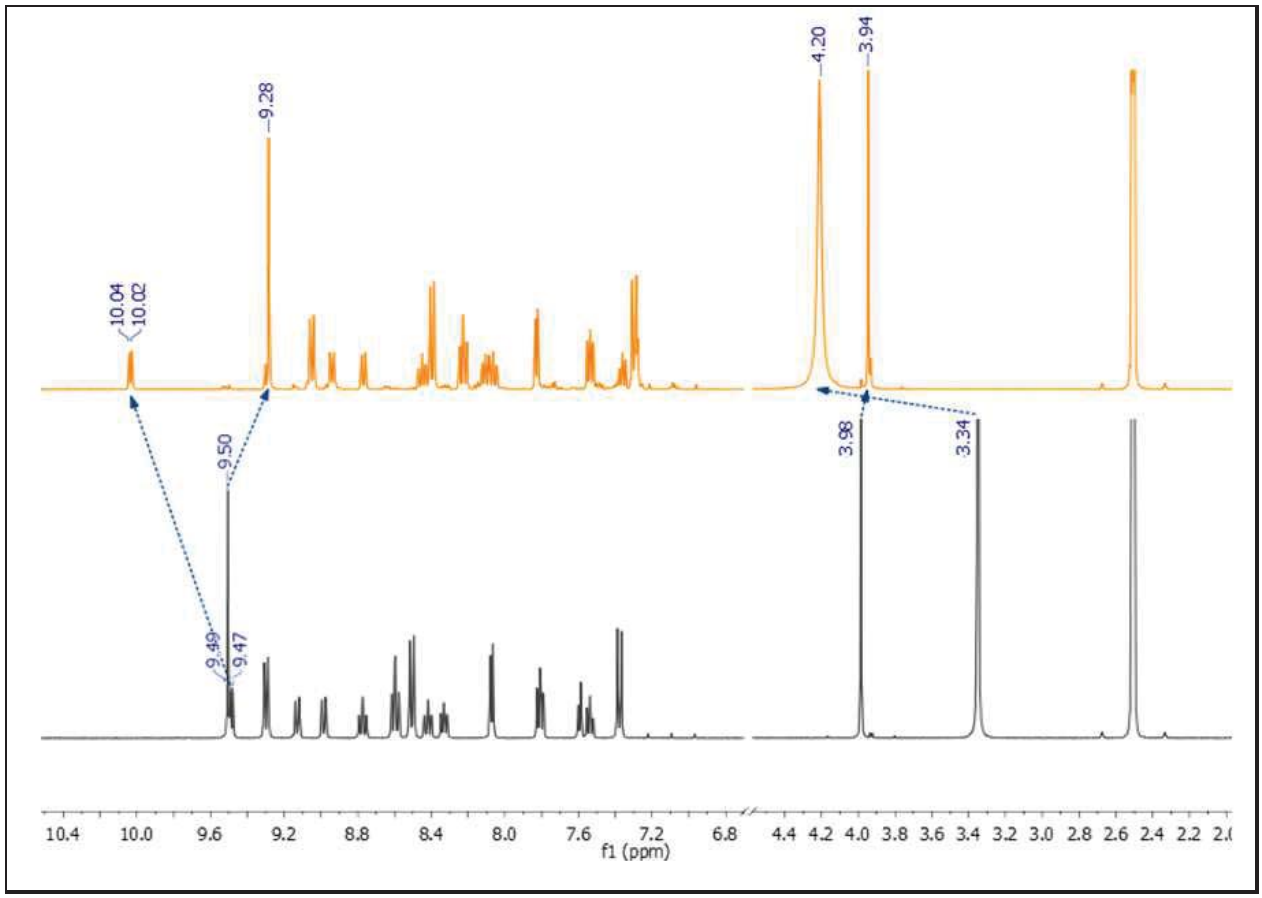

Figure 5.7. ^{1}H-NMR spectra of $[Ru^{II}(MeO\text{-}Phtpy)(bpy)(NO)](PF_6)_3$ in DMSO-d_6 (bottom) and the obtained solution of photoproduct (top).

In contrast to the previous experiment with the acetonitrile solution of the complex, the broadening of signals was not observed at any of the steps of photoreaction, and the spectrum of the complex after the NO-release completion is similar to the spectrum of the initial substance in relative position of the signals and their integral intensity. A singlet at 3.34 ppm, characteristic for protons of water molecules is not shifted strongly in the weak field, the main shifting is observed in first minutes of irradiation. So, after 5 minutes of the sample exposure to electromagnetic radiation, the peak of water shifts from 3.34 to 4.09 ppm, and then,

its position remains almost unchanged, moving in a weak field in general by another 0.11 ppm until the end of the photoreaction.

A good correspondence of the spectra of the initial complex and the photoproduct allows us to assume that the structure of the complex has not changed significantly, and apart from replacing the nitrosyl ligand with the solvent molecule, the constitution of the molecular ion has not changed.

The structure of the cationic part of the photoproduct was confirmed by the single crystal X-ray diffraction analysis of the photoproduct. The crystal was grown from an acetonitrile solution of a photoproduct that was obtained after irradiation of the solution of $[Ru^{II}(MeO\text{-}Phtpy)(bpy)(NO)](PF_6)_3$ in CH_3CN.

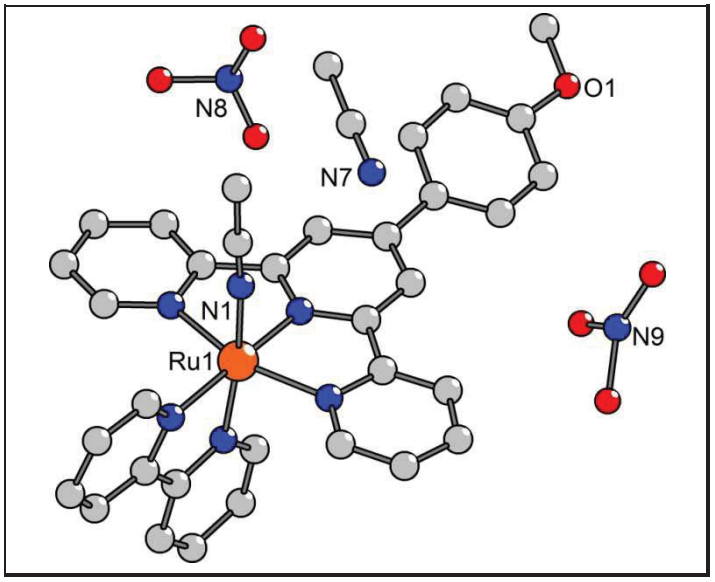

Figure 5.8. The structure of the asymmetric unit of the elementary cell of the complex $[Ru^{II}(MeO\text{-}Phtpy)(bpy)(CH_3CN)](NO_3)_2$.

The photoproduct crystallizes in $P2_1c$ monoclinic space group. The asymmetric unit of the elementary cell of the crystal is shown in Figure 5.8. It consists of one cation $[Ru^{II}(MeO\text{-}Phtpy)(bpy)(CH_3CN)]^{2+}$, two NO_3^- anions and a molecule of acetonitrile.

As predicted, the structure of the cation of the photoproduct differs from the cation of the initial complex only in the presence of a coordinated molecule of acetonitrile instead of the nitrosyl ligand. But unexpectedly, the anions in the structure of the photoproduct are not PF_6^-, but ions $NO3^-$. The presence of nitrate anions could apparently be explained by the release and subsequent oxidation of nitric oxide, which confirms the assumption that the acidity of the solution during the irradiation of the initial complex (Figure 5.6) may increase as a result of the formation of the species containing nitrogen in higher oxidation states. The change of the anion from PF_6^- to NO_3^- was already observed earlier for ruthenium-nitrosyl complexes, in particular for the compound

$[Ru^{II}(FT)Cl_2(NO)](PF_6)$.[146] The geometry of the nitrate anions in the structure of the complex somewhat deviate from the absolute planarity. The nitrogen atoms N(8) and N(9) are located in 0.217 Å and 0.405 Å above the average plane of the three oxygen atoms. A high disorder of anions may partially be caused by this deviation. It is important that the structure of the complex consists of only two anions, which indicates that the ruthenium atom is in the oxidation state +2.

The coordination sphere of the ruthenium atom in the complex ion $[Ru^{II}(MeO\text{-}Phtpy)(bpy)(CH_3CN)]^{2+}$ is similar to that in the starting complex $[Ru^{II}(MeO\ Phtpy)(bpy)(NO)](PF_6)_3$. In particular, there are slight differences in the lengths of the Ru-N_{py} bonds. Thus, in both structures, the length of the bond between the central atom and the nitrogens atom of the central pyridine ring of terpyridine is approximately 0.1 Å shorter in comparison with the bonds of the ruthenium atom with the pyridine rings. Also, on the average, Ru-N_{bpy} bonds are slightly longer than Ru-N_{tpy} bonds. The terpyridine fragment is more flat than in the initial complex with a maximum deviation from the average plane in 0.059 Å for the C(19) atom. The angle between the terpyridine and bipyridine planes is 85.91 °, and the torsion angle between the terpyridine and methoxyphenyl moieties is slightly higher than the value in the initial complex - 8.50 °.

This is likely to indicate a less efficient conjugation between the phenyl and pyridine rings, which by-turn is caused by the reduced withdrawing effect of the {Ru(tpy)(bpy)(CH_3CN)} fragment compared with the highly accepting ruthenium-nitrosyl group. Some parameters of the ruthenium coordination sphere, in particular the important interatomic distances and angles, are given in Table 5.4.

Acetonitrile		*Terpyridine*		*Bipyridine*	
Ru(1) – N(1)	2.031(6)	Ru(1) – N(4)	2.080(6)	Ru(1) – N(2)	2.071(6)
Ru(1)-N(1)-C(1)	175.1(6)	Ru(1) – N(5)	1.967(6)	Ru(1) – N(3)	2.039(6)
		Ru(1) – N(6)	2.072(6)		

Table 5.4. Main bond lengths (Å) and angles (°) in the coordination sphere of ruthenium in $[Ru^{II}(MeO\text{-}Phtpy)(bpy)(MeCN)]^{2+}$.

The fact that NO-release leads to the formation of a photoproduct in the oxidation state +2 raises the issue of the real nature of the NO-species liberated under irradiation, which might not be NO-radicals, but the alternative, and undesirable NO^+-cation produced by the following reaction:

$$[Ru^{II}(NO)^+] + \text{solvent} \rightarrow [Ru^{II}(\textit{solvent})] + NO^+.$$

Nevertheless, the photo-generation of NO· instead of NO^+ can be demonstrated experimentally, by EPR spectroscopy under standard excitation at λ = 365 nm or 436 nm, since spin trapping combined with EPR spectroscopy is considered as one of the best methods for the direct detection of NO· radicals.[89] Namely, we used Iron(II)-N-methyl-D-glucamine dithiocarbamato $[Fe^{II}(MGD)_2]$ to trap NO· due to its high probability of adduct formation and to the high stability of its spin adduct. The appearance of the characteristic triplet signal of NO· is shown in Figure 5.9.

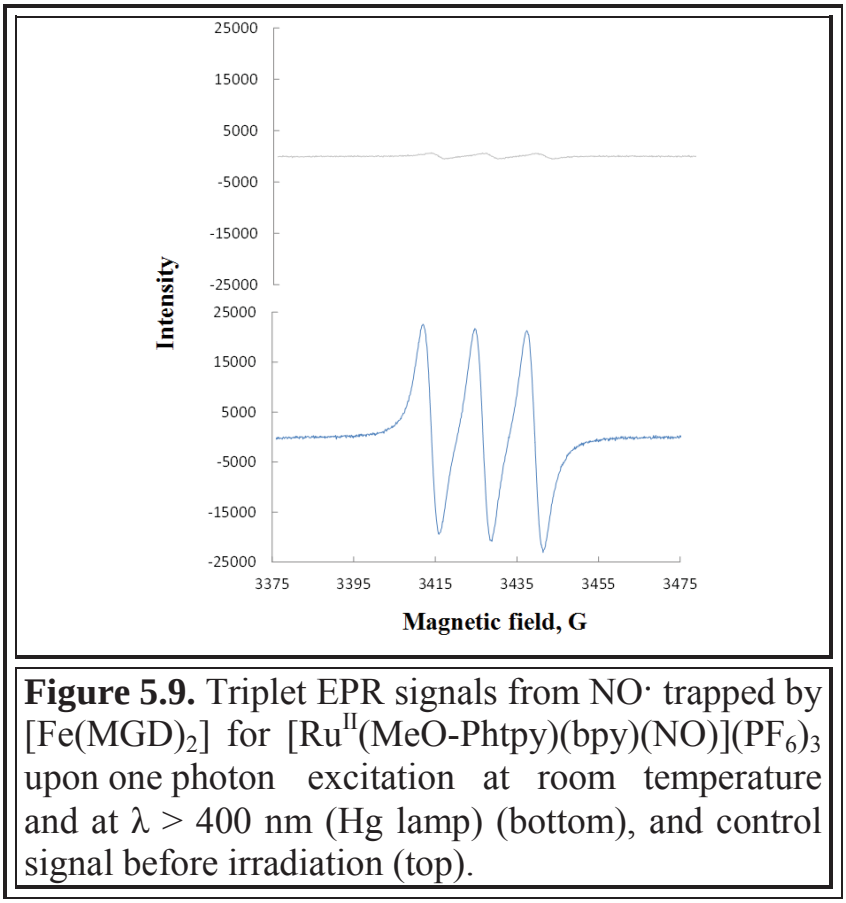

Figure 5.9. Triplet EPR signals from NO· trapped by $[Fe(MGD)_2]$ for $[Ru^{II}(MeO\text{-}Phtpy)(bpy)(NO)](PF_6)_3$ upon one photon excitation at room temperature and at $\lambda > 400$ nm (Hg lamp) (bottom), and control signal before irradiation (top).

The hyperfine splitting constant value is $a_N = 1.24\ 10^{-3}$ cm^{-1}, *g*-factor is equal to 2.040. These values are fully consistent with the literature report for $[Fe^{II}(MGD)_2$-NO] adduct.[89]

The weak signal observed in the control spectrum (top of Figure5.9) is due to a trace of NO· and related to the fact that the manipulation is never strictly conducted in the dark.

Investigation of the initial complex $[Ru^{II}(MeO\text{-}Phtpy)(bpy)(NO)](PF_6)_3$ and the corresponding photoproduct by electrochemical methods gave an opportunity to explain why the oxidation state of ruthenium in photoproduct is +2. Obtained voltamperograms are shown in Figure 5.10. The results of electrochemical studies are summarized in Table 5.5, data for the cis- $[Ru^{II}(MeO\text{-}Phtpy)Cl_2(NO)](PF_6)$ compound are given as reference. The reference electrode consisted of a saturated calomel electrode (SCE) separated from the solution by a bridge compartment.

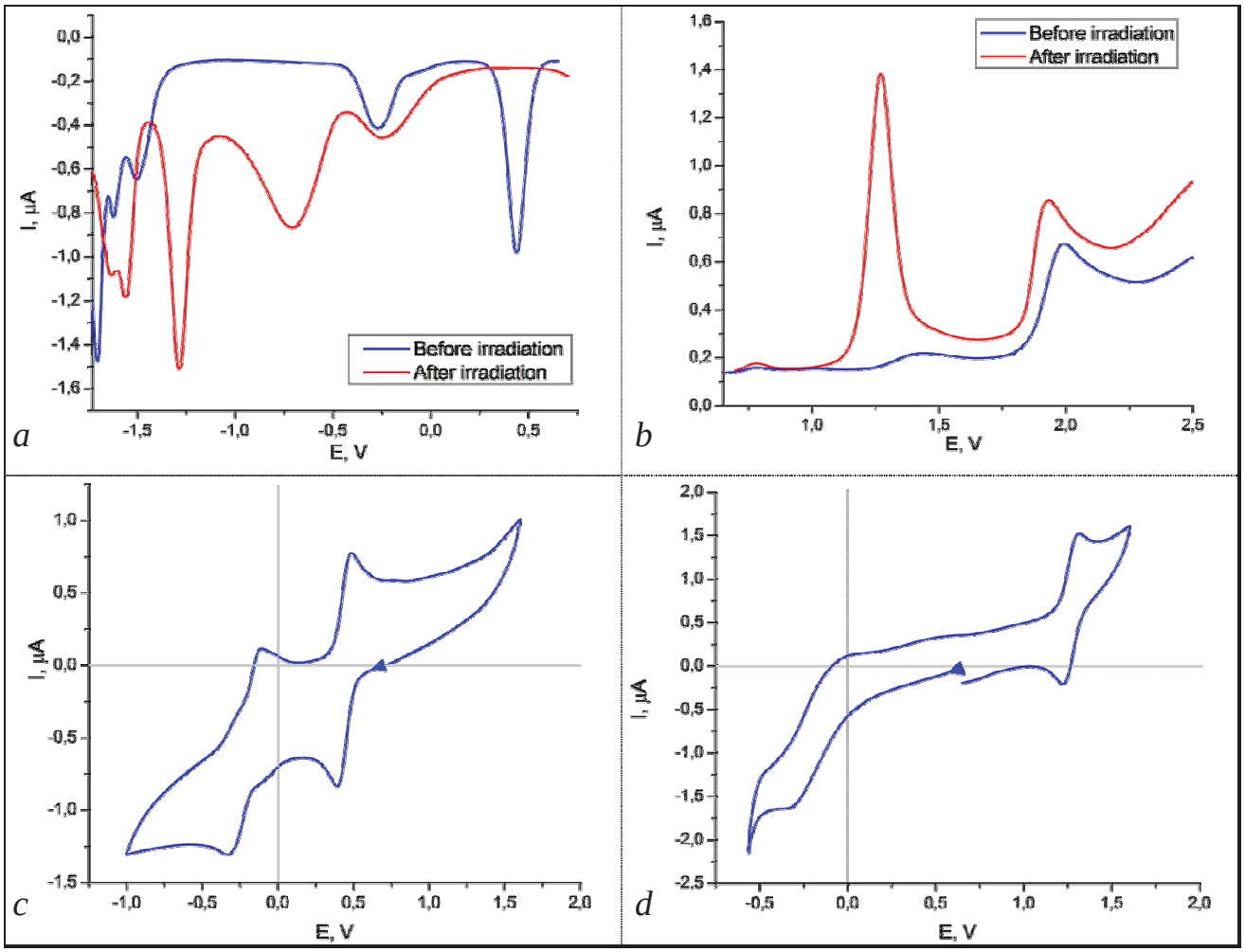

Figure 5.10. Square-wave voltamperograms for the acetonitrile solutions of the complex $[Ru^{II}(MeO\text{-}Phtpy)(bpy)(NO)](PF_6)_3$ (a and b). Cyclic voltamperograms of the solution before (c) and after irradiation (d).

Compound	Before irradiation				After irradiation			
	E_{eq}	Reduction	Oxidation		E_{eq}	Reduction	Oxidation	
		$NO^+/NO^\bullet$	*MeOPh-tpy and bpy*	*MeOPh-tpy*		*MeOPh-tpy*	*$Ru^{III/II}$*	*MeOPh-tpy*
$[Ru^{II}(MeO\text{-}Phtpy)(bpy)(NO)](PF_6)_3$	0.48	0.44	-1.49 -1.62 -1.71	1.99	0.69	-1.29 -1.56 -1.63 -1.71	1.27	1.93
cis-$[Ru^{II}(MeO\text{-}Phtpy)Cl_2(NO)](PF_6)$	-	-0.13	-	1.9	-	-	0.4	-

Table 5.5. The data of electrochemical investigation of the complex $[Ru^{II}(MeO\text{-}Phtpy)(bpy)(NO)](PF_6)_3$ before and after irradiation with the light of 350-450 nm region. Data for $[Ru^{II}(MeO\text{-}Phtpy)Cl_2(NO)](PF_6)$ are given as references.

The initial complex shows first two reduction waves at 0.44 V and 0.27 V (Figure 5.10a). At the same time, the process corresponding to the first one is reversible (Fig. 5.10c), and, according to the literature data for similar complexes, corresponds to the process of reduction of nitrosyl ligand $Ru^{II}NO^{+} \rightarrow Ru^{II}NO^{\cdot}$.[147,148] Naturally, after irradiation and NO release completion, this reduction wave disappears.

The second wave of reduction is likely to correspond to the $Ru^{II}NO^{\cdot} \rightarrow Ru^{II}NO^{-}$ process, which is not reversible. This attribution is also consistent with the published data.[148] Additional waves observed at significantly lower potentials appear due to the processes of reduction of organic ligands that are present in the complex.

The oxidation of the initial ruthenium-nitrosyl complex occurs at a potential of 1.99 V. The corresponding potential for the photoproduct is 1.93 V. The processes that determine the appearance of these waves are associated with the oxidation of ligands, most likely terpyridine, which is more enriched with electronic density. A similar behavior was observed earlier for the compound cis-$[Ru^{II}(MeO\text{-}Phtpy)Cl_2(NO)](PF_6)$: the oxidation was observed at a potential of 1.9 V. The most important result of the study of electrochemical oxidation of the photoproduct solution was the value of the redox potential for Ru^{III}/Ru^{II} pair , which makes 1.27 V. Observation of this wave in the process of the complex oxidation confirms the fact that ruthenium is in the oxidation state +2 in the compound[149].

The data of electrochemical study can be used to evaluate the stability of Ru^{II}/Ru^{III} forms in solution depending on the coordination environment of the metal center. Indeed, Ru^{III} complexes should be more prone to reduction in the case when the coordination sphere of the central atom contains five pyridine rings, i.e. {Ru(bpy)(tpy)}, than when it contains strong σ-donating ligands, such as chloro-ligands. This conclusion comes from the fact that the greater possibility of ruthenium electron density delocalization through π-backdonating interaction is possible in the case of pyridine ligands. This effect stabilizes the lower oxidation state of the metal, in other words, it increases the redox potential of the Ru^{III}/Ru^{II} pair. As can be seen from Table 5.5, the replacement of chloro-ligands with 2,2'-bipyridine results in an

increase in the potential of Ru^{III}/Ru^{II} pair from 0.4 V (for the compound cis-$[Ru^{II}(MeO\text{-}Phtpy)Cl_2(CH_3CN)]^{+/0}$ to 1.27 V (for the compound $[Ru^{II}(MeO\text{-}Phtpy)(bpy)(NO)]^{+3/+2}$).

Taking into account the results of the physical-chemical studies of the complex and the resulting photoproduct, it can be concluded that the release of nitric oxide from the ruthenium-nitrosyl complex $[Ru^{II}(MeO\text{-}Phtpy)(bpy)(NO)](PF_6)_3$ leads to the formation of a product containing ruthenium atom in the oxidation state +3, which, immediately reducing transforms into $[Ru^{II}(MeO\text{-}Phtpy)(bpy)(CH_3CN)]^{2+}$. The nature of the reductant, however, has not been investigated. On the one hand, the presence of nitrate anions in the crystalline structure of the photoproduct may indicate that the released nitric oxide can act as a reducing agent for compounds of Ru(III). On the other hand, the oxygen present in the solution can cause oxidation of NO, so there is no undeniable evidence of the direct interaction of Ru(III) complex with nitric oxide after its photorelease.

5.5. The by-product of the reaction of NO-release from the complex $[Ru^{II}(MeO\text{-}Phtpy)(bpy)(NO)](PF_6)_3$

An attempt to crystallize a photoproduct resulted in the formation of two types of crystals. Some of the crystals corresponded to the structure of the compound $[Ru^{II}(MeO\text{-}Phtpy)(bpy)(CH_3CN)](NO_3)_2$ described above. While the X-ray diffraction analysis of crystals of the second type revealed the structure of another photoproduct formed during the release of nitric oxide from the initial complex. Unfortunately, crystals of the second type were of a quality not good enough for X-ray study and obtaining a crystal of higher quality of this photoproduct failed. So at this stage only the structure of the cationic part of the complex was obtained with sufficient accuracy. Its structure is shown in Figure 5.11.

As in the case with the main photoproduct, the nitrosyl ligand in the by-product is replaced with the molecule of acetonitrile, but the main difference is that the phenyl ring of the terpyridine ligand in the case of a by-product is substituted with the nitrogroup in the third position. The formation of this compound was not detected

either by UV visible spectroscopy or NMR spectroscopy during a direct experiment on the release of nitrogen monoxide from the ruthenium-nitrosyl complex. This fact indicates that the formation of such a cation occurs during some time after irradiation.

Interestingly, the structure of the obtained nitro-derivative or rather 3-nitro-4-methoxyphenyl substituent is similar to the product of tyrosine amino acid nitration in living organisms.

As described in section 1.2, the formation of various reactive nitrogen species (RNS) capable of oxidizing and nitrating biomolecules takes place in tissues in the presence of nitric oxide and high concentrations of reactive oxygen forms. Such RNS are peroxynitrite anion, nitrogen(IV) oxide and some others. Although several hypothetical mechanisms for nitration of the amino acid residues of tyrosine are proposed, all of them suggest a radical mechanism of the process.[150,151] One of the possible ways of nitration is shown in Figure 5.12.[151]

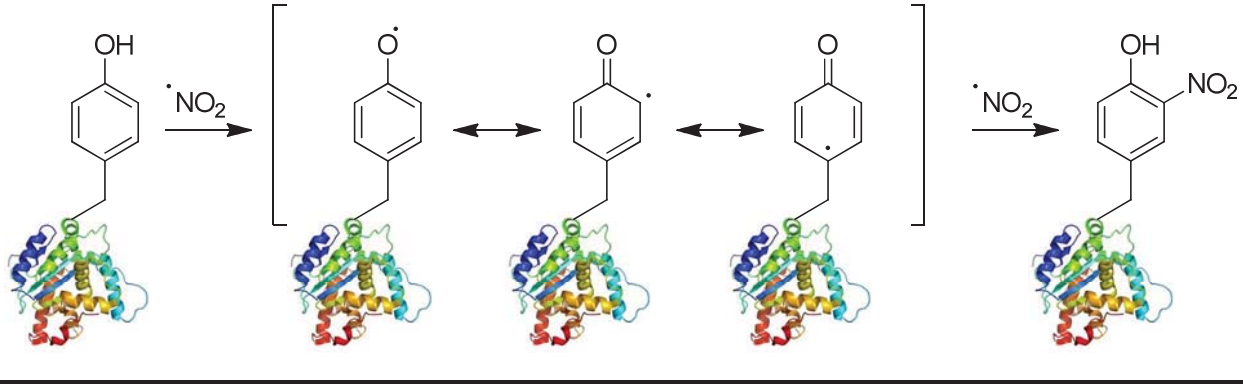

Figure 5.12. One of possible radical mechanisms of nitration of tyrosine with the formation of 3-nitrotyrosine.

Given that the methoxyphenyl substituent present in the MeO-Phtpy ligand cannot form a stable radical particle, the radical mechanism of the formation of the cation shown in Figure 5.11 is hardly probable. Possibly, nitration could occur through the mechanism of aromatic electrophilic substitution. In this case nitration could be attributed to the compounds of nitrogen in higher oxidation states, the presence of which in the system is confirmed by the presence of nitrate anions in the crystalline structure of the main photoproduct.

$[Ru^{II}(MeO\text{-}Phtpy)(bpy)(NO)]^{3+}$ releases NO· under irradiation in the UV-visible domain, with a quantum yield which appears significantly reduced when the involved transition exhibits a stronger push-pull charge transfer towards NO. This behavior indicates that the real mechanism of the NO-release cannot be restricted to the effect of an individual transition. Although NO is undoubtedly generated as NO· radical, the concomitant Ru^{III} photoproduct is readily reduced to a Ru^{II} complex of formula $[Ru^{II}(MeO\text{-}Phtpy)(bpy)(MeCN)]^{2+}$, probably by the action of a fraction of the nitric oxide photo-released during the irradiation process. In the presence of oxygen and water nitrogen monoxide is capable of being converted into species containing nitrogen at higher oxidation states that are capable of further interaction with the photoproduct $[Ru^{II}(MeO\text{-}Phtpy)(bpy)(CH_3CN)]^{2+}$ forming its nitro-derivative.

EXPERIMENTAL PART

Instrumentation.

Elemental analysis was performed on Perkin Elmer 2400 series II Instrument in LCC. ^{1}H NMR and ^{13}C NMR spectra were recorded on Bruker Avance III 400 (400 and 101 MHz respectively) or Bruker Avance 300 (300 and 75 MHz respectively) spectrometer at 298 K in DMSO-d_6, $CDCl_3$,CD_3OD, CD_3CN or THF-d_8; the internal standard is the residual peaks of deuterated solvents. The degree of carbon atom substitution was determined by NMR spectra acquired according to the DEPT-135 or JMOD methods. Two-dimensional (2D) (COSY, HMQC, HMBC) spectra were recorded on a Bruker Avance III 400 (400 MHz) spectrometer. Coupling constants (J) are reported in Hz, chemical shift (δ) in ppm. The multiplicity of signals is indicated using the following abbreviations: s = singlet, bs = broad singlet, d = doublet, t = triplet, q = quartet, quint = quintet, dd = doublet of doublets, ddd = doublet of doublets of doublets, dt = doublet of triplets, td = triplet of doublets and m = multiplet.

Electronic spectra were recorded on Hewlett Packard 8454A. IR-spectra were recorded on Perkin–Elmer 1725.

Electron paramagnetic resonance spectra (EPR) were recorded on Bruker ESP 500E. The following parameters and methods were used: microwave power 20 mW, amplitude of field modulation 0.1 mT, field modulation frequency 100 kHz, microwave frequency 9.782512 GHz. *N*-Methyl-*D*-glucamine dithiocarbamate was synthesized in advance and injected into the reaction with ammonium iron(II) sulfate to obtain $[Fe(MGD)_2]$.[152] The 90 μl 1 mM of $[Ru(MeO\text{-}Phtpy)(bpy)(NO)](PF_6)_3$ in acetonitrile was mixed with 10 μl of 2 mM $[Fe(MGD)_2]$ (in water) and injected into a quartz capillary. The sample was irradiated in EPR spectrometer by mercury lamp 250 W Oriel (Palaiseau, France). The emission light passed through the filter Oriel WG 400 UV (Palaiseau, France, $\lambda > 400$ nm) and was directed with the help of optical fiber.

High resolution mass spectra (HRMS) were recorded on GCT Premier spectrometer upon electron spray ionization (ESI).

The melting points were determined on Stuart melting point apparatus SMP10.

In the experiment when NO-release was studied by NMR-spectroscopy, the irradiation of complex was carried out by homemade LED device at 350-450 nm wavelength range. The study was made on the samples dissolved in CD_3CN introduced into NMR ampoules in the following conditions: 5 min of irradiation – ^1H NMR – 5 min of irradiation and so on until the disappearance of peaks of starting material.

Electrochemical investigations were carried out at room temperature in a homemade sealed tri-electrode cell connected to vacuum-argon line using the Autolab PGSTAT100 potentiostat. A reference electrode was a saturated calomel electrode (SCE), separated from the solution by a bridge. Counter electrode was Pt wire with approximate surface area of 1 cm^2. Main electrode was Pt microdisk (0.5 mm diameter). Electrolyte, which was used for experiment was tetrabtylammonium hexafluorophosphate (n-Bu_4N)[PF_6] (Fluka, 99%, puriss, electrochemical grade) which was used directly after degassing with argon. Complex and electrolyte concentrations were about 10^{-3} M and 0.1 M, respectively. Before each experiment, the solution was degassed by Ar flow, and the main electrode was polished using a Presi P230 machine. Irradiation aimed at obtaining a photoproduct with the purpose of the study of the latter by electrochemical method was carried out using homemade LED device with a wavelength range of 350-450 nm. The irradiation continued until disappearance of a characteristic signal of 2,2'-bipyridine proton at 9.32 ppm and disappearance of $NO^+ \rightarrow NO\cdot$ reduction band in voltamperometric analysis.

Photochemical studies.

Kinetic studies of photolysis reactions were performed using a diode-array Hewlett Packard 8454A spectrophotometer. All experiments were performed for acetonitrile non-deoxygenated solutions (volume 2 ml) of substances with concentrations: [Ru(FT)(bpy)NO]$(PF_6)_3$ (bpy1) – $4.94\cdot10^{-5}$ M, [Ru(FCCT)(bpy)NO]$(PF_6)_3$ – $4.43\cdot10^{-5}$ M, [Ru(FCC3T)(bpy)NO]$(PF_6)_3$ –

$4.48 \cdot 10^{-5}$ M, [Ru(MeO-Phtpy)(bpy)(NO)]$(PF_6)_3$– $3.64 \cdot 10^{-5}$ M (under irradiation with 365 nm wavelength), $4.42 \cdot 10^{-5}$ M (under irradiation with 436 nm wavelength). Optical fiber was fixed from the outside of the solution cuvettes. Absorption spectra were recorded every 10 seconds in fast scan mode. Irradiation was performed until a stable absorption value was achieved. The source of radiation was a mercury lamp, equipped with light filters, allowing to receive a monochromatic light of different wavelengths. The temperature was maintained at 25 °C throughout the experiment.

Measurement of the quantum yield of NO-release reaction.

Light intensities were determined before each photolysis experiment by chemical actinometry procedure. The actinometer used was potassium ferrioxalate trihydrate $K_3[Fe(C_2O_4)_3] \cdot 3H_2O$. The determined light intensity for bpy1 is 10^{-6} $M \cdot s^{-1}$, for [Ru(FCCT)(bpy)NO]$(PF_6)_3$ is $7.05 \cdot 10^{-7}$ $M \cdot s^{-1}$, [Ru(FCC3T)(bpy)NO]$(PF_6)_3$ is $8.66 \cdot 10^{-7}$ $M \cdot s^{-1}$, [Ru(MeO-Phtpy)(bpy)(NO)]$(PF_6)_3$ is $8.2 \cdot 10^{-7}$ $M \cdot c^{-1}$ (under irradiation with 365 nm wavelenght), $7.81 \cdot 10^{-7}$ $M \cdot c^{-1}$ (under irradiation with 436 nm wavelength). The quantum yield (ϕ_A) was determined by the program Sa3.3 written by D. Lavabre and V. Pimienta.[153] It allows the resolution of the differential eq. 6.1

$$\frac{\mathbf{d[A]}}{\mathbf{dt}} = -\boldsymbol{\varphi}_{\mathbf{A}}\, \mathbf{I}_{\mathbf{a}}^{\mathbf{A}} = -\boldsymbol{\varphi}_{\mathbf{A}}\, \mathbf{Abs}_{\mathbf{A}}^{\boldsymbol{\lambda}} \mathbf{I_0 F} \quad (6.1),$$

where $\mathbf{I}_{\mathbf{a}}^{\mathbf{A}}$ is the intensity of the light absorbed by the precursor; $\mathbf{Abs}_{\mathbf{A}}^{\boldsymbol{\lambda}}$ is the optical density before irradiation; $\mathbf{I_0}$, the incident intensity measured at 365 or 436 nm and **F** the photokinetic factor depending on total optical density $\mathbf{Abs}_{\mathbf{Tot}}^{\boldsymbol{\lambda}}$ and given by eq. 6.2:

$$\mathbf{F} = \frac{\left(\mathbf{1} - \mathbf{10}^{-\mathbf{Abs}_{\mathbf{Tot}}^{\boldsymbol{\lambda}}}\right)}{\mathbf{Abs}_{\mathbf{Tot}}^{\boldsymbol{\lambda}}} \qquad (6.2).$$

The equation was fitted with the experimental data parameters φ_A and ε_B (ε_B is the molar extinction coefficient measured at the end of the reaction) at two wavelengths, namely, the wavelength of irradiation λ_{irr} and the wavelength of observation λ_{obs}, which corresponds to the largest difference between molar extinction coefficient at the initial and final moment of the photochemical reaction. Optimization procedures were performed by using numerical integration and a non-linear minimization algorithm.[154]

bpy1:

$[A]_0 = 4.94 \cdot 10^{-5}$ M, $\boldsymbol{\varepsilon_A^{405}} = 15729$ $M^{-1} \cdot cm^{-1}$, $\boldsymbol{\varepsilon_A^{470}} = 12579$ $M^{-1} \cdot cm^{-1}$,

$\boldsymbol{\varepsilon_B^{405}} = 7969$ $M^{-1} \cdot cm^{-1}$, $\boldsymbol{\varepsilon_B^{470}} = 21422$ $M^{-1} \cdot cm^{-1}$

[Ru(FCCT)(bpy)NO](PF$_6$)$_3$:

$[A]_0 = 4.43 \cdot 10^{-5}$ M, $\boldsymbol{\varepsilon_A^{436}} = 19639$ $M^{-1} \cdot cm^{-1}$, $\boldsymbol{\varepsilon_A^{370}} = 17156$ $M^{-1} \cdot cm^{-1}$,

$\boldsymbol{\varepsilon_B^{436}} = 14756$ $M^{-1} \cdot cm^{-1}$, $\boldsymbol{\varepsilon_B^{370}} = 20442$ $M^{-1} \cdot cm^{-1}$

[Ru(FCC3T)(bpy)NO](PF$_6$)$_3$:

$[A]_0 = 4.48 \cdot 10^{-5}$ M, $\boldsymbol{\varepsilon_A^{436}} = 17411$ $M^{-1} \cdot cm^{-1}$, $\boldsymbol{\varepsilon_A^{370}} = 18973$ $M^{-1} \cdot cm^{-1}$,

$\boldsymbol{\varepsilon_B^{436}} = 15106$ $M^{-1} \cdot cm^{-1}$, $\boldsymbol{\varepsilon_B^{370}} = 30437$ $M^{-1} \cdot cm^{-1}$

[Ru(MeO-Phtpy)(bpy)(NO)](PF$_6$)$_3$:

under irradiation with 365 nm wavelength:

$[A]_0 = 3.64 \cdot 10^{-5}$ M, $\boldsymbol{\varepsilon_A^{365}} = 18874$ $M^{-1} \cdot cm^{-1}$, $\boldsymbol{\varepsilon_A^{470}} = 7335$ $M^{-1} \cdot cm^{-1}$,

$\boldsymbol{\varepsilon_B^{365}} = 5244$ $M^{-1} \cdot cm^{-1}$, $\boldsymbol{\varepsilon_B^{470}} = 17672$ $M^{-1} \cdot cm^{-1}$

Under irradiation with 436 nm wavelength:

$[A]_0 = 4.42 \cdot 10^{-5}$ M, $\boldsymbol{\varepsilon_A^{436}} = 11292$ $M^{-1} \cdot cm^{-1}$, $\boldsymbol{\varepsilon_A^{370}} = 18735$ $M^{-1} \cdot cm^{-1}$,

$\boldsymbol{\varepsilon_B^{436}} = 13412$ $M^{-1} \cdot cm^{-1}$, $\boldsymbol{\varepsilon_B^{370}} = 5554$ $M^{-1} \cdot cm^{-1}$

X-Ray analysis.

The data were collected at low temperature (100(2) K) with a Bruker Apex II diffractometer equipped with a 30 W air-cooled microfocus Mo-*K*α radiation source (λ = 0.71073 A) and an Oxford Cryosystems Cryostream cooler device, and φ and ω scans were used for data collection. An empirical correction using SADABS was used.[155] The structure was solved by direct methods with SHELXT. All non-hydrogen atoms were refined anisotropically by least-squares procedures on F^2 with the aid of the program SHELXL.[156,157] All hydrogen atoms were refined isotropically at calculated positions in a riding model with their isotropic displacement parameters constrained to 1.5 times the equivalent isotropic displacement parameters of their pivot atoms for terminal sp^3 carbon atom and 1.2 times for all other carbon atoms. In the crystal structure counter anions were highly disordered. In [Ru(MeO-Phtpy)(bpy)(NO)]$(PF_6)_3$ one hexafluorophosphate anion was disordered over two positions in 74:26 ratio; in $[Ru^{II}$(MeO-Phtpy)(bpy)(MeCN)]$(NO_3)_2$ two nitrate anions were disordered over three positions in 48:22:30 and 40:29:3 ratios. Each disorder was modeled successfully with the atom ellipsoids restrained by SIMU, DELU and ISOR commands.

Computational studies.

All the calculations were performed using Gaussian-09 program package within the framework of Density Functional Theory (DFT). Optimization of structures of all ions was performed using the hybrid functional B3PW91, which for these systems shows the best match between the theoretical results and the experimental data. This choice is also in agreement with a previous investigation of ruthenium-nitrosyl complexes made by Mascharak[158] and I. Malfant[86] group. B3PW91 has been shown to outperform other hybrid functionals (e.g., B3LYP) and pure functionals (e.g., PW91) for numerous ruthenium complexes, especially when backbonding ligands (such as NO) are present. The vibrational analysis performed at the same level of theory as the oprimization of geometry was made to verify that the stationary points corresponded to minima on the potential energy surfaces.

The «double-ζ» basis 6-31G* was used for all atoms except the heavy ruthenium atom, for which the LANL2DZ basis set was applied to account for relativistic effects.

Complexes cis1', trans1' and bpy1' were optimized in a gas phase, UV/Vis electronic spectra were then computed at the CAM-B3LYP/6-31G* level, which was selected for its efficient reproduction of experimental transition energies within a maximum uncertainty of 0.3 eV.

Solvent effects were included by using the polarizable continuum model (PCM) implemented in Gaussian09 for acetonitrile (ε = 35.688).

Compounds **3.1-3.22** were optimized at a gas phase. For each molecule the two possible conformers resulting from the rotation around σ-bond between the fused heterocyclic system and the C=C double bond of the ethenyl linkage were considered (*vide infra*). The most stable one was selected by comparison of their Gibbs free energies (ΔG°). UV/Vis electronic spectra were then computed at the CAM-B3LYP/6-31G* level of theory. The total hyperpolarizabilities (β) were computed at CAM-B3PYP/6-31G** level, in which *p* polarization functions are used on hydrogen atoms. The ten independent β_{ijk} tensor components were computed by the derivative procedure implemented in Gaussian-09, according to the following equation:

$$\boldsymbol{\beta_{ijk} = -\left(\frac{\partial^3 W}{\partial E_i \partial E_j \partial E_j}\right)_{E=0}} \qquad (6.3),$$

where *W* is the energy and *E* the electric field. This expression is only valid for the static field limit, which corresponds to Kleinman conditions.[159] The final β value is given as the magnitude of the β vector ($\sqrt{\beta_x^2 + \beta_y^2 + \beta_z^2}$). The vectorial component β_i is computed from the tensor components as: $\beta_i = \beta_{ixx} + \beta_{iyy} + \beta_{izz}$.

Ions [Ru(FCC3T)(bpy)(NO)]$^{3+}$, [Ru(FCCT)(bpy)(NO)]$^{3+}$, [Ru(MeO-Phtpy)(bpy)(NO)] $^{3+}$ and [Ru(FT)Cl_2(CH_3CN)]$^{+}$ were optimized using PCM model for acetonitrile; UV/Vis electronic spectra were computed at the CAM-B3LYP/6-31G* level of theory.

Molecular orbitals were plotted with GABEDIT 2.4.8.

Two-photon absorption study.

The z-scan technique was used to measure the nonlinear absorption coefficients of the samples at λ = 800 nm through the application of short laser pulses of 90 fs at a repetition rate of 1 kHz. The molecules under study were dissolved in acetonitrile at a concentration of $1 \cdot 10^{-2}$ mol·L^{-1}. *Z*-scan traces for each solution were measured at different energies, namely, 30, 50, 75, and 95 nJ for cis2, trans2, bpy2; 40, 65, 75 nJ for *cis*(Cl,Cl)-[Ru(MeOPh-tpy)Cl_2NO]PF_6, *trans*(Cl,Cl)-[Ru(MeOPh-tpy)Cl_2NO]PF_6, *cis*(Cl,Cl)-[Ru(Et_2NPh-tpy)Cl_2NO]PF_6, *trans*(Cl,Cl)-[Ru(Et_2NPh-tpy)Cl_2NO]PF_6); 40, 62, 100 nJ for [Ru(FCCT)(bpy)NO]$(PF_6)_3$ and [Ru(FCC3T)(bpy)NO]$(PF_6)_3$. All samples were measured at least ten times at each energy. The increase in the energy of the radiation should be linearly related to the decrease in the transmission of the sample, which has been confirmed for each of the complexes. To verify the validity of our measurements, the same z-scan apparatus was first utilized in the closed-aperture approach to measure the nonlinear refractive index n_2 of the standard CS_2. The results led to n_2 values in the range $1.2 \cdot 10^{-15}$ cm^2/W, which are in very good agreement with the values accepted for this standard reference. Then, the laser dye rhodamine 6G (R6G) was measured along with the set of samples under test in the open-aperture approach. In this case, the σ_{TPA} value of R6G was (67.5) GM, which is also in very good agreement with the value accepted in the literature.[160]

The nonlinear absorption coefficient β of each sample was obtained after fitting the normalized transmission *T*(z) according to eq. 6.4:

$$\mathbf{T(z) = 1 - \frac{1}{2\sqrt{2}} \beta \frac{I_0 l_{eff}}{1 + \left(\frac{z}{z_0}\right)^2}} \qquad (6.4),$$

where I_0 – laser pulse energy, l_{eff} – sample thickness (0.1 cm for all the experiments), z – sample position, z_0 – Rayleigh length (parameter of the laser beam). Rayleigh

length was established by the «knife-edge method», and was 0.190 cm when studying cis2, trans2 and bpy2; 0.066 cm when studying *cis*(Cl,Cl)-[Ru(MeOPh-tpy)Cl_2NO]PF_6, *trans*(Cl,Cl)-[Ru(MeOPh-tpy)Cl_2NO]PF_6, *cis*(Cl,Cl)-[Ru(Et_2NPh-tpy)Cl_2NO]PF_6, *trans*(Cl,Cl)-[Ru(Et_2NPh-tpy)Cl_2NO]PF_6; 0.101 cm when studying [Ru(FCCT)(bpy)NO]$(PF_6)_3$ and [Ru(FCC3T)(bpy)NO]$(PF_6)_3$. The values of absorption cross-sections were calculated according to formula 6.5:

$$\sigma = \frac{h\nu\beta}{N} \qquad (6.5),$$

where N – concentration of the molecule (molecule/l), ν – frequency of laser radiation.

The procedures for the syntheses of ligands and their precursors.

Compounds **4.1**[126], **4.2**[126], **4.5**[129], **4.7**[161], 1-(2-oxo-2-(pyridin-2-yl)ethyl)pyridin-1-ium iodide[132], **4.15**[137], **4.16**[162], **4.17**[137], 4'-(4-methoxyphenyl)-2,2':6',2''-terpyridine[142] were synthesized according to the reported procedures.

The synthesis of FCCT and FCC3T ligands:

4'-bromo-2,2':6',2''-terpyridine ***(4.3)*****.**

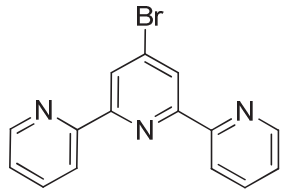

PBr_5 (8.09 g, 19 mmol) was added to the suspension of (2,2':6',2''-terpyridin)-4'(1'*H*)-one **4.2** (1.93 g, 7.75 mmol) in DMF (50 mL) and heated at 90-93 °C for 20 h. The reaction mixture was then cooled down and 80-100 mL of water were carefully added followed by neutralization with Na_2CO_3. The mixture was extracted with CH_2Cl_2. The organic phase was washed with brine, dried over Na_2SO_4 and filtrated. The solvent was evaporated under reduced pressure and the residues were purified by column chromatography (elution system: CH_2Cl_2 – hexane, 2:1) on alumina yielding 1.69 g (5.42 mmol, 70%) of light beige solid.

2-bromo-9,9-dihexyl-9H-fluorene ***(4.6)*****.**

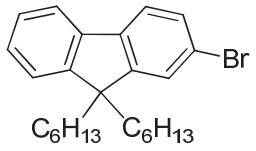

2-Bromofluorene (11.65 g, 0.048 mol) and KI (0.79 g, 4.76 mmol) were dissolved in DMSO (96 mL) upon slight heating. After complete dissolving the mixture was degassed and put under inert atmosphere. KOH (9.16 g, 0.164 mol) was then pestled and added to the solution under Ar flow. The mixture was stirred for 20 min followed by *n*-bromohexane (17 mL, 0.121 mol) dropping into the reaction mixture in 5 portions, very slowly, with intensive stirring. The interval between portions was 10 min. After the addition was completed, the mixture was left stirring at room temperature for 3 hours followed by water addition and extraction with EtOAc. The organic layer was washed with brine and dried over Na_2SO_4. The product was purified by column chromatography (eluent: pentane, 100%) to yield 19.63 g (99.9%) of colorless oil.

9,9-dihexyl-2-vinyl-9H-fluorene ***(4.8)*****.**

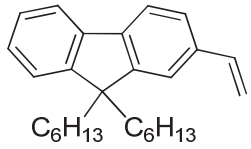

2-Bromo-9,9-dihexyl-9*H*-fluorene (960 mg, 2.32 mmol), $KBF_3C_2H_3$ (334 mg, 2.49 mmol), $Pd(OAc)_2$ (70 mg, 0.31 mmol), PPh_3 (233 mg, 0.89 mmol) and Cs_2CO_3 (1936 mg, 5.94 mmol) were suspended in THF (30 mL) and H_2O (1.5 mL) mixture and placed into teflon reactor. The mixture was degassed under the intense Ar flow and sealed. The mixture was heated at 100 °C under the vigorous stirring over 48 h. The resulting mixture was diluted with H_2O and extracted with CH_2Cl_2. Organic extracts were washed with brine, dried over Na_2SO_4 and filtrated. The solvent was evaporated under reduced pressure and the residues were purified by column chromatography (eluent: hexane, 100%) on silica gel to yield 227 g (0.63 mmol, 27%) of colorless oil.

(E)-ethyl 3-(9,9-dihexyl-9H-fluoren-2-yl)acrylate ***(4.9)*****.**

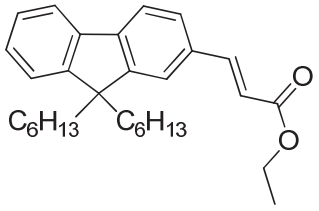

Ethylacrylate (1.12 mL, 10.50 mmol) and anhydrous DMF (7 mL) was added to the mixture of 2-bromo-9,9-dihexyl-9H-fluorene **4.6** (2.89 g, 7.00 mmol), $Pd(OAc)_2$ (47 mg,

0.21 mmol), PPh_3 (138 mg, 0.53 mmol) and Et_3N (0.98 mL, 7.00 mmol) in inert atmosphere. The resulting suspension was heated at 90 °C under vigorous stirring over 14 h. After the completion of the reaction was cooled down to rt followed by H_2O (70 mL) adding. The mixture was extracted with EtOAc; the organic extracts were washed with brine, dried over Na_2SO_4 and filtrated. The solvent was evaporated under reduced pressure and the residues were purified by column chromatography (elution system: *n*-hexane – EtOAc, 200:1) on silica gel to yield 2.48 g (5.73 mmol, 82%) of yellow oil.

(E)-3-(9,9-dihexyl-9H-fluoren-2-yl)acrylaldehyde ***(4.11)*****.**

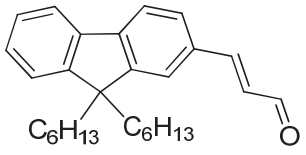

The solution of DIBAL-H (30 mL, 1.5 M, 45 mmol) was dropped into the solution of (*E*)-ethyl 3-(9,9-dihexyl-9*H*-fluoren-2-yl)acrylate **4.9** (6.49 g, 15 mmol) in anhydrous toluene (150 mL) under inert atmosphere at -78 °C. The reaction mixture was stirred vigorously until the complete disappearance of the starting material (TLC control). Then MeOH (3.6 mL) was added slowly to the reaction mixture until complete liberation of H_2 followed by quick addition of AcOEt (300 mL). The mixture was allowed to reach a room temperature and left at intensive stirring for 1 hour followed by filtration through celite; the filtrate was evaporated under reduced pressure.

The resulting mixture was dissolved in $CHCl_3$ (225 mL) and MnO_2 (9.78 g, 112.5 mmol) was added. Heterogenic mixture was stirred at room temperature until complete disappearance of starting material (TLC control, for 2-3 days). After the reaction completion the mixture was filtrated through a plug of celite and filtrate was concentrated under reduced pressure. The residues were purified by column chromatography (elution system: *n*-hexane – EtOAc, 99:1) on silica gel to yield 3.43 g (8.2 mmol, 70%) of yellow oil.

(2E,4E)-5-(9,9-dihexyl-9H-fluoren-2-yl)-1-(pyridin-2-yl)penta-2,4-dien-1-one ***(4.12).***

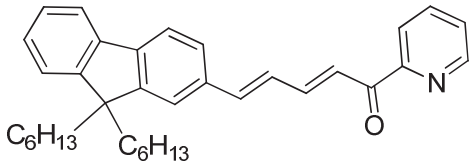

A solution of NaOH (1.35 mL, 1M, 1.35 mmol) in water was dropped into the solution of (*E*)-3-(9,9-dihexyl-9H-fluoren-2-yl)acrylaldehyde **4.11** (0.35 g, 0.90 mmol) and 2-acetylpyridine (0.10 mL, 0.90 mmol) in EtOH under vigorous stirring. The reaction mixture was stirred at rt until complete conversion of starting material (TLC control) The resulting precipitate was filtered off, rinsed with water and cold EtOH and dried under vacuum. The yield of **4.12** was 0.20 g (0.52 mmol, 45%). After purification of filtrate by column chromatography (elution system: hexane – AcOEt, 9:1) the extra 0.06 g was obtained (13%). The total yield was 58%, yellow powder.

(E)-4'-(2-(9,9-dihexyl-9H-fluoren-2-yl)vinyl)-2,2':6',2''-terpyridine ***(FCCT).***

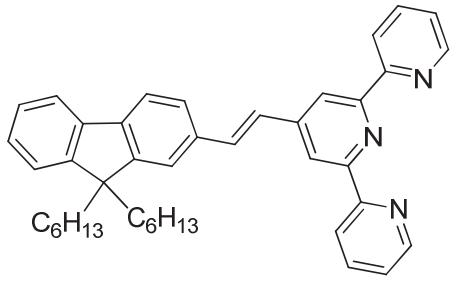

1-(2-Oxo-2-(pyridin-2-yl)ethyl)pyridin-1-ium iodide (0.32 g, 0.99 mmol) and NH_4OAc (1.04 g, 13.5 mmol) were added to the suspension of (2*E*,4*E*)-5-(9,9-dihexyl-9H-fluoren-2-yl)-1-(pyridin-2-yl) penta-2,4-dien-1-one **4.12** (0.44 g, 0.9 mmol) in EtOH (5 mL) and the mixture was refluxed until complete conversion of starting ketone **4.12** (TLC control). After the reaction finished the mixture was cooled down and evaporated under reduced pressure. The residue was diluted with water and extracted with EtOAc. The organic extracts were dried over Na_2SO_4 followed by filtration and solvent evaporation under educed pressure. The residue was purified by column chromatography: primarily – eluent: CH_2Cl_2, 100%; second time – elution system: hexane – acetone, 9:1 on alumina oxide to yield 0.19 g (0.32 mmol, 36%) of yellow oil. R_f 0.48 (heptane – acetone, 4:1, alumina oxide).

2-ethynyl-9,9-dihexyl-9H-fluorene ***(4.14)*****.**

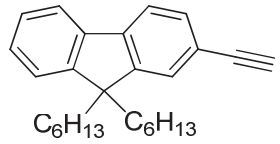

The mixture of 2-bromo-9,9-dihexyl-9*H*-fluorene **4.6** (3.14 g, 7.60 mmol), activated CuI (72 mg, 0.38 mmol) and $PdCl_2(PPh_3)_2$ (133 mg, 0.189 mmol) were placed in inert atmosphere followed by addition of anhydrous THF (10 mL). The reaction mixture was heated to reflux followed by dropwise addition of DIPA (6 mL, 43 mmol) and ethynyltrimethylsilane (2.7 mL, 19 mmol); the condenser should be kept cold (the boiling point of ethynyltrimethylsilane is 57 °C). After 12 h the reaction was stopped, the solution was cooled down, and EtOAc (15 mL) was added followed by washing with saturated NH_4Cl solution. The product was purified by column chromatography (eluent: hexane, 100%) on silica gel to yield 1.84 g (4.26 mmol, 56%) of ((9,9-dihexyl-9*H*-fluoren-2-yl)ethynyl) which was then suspended in the mixture of metanol (10 mL) and diethyl ether (10 mL) followed by potassium carbonate addition (2.11 g, 15 mmol). The mixture was stirred over 90 min and filtrated, filtrate was evaporated under reduced pressure. The residue was dissolved in hexane and filtrated through a plug of silica gel. Silica gel was thoroughly rinsed with hexane. Filtrate was evaporated under reduced pressure to yield 1.24 g (3.46 mmol, 81%) of colorless oil.

4'-((9,9-dihexyl-9H-fluoren-2-yl)ethynyl)-2,2':6',2''-terpyridine ***(FCC3T)*****.**

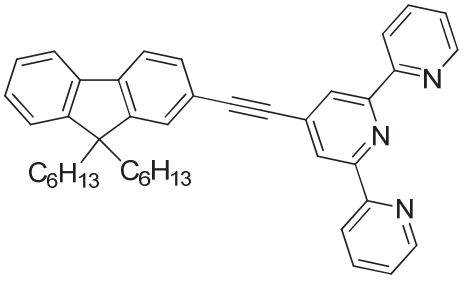

The mixture of 2-ethynyl-9,9-dihexyl-9*H*-fluorene **4.14** (311 mg, 0.87 mmol), (2,2':6',2''-terpyridin)-4'-yl trifluoromethylsulfonate **4.7** (330 mg, 0.87 mmol), $[Pd(PPh_3)_4]$ (50 mg, 0.043 mmol) was degassed and placed into inert atmosphere. Anhydrous PhMe (60 mL) and DIPA (8.2 mL) were after added to the reaction mixture and the resulting mixture was heated at 80 °C over 36 h (TLC control). After the reaction completion it was cooled down and evaporated under reduced pressure. The residue was dissolved in CH_2Cl_2, rinsed with water, brine and dried over Na_2SO_4. The solvent was evaporated at reduced pressure. The product was purified by column

chromatography on silica gel in two steps: 1) elution system: pentane – CH_2Cl_2, 9:1; 2) elution system pentane – EtOAc, 10:1 to yield 213 mg (42%) of yellowish oil.

Synthesis of complexes.

General procedure for the synthesis of [Ru(R-tpy)Cl_3] (A).

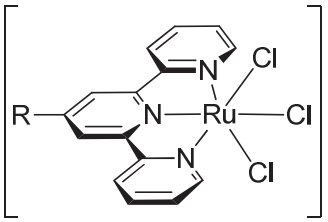

A

Ligand (1 mmol) and $RuCl_3 \cdot xH_2O$ (Ru: 40-49%; 251 mg for 1 mmol of ligand, 1-1.22 equiv) were suspended in ethanol (65 mL for 1 mmol of ligand). The mixture was refluxed over 3h; the flask was covered by aluminium foil to protect the complex from radiation. After 3h the flask was cooled down and the volume of solvent was reduced to 1/3 of the initial volume upon evaporation under reduced pressure. The residue was left in the fridge for 2 h. The obtained precipitate was filtrated off and was thoroughly rinsed with cold water (until the colorless drops of filtrate), chilled EtOH and diethyl ether. The complex was dried under vacuum to yield brown-black solids. .

[Ru(FCCT)Cl_3]:

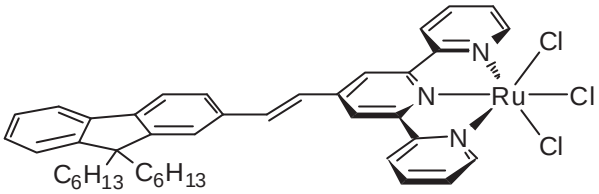

Starting materials: (*E*)-4'-(2-(9,9-dihexyl-9*H*-fluoren-2-yl)vinyl)-2,2':6',2''-terpyridine **FCCT** (216 mg, 0.364 mmol), $RuCl_3 \cdot xH_2O$ (Ru: 40-49%; 96 mg), EtOH (22 mL). Yield – 262 mg (0.327 mmol, 90%).

[Ru(FCC3T)Cl_3]:

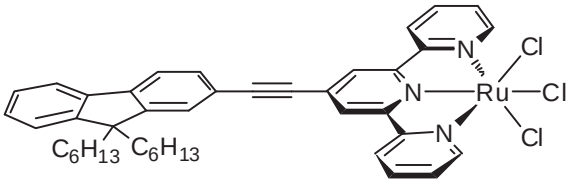

Starting materials: 4'-((9,9-dihexyl-9*H*-fluoren-2-yl)ethynyl)-2,2':6',2''-terpyridine **FCC3T** (214 mg, 0.36 mmol), $RuCl_3 \cdot xH_2O$ (Ru: 40-49%; 91 mg), EtOH (30 mL). Yield – 169 mg (0.34 mmol, 58 %).

[Ru(MeO-Phtpy)Cl_3]:

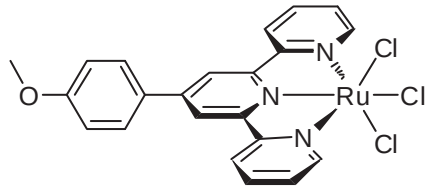

Starting materials: 4'-(4-methoxyphenyl)-2,2':6',2''-terpyridine **MeO-Phtpy** (250 mg, 0.74 mmol), $RuCl_3 \cdot xH_2O$ (Ru: 40-49%; 192 mg). EtOH (48 mL) Yield – 335 mg (0.61 mmol, 83 %).

General procedure for the synthesis of [Ru(R-tpy)(bpy)Cl]Cl (B).

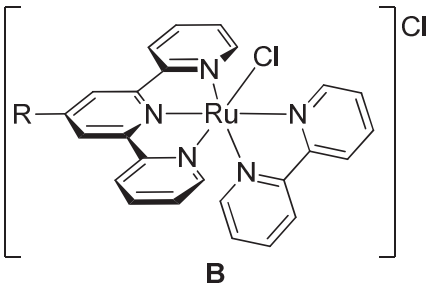

Complex [Ru(R-tpy)Cl_3] (**A**) (1 equiv), 2,2'-bipyridine (1 equiv), LiCl (6 equiv) were added to 75% EtOH/25% H_2O mixture (92 mL for 1 mmol of **A**), followed by Et_3N (1.6 equiv) addition. The mixture was refluxed over 3h; the flask was covered with aluminium foil to protect the complex from irradiation. After the reaction completion an undesired precipitate was immediately filtrated off from the hot solution. The precipitate was washed by ethanol and the filtrate was concentrated under reduced pressure until 1/6 of initial volume and left in the fridge over 2 h. The obtained precipitate was filtrated off and rinsed with aqueous HCl solution (3M) (until the colorless drops of filtrate), a small amount of chilled EtOH and diethyl ether. The product was dried under the vacuum to yield purple solids.

[Ru(FCCT)(bpy)Cl]Cl:

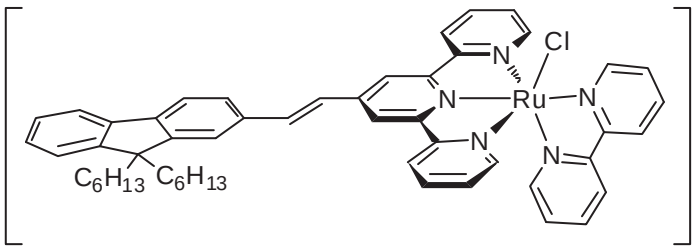

Starting materials: [Ru(FCCT)Cl_3] (262 mg, 0.33 mmol), 2,2'-bipyridine (51 mg, 0.33 mmol), LiCl (77 mg, 1.80 mmol), Et_3N (74 µL, 0.52 mmol), 75% EtOH/25% H_2O (30 mL). Yield – 208 mg (0.23 mmol, 69%).

[Ru(FCC3T)(bpy)Cl]Cl:

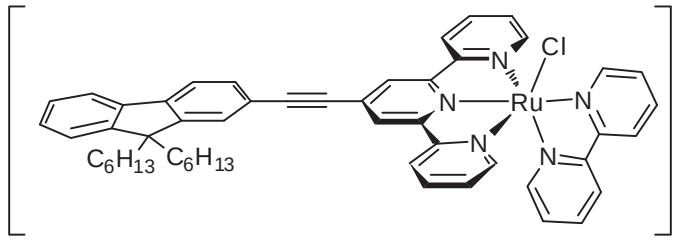

Starting materials: $[Ru(FCC3T)Cl_3]$ (169 mg, 0.21 mmol), 2,2'-bipyridine (33 mg, 0.21 mmol), LiCl (64 mg, 1.5 mmol), Et_3N (60 µL, 0.42 mmol), 75% EtOH/25% H_2O (25 mL). Yield – 162 mg (0.23 mmol, 83%).

[Ru(MeO-Phtpy)(bpy)Cl]Cl:

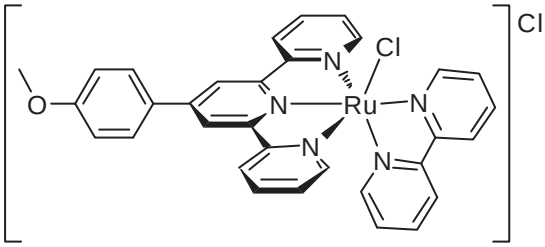

Starting materials: $[Ru(MeO\text{-}Phtpy)Cl_3]$ (335 mg, 0.61 mmol), 2,2'-bipyridine (96 mg, 0.62 mmol), LiCl (146 mg, 3.5 mmol), Et_3N (138 µL, 1 mmol), 75% EtOH/25% H_2O (56 mL). Yield – 390 mg (0.23 mmol, 69%).

General procedure for the synthesis of [Ru(R-tpy)(bpy)NO_2]Cl (C).

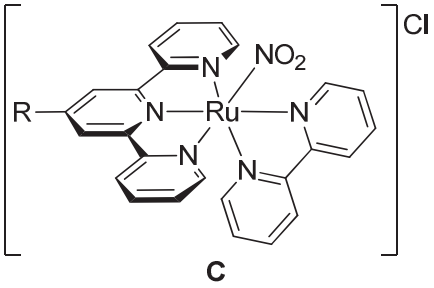

C

Complex [Ru(R-tpy)(bpy)Cl]Cl **(B)** (1 equiv) and $NaNO_2$ (10 equiv) were dissolved in 75% EtOH/25% H_2O mixture(124 mL for 1 mmol). The mixture was refluxed over 3h; the flask was covered with aluminium foil to protect the complex from irradiation. After the reaction completion the flask was cooled down and the volume of solvent was reduced to 1/6 of the initial volume upon concentration. The residue was left in the fridge for 2 h. The obtained precipitate was filtrated off and rinsed with cold water, a small amount of cold EtOH and diethyl ether. The complex was dried under the vacuum to yield dark red solids. .

[Ru(FCCT)(bpy)NO$_2$]Cl:

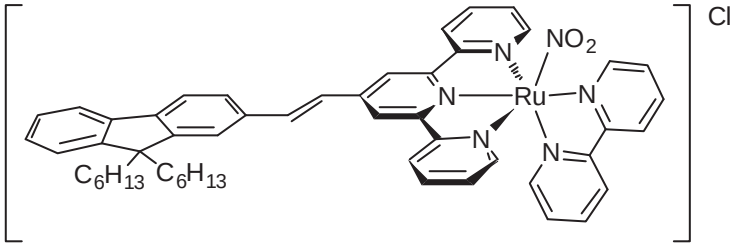

Starting materials: [Ru(FCCT)(bpy)Cl]Cl (208 mg, 0.23 mmol), $NaNO_2$ (156 mg, 2.26 mmol), 75% EtOH/25% H_2O (28 mL). Yield – 139 mg (0.149 mmol, 66%).

[Ru(FCC3T)(bpy)NO$_2$]Cl:

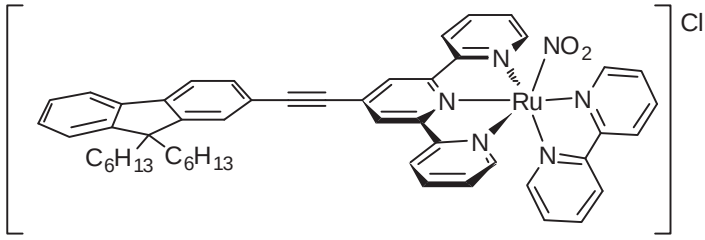

Staring materials: [Ru(FCC3T)(bpy)Cl]Cl (162 mg, 0.22 mmol), $NaNO_2$ (150 mg, 2.17 mmol), 75% EtOH/25% H_2O (28 mL). Yield – 95 mg (0.10 mmol, 46%).

[Ru(MeO-Phtpy)(bpy)NO$_2$]Cl:

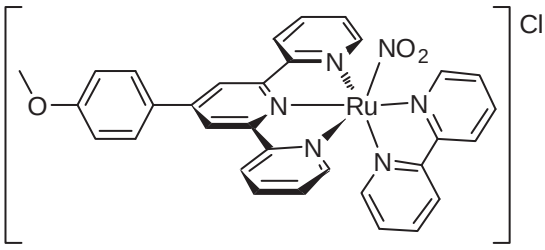

Starting material: [Ru(MeO-Phtpy)(bpy)Cl]Cl (390 mg, 0.58 mmol), $NaNO_2$ (402 mg, 5.83 mmol), 75% EtOH/25% H_2O (72 mL). Yield – 357 mg (0.53 mmol, 90%).

General procedure for the synthesis of [Ru(R-tpy)(bpy)NO](PF$_6$)$_3$ (D).

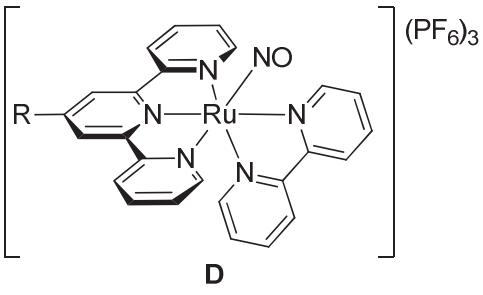

D

Complex [Ru(R-tpy)(bpy)NO_2]Cl (**C**) (1 equiv) was dissolved in EtOH (108 mL for 1 mmol of **C**), and the solution was mixed with the solution of HCl (12M, 108 mL for 1 mmol of **C**, 1300 equiv) in EtOH (216 mL for 1 mmol of **C**). The mixture was heated to 60 °C and left stirring over 1 h; the flask was covered by aluminium foil to protect the complex from radiation. After the reaction completion the flask was cooled down and the volume of solvent was reduced to 1/5 of the initial volume followed by addition of saturated solution of NH_4PF_6 (15 equiv) in water. The

mixture was left in the fridge for 2 h. The obtained precipitate was filtrated off, rinsed with a small amount of cold EtOH and diethyl ether. The complex was dried under vacuum.

[Ru(FCCT)(bpy)NO](PF$_6$)$_3$:

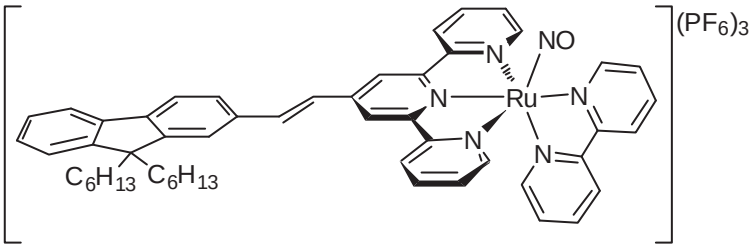

Starting materials: [Ru(FCCT)(bpy)NO$_2$]Cl (60 mg, 0.064 mmol), HCl (12M, 6.9 mL, 83.8 mmol), EtOH (21 mL). Yield – 53 mg (0.041 mmol, 63%).

[Ru(FCC3T)(bpy)NO](PF$_6$)$_3$:

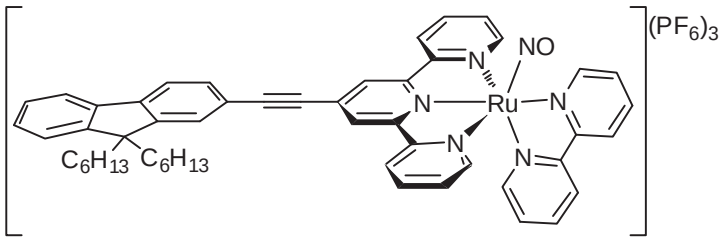

Starting materials: [Ru(FCC3T)(bpy)NO$_2$]Cl (72 mg, 0.078 mmol), HCl (12M, 8.3 mL, 63.2 mmol), EtOH (16 mL). Yield – 68 mg (0.051 mmol, 66%).

[Ru(MeO-Phtpy)(bpy)NO](PF$_6$)$_3$:

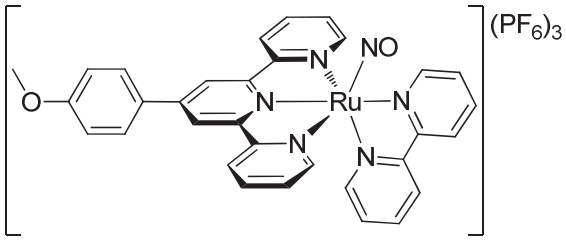

Starting materials: [Ru(MeO-Phtpy)(bpy)Cl]Cl (390 mg, 0.58 mmol), $NaNO_2$ (402 mg, 5.83 mmol), 75% EtOH/25% H_2O (72 mL). Yield – 357 mg (0.53 mmol, 90%).

Procedure for the synthesis of DMAFT and DMACCT:

7-bromo-9,9-dihexyl-N,N-dimethyl-9H-fluoren-2-amine ***(4.17)*****.**

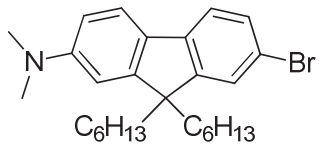

2-Bromo-9,9-dihexyl-7-nitro-9*H*-fluorene **4.15** (1 g, 2.18 mmol), HCOOH (96%, 2.24 mL, 57 mmol), Et_3N (6.4 mL,

46 mmol) and DMSO (6.5 mL) were placed in the reactor intended for conducting the reactions under pressure and the mixture was thoroughly degassed by Ar bubbling. $FeCl_2 \cdot 4H_2O$ (9 mg, 0.045 mmol) was then added to the reaction mixture keeping the inert atmosphere in the flask. The reactor was sealed and heated at 150 °C over 14 h. Then the reactor was cooled down to room temperature. The water (20 ml) was then added and the misture was extracted with EtOAc, organic phases were combined, washed with brine, dried over Na_2SO_4 and filtrated off. The solvent was evaporated under reduced pressure. The residue was purified by column chromatography (elution system: hexane – EtOAc, 40:1) to yield 0.628 g (1.37 mmol , 63%) of colorless oil.

7-(dimethylamino)-9,9-dihexyl-9H-fluorene-2-carbaldehyde ***(4.18)*****.**

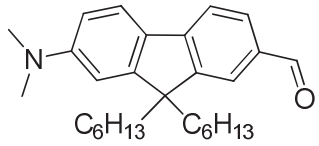

Solution of 7-bromo-9,9-dihexyl-*N*,*N*-dimethyl-9*H*-fluoren-2-amine **4.17** (2.487 g, 5.44 mmol) in anhydrous THF (57 mL) was placed into inert atmosphere and cooled down to -78 °C. The solution of n-BuLi (2.5 M, 4.84 mL, 12.1 mmol) was adeed to the solution dropwise and the mixture was stirred over 1 h. At this point anhydrous DMF (2.12 mL, 27.4 mmol) was added dropwise to the mixture and the stirring continued for 2 h at -78 °C. The solution was then left stirring at room temperature overnight, then quenched with 1M solution of HCl. The mixture is extracted with EtOAc, organic phases were combined, washed with brine, dried over Na_2SO_4 and filtrated off. The solvent was evaporated under reduced pressure. The residue was purified by column chromatography (elution system: CH_2Cl_2 – hexane, 7:1) to yield 1.39 g (3.41 mmol, 63%) of yellow-green fluorescent oil.

(E)-3-(7-(dimethylamino)-9,9-dihexyl-9H-fluoren-2-yl)-1-(pyridin-2-yl)prop-2-en-1-one ***(4.19)*****.**

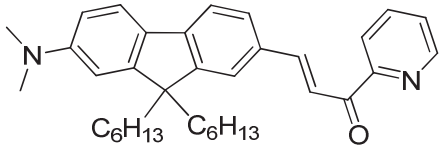

To the solution of 7-(dimethylamino)-9,9-dihexyl-9*H*-fluorene-2-carbaldehyde **4.18** (736 mg, 1.81 mmol) in EtOH (10 mL), 2-acetylpyridine (204 μл, 1.82 mmol) and then ground KOH (155 mg, 2.77 mmol) were added. The reaction

was controlled by TLC. After the reaction completion (around 3 h) the mixture was diluted with water and extracted with EtOAc. Organic extracts were washed with brine and dried over Na_2SO_4; the solvent was evaporated under reduced pressure. The residue was purified by column chromatography (elution system: pentane – EtOAc, 100:1, with gradual increase of the polarity of the system during the elution) to yield 517 mg (1.02 mmol, 56%) of red oil.

7-([2,2':6',2''-terpyridin]-4'-yl)-9,9-dihexyl-N,N-dimethyl-9H-fluoren-2-amine ***(DMAFT).***

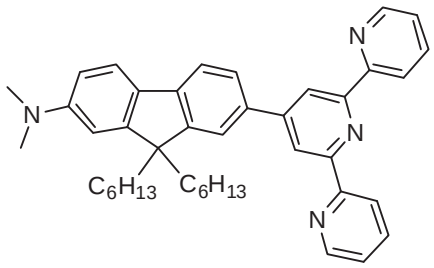

1-(2-Oxo-2-(pyridin-2-yl)ethyl)pyridin-1-yl iodide (180 mg, 0.55 mmol) and NH_4OAc (638 mg, 8.28 mmol) were added to a solution of (*E*)-3-(7-(dimethylamino)-9,9-dihexyl-9*H*-fluoren-2-yl)-1-(pyridin-2-yl)prop-2-en-1-one **4.19** (247 mg, 0.49 mmol) in MeOH (5 mL). The mixture was refluxed until the complete conversion of starting ketone **4.12** (TLC control). When the reaction finished the flask was cooled down to room temperature and the solvent was evaporated. Water was then added and the mixture was extracted with EtOAc. The organic phases were then combined, washed with brine, dried over Na_2SO_4 and filtrated off. The residue was purified by column chromatography 2 times: 1) eluent: CH_2Cl_2, 100%; 2) elution system: *n*-hexane – EtOAc, 15:1. The obtained oil was crystallized upon recrystallization from hexane to yield 84 mg (0.14 mmol, 28%) of yellow powder.

(E)-ethyl 3-(7-(dimethylamino)-9,9-dihexyl-9H-fluoren-2-yl)acrylate ***(4.24).***

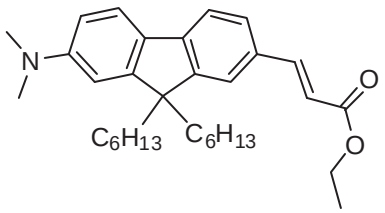

The mixture of 7-bromo-9,9-dihexyl-*N*,*N*-dimethyl-9*H*-fluoren-2-amine **4.17** (1.012 g, 2.22 mmol), $Pd(OAc)_2$ (25 mg, 0.11 mmol), P(o-tolyl)$_3$ (118 mg, 0.39 mmol) and $[Pd(PPh_3)_4]$ (131 mg, 0.11 mmol) was carefully degassed and placed into inert atmosphere. Et_3N (1.3 mL, 9.34 mmol), ethylacrylate (1 mL, 9.2 mmol) and anhydrous DMF (2.53 mL) were then added to the reaction

mixture. The suspension was heated at 90 °C for 14 h upon vigorous stirring. After the reaction completion the flask was cooled down to room temperature, and 30 ml of water was added to the mixture, that was then extracted with EtOAc. The organic phase is then washed with brine, dried over anhydrous Na_2SO_4, filtrated off, and the solvent was evaporated under reduced pressure. The residue was purified by column chromatography (elution system: *n*-hexane – EtOAc, 20:1. Yield – 814 mg (1.71 mmol, 77%) of bright yellow fluorescent powder.

(E)-3-(7-(dimethylamino)-9,9-dihexyl-9H-fluoren-2-yl)acrylaldehyde ***(4.26)*****.**

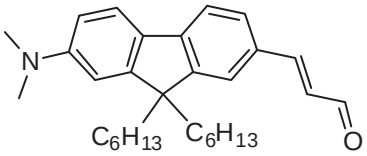

DIBAL-H (545 µl, 1.5 M, 0.82 mmol) was added slowly in a dropwise manner to the solution of (*E*)-ethyl 3-(7-(dimethylamino)-9,9-dihexyl-9*H*-fluoren-2-yl)acrylate **4.24** (125 mg, 0.26 mmol) in anhydrous toluene (2.8 mL) in inert atmosphere at -78 °C. The reaction mixture was vigorously stirred until complete conversion of starting material (TLC control, around 4 h). Then MeOH (80 µl) was added slowly to the reaction mixture until complete liberation of H_2 followed by quick addition of AcOEt (6 mL). The mixture was allowed to reach a room temperature and left at intensive stirring for 1.5 hour followed by filtration through celite; the filtrate was evaporated under reduced pressure.

The obtained alcohol 106 mg (the spectrum is given below) was placed under vacuum and was introduced in the next step as fast as possible. 1,1,1-Triacetoxy-1,1-dihydro-1,2-benziodoxol-3(1*H*)-one (Dess-Martin periodinane (DMP), 114 mg, 0.27 mmol) was suspended in CH_2Cl_2 (2 mL) and mixed with *tert*-butyl alcohol (26 µl, 0.27 mmol). The mixture was left stirring for 20 min, then the solution of obtained alcohol in CH_2Cl_2 (2 mL) was added and the stirring continued for 2h in a closed system. Meanwhile (after 1 h 40 min of stirring) the suspension of DMP (73 mg, 0.17 mmol) in CH_2Cl_2 (1.5 mL) and *tert*-buthanol (16 µL, 0.17 mmol) was prepared. It was stirred for 20 min and after added to the reaction mixture. The final mixture was stirred for 2 h. After the reaction finished the solvent was evaporated under reduced pressure and the residue was suspended in diethyl ether followed by rinsing with

$Na_2S_2O_3$ (10%) and saturated aq. solution of $NaHCO_3$ (1:1). The organic phase was rinsed with water and back extracted with small quantity of diethyl ether. Organic layers were combined, dried over Na_2SO_4, and the salt was filtrated off; the solvent was evaporated under reduced pressure. The residue was purified by column chromatography (*n*-hexane –EtOAc, 20:1) on silica gel to yield 84 mg (1.71 mmol, 79%) of bright red oil.

(2E,4E)-5-(7-(dimethylamino)-9,9-dihexyl-9H-fluoren-2-yl)-1-(pyridin-2-yl)penta-2,4-dien-1-one ***(4.27)*****.**

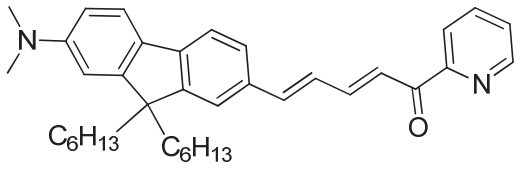

2-Acetylpyridine (12 μл, 0.1 mmol) was added to the solution of (*E*)-3-(7-(dimethylamino)-9,9-dihexyl-9*H*-fluoren-2-yl)acrylaldehyde **4.26** (46 mg, 0.11 mmol) in EtOH (0.5 mL). Ground KOH (9 mg, 0.16 mmol) was then added. The reaction course was controlled by TLC. After the reaction finished (around 3 h) the mixture was diluted with water and extracted with EtOAc. Organic extracts were washed with brine and dried over Na_2SO_4; the solvent was evaporated under reduced pressure. The residue was purified by column chromatography (elution system: pentane – EtOAc, 100:1, with gradual increase of the polarity of the system during the elution) to yield 35 mg (0.065 mmol, 61%) of red oil.

(E)-7-(2-([2,2':6',2''-terpyridin]-4'-yl)vinyl)-9,9-dihexyl-N,N-dimethyl-9H-fluoren-2-amine ***(DMAFCCT)*****.**

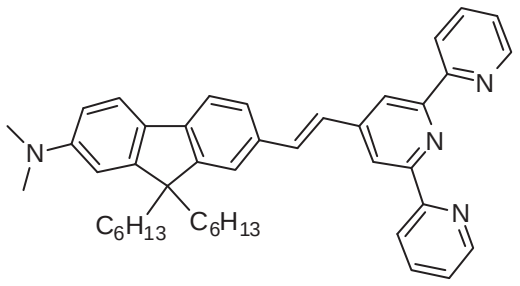

1-(2-Oxo-2-(pyridin-2-yl)ethyl)pyridin-1-yl iodide (99 mg, 0.30 mmol) and NH_4OAc (350 mg, 4.54 mmol) were added to a solution of (2*E*,4*E*)-5-(7-(dimethylamino)-9,9-dihexyl-9*H*-fluoren-2-yl)-1-(pyridin-2-yl)penta-2,4-dien-1-one **4.27** (143 mg, 0.27 mmol) in MeOH (5 mL). The mixture was refluxed until the complete conversion of starting ketone **4.27** (TLC control). After the reaction completed the flask was cooled down to room temperature. After the solvent was

evaporated under reduced pressure, water was added. The mixture was then extracted with EtOAc, organic phases were combined, washed with brine, dried over Na_2SO_4 and filtrated off. The residue was purified by column chromatography 2 times: 1) eluent: CH_2Cl_2, 100%; 2) elution system: *n*-hexane – EtOAc, 15:1 with gradual increase of the polarity of the system during the elution. Yield – 52 mg (0.08 mmol, 31%) of yellow oil.

Compound	Characterization
4'-bromo-2,2':6',2''-terpyridine ***(4.3)***. 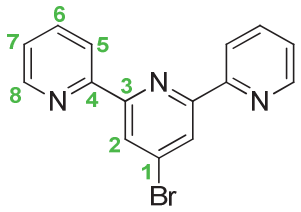	mp. 134-135 °C. **NMR ^{1}H** (400 MHz, $CDCl_3$) δ 8.71 (ddd, *J* = 4.8, 1.8, 0.8 Hz, 2H, H-8), 8.66 (s, 2H, H-2), 8.59 (d, *J* = 8.0 Hz, 2H, H-5), 7.87 (td, *J* = 7.7, 1.7 Hz, 2H, H-6), 7.36 (ddd, *J* = 7.4, 4.9, 1.1 Hz, 1H, H-7).
2-bromo-9,9-dihexyl-9H-fluorene ***(4.6)***. 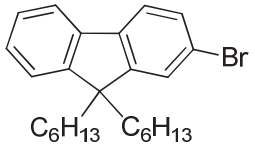	**NMR ^{1}H** (300 MHz, $CDCl_3$) δ 7.70 – 7.64 (m, 1H), 7.56 (dd, *J* = 7.5, 1.0 Hz, 1H), 7.46 (s, 1H), 7.45 (dd, *J* = 8.0, 1.9 Hz, 1H), 7.34 – 7.31 (m, 2H), 2.02 – 1.85 (m, 4H), 1.19 – 0.97 (m, 12H), 0.78 (t, *J* = 7.0 Hz, 6H), 0.69 – 0.51 (m, 4H).
9,9-dihexyl-2-vinyl-9H-fluorene ***(4.8)***. 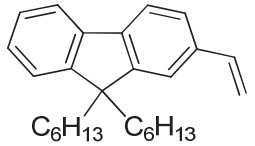	**NMR ^{1}H** (300 MHz, $CDCl_3$) δ 7.78 – 7.66 (m, 2H), 7.48 – 7.31 (m, 5H), 6.86 (dd, *J* = 17.6, 10.9 Hz, 1H), 5.85 (dd, *J* = 17.6, 0.9 Hz, 1H), 5.30 (dd, *J* = 10.9, 0.9 Hz, 1H), 2.06 – 1.97 (m, 4H), 1.22 – 1.03 (m, 12H), 0.82 (t, *J* = 6.9 Hz, 6H), 0.75 – 0.62 (m, 4H).
(E)-ethyl 3-(9,9-dihexyl-9H-fluoren-2-yl)acrylate ***(4.9)***.	**NMR ^{1}H** (300 MHz, $CDCl_3$) δ 7.78 (d, *J* = 16.0 Hz, 1H, H-16), 7.73 – 7.66 (m, 2H, H-4, H-5), 7.51 (dd, *J* = 7.9 Hz, 1.4 Hz, 1H, H-3), 7.49 (d, *J* = 1.4 Hz, 1H. H-l), 7.36 – 7.31 (m, 3H,

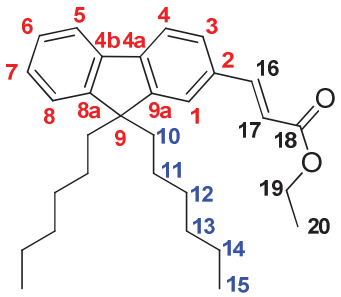	H-6, H-7, H-8), 6.49 (d, *J* = 16.0 Hz, 1H, H-17), 4.29 (q, *J* = 7.1 Hz, 2H, H-19), 2.04 – 1.91 (m, 4H, H-10), 1.36 (t, *J* = 7.1 Hz, 3H, H-20), 1.18-0.96 (m, 12H, H-12, H-13, H-14), 0.76 (t, *J* = 7.0 Hz, 6H, H-15), 0.67 - 0.48 (m, 4H, H-11); **NMR ^{13}C** (75 MHz, $CDCl_3$), δ 167.29 (C-18), 151.45 (C-8a або C-9a), 151.42 (C-8a або C-9a), 145.35 (C-16), 143.68 (C-4a), 140.32 (C-4b), 133.35 (C-2), 127.90 (C-6 або C-7), 127.57 (C-3), 127.04 (C-6 або C-7), 123.04 (C-8), 122.36 (C-l), 120.25 (C-4 або C-5), 120.11 (C-4 або C-5), 117.27 (C-17), 60.51 (C-19), 55.19 (C-9), 40.45 (C-10), 31.58 (C-13), 29.77 (C-12),23.83 (C-11), 22.66 (C-14), 14.50 (C-20), 14.12 (C-15). **HRMS (ESI):** calculated for $C_{30}H_{41}O_2$ $(M + H)^+$: 433.310107, found: 433.310186
(E)-3-(9,9-dihexyl-9H-fluoren-2-yl)acrylaldehyde ***(4.11)***. 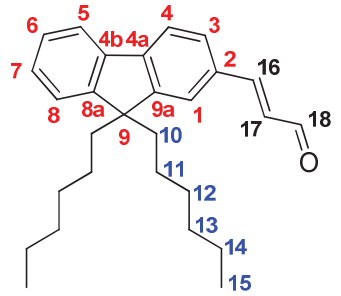	**NMR ^{1}H** (300 MHz, $CDCl_3$), δ 9.74 (d. *J*= 7.7 Hz, 1H, H-18), 7.77 - 7.70 (m, 2H, H-4, H-5), 7.58 (d, *J* = 15.9 Hz, 1H, H-16), 7.56 (dd, *J* = 7.9 Hz, 1.6 Hz, 1H. H-3), 7.53 (d, *J*= 1.6 Hz, 1H, H-l), 7.39 - 7.34 (m, 3H, H-6, H-7, H-8), 6.79 (dd, *J* = 15.9 Hz, 7.7 Hz, 1H, H-17), 2.03 - 1.94 (m, 4H, H-10), 1.15 - 0.97 (m, 12H, H-12, H-13, H -l4), 0.75 (t, *J* = 6.9 Hz, 6H, H-15), 0.67 - 0.55 (m, 4H, H-11): **NMR ^{13}C** (75 MHz, $CDCl_3$) δ 193.89 (C-18), 153.74 (C-16), 151.72 (C-8a або C-9a), 151.62 (C-8a або C-9a), 144.83 (C-4a), 140.04 (C-4b), 132.88 (C-2), 128.34 (C-6 або C-7), 128.18 (C-3), 127.84 (C-17), 127.17 (C-6 або C-7), 123.15 (C-8), 122.82 (C-l), 120.52 (C-4 або C-5), 120.34 (C-4 або C-5), 55.30 (C-9), 40.42 (C-10), 31.59 (C-13), 29.76 (C-12), 23.85 (C -11), 22.68 (C-14), 14.12 (C-15). **HRMS (ESI):** calculated for

	$C_{28}H_{37}O$ $(M + H)^+$: 389.283892, found: 389.284019.
(2E,4E)-5-(9,9-dihexyl-9H-fluoren-2-yl)-1-(pyridin-2-yl)penta-2,4-dien-1-one ***(4.12)***. 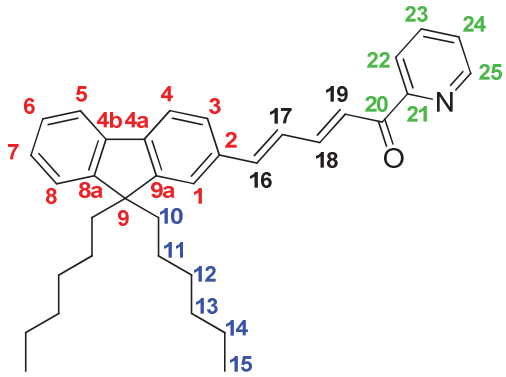	mp. 104 – 105 °C; **NMR ^{1}H** (400 MHz, THF-*d*8) δ 8.69 (ddd, *J* = 4.7 Hz, 1.7 Hz, 0.9 Hz, 1H, H-25), 8.11 (dt, *J* = 7.7 Hz, 1.3 Hz, 0.9 Hz, 1H, H-22), 7.93 (d, *J* = 15.3 Hz, 1H , H-19), 7.90 (td, *J* = 7.7 Hz, 7.5 Hz, 1.7 Hz, 1H, H-23), 7.77 – 7.65 (m, 3H, H-4, H-5, H-18), 7.65 (d, *J* = 1.5 Hz, 1H, H-1), 7.55 (dd, *J* = 7.9 Hz, 1.5 Hz, 1H, H-3), 7.50 (ddd, *J* = 7.5 Hz, 4.7 Hz, 1.3 Hz, 1H, H-24), 7.41 – 7.33 (m, 1H, H-8), 7.35 – 7.23 (m, 3H, H-6, H-7, H-17), 7.19 (d, *J* = 15.5 Hz, 1H, H-16), 2.14 – 1.97 (m, 4H, H-10), 1.17 – 0.96 (m, 12H, H-12, H-13, H-14), 0.75 (t, *J* = 7.0 Hz, 6H, H-15), 0.70 – 0.55 (m, 4H, H-11); **NMR ^{13}C** (101 MHz, ТГФ-*d*8) δ 189.02 (C-20), 155.49 (C-21), 152.11 (C-8a або C-9a), 151.99 (C-8a або C-9a), 149.76 (C-25), 144.95 (C-18), 143.52 (C-4a), 143.21 (C-16), 141.70 (C-4b), 137.78 (C-23), 136.70 (C-2), 128.34 (C-17), 128.06 (C-3 або C-6, або C-7), 127.80 (C-3 або C-6, або C-7), 127.78 (C-3 або C-6, або C-7), 127.54 (C-24), 125.09 (C-19), 123.68 (C-8), 123.07 (C-22), 122.29 (C-1), 120.85 (C-4 або C-5), 120.84 (C-4 або C-5), 55.93 (C-9), 41.28 (C-10), 32.49 (C-13), 30.69 (C-12), 24.70 (C-11), 23.48 (C-14), 14.37 (C-15). **HRMS (ESI):** calculated for $C_{35}H_{42}NO$ $(M + H)^+$: 492.326091, found: 491.326093.
(E)-4'-(2-(9,9-dihexyl-9H-fluoren-2-yl)vinyl)-2,2':6',2''-terpyridine	**NMR ^{1}H** (400 MHz, CD_3CN) δ 8.72 (ddd, *J* = 4.8 Hz, 1.8 Hz, 0.9 Hz, 2H, H-25), 8.66 (dt, *J* = 7.8 Hz, 1.2 Hz, 0.9 Hz, 2H, H-22), 8.64 (s, 2H, H-19), 7.95 (td, *J* = 7.8 Hz, 7.6 Hz, 1.8 Hz,

(FCCT). 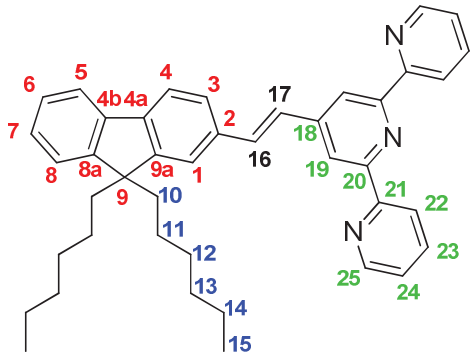 	2H, H-23), 7.79 – 7.75 (m, 3H, H-1, H-4, H-5), 7.68 (d, *J* = 16.4 Hz, 1H, H-16), 7.65 (dd, *J* = 7.8 Hz, 1.5 Hz, 1H, H-3), 7.48 (d, *J* = 16.4 Hz, 1H, H-17), 7.43 (ddd, *J* = 7.6 Hz, 4.8 Hz, 1.2 Hz, 2H, H-24), 7.43 – 7.40 (m, 1H, H-6), 7.37 – 7.31 (m, 2H, H-7, H-8), 2.12 – 1.98 (m, 4H, H-10), 1.14 – 0.94 (m, 12H, H-12, H-13, H-14), 0.73 (t, *J* = 7.0 Hz, 6H, H-15), 0.62 – 0.45 (m, 4H, H-11); **NMR ^{13}C** (101 MHz, CD_3CN) δ 156.93 (C-21), 156.78 (C-20), 152.32 (C-8a або C-9a), 152.07 (C-8a або C-9a), 150.23 (C-25), 148.02 (C-18), 142.88 (C-4a), 141.59 (C-4b), 138.09 (C-23), 136.58 (C-2), 134.57 (C-16), 128.44 (C-3), 127.98 (C-6 або C-7), 127.74 (C-6 або C-7), 126.89 (C-17), 125.13 (C-24), 124.00 (C-8), 122.45 (C-1), 121.91 (C-22), 120.88 (C-4 або C-5), 120.83 (C-4 або C-5), 118.65 (C-19), 56.02 (C-9), 40.82 (C-10), 32.18 (C-13), 30.21 (C-12), 24.64 (C-11), 23.16 (C-14), 14.20 (C-15). **HRMS (ESI):** calculated for $C_{42}H_{46}N_3$ $(M + H)^+$: 592.368625, found for: 592.368897.
2-ethynyl-9,9-dihexyl-9H-fluorene ***(4.14)***. 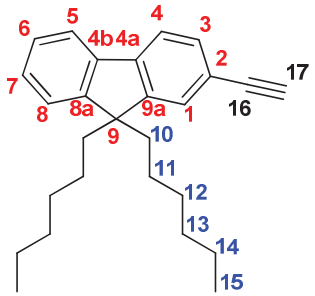 	**NMR ^{1}H**(400 MHz, $CDCl_3$) δ 7.73 – 7.70 (m, 1H, H-3), 7.67 (dd, *J* = 7.0, 1.3 Hz, 1H, H-5), 7.51 (dd, *J* = 7.0, 1.4 Hz, 1H, H-4), 7.50 (s, 1H, H-1), 7.40 – 7.31 (m, 3H, H-6,H-7, H-8), 2.01 – 1.95 (m, 4H, H-10), 1.22 – 0.98 (m, 12H, H-12, H-13, H-14), 0.79 (t, *J* = 7.1 Hz, 6H, H-15), 0.68 – 0.56 (m, 4H, H-11).

4'-((9,9-dihexyl-9H-fluoren-2-yl)ethynyl)-2,2':6',2''-terpyridine ***(FCC3T).*** 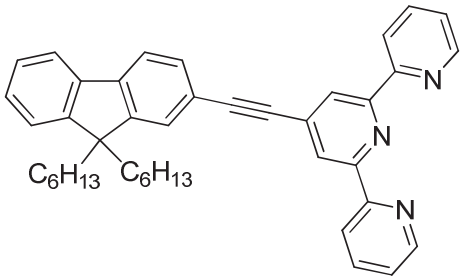	**NMR ^{1}H** (400 MHz, $CDCl_3$) δ 8.75 (d, *J* = 4.0 Hz, 2H), 8.67 (c, 2H), 8.66 (d, 2H), 7.94 – 7.84 (m, 2H), 7.77 – 7.70 (d, *J* = 7.7 Hz, 2H), 7.60 (s, 1H), 7.59 (d, *J* = 8.8 Hz, 1H), 7.42 – 7.32 (m, 5H), 2.09 – 1.96 (m, 4H), 1.22 – 1.02 (m, 12H), 0.80 (t, *J* = 7.0 Hz, 6H), 0.75 – 0.58 (m, 4H). **NMR ^{13}C** (101 MHz, $CDCl_3$) δ 155.7 (2C), 155.5 (2C), 151.2 (C), 150.9 (C), 149.2 (2CH), 142.2 (C), 140.2 (C), 136.9 (2CH), 133.7 (C), 130.9 (CH), 127.7 (CH), 126.9 (CH), 126.5 (CH), 124.0 (2CH), 122.9 (CH), 122.8 (2CH), 121.2 (2CH), 120.5 (C), 120.2 (CH), 119.7 (CH), 95.2 (C), 87.6 (C), 55.2 (C), 40.4 ($2CH_2$), 31.5 ($2CH_2$), 29.7 ($2CH_2$), 23.8 ($2CH_2$), 22.6 ($2CH_2$), 14.0 ($2CH_3$). **Calculated, %:** C, 85.53; H, 7.35; N, 7.12. $C_{42}H_{43}N_3$. **Found, %:** C, 85.31; H, 7.47; N, 7.01.
[Ru(FCCT)(bpy)Cl]Cl. 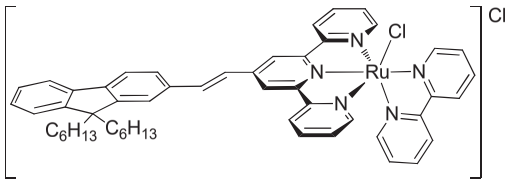	**NMR ^{1}H** (400 MHz, CD_3OD) δ 10.29 (d, *J* = 5.1 Hz, 1H), 8.89 (s, 2H), 8.78 (d, *J* = 8.0 Hz, 1H), 8.56 (d, *J* = 7.8 Hz, 2H), 8.49 (d, *J* = 8.0 Hz, 1H), 8.31 (t, *J* = 7.8 Hz, 1H), 8.10 (d, *J* = 16.2 Hz, 1H), 8.05 - 8.00 (m, 1H), 7.88 - 7.65 (m, 9H), 7.59 (d, *J* = 16.6 Hz, 1H), 7.42 (ddd, *J* = 8.3 Hz, 6.7 Hz, 3.5 Hz, 4H), 7.33 - 7.26 (m, 2H), 7.05 (t, *J* = 6.5 Hz, 1H), 2.23 - 2.07 (m, 4H), 1.17-1.00 (m, 12H), 0.78 (t, *J* = 7.0 Hz, 6H), 0.72 - 0.59 (m, 4H). **Calculated, %:** C, 67.89; H, 5.81; N, 7.61. $C_{52}H_{53}Cl_2N_5Ru$ **Found, %:** C 67.87; H, 5.86; N, 7.53.
[Ru(FCC3T)(bpy)Cl]Cl.	**NMR ^{1}H** (400 MHz, CD_3OD) δ 10.25 – 10.22 (m, 1H), 0.66 – 0.56 (m, 4H), 8.82 (s, 2H),

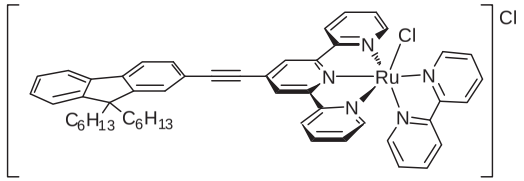	8.79 (d, *J* = 8.2 Hz, 1H), 8.57 (d, *J* = 8.0 Hz, 2H), 8.50 (d, *J* = 7.9 Hz, 1H), 8.34 (td, *J* = 7.9, 1.5 Hz, 1H), 8.02 (ddd, *J* = 7.5, 5.6, 1.2 Hz, 1H), 7.91 (td, *J* = 7.9, 1.5 Hz, 2H), 7.87 (d, *J* = 7.8 Hz, 1H), 7.85 – 7.83 (m, 1H), 7.75 (ddd, 8.5, 7.8, 1.3 Hz, 1H), 7.73 (dd, 8.5, 1.4 Hz, 2H), 7.70 (s, 1H), 7.69 (ddd, 8.3, 1.4 Hz, 1H), 7.47 – 7.38 (m, 4H), 7.36 (dd, *J* = 7.5, 1.1 Hz, 1H), 7.34 (dd, *J* = 7.5, 1.1 Hz, 1H), 7.06 (ddd, *J* = 7.3, 5.8, 1.3 Hz, 1H), 2.14 – 2.07 (m, 4H), 1.19 – 0.99 (m, 12H), 0.79 (t, *J* = 7.0 Hz, 6H). **Calculated, %:** C, 68.04; H, 5.60; N, 7.63. $C_{52}H_{51}Cl_2N_5Ru$. **Found, %:** C 67.99; H, 5.91; N, 7.33.
[Ru(MeO-Phtpy)(bpy)Cl]Cl. 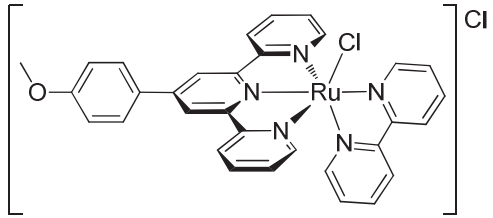	**NMR ^{1}H** (400 MHz, CD_3OD) δ 10.26 (d, *J* = 5.5 Hz, 1H, H-1), 8.82 (s, 2H, H-19, H-20), 8.77 (d, *J* = 7.5 Hz, 1H, H-4), 8.60 (d, *J* = 8.0, 2H, H-15, H-23), 8.48 (d, *J* = 8.9, 1H, H-7), 8.32 (td, *J* = 7.9, 1.6 Hz, 1H, H-3), 8.13 – 8.06 (m, 2H, H-28, H-32), 8.32 (ddd, *J* = 7.2, 5.6, 1.3 Hz, 1H, H-8), 7.85 (td, *J* = 7.9, 1.5 Hz, 2H, H-14, H-24), 7.77 – 7.64 (m, 3H, H-12, H-26, H-2), 7.38 (d, *J* = 6.1 Hz, 1H, H-10), 7.30 (ddd, *J* = 7.1, 5.5, 1.2 Hz, 2 H, H-13, H-25), 7.18 – 7.10 (m, 2H, H-29, H-31), 7.02 (ddd, *J* = 7.3, 5.7, 1.3 Hz, 1H, H-9), 3.9 (s, 3H, H-33). **Calculated, %:** C, 57.58; H, 3.77; N, 10.49; $C_{32}H_{25}Cl_2N_5ORu$. **Found, %:** C, 57.59; H, 3.81; N, 10.38;
[Ru(FCCT)(bpy)NO$_2$]Cl.	**NMR ^{1}H** (400 MHz, CD_3OD) δ 9.91 (d, *J* = 4.8 Hz, 1H), 8.78 (d, *J* = 8.1 Hz, 1H), 8.74 (s, 2H), 8.55 (d, *J* = 8.2 Hz, 1H), 8.46 (d, *J* = 8.0 Hz, 2H), 8.32 (td, *J* = 8.0, 1.5 Hz, 1H), 8.04 - 7.99 (m, 1H), 7.96 (d, *J* = 16.3 Hz, 1H), 7.92 - 7.80 (m, 6H), 7.77 - 7.73 (m, 2H), 7.73 - 7.68

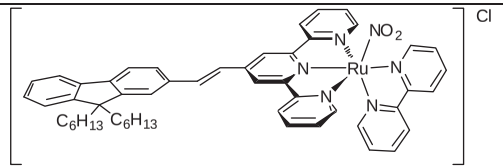	(m, 1H), 7.52 (d, *J* = 16.3 Hz, 1H), 7.47 - 7.43 (m, 2H), 7.42 - 7.36 (m, 2H), 7.36 - 7.31 (m, 2H), 7.19 - 7.13 (m, 1H), 2.21 - 2.07 (m, 4H), 1.16 – 1.00 (m, 12H), 0.76 (t, *J* = 7.0 Hz, 6H), 0.70 – 0.58 (m, 4H). **Calculated, %:** C, 67.12; H, 5.74; N, 9.03. $C_{52}H_{53}ClN_6O_2Ru$. **Found, %:** C, 67.32; H, 5.82; N, 8.95
[Ru(FCC3T)(bpy)NO$_2$]Cl. 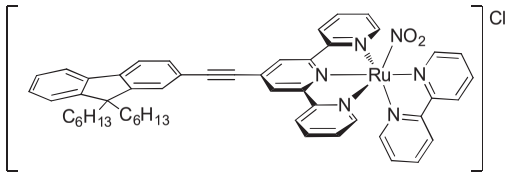	**NMR ^{1}H** (400 MHz, CD_3OD) δ 9.90 (d, *J* = 5.3 Hz, 1H), 8.78 (d, *J* = 8.2 Hz, 2H), 8.76 (s, 1H), 8.55 (d, *J* = 8.1 Hz, 1H), 8.50 (d, *J* = 8.0 Hz, 2H), 8.34 (td, *J* = 7.9, 1.4 Hz, 1H), 8.02 (ddd, *J* = 7.5, 5.9, 1.1 Hz, 1H), 7.93 (td, *J* = 7.9, 1.4 Hz, 2H), 7.90 – 7. 81 (m, 3H), 7.79 (s, 1H), 7.75 (d, *J* = 8.6 Hz, 2H), 7.67 (dd, *J* = 7.8, 1.3 Hz, 1H), 7.52 – 7.32 (m, 6H), 7.18 (ddd, *J* = 7.6, 5.7,1.3 Hz, 1H), 2.19 – 2.00 (m, 4H), 1.21 – 1.01 (m, 12H), 0.78 (t, *J* = 6.9 Hz, 6H), 0.70 – 0.54 (m, 4H). **Calculated, %:** C, 67.26; H, 5.54; N, 9.05. $C_{52}H_{51}ClN_6O_2Ru$. **Found, %:** C, 66.97; H, 5.63; N, 8.93
[Ru(MeO-Phtpy)(bpy)NO$_2$]Cl: 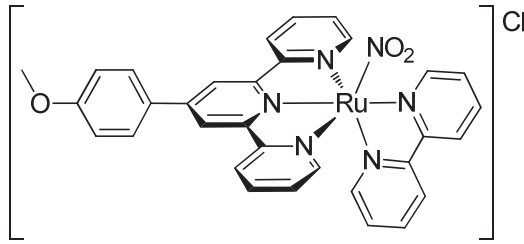	**NMR ^{1}H** (400 MHz, CD_3OD) δ 9.90 (d, *J* = 5.8 Hz, 1H, H-1), 8.82 – 8.73 (m, 3H, H-19, H-20, H-4), 8.59 – 8.51 (m, 3H, H-15, H-23, H-7), 8.33 (td, *J* = 7.9, 1.5 Hz, 1H, H-3), 8.08 – 7.99 (m, 3H, H-28, H-32, H-8), 7.93 (td, *J* = 7.9, 1.6 Hz, 2H, H-14, H-24), 7.85 (td, *J* = 7.9, 1.5 Hz, 1H, H-2), 7.78 (dd, J_1 = 5.5, 1.5 Hz, 2H, H-12, H-26), 7.49 – 7.45 (m, 1H, H-10), 7.35 (ddd, *J* = 7.2, 5.5, 1.3 Hz, 2H, H-13, H-25), 7.19 – 7.10 (m, 3H, H-29, H-31, H-9), 3.93 (s, 3H, H-33). **NMR ^{13}C** (CD_3OD, 75 MHz) δ 163.2, 160.2, 159.2, 158.2, 157.4, 154.0, 153.6, 151.7, 149.7, 139.1, 138.5, 138.4, 130.1, 129.7, 128.6, 128.2, 127.5, 125.1, 125.0, 124.4,

	120.8, 115.9, 56.0. **Calculated, %:** C, 56.68; H, 3.72; N, 12.39. $C_{32}H_{25}ClN_6O_3Ru$. **Found, %:** C, 56.81; H, 3.94; N, 12.10.
[Ru(FCCT)(bpy)NO](PF$_6$)$_3$ 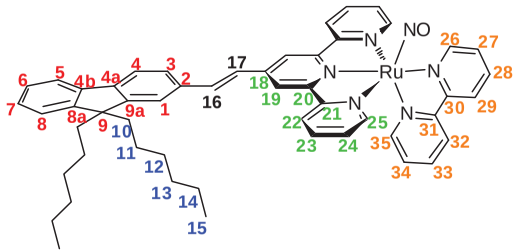	**NMR ^{1}H** (400 MHz, CD_3CN) δ 9.30 (d, *J* = 5.7 Hz, 1H, H-26), 8.92 (s, 2H, H-19), 8.81 (d, *J* = 7.8 Hz, 1H, H-29), 8.74 (d, *J* = 7.4 Hz, 2H, H-22), 8.69 (td, *J* = 8.1, 1.4 Hz, 1H, H-28), 8.61 (d, *J* = 7.7 Hz, 1H, H-32), 8.49 (td, *J* = 7.9, 1.4 Hz, 2H, H-23), 8.32 (d, *J* = 16.3 Hz, 1H, H-16), 8.33 – 8.27 (m, 1H, C-33), 8.27 – 8.23 (m, 1H, H-27), 8.01 (dd, *J* = 5.6, 1.1 Hz, 2H, H-25), 7.95 (d, *J* = 8.1 Hz,1H, H-4), 7.94 (s, H-1), 7.90 – 7.83 (m, 2H, H-3,H-5), 7.74 (d, *J* = 16.2 Hz, 1H, H-17), 7.71 (ddd, *J* = 7.5, 5.4, 1.1 Hz, 2H, H-24), 7.53 – 7.39 (m, 4H, H-6,H-7, H-8, H-34), 7.32 (dd, *J* = 6.0, 0.9 Hz, 1H, H-35), 2.21 – 2.09 (m, 4H, H-10), 1.15 – 0.97 (m, 12H, H-12, H-13, H-14), 0.77 (t, *J* = 6.9 Hz, 6H, H-15), 0.61 (d, *J* = 6.4 Hz, 4H, H-11). **Calculated, %:** C, 47.53; H, 4.07; N, 6.40. $C_{52}H_{53}F_{18}N_6OP_3Ru$. **Found, %:** C, 43.36; H, 3.75; N, 6.21. **IR (neat film):** 1942 cm^{-1} ν(NO).
[Ru(FCC3T)(bpy)NO](PF$_6$)$_3$: 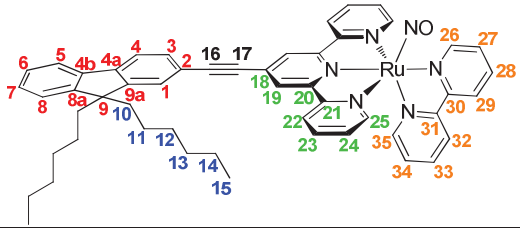	**NMR ^{1}H** (300 MHz, CD_3CN) δ 9.31 (d, *J* = 5.8 Hz, 1H, H-26), 8.96 (s, 2H, H-19), 8.82 (d, *J* = 8.1 Hz, 1H, H-29), 8.75 – 8.66 (m, 3H, H-22, H-28), 8.63 (d, *J* = 8.1 Hz, 1H, H-32), 8.48 (t, *J* = 8.2 Hz, 2H, H-23), 8.31 (t, *J* = 8.0, 1H, H-33), 8.28 – 8.21 (m, 1H, H-27), 8.02 (d, *J* = 5.2 Hz, 2H, H-25), 7.97 (d, *J* = 7.8 Hz, 1H, H-4), 7.92 – 7.79 (m, 3H, H-1,H-3,H-5), 7.78 – 7.68 (m, 2H, H-24), 7.56 – 7.39 (m, 4H, H-6,H-7, H-8, H-34), 7.34 (d, *J* = 5.9 Hz, 1H, H-35), 2.27 – 2.05 (m, 4H, H-10), 1.21 – 0.95 (m, 12H, H-12, H-13, H-14), 0.77 (t, *J* = 6.8 Hz, 6H, H-15),

	0.66 – 0.46 (m, 4H, H-11). **NMR ^{13}C** (75 MHz, CD_3CN) δ 156.2 (2C), 154.9 (2CH), 154.2 (C), 153.8 (2C), 153.4 (C), 153.0 (CH), 151.5 (C), 151.4 (C), 148.1 (CH), 144.8 (C), 144.7 (CH), 144.4 (2CH), 144.0 (CH), 142.0 (C), 139.7 (C), 132.3 (CH), 130.6 (CH), 130.4 (2CH), 130.1 (CH), 128.8 (CH), 128.2 (2CH), 127.5 (2CH), 127.4 (CH), 127.1 (CH), 126.9 (CH), 126.3 (C), 123.3 (CH), 120.8 (CH), 120.5 (CH), 118.2 (C), 106.3 (CH), 86.5 (C), 55.4 (C), 39.7 (CH_2), 31.1 (CH_2), 29.2 (CH_2), 23.6 (CH_2), 22.1 (CH_2), 13.2 (CH_3). **Calculated, %:** C, 47.60; H, 3.92; N, 6.41. $C_{52}H_{51}F_{18}N_6OP_3Ru$. **Found, %:** C, 45.78; H, 3.52; N, 6.17. **IR (neat film):** 1946 cm^{-1} ν(NO), 2200 ν(C≡C).
[Ru(MeO-Phtpy)(bpy)NO](PF$_6$)$_3$: 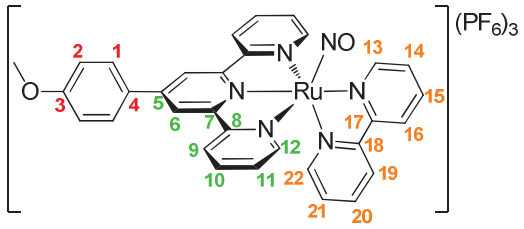	**NMR ^{1}H** (400 MHz, CD_3CN) δ 9.32 (d, *J* = 5.51 Hz, 1H, H-13), 9.04 (c, 2H, H-6), 8.86 (d, *J* = 8.02 Hz, 2H, H-9), 8.81 (d, *J* = 8.26 Hz, 1H, H-16), 8.69 (m, 1H, H-15), 8.62 (d, *J* = 8.03 Hz, 1H, H-19), 8.47 (t, *J* = 7.77, 2H, H-10), 8.28 (m, 4H, H-1, H-14, H-20), 8.02 (d, *J* = 5.37 Hz, 2H, H-12), 7.71 (t, *J* = 6.42 Hz, 2H, H-11), 7.50 (t, *J* = 6.66 Hz, 1H, H-21), 7.33 (m, 3H, H-2), 3.99 (s, 3H, OCH_3). **NMR ^{13}C** (101 MHz, CD_3CN) δ 164.8 (C-3), 159.1 (C-5), 157.7 (2C-8), 155.8 (2C-12), 155.3 (C-18), 154.6 (2C-7), 154.4 (C-17), 153.9 (C-13), 149.0 (C-22), 145.6 (C-20), 145.2 (2C-10), 144.9 (C-15), 131.6 (C-14), 131.5 (2C-1), 131.1 (C-21), 131.1 (2C-11), 128.5 (2C-9), 127.9 (C-16), 127.5 (C-4), 127.3 (C-19), 124.5 (2C-6), 116.5 (2C-2), 56.7 ($O\underline{C}H_3$). **IR (neat film):** 1940 cm^{-1} ν(NO). **Calculated, %:** C, 36.21; H, 2.37; N, 7.92. $C_{32}H_{25}F_{18}N_6O_2P_3Ru$. **Found, %:** C, 36.02; H, 2.48; N, 7.67.

7-bromo-9,9-dihexyl-N,N-dimethyl-9H-fluoren-2-amine ***(4.17)***. 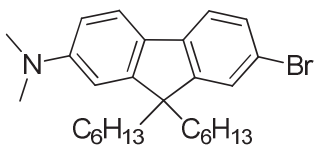	**NMR ^{1}H** (300 MHz, $CDCl_3$) δ 7.54 (d, *J* = 8.4 Hz, 1H), 7.44 – 7.40 (m, 2H), 7.42 (s, 1H), 6.73 (dd, *J* = 8.4, 2.4 Hz, 1H), 6.68 (d, *J* = 2.3 Hz, 1H), 3.05 (s, 6H), 2.08 – 1.81 (m, 4H), 1.28 – 0.97 (m, 12H), 0.82 (t, *J* = 6.9 Hz, 6H), 0.76 – 0.61 (m, 4H). **Calculated, %:** C, 71.04; H, 8.39; N, 3.07. $C_{27}H_{38}BrN$. **Found, %:** C, 70.71; H, 8.42; N, 2.94.
7-(dimethylamino)-9,9-dihexyl-9H-fluorene-2-carbaldehyde ***(4.18)***. 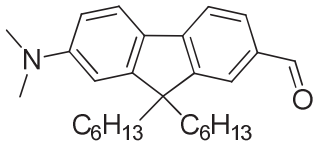	mp. 51-52 °C. **NMR ^{1}H** (400 MHz, $CDCl_3$) δ 9.99 (s, 1H, COH), 7.80 – 7.79 (m, 1H, H-1), 7.77 (dd, *J* = 7.7, 1.5 Hz, 1H, H-3), 7.64 (d, *J* = 8.1 Hz, 1H, H-4), 7.61 (d, *J* = 8.5 Hz, 1H, H-5), 6.73 (dd, *J* = 8.5, 2.4 Hz, 1H, H-6), 6.64 (d, *J* = 2.3 Hz, 1H, H-8), 3.07 (c, 6H, $N(CH_3)_2$), 2.07 – 1.85 (m, 4H, H-10), 1.15 – 0.98 (m, 12H, H-12, H-13, H-14), 0.76 (t, *J* = 7.1 Hz, 6H, H-15), 0.68 – 0.53 (m, 4H, H-11). **NMR ^{13}C** (101 MHz, $CDCl_3$) δ 192.4 (CH), 154.4 (C), 151.7 (C), 150.6 (C), 148.9 (C), 133.6 (C), 131.3 (CH), 128.5 (C), 122.6 (CH), 121.9 (CH), 118.2 (CH), 111.5 (CH), 106.3 (CH), 55.1 (C), 40.9 ($2CH_3$), 40.7 ($2CH_2$), 31.6 ($2CH_2$), 29.8 ($2CH_2$), 23.8 ($2CH_2$), 22.7 ($2CH_2$), 14.1 ($2CH_3$). **Calculated, %:** C, 82.91; H, 9.69; N, 3.45. $C_{28}H_{39}NO$. **Found, %:** C, 82.69; H, 9.73; N, 3.42.
(E)-3-(7-(dimethylamino)-9,9-dihexyl-9H-fluoren-2-yl)-1-(pyridin-2-yl)prop-2-en-1-one	**NMR ^{1}H** (300 MHz, $CDCl_3$) δ 8.80 – 8.75 (m, 1H, H-23), 8.25 (d, *J* = 16.0 Hz, 1H, H-16), 8.21 (dd, *J* = 7.7 Hz, 1H, H-20), 8.05 (d, *J* = 15.9 Hz, 1H, H-17), 7.89 (td, *J* = 7.7, 1.6 Hz, 1H, H-21), 7.68 – 7.62 (m, 1H, H-3), 7.64 (s, 1H, H-1), 7.58 (d, *J* = 8.2, 1H, H-4), 7.56 (d, *J*

(4.19). 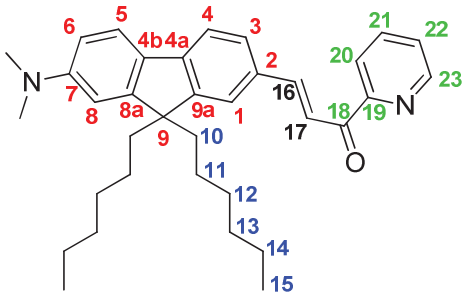	= 8.1, 1H, H-5), 7.53 – 7.46 (m, 1H, H-22), 6.83 – 6.61 (m, 2H, H-6, H-8), 3.06 (s, 6H, $N(CH_3)_2$), 2.08 – 1.86 (m, 4H, H-10), 1.17 – 0.98 (m, 12H, H-12, H-13, H-14), 0.75 (t, *J* = 6.9 Hz, 6H, H-15), 0.70 – 0.57 (m, 4H, H-11). **Calculated, %:** C, 82.63; H, 8.72; N, 5.51. $C_{35}H_{44}N_2O$. **Found, %:** C, 82.47; H, 8.69; N, 5.43.
7-([2,2':6',2''-terpyridin]-4'-yl)-9,9-dihexyl-N,N-dimethyl-9H-fluoren-2-amine ***(DMAFT)***. 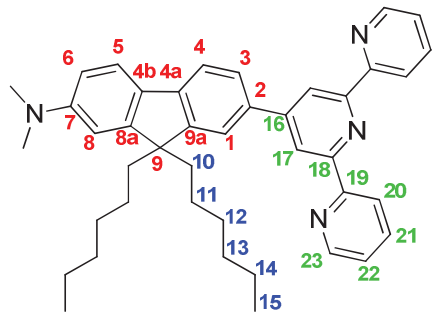	mp. 107-108 °C. **NMR ^{1}H** (300 MHz, $CDCl_3$) δ 8.83 (s, 2H, H-19), 8.77 (d, *J* = 4.0 Hz, 2H, H-25), 8.70 (d, *J* = 8.0 Hz, 2H, H-22), 7.93 – 7.81 (m, 4H, H-23, H-1, H-3), 7.69 (d, *J* = 7.9 Hz, 1H, H-4), 7.62 (d, *J* = 8.2 Hz, 1H, H-5), 7.34 (ddd, *J* = 7.4, 4.8, 1.0 Hz, 2H, H-24), 6.75 (d, *J* = 7.8, 2.2 Hz, 1H, H-6), 6.73 (s, 1H, H-8), 3.04 (s, 6H, $N(CH_3)_2$), 2.22 – 1.87 (m, 4H, H-10), 1.22 – 1.02 (m, 12H, H-12, H-13, H-14), 0.78 (t, *J* = 6.8 Hz, 6H, H-15), 0,89 – 0.60 (m, 4H, H-11). **NMR ^{13}C** (101 MHz, $CDCl_3$) δ 156.7 (2C), 156.0 (2C), 153.0 (C), 151.4 (C), 150.9 (C), 150.8 (C), 149.2 (2CH), 143.2 (C), 137.0 (2CH), 135.2 (C), 129.9 (C), 126.5 (CH), 123.8 (2CH), 121.6 (2CH), 121.2 (CH), 120.7 (CH), 118.9 (2CH), 118.7 (CH), 111.5 (CH), 107.0 (CH), 55.4 (C), 41.1 ($2CH_3$), 40.9 ($2CH_2$), 31.6 ($2CH_2$), 29.9 ($2CH_2$), 23.8 ($2CH_2$), 22.7 ($2CH_2$), 14.2 ($2CH_3$). **Calculated, %:** C, 82.85; H, 7.95; N, 9.20. $C_{42}H_{48}N_4$. **Found, %:** C, 82.51; H, 8.08; N, 8.98.

(E)-ethyl 3-(7-(dimethylamino)-9,9-dihexyl-9H-fluoren-2-yl)acrylate ***(4.24)***. 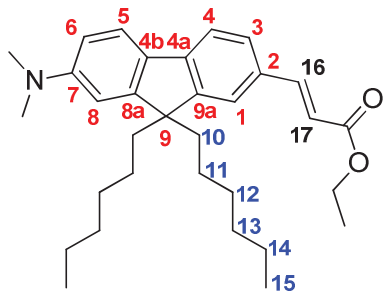	mp. 95-96 °C. **NMR ^{1}H** (400 MHz, $CDCl_3$) δ 7.77 (d, *J* = 16.0 Hz, 1H, H-16), 7.55 (d, *J* = 8.5 Hz, 1H, H-4), 7.52 (d, *J* = 8.5 Hz, 1H, H-5), 7.45 (dd, J = 8.4, 1.3 Hz, 1H, H-3), 7.44 (s, 1H, H-1), 6.71 (dd, *J* = 8.4, 2.1 Hz, 1H, H-6), 6.65 (d, *J* = 1.8 Hz, 1H, H-8), 6.44 (d, *J* = 15.9 Hz, 1H, H-17), 4.28 (q, *J* = 7.1 Hz, 2H, $C\underline{H_2}CH_3$), 3.04 (s, 6H, $N(CH_3)_2$), 2.04 – 1.82 (m, 4H, H-10), 1.35 (t, *J* = 7.1 Hz, 3H, $CH_2C\underline{H_3}$), 1.18 – 0.99 (m, 12H, H-12, H-13, H-14), 0.77 (t, *J* = 7.1 Hz, 6H, H-15), 0.71 – 0.57 (m, 4H, H-11); **NMR ^{13}C** (101 MHz, $CDCl_3$) δ 167.6 (C), 153.3 (C), 151.1 (C), 150.5 (C), 145.8 (CH), 144.7 (C), 131.2 (C), 129.5 (C), 127.9 (CH), 122.0 (CH), 121.0 (CH), 118.5 (CH), 115.8 (CH), 111.5 (CH), 106.7 (CH), 60.4 (CH_2), 55.0 (C), 41.0 ($2CH_3$), 40.8 ($2CH_2$), 31.6 ($2CH_2$), 29.8 ($2CH_2$), 23.8 ($2CH_2$), 22.7 ($2CH_2$), 14.5 (CH_3), 14.1 ($2CH_3$). **Calculated, %:** C, 80.79; H, 9.53; N, 2.94. $C_{32}H_{45}NO_2$. **Found, %:** C, 80.45; H, 9.64; N, 2.65. **IR (neat film):** 1704 cm^{-1} (ν(C=O)).
(E)-3-(7-(dimethylamino)-9,9-dihexyl-9H-fluoren-2-yl)prop-2-en-1-ol ***(4.25)***.	**NMR ^{1}H** (400 MHz, $CDCl_3$) δ 7.52 (d, *J* = 8.3 Hz, 1H, H-4), 7.49 (d, *J* = 8.2 Hz, 1H, H-5), 7.32 – 7.28 (m, 2H, H-1, H-3), 6.72 – 6.63 (m, 2H, H-6, H-8), 6.68 (d, *J* = 15.9, 1H, H-16), 6.38 (dt, *J* = 15.8, 6.0 Hz, 1H, H-17), 4.35 (d, *J* = 5.6 Hz, 2H, H-18), 3.02 (s, 6H, $N(CH_3)_2$), 2.00 – 1.80 (m, 4H, H-10), 1.16 – 0.97 (m, 12H, H-12, H-13, H-14), 0.76 (t, *J* = 7.1 Hz, 6H, H-15), 0.69 – 0.60 (m, 4H, H-11). **NMR ^{13}C** (101 MHz, $CDCl_3$) δ 152.7 (C), 150.6 (C), 150.4 (C), 141.9 (C), 133.5 (C), 132.6 (CH), 130.3 (C), 126.5 (CH), 125.7 (CH), 120.5 (CH),

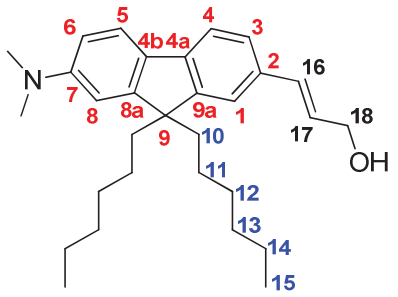	120.4 (CH), 118.3 (CH), 111.5 (CH), 107.1 (CH), 64.2 (CH_2), 54.9 (C), 41.1 ($2CH_3$), 40.9 ($2CH_2$), 31.6 ($2CH_2$), 29.9 ($2CH_2$), 23.8 ($2CH_2$), 22.7 ($2CH_2$), 14.1 ($2CH_3$).
(E)-3-(7-(dimethylamino)-9,9-dihexyl-9H-fluoren-2-yl)acrylaldehyde ***(4.26)***. 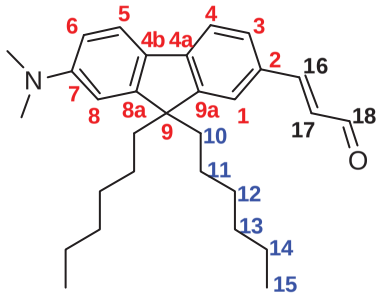	**NMR ^{1}H** (400 MHz, $CDCl_3$) δ 9.70 (d, *J* = 7.8 Hz, 1H, COH), 7.58 (d, *J* = 8.5 Hz, 1H, H-5), 7.58 (d, *J* = 7.5 Hz, 1H, H-4), 7.54 (d, *J* = 15.3 Hz, 1H, H-16), 7.49 (dd, *J* = 7.9, 1.4 Hz, 1H, H-3), 7.46 – 7.44 (m, 1H, H-1), 6.75 – 6.70 (m, 1H, H-6), 6.74 (dd, *J* = 15.8, 7.8 Hz, 1H, H-17), 6.65 (s, 1H, H-8), 3.06 (s, 6H, $N(CH_3)_2$), 2.01 – 1.85 (m, 4H, H-10), 1.17 – 0.98 (m, 12H, H-12, H-13, H-14), 0.76 (t, *J* = 7.1 Hz, 6H, H-15), 0.69 – 0.58 (m, 4H, H-11). **NMR ^{13}C** (101 MHz, $CDCl_3$) δ 193.9 (CH), 154.4 (CH), 153.6 (C), 151.3 (C), 150.7 (C), 146.0 (C), 130.8 (C), 129.1 (C), 128.6 (CH), 126.6 (CH), 122.4 (CH), 121.3 (CH), 118.6 (CH), 111.5 (CH), 106.5 (CH), 55.1 (C), 41.0 ($2CH_3$), 40.7 ($2CH_2$), 31.6 ($2CH_2$), 29.8 ($2CH_2$), 23.8 ($2CH_2$), 22.7 ($2CH_2$), 14.1 ($2CH_3$). **Calculated, %:** C, 83.47; H, 9.57; N, 3.24. $C_{30}H_{41}NO$. **Found, %:** C, 83.09; H, 9.70; N, 3.11. **IR (neat film):** 1674 cm^{-1} (ν(C=O)).
(2E,4E)-5-(7-(dimethylamino)-9,9-dihexyl-9H-fluoren-2-yl)-1-(pyridin-2-yl)penta-2,4-dien-1-	**NMR ^{1}H** (400 MHz, $CDCl_3$) δ 8.73 (ddd, *J* = 4.7, 1.6, 0.9 Hz, 1H, H-25), 8.17 (dt, *J* = 7.9, 1.0 Hz, 1H, H-22), 7.86 (td, *J* = 7.7, 1.7 Hz, 1H, H-23), 7.82 – 7.77 (m, 2H, H-4, H-5), 7.55 (d, *J* = 8.6 Hz, 1H, H-18), 7.53 (d, *J* = 8.6 Hz, 1H, H-16), 7.46 (ddd, *J* = 7.5, 4.8, 1.2 Hz, 1H,

*one **(4.27)**.* 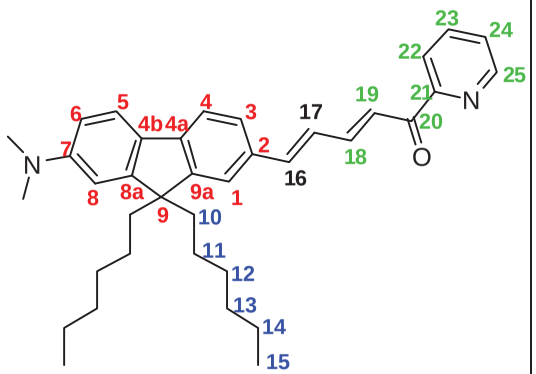	H-24), 7.43 (dd, *J* = 7.9, 1.4 Hz, 1H, H-3), 7.41 – 7.39 (m, 1H, H-1), 7.15 – 7.11 (m, 2H, H-17, 18), 6.71 (dd, *J* = 8.4, 2.2 Hz, 1H, H-6), 6.65 (d, *J* = 2.0 Hz, 1H, H-8), 3.04 (s, 6H, $N(CH_3)_2$), 2.00 – 1.85 (m, 4H, H-10), 1.19 – 0.99 (m, 12H, H-12, H-13, H-14), 0.77 (t, *J* = 7.0 Hz, 6H, H-15), 0.71 – 0.61 (m, 4H, H-11). **Calculated, %:** C, 83.10; H, 8.67; N, 5.24. $C_{37}H_{46}N_2O$. **Found, %:** C, 82.96; H, 8.48; N, 5.07.
*(E)-7-(2-([2,2':6',2''-terpyridin]-4'-yl)vinyl)-9,9-dihexyl-N,N-dimethyl-9H-fluoren-2-amine **(DMAFCCT)**.* 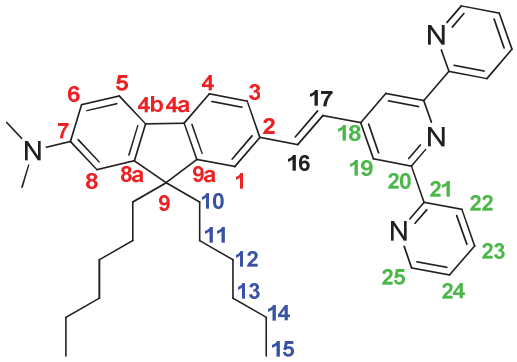	**NMR ^{1}H** (400 MHz, $CDCl_3$) δ 8.77 (ddd, *J* = 4.8, 1.7, 0.8 Hz, 2H, H-25), 8.69 (dt, *J* = 7.9, 1.0 Hz, 2H, H-22), 8.62 (s, 2H, H-19), 7.90 (td, *J* = 7.7, 1.8 Hz, 2H, H-23), 7.71 (d, *J* = 16.3 Hz, 1H, H-16), 7.61 – 7.51 (m, 4H, H-1, H-3, H-4, H-5), 7.38 (ddd, *J* = 7.5, 4.8, 1.2 Hz, 2H, H-24), 7.29 (d, *J* = 16.4 Hz, 1H, H-17), 6.79 – 6.66 (m, 1H, H-6), 6.71 (s, 1H, H-8), 3.07 (s, 6H, $N(CH_3)_2$), 2.06 – 1.88 (m, 4H, H-10), 1.18 – 1.03 (m, 12H, H-12, H-13, H-14), 0.79 (t, *J* = 7.0 Hz, 6H, H-15), 0.76 – 0.66 (m, 4H, H-11). **NMR ^{13}C** (75 MHz, $CDCl_3$) δ 156.5 (2C), 155.8 (2C), 153.1 (C), 150.8 (C), 150.5 (C), 149.2 (2CH), 147.4 (C), 143.0 (C), 137.0 (2CH), 133.4 (C), 130.0 (C), 126.4 (CH), 123.9 (2CH), 121.4 (2CH), 121.3 (CH), 120.7 (CH), 118.6 (CH), 118.1 (2CH), 111.5 (CH), 106.9 (CH), 55.0 (C), 41.1 ($2CH_3$), 40.9 ($2CH_2$), 31.6 ($2CH_2$), 31.6 (CH), 30.3 (CH), 29.9 ($2CH_2$), 23.9 ($2CH_2$), 22.8 ($2CH_2$), 14.2 ($2CH_3$). **Calculated, %:** C, 83.24; H, 7.94; N, 8.82. $C_{44}H_{50}N_4$. **Found, %:** C, 82.92; H, 7.81; N, 8.49.

GENERAL CONCLUSIONS

1. It was shown that the introduction of 2,2'-bipyridine as a ligand into the structure of ruthenium-nitrosyl complexes instead of the two chloro-ligands leads to a decrease in the quantum yield of nitric oxide photorelease from 0.11 (trans(Cl,Cl)-$[Ru^{II}(FT)Cl_2(NO)](PF_6)$) to 0.06, however, it leads to an increase in the TPA cross-section from 90-100 GM to 108 GM.
2. By means of quantum-chemical calculations it has been demonstrated that the introduction of azaheterotricyclic systems with a 14π-electron conjugation system into the structure of the terpyridine ligand in the ruthenium-nitrosyl complex may contribute to a weak increase in the efficiency of the compounds in two-photon absorption (the maximum TPA cross-section obtained for the compound 1-methyl-1*H* -benzo[f] indole (compound 3.3) is only 1% higher than that for the reference compound trans1, the TPA cross-section for which is 87GM) However, the replacement of fluorene with such heterocyclic analogues substantially alters the ability of compounds to hyperpolarization, the value of which varies depending on the heterocycle from 233.1·10-30 $cm^5 \cdot esu^{-1}$ (compound **3.12**) to 2751.7 ·10-30 $cm^5 \cdot esu^{-1}$ (compound **3.8**)
3. Preparative methods for synthess of ruthenium-nitrosyl complexes with ligands containing different types of linker between donor fluorenyl and withdrawing terpyridine fragments have been developed – $[Ru(FCCT)(bpy)NO](PF_6)_3$, $[Ru(FCC3T)(bpy)NO](PF_6)_3$.
4. It was shown that the enlargement of the conjugation and its efficiency enhancement through the decrease of the torsion angle between the donating and withdrawing fragments of the complex increases the efficiency of the compound in two-photon absorption due to an increase of the push-pull character of the compound (an increase in TPA cross-section observed is 20-40%).
5. It has been demonstrated on the series of ruthenium-nitrosyl complexes with substituted phenyl-terpiridines that electron donating substituents increase the efficiency of compounds in two-photon absorption, while withdrawing groups do not lead to such improvement. The maximum TPA cross-section value is observed

for the complex with the ligand 4'-(4-methoxyphenyl)-2,2':6',2"-terpyridine – trans(Cl,Cl)-[Ru(MeOPh-tpy)Cl_2($^{\prime}$NO)]PF_6 – 154 GM.

6. The structure of the photoproduct formed during the release of nitric oxide from the ruthenium-nitrosyl complex containing 4'-(4-methoxyphenyl)-2,2':6',2"- terpyridine and 2,2'-bipyridine has been established. It has been proved that in contrast to complexes with chloro-ligands instead of 2,2'-bipyridine, the oxidation state of ruthenium in them is +2. It was also confirmed by means of EPR spectroscopy with the use of spin trap that NO is released in a form of radical.
7. It has been established that, contrary to previous notions, the irradiation of compounds with electromagnetic waves of the energies corresponding to the energy of electron density transfer from donor to ruthenium-nitrosyl fragment does not play a decisive role in the efficiency of the compound in the process of NO release. Irradiation at higher energies could result in photorelase with higher quantum yields.

PUBLICATION LIST

1. Lacroix, P. G.; Akl, J.; Malfant, I.; Sasaki, I.; Vicendo, P.; Blanchard-Desce, M.; Farfán, N.; Santillán, R.; Bukhanko, V.; Voitenko, Z. Nitric Oxide (NO) Delivery from [Ru(NO)] Metal Complexes with Substituted Terpyridine Ligands. *Polymat Contrib.* 2016, *1*, 97–100
2. Enriquez-Cabrera, A.; Sasaki, I.; Bukhanko, V.; Tassé, M.; Mallet-Ladeira, S.; Lacroix, P. G.; Barba-Barba, R. M.; Ramos-Ortiz, G.; Farfán, N.; Voitenko, Z.; Malfant I. Replacing Two Chlorido Ligands by a Bipyridine Ligand in Ruthenium Nitrosyl Complexes with NO-Release Capabilities: A Comparative Study. *Eur. J. Inorg. Chem* 2017, No. 11, 1446–1456.
3. Буханько, В.; Войтенко, З.; Лакруа, П. Д.; Мальфант І., Рутеній-Нітрозильні Комплекси З Терпіридиновими Лігандами Як Донори нітроген(II) Оксиду. *Вісник Київського національного університету імені Тараса Шевченка* 2017, *1(53)*, 22–24.
4. Bukhanko, V.; Malfant, I.; Voitenko, Z.; Lacroix, P. G. Isoindole and Isomeric Heterocyclic Donating Substituents in Ruthenium(II) Nitrosyl Complexes with Large First Hyperpolarizabilities and Potential Two-Photon Absorption Capabilities: A Computational Approach. *Fr. Ukr. J. Chem.* 2017, *5* (1), 8–23.
5. Roose, M.; Sasaki, I.; Bukhanko, V.; Mallet-Ladeira, S.; Barba-Barba, R. M.; Ramos-Ortiz, G.; Enriquez-Cabrera, A.; Farfán, N.; Lacroix, P. G.; Malfant, I. Nitric Oxide Photo-Release from a Ruthenium Nitrosyl Complex with a 4,4'-Bisfluorenyl-2,2'-Bipyridine Ligand. *Polyhedron* 2018, *151*, 101–111.
6. Bukhanko, V.; Lacroix, P. G.; Sasaki, I.; Tassé, M.; Voitenko, Z.; Malfant, I. Mechanism and Oxidation State Involved in the Nitric Oxide (NO) Photorelease in a Terpyridine-Bipyridine-Based Ruthenium Nitrosyl Complex. *Inorganica Chim. Acta* 2018, *482*, 195–205.

Participation in conferences:

1. Bukhanko V., Lacroix P. G. Voitenko Z., Sasaki I., Ramos G., Malfant I. Terpyridine Ruthenium-Nitrosyl Complexes as NO-Donors In Photodynamic Therapy. *Modern chemistry problems,* Book of abstracts of 17th International conference for Students and PhD students, Kyiv, Ukraine, 18-20th May, 2016 ; p. 42.
2. Bukhanko V., Leon-Rojas A. F., Lacroix P. G., Sasaki I., Voitenko Z. V., Malfant I., Farfan N. The Enhancement of Conjugation In Terpyridine Ligands and Its Effect on NO-Release From Ruthenium-Nitrosyl Complexes. *9th International conference in chemistry Kyiv-Toulouse,* Materials of reports and performances, Kyiv, Ukraine, 4-9th June 2017; p.70.
3. Bukhanko V., Leon-Rojas A. F., Lacroix P. G., Sasaki I., Voitenko Z. V., Malfant I., Farfan N. The Effect of Enhanced Conjugation In Terpyridine Ligands on NO-Release From Ruthenium-Nitrosyl Complexes. *Modern chemistry problems,* Book of abstracts of 18th International conference for Students and PhD students, Kyiv, Ukraine, 17-19th May, 2017 ; p. 82.
4. Bukhanko V., Leon-Rojas A. F., Lacroix P. G., Sasaki I., Voitenko Z. V., Malfant I., Farfan N. Extension de la Conjugaison dans des Ligands Terpyridine : Effets sur la Libération de NO à Partir de Complexes Ruthénium-Nitrosyle. *Langues, sciences et pratiques,* Actes du 1er Colloque international francophone en Ukraine, Kiev, Ukraine, 19-20 octobre 2017.

REFERENCES

(1) Greenwood, N. N.; Earnshaw, A. *Chemistry of the Elements*, Second edi.; Butterworth-Heinemann, Oxford, 1997.

(2) McCleverty, J. A. Chemistry of Nitric Oxide Relevant to Biology. *Chem. Rev.* **2004**, *104* (2), 403–418.

(3) Jones, K. *Comprehensive Inorganic Chemistry*; Pergamon Pr.: Oxford, 1973.

(4) Linnett, J. W. Binding in Some Diatomic Molecules. *J. Chem. Soc.* **1956**, No. 2, 275–287.

(5) Tretiakov, J. D.; Martynenko, L. I.; Grigoriev, A. N.; Cyvadze, A. J. *Inorganic Chemistry. Chemistry of Elements*; Chemistry, 2001.

(6) Rodebush, W. H. The Reaction between Nitric Oxide and Atomic Oxygen. *Chem. Rev.* **1935**, *17* (3), 409–412.

(7) Lewis, R. S.; Deen, W. M. Kinetics of the Reaction of Nitric Oxide with Oxygen in Aqueous Solutions. *Chem. Res. Toxicol.* **1994**, *7* (4), 568–574.

(8) Wink, D. A.; Feelisch, M.; Fukuto, J.; Chistodoulou, D.; Jourd'heuil, D.; Grisham, M. B.; Vodovotz, Y.; Cook, J. A.; Krishna, M.; DeGraff, W. G.; et al. The Cytotoxicity of Nitroxyl: Possible Implications for the Pathophysiological Role of NO. *Arch. Biochem. Biophys.* **1998**, *351* (1), 66–74.

(9) Thomas, D. D.; Ridnour, L. A.; Isenberg, J. S.; Flores-santana, W.; Switzer, C. H.; Donzelli, S.; Hussain, P.; Vecoli, C.; Paolocci, N.; Ambs, S.; et al. Free Radical Biology & Medicine The Chemical Biology of Nitric Oxide : Implications in Cellular Signaling. **2008**, *45*, 18–31.

(10) Hill, B. G.; Dranka, B. P.; Bailey, S. M.; Lancaster, J. R.; Darley-Usmar, V. M. What Part of NO Don't You Understand? Some Answers to the Cardinal Questions in Nitric Oxide Biology. *J. Biol. Chem.* **2010**, *285* (26), 19699–19704.

(11) Feelisch, M. The Chemical Biology of Nitric Oxide – an Outsider ' S Reflections about Its Role in Osteoarthritis. *Osteoarthr. Cartil.* **2008**, *16*, S3–

S13.

(12) Miranda, K. M.; Espey, M. G.; Jourd'heuil, D.; Grisham, M. B.; Fukuto, J. M.; Feelisch, M.; Wink, D. A. The Chemical Biology of Nitric Oxide. In *Nitric oxide: Biology and Pathobiology.*; Ignarro, L. J., Ed.; San Diego: Academic Press, 2000.

(13) Lepoivres, M.; Bob, P.; Lemaire, G. Quenching of the Tyrosyl Free Radical of Ribonucleotide Reductase by Nitric Oxide. **1994**, *269* (34), 21891–21897.

(14) Padmaja, S.; Huie, R. E. The Reaction of Nitric Oxide with Organic Peroxyl Radicals. *Biochem. Biophys. Res. Commun.* **1993**, *195* (2), 539–544.

(15) Routledge, M. N.; Mirsky, F. J.; Wink, D. A.; Keefer, L. K.; Dipple, A. Nitrite-Induced Mutations in a Forward Mutation Assay: Influence of Nitrite Concentration and pH. *Mutat. Res. Toxicol.* **1994**, *322* (4), 341–346.

(16) Koppenol, W. H.; Moreno, J. J.; Pryor, W. A.; Ischiropoulos, H.; Beckman, J. S. Peroxynitrite, a Cloaked Oxidant Formed by Nitric Oxide and Superoxide. *Chem. Res. Toxicol.* **1992**, *5* (6), 834–842.

(17) Bonavida, B.; Khineche, S.; Huerta-Yepez, S.; Garban, H. Therapeutic Potential of Nitric Oxide in Cancer. *Drug Resist. Updat.* **2006**, *9*, 157–173.

(18) Choudhari, S. K.; Chaudhary, M.; Bagde, S.; Gadbail, A. R.; Joshi, V. Nitric Oxide and Cancer : A Review. *World J Surg Oncol.* **2013**, *11* (118), 1–11.

(19) Fukumura, D.; Kashiwagi, S.; Jain, R. K. The Role of Nitric Oxide in Tumour Progression. *Nat Rev Cancer.* **2006**, *6* (July), 521–534.

(20) Oronsky, B.; Fanger, G. R.; Oronsky, N.; Knox, S.; Scicinski, J. The Implications of Hyponitroxia in Cancer. *Trans. Oncol.* **2014**, *7* (2), 167–173.

(21) Furchgott, R. F.; Zawadzki, J. V. The Obligatory Role of Endothelial Cells in the Relaxation of Arterial Smooth Muscle by Acetylcholine. *Nature* **1980**, *288* (373–6).

(22) Pereira, A. C.; Paulo, M.; Araújo, A. V.; Rodrigues, G. J.; Bendhack, L. M. Nitric Oxide Synthesis and Biological Functions of Nitric Oxide Released from Ruthenium Compounds. *Brazilian J. Med. Biol. Res.* **2011**, *44* (9), 947–957.

(23) Knowles, R. G.; Moncada, S. Nitric Oxide Synthases in Mammals. *Biochem. J.* **1994**, *298*, 249–258.

(24) Kwon, N. S.; Nathan, C. F.; Gilker, C.; Griffith, O. W.; Matthews, D. E.; Stuehr, D. J. L-Citrulline Production from L-Arginine by Macrophage Nitric Oxide Synthase. *J. Biol. Chem.* **1990**, *265* (23), 13442–13445.

(25) Sonveaux, P.; Jordan, B. F.; Gallez, B.; Feron, O. Nitric Oxide Delivery to Cancer : Why and How ? *Eur. J. Cancer* **2009**, *45*, 1352–1369.

(26) Nathan, C.; Xie, Q. Nitric Oxide Synthases : Roles , Tolls , and Controls. *Cell* **1994**, *78*, 915–918.

(27) Kim, J.; Saravanakumar, G.; Choi, H. W.; Park, D.; Kim, W. J. A Platform for Nitric Oxide Delivery. *J. Mater. Chem. B* **2014**, *2* (4), 341–356.

(28) Carpenter, A. W.; Schoenfisch, M. H. Nitric Oxide Release : Part II . Therapeutic Applications. *Chem. Soc. Rev.* **2012**, *41*, 3742–3752.

(29) Ivy, D. D.; Abman, S. H.; Barst, R. J.; Berger, R. M. F.; Bonnet, D.; Fleming, T. R.; Haworth, S. G.; Raj, J. U.; Rosenzweig, E. B.; Neick, S.; et al. Pediatric Pulmonary Hypertension. *JACC* **2013**, *62* (25), D117–D126.

(30) Feelisch, M.; Stamler, J. S. Donors of Nitrogen Oxides. In *Methods in Nitric Oxide Research*; Wiley: Chichester, 1996; pp 77–115.

(31) Agvald, P.; Adding, L. C.; Artlich, A.; Persson, M. G.; Gustafsson, L. E. Mechanisms of Nitric Oxide Generation from Nitroglycerin and Endogenous Sources during Hypoxia in Vivo. *Br. J. Pharmacol* **2002**, *135* (2), 373–382.

(32) Huerta, S.; Chilka, S.; Bonavida, B. Nitric Oxide Donors : Novel Cancer Therapeutics (Review). *Int. J. Oncol* **2008**, *33* (5), 909–927.

(33) Yasuda, H. Nitric Oxide Solid Tumor Physiology and Hypoxia-Induced Chemo / Radio-Resistance : Novel Strategy for Cancer Therapy : Nitric Oxide Donor as a Therapeutic Enhancer. *Nitric Oxide* **2008**, *19*, 205–216.

(34) Daiber, A.; Munzel Abstract, T. Organic Nitrate Therapy, Nitrate Tolerance, and Nitrate-Induced Endothelial Dysfunction: Emphasis on Redox Biology and Oxidative Stress. *Antioxid Redox Signal.* **2015**, *23* (11), 899–942.

(35) Parker, J. D.; Parker, J. O. Nitrate Therapy for Stable Angina Pectoris. *N*

Engl J Med **1998**, *338* (8), 520–531.

(36) Bogaert, M. G.; De Schaepdryver, A. F. Tolerance towards Glyceryl Trinitrate (Trinitrin) in Dogs. *Arch Int Pharmacodyn Ther.* **1968**, *171* (1), 221–224.

(37) Frederiksen, L. J.; R., S.; Maxwell, L. R.; Macdonald-Goodfellow, S. K.; Adams, M. A.; Bennett, B. M.; R., S. D.; Graham, C. H. Chemosensitization of Cancer in Vitro and in Vivo by Nitric Oxide Signaling. *Clin. Cancer Res.* **2007**, *13* (7), 2199–2206.

(38) Michele, C. J.; Serrano, M. C.; van Lith, R.; Ameer, G. A. Polymer-Based Nitric Oxide Therapies: Recent Insights for Biomedical Applications. *Adv Funct Mater.* **2012**, *22* (2), 239–260.

(39) Miller, M. R.; Megson, I. L. Recent Developments in Nitric Oxide Donor Drugs. *Br. J. Pharmacol.* **2007**, *151* (3), 305–321.

(40) Drago, R. S.; Paulik, F. E. The Reaction of Nitrogen(II) Oxide with Diethylamine. *J. Am. Chem. Soc.* **1960**, *82* (1), 96–98.

(41) Reynolds, M. M.; Frost, M. C.; Meyerhoff, M. E. Nitric Oxide-Releasing Hydrophobic Polymers: Preparation, Characterization, and Potential Biomedical Applications. *Free Radic. Biol. Med.* **2004**, *37* (7), 926–936.

(42) Tang, X.; Xian, M.; Trikha, M.; Honn, K. V.; Wang, P. G. Synthesis of Peptide-Diazeniumdiolate Conjugates: Towards Enzyme Activated Antitumor Agents. *Tetrahedron Lett.* **2001**, *42* (14), 2625–2629.

(43) Brookes, P.; Walker, J. Formation and Properties of Sydnone Imines, a New Class of Meso-Ionic Compound, and Some Sydnones Related to Natural a-Amino-Acids. *J. Chem. Soc.* **1957**, 4409.

(44) Wang, P. G.; Xian, M.; Tang, X.; Wu, X.; Wen, Z.; Cai, T.; Janczuk, A. J. Nitric Oxide Donors: Chemical Activities and Biological Applications. *Chem. Rev.* **2002**, *102* (4), 1091–1134.

(45) Bohn, H.; Schonafinger, K. Oxygen and Oxidation Promote the Release of Nitric Oxide from Sydnonimines. *J Cardiovasc Pharmacol.* **1989**, *14* (11), S6–S12.

(46) Riccio, D. A.; Schoenfisch, M. H. Nitric Oxide Release Part I. Macromolecular Scaffolds. *Chem. Soc. Rev.* **2012**, *41* (10), 3731–3741.

(47) Nie, Y.; Li, Z. Controlled Nitric Oxide Release for Tissue Repair and Regeneration. *Turkish J. Biol.* **2016**, *40*, 316–326.

(48) Xiang, H.-J.; Guo, M.; Liu, J.-G. Transition-Metal Nitrosyls for Photocontrolled Nitric Oxide Delivery. *Eur. J. Inorg. Chem* **2017**, No. 12, 1586–1595.

(49) Frost, M. C.; Reynolds, M. M.; Meyerhoff, M. E. Polymers Incorporating Nitric Oxide Releasing/generating Substances for Improved Biocompatibility of Blood-Contacting Medical Devices. *Biomaterials* **2005**, *26* (14), 1685–1693.

(50) Shishido, S. M.; Seabra, A. B.; Loh, W.; De Oliveira, M. G. Thermal and Photochemical Nitric Oxide Release from S-Nitrosothiols Incorporated in Pluronic F127 Gel: Potential Uses for Local and Controlled Nitric Oxide Release. *Biomaterials* **2003**, *24* (20), 3543–3553.

(51) Frost, M. C.; Meyerhoff, M. E. Controlled Photoinitiated Release of Nitric Oxide from Polymer Films Containing S-Nitroso-N-Acetyl-DL-Penicillamine Derivatized Fumed Silica Filler. *J. Am. Chem. Soc.* **2004**, *126* (5), 1348–1349.

(52) Riccio, D. A.; Coneski, P. N.; Nichols, S. P.; Broadnax, A. D.; Schoenfisch, M. H. Photoinitiated Nitric Oxide-Releasing Tertiary S-Nitrosothiol-Modified Xerogels. *ACS Appl Mater Interfaces* **2012**, *4* (2), 796–804.

(53) Sortino, S.; Petralia, S.; Compagnini, G.; Conoci, S.; Condorelli, G. Light-Controlled Nitric Oxide Generation from a Novel Self-Assembled Monolayer on a Gold Surface. *Angew. Chem. Int. Ed. Engl.* **2002**, *41* (11), 1914–1917.

(54) Sortino, S.; Giuffrida, S.; De Guldi, G.; Chillemi, R.; Petralia, S.; Marconi, G.; Condorelli, G.; Sciuto, S. The Photochemistry of Flutamide and Its Inclusion Complex with Beta-Cyclodextrin. Dramatic Effect of the Microenvironment on the Nature and on the Efficiency of the Photodegradation Pathways. *Photochem. Photobiol.* **2001**, *73* (1), 6–13.

(55) Hishikawa, K.; Nakagawa, H.; Furuta, T.; Fukuhara, K.; Tsumoto, H.; Suzuki, T.; Miyata, N. Photoinduced Nitric Oxide Release from a Hindered Nitrobenzene Derivative by Two-Photon Excitation. *J. Am. Chem. Soc.* **2009**, *131* (22), 7488–7489.

(56) Fukuhara, K.; Kurihara, M.; Miyata, N. Photochemical Generation of Nitric Oxide from 6-Nitrobenzo[a]pyrene. *J. Am. Chem. Soc.* **2001**, *123* (36), 8662–8666.

(57) Kitamura, K.; Ieda, N.; Hishikawa, K.; Suzuki, T.; Miyata, N.; Fukuhara, K.; Nakagawa, H. Visible Light-Induced Nitric Oxide Release from a Novel Nitrobenzene Derivative Cross-Conjugated with a Coumarin Fluorophore. *Bioorganic Med. Chem. Lett.* **2014**, *24* (24), 5660–5662.

(58) Xu, C.; Webb, W. W. Measurement of Two-Photon Excitation Cross Sections of Molecular Fluorophores with Data from 690 to 1050 Nm. *J. Opt. Soc. Am. B* **1996**, *13* (3), 481–491.

(59) Ford, P. C.; Bourassa, J.; Miranda, K.; Lee, B.; Lorkovic, I.; Boggs, S.; Kudo, S.; Laverman, L. Photochemistry of Metal Nitrosyl Complexes. Delivery of Nitric Oxide to Biological Targets. *Coord. Chem. Rev.* **1998**, *171*, 185–202.

(60) Mingos, M. P. Historical Introduction to Nitrosyl Complexes. In *Nitrosyl Complexes in Inorganic Chemistry, Biochemistry and Medicine I*; Mingos, M. P., Ed.; Springer, 2014; pp 1–44.

(61) Frenz, B. A.; Enemark, J. H.; Ibers, J. A. The Structure of Nitrosyltetracarbonylmanganese, Mn(NO)(CO)4. *Inorg. Chem.* **1969**, *8* (6), 1288–1293.

(62) P., M. D. M.; Ibers, J. A. The Crystal and Molecular Structure of Dinitrosylbis(triphenylphosphine)iridium Perchlorate. *Inorg. Chem.* **1970**, *9* (5), 1105–1111.

(63) Fomitchev, D. V; Furlani, T. R.; Coppens, P. Combined X-Ray Diffraction and Density Functional Study of [Ni (NO)(η 5 -Cp *)] in the Ground and Light-Induced Metastable States. *Inorg. Chem.* **1998**, *37* (1), 1519–1526.

(64) Enemark, J. H.; Feltham, R. D. Principles of Structure, Bonding, and Reactivity for Metal Nitrosyl Complexes. *Coord. Chem. Rev.* **1974**, *13* (4), 339–406.

(65) Pierpont, C. G.; Eisenberg, R. The Molecular Structure of Chlorodinitrosylbis(triphenylphosphine)ruthenium Hexafluorophosphate-Benzene. A Complex Having Linear and Bent Nitrosyl Groups. *Inorg. Chem.* **1972**, *11* (5), 1088–1094.

(66) Lichtenberger, D. L.; Gruhn, N. E.; Renshaw, S. K. Relative Bonding Capabilities of Molecules to Metals as Measured by Gas-Phase Photoelectron Spectroscopy. *J. Mol. Struct.* **1997**, *405* (1), 79–86.

(67) Paul, P. P.; Tyeklár, Z.; Farooq, A.; Karlin, K. D.; Liu, S.; Zubieta, J.; Karlin, K. D. Isolation and X-Ray Structure of a Dinuclear Copper-Nitrosyl Complex. *J. Am. Chem. Soc.* **1990**, *112* (6), 2430–2432.

(68) Ellis, D.; Farrugia, L. J. Synthesis of Platinum-Triruthenium Clusters Using the Zero-Valent Platinum Reagent Pt(nb)3. *J. Clust. Sci.* **2001**, *11* (1), 243–257.

(69) Beringhelli, T.; Ciani, G.; D'Alfonso, G.; Molinari, H.; Sironi, A.; Freni, M. A Novel Co-Ordination Mode of Nitric Oxide. Synthesis and Crystal Structure of the [{Re3(μ-H)3(CO)10}2(μ4-η2-NO)]-. *J. Chem. Soc.* **1984**, *0* (20), 1327–1329.

(70) Hayton, T. W.; Legzdins, P.; Sharp, W. B. Coordination and Organometallic Chemistry of Metal-NO Complexes. *Chem. Rev.* **2002**, *102* (4), 935–991.

(71) Lewandowska, H. Spectroscopic Characterization of Nitrosyl Complexes. In *Nitrosyl Complexes in Inorganic Chemistry, Biochemistry and Medicine I. Structure and Bonding*; Mingos, D., Ed.; Springer: Berlin, Heidelberg, 2013; Vol. 153.

(72) De La Cruz, C.; Sheppard, N. A Structure-Based Analysis of the Vibrational Spectra of Nitrosyl Ligands in Transition-Metal Coordination Complexes and Clusters. *Spectrochim. Acta A* **2011**, *78* (1), 7–28.

(73) Rose, M. J.; Mascharak, P. K. Fiat Lux: Selective Delivery of High Flux of

Nitric Oxide (NO) to Biological Targets Using Photoactive Metal Nitrosyls. *Curr. Opin. Chem. Biol.* **2008**, *12* (2), 238–244.

(74) Huang, Z.; Fu, J.; Zhang, Y. Nitric Oxide Donor-Based Cancer Therapy: Advances and Prospects. *J. Med. Chem.* **2017**, *60*, 7617–7635.

(75) Clarke, M. J. Ruthenium Metallopharmaceuticals. *Coord. Chem. Rev.* **2003**, *236*, 209–233.

(76) Tfouni, E.; Truzzi, D. R.; Tavares, A.; Gomes, A. J.; Figueiredo, L. E.; Franco, D. W. Biological Activity of Ruthenium Nitrosyl Complexes. *Nitric Oxide - Biol. Chem.* **2012**, *26* (1), 38–53.

(77) Rose, M. J.; Mascharak, P. K. Photoactive Ruthenium Nitrosyls: Effects of Light and Potential Application as NO Donors. *Coord. Chem. Rev.* **2008**, *252* (18–20), 2093–2114.

(78) Bettache, N.; Carter, T.; E., C. J.; Ogden, D.; Trentham, D. R. Photolabile Donors of Nitric Oxide: Ruthenium Nitrosyl Chlorides as Caged Nitric Oxide. *Methods Enzym.* **1996**, *268*, 266–281.

(79) Lorković, I. M.; Ford, P. C. Kinetics and Mechanism of Nitric Oxide Disproportionation upon Reaction with Ruthenium(II) Porphyrin Carbonyls: Evidence for Dinitrosyl Intermediates. *Inorg. Chem.* **1999**, *38* (7), 1467–1473.

(80) Works, C. F.; Jocher, C. J.; Bart, G. D.; Bu, X.; Ford, P. C. Photochemical Nitric Oxide Precursors : Synthesis , Photochemistry , and Ligand Substitution Kinetics of Ruthenium Salen Nitrosyl and Ruthenium Salophen Nitrosyl Complexes 1. *Inorg. Chem.* **2002**, *41* (14), 3728–3739.

(81) Endo, I.; Nojiri, M.; Tsujimura, M.; Nakasako, M.; Shigehiro, N.; Yohda, M.; Odaka, M. Fe-Type Nitrile Hydratase. *J. Inorg. Biochem.* **2001**, *83*, 247–253.

(82) Szundi, I.; Rose, M. J.; Sen, I.; Eroy-reveles, A. A.; Mascharak, P. K.; Einarsdottir, O. Rapid Communication A New Approach for Studying Fast Biological Reactions Involving Nitric Oxide : Generation of NO Using Photolabile Ruthenium and Manganese NO Donors. *Photochem. Photobiol.*

2006, No. 80, 1377–1384.

(83) Rose, M. J.; Fry, N. L.; Marlow, R.; Hinck, L.; Mascharak, P. K. Sensitization of Ruthenium Nitrosyls to Visible Light via Direct Coordination of the Dye Resorufin : Trackable NO Donors for Light-Triggered NO Delivery to Cellular Targets. *J. Am. Chem. Soc.* **2008**, No. 130, 8834–8846.

(84) Fry, N. L.; Wei, J.; Mascharak, P. K. Triggered Dye Release via Photodissociation of Nitric Oxide from Designed Ruthenium Nitrosyls : Turn-ON Fluorescence Signaling of Nitric Oxide Delivery. *Inorg. Chem.* **2011**, *50* (18), 9045–9052.

(85) Schubert, U. S.; Hofmeier, G. R.; Newkome, G. R. Chemistry and Properties of Terpyridine Metal Complexes. In *Modern Terpyridine Chemistry*; Wiley-VCH Verlag GmbH & Co. KGaA: Weinheim, 2006; pp 37–68.

(86) Akl, J.; Sasaki, I.; Lacroix, P. G.; Malfant, I.; Mallet-ladeira, S.; Vicendo, P.; Farfán, N.; Santillan, R. Comparative Photo-Release of Nitric Oxide from Isomers of Substituted terpyridinenitrosylruthenium(II) Complexes: Experimental and Computational Investigations. *Dalt. Trans.* **2014**, *43*, 12721–12733.

(87) Nagao, H.; Enomoto, K.; Wakabayashi, Y.; Komiya, G.; Hirano, T.; Oi, T. Synthesis of Nitrosylruthenium Complexes Containing 2 ,2′:6′,2″-Terpyridine by Reactions of Alkoxo Complexes with Acids. *Inorg. Chem.* **2007**, *46* (4), 1431–1439.

(88) Tsikas, D. Analysis of Nitrite and Nitrate in Biological Fluids by Assays Based on the Griess Reaction: Appraisal of the Griess Reaction in the L-Arginine/nitric Oxide Area of Research. *J. Chromatogr. B Anal. Technol. Biomed. Life Sci.* **2007**, *851* (1–2), 51–70.

(89) Vanin, A. F.; Poltorakov, A. P.; Mikoyan, V. D.; Kubrina, L. N.; van Faassen, E. Why Iron-Dithiocarbamates Ensure Detection of Nitric Oxide in Cells and Tissues. *Nitric Oxide - Biol. Chem.* **2006**, *15* (4), 295–311.

(90) Xiang, H.-J.; An, L.; Tang, W.-W.; Yang, S.-P.; Liu, J.-G. Photo-Controlled

Targeted Intracellular Delivery of Both Nitric Oxide and Singlet Oxygen Using a Fluorescence-Trackable Ruthenium Nitrosyl Functional Nanoplatform. *Chem. Commun.* **2015**, *51* (13), 2555–2558.

(91) García, J. S.; Alary, F.; Boggio-Pasqua, M.; Dixon, I. M.; Heully, J. L. Is Photoisomerization Required for NO Photorelease in Ruthenium Nitrosyl Complexes? *J. Mol. Model.* **2016**, *22*, 284.

(92) Cormary, B.; Ladeira, S.; Jacob, K.; Lacroix, P. G.; Woike, T.; Schaniel, D.; Malfant, I. Structural Influence on the Photochromic Response of a Series of Ruthenium Mononitrosyl Complexes. *Inorg. Chem.* **2012**, *51* (14), 7492–7501.

(93) Garcia, J. S.; Alary, F.; Boggio-Pasqua, M.; Dixon, I. M.; Malfant, I.; Heully, J. Establishing the Two-Photon Linkage Isomerization Mechanism in the Nitrosyl Complex Trans-[RuCl(NO)(py)4]2+ by DFT and TDDFT. *Inorg. Chem.* **2015**, *54* (17), 8310–8318.

(94) Bitterwolf, T. E. Photolysis of [Ru(bipy)2(NO)Cl](PF6)2 in Frozen Ionic Glass Matrices. Evidence for Nitrosyl Linkage Isomerism and NO-Loss in a Physiologically Relevant Nitric Oxide Source. *Inorg. Chem. Commun.* **2008**, *11* (7), 772–773.

(95) Giglmeier, H.; Kerscher, T.; Klüfers, P.; Schaniel, D.; Woike, T. Nitric-Oxide Photorelease and Photoinduced Linkage Isomerism on Solid [Ru(NO)(terpy)(L)]BPh4 (L = Glycolate Dianion). *Dalt. Trans.* **2009**, *4* (42), 9113.

(96) Göppert-Mayer, M. Uber Elementarakte Mit Zwei Quantensprüngen. *Ann. Phys.* **1931**, *401* (3), 273–294.

(97) Kaiser, W.; Garrett, C. Two-Photon Excitation in CaF2:Eu2+. *Phys. Rev. Lett.* **1961**, *7* (6), 229–231.

(98) Belfield, K. D.; Schafer, K. J.; Mourad, W.; Reinhardt, B. A. Synthesis of New Two-Photon Absorbing Fluorene Derivatives via Cu-Mediated Ullmann Condensations. *J. Org. Chem.* **2000**, *65* (15), 4475–4481.

(99) Przhonska, O. V; Webster, S.; Padilha, L. A.; Hu, H.; Kachkovski, A. D.;

Hagan, D. J.; Stryland, E. W. Van. Two-Photon Absorption in Near-IR Conjugated Molecules: Design Strategy and Structure–Property Relations. In *Advanced Fluorescence Reporters in Chemistry and Biology I. Springer Series on Fluorescence (Methods and Applications)*; Springer: Berlin, Heidelberg, 2010; Vol. 8.

(100) He, G. S.; Tan, L. S.; Zheng, Q.; Prasad, P. N. Multiphoton Absorbing Materials: Molecular Designs, Characterizations, and Applications. *Chem. Rev.* **2008**, *108* (4), 1245–1330.

(101) Akl, J.; Sasaki, I.; Lacroix, P. G.; Hugues, V.; Vicendo, P.; Bocé, M.; Mallet-ladeira, S.; Blanchard-desce, M.; Malfant, I. Trans- and Cis-(Cl,Cl)-[RuII(FT)Cl2(NO)](PF6): Promising Candidates for NO Release in the NIR Region. *Photochem. Photobiol. Sci.* **2016**, *15*, 1484–1491.

(102) Amabilino, S.; Tasse, M.; Lacroix, P. G.; Mallet-Ladeira, S.; Pimienta, V.; Akl, J.; Sasaki, I.; Malfant, I. Photorelease of Nitric Oxide (NO) on Ruthenium Nitrosyl Complexes with Phenyl Substituted Terpyridines. *New J. Chem.* **2017**, *41* (15), 7371–7383.

(103) Kokou, D. (Honorat) D.; Sungur, E.; Bulou, H.; Taupier, G.; Boeglin, A. Monitoring the Contractile Properties of Optically Patterned Liquid Crystal Based Elastomers. In *Advanced Elastomers - Technology, Properties and Applications*; Boczkowska, A., Ed.; InTech, 2012.

(104) Aparicio-Ixta, L.; Rodriguez, M.; Ramos-ortiz, G. Organic Nanomaterials with Two-Photon Absorption Properties for Biomedical Applications. In *Contemporary Optoelectronics Springer Series in Optical Sciences*; Shulika, O., Sukhoivanov, I., Eds.; Springer: Dordrecht, 2016; Vol. 199.

(105) Lacroix, P. G.; Akl, J.; Malfant, I.; Sasaki, I.; Vicendo, P.; Blanchard-desce, M.; Farfán, N.; Santillán, R.; Bukhanko, V.; Voitenko, Z. Nitric Oxide (NO) Delivery from [Ru(NO) Metal Complexes with Substituted Terpyridine Ligands. *Polymat Contrib.* **2016**, *1*, 97–100.

(106) Chauvin, R.; Lepetit, C. The Fundamental Chemical Equation of Aromaticity. *Phys. Chem. Chem. Phys.* **2013**, *15* (11), 3855.

(107) Enriquez-Cabrera, A.; Sasaki, I.; Bukhanko, V.; Tassé, M.; Mallet-Ladeira, S.; Lacroix, P. G.; Barba-Barba, R. M.; Ramos-Ortiz, G.; Farfán, N.; Voitenko, Z.; et al. Replacing Two Chlorido Ligands by a Bipyridine Ligand in Ruthenium Nitrosyl Complexes with NO-Release Capabilities: A Comparative Study. *Eur. J. Inorg. Chem* **2017**, No. 11, 1446–1456.

(108) Garcia, J. S. Theoretical Study of New Nitrosyl Ruthenium Complexes: Mechanisms of Photoisomerization and Photorelease of NO, University Toulouse III - Paul Sabatier, 2016.

(109) Juris, A.; Balzani, V.; Barigelletti, F.; Campagna, S.; Belser, P.; von Zelewsky, A. Ru(II) Polypyridine Complexes: Photophysics, Photochemistry, Eletrochemistry, and Chemiluminescence. *Coord. Chem. Rev.* **1988**, *84* (C), 85–277.

(110) de Lima, R. G.; Sauaia, M. G.; Bonaventura, D.; Tedesco, A. C.; Bendhack, L. M.; da Silva, R. S. Influence of Ancillary Ligand L in the Nitric Oxide Photorelease by the [Ru(L)(tpy)NO]3+complex and Its Vasodilator Activity Based on Visible Light Irradiation. *Inorganica Chim. Acta* **2006**, *359* (8), 2543–2549.

(111) Буханько, В.; Войтенко, З.; Лакруа, П. Д.; І., М. Рутеній-Нітрозильні Комплекси З Терпіридиновими Лігандами Як Донори нітроген(II) Оксиду. *Вісник Київського національного університету імені Тараса Шевченка* **2017**, *1(53)*, 22–24.

(112) Bordini, J.; Hughes, D. L.; Da Motta Neto, J. D.; Da Cunha, C. J. Nitric Oxide Photorelease from Ruthenium Salen Complexes in Aqueous and Organic Solutions. *Inorg. Chem.* **2002**, *41* (21), 5410–5416.

(113) Feuvrie, C.; Maury, O.; Le Bozec, H.; Ledoux, I.; Morrall, J. P.; Dalton, G. T.; Samoc, M.; Humphrey, M. G. Nonlinear Optical and Two-Photon Absorption Properties of Octupolar Tris(bipyridyl)metal Complexes. *J. Phys. Chem. A* **2007**, *111* (37), 8980–8985.

(114) Wang, X.; Nguyen, D. M.; Yanez, C. O.; Rodriguez, L.; Ahn, H. Y.; Bondar, M. V.; Belfield, K. D. High-Fidelity Hydrophilic Probe for Two-Photon

Fluorescence Lysosomal Imaging. *J. Am. Chem. Soc.* **2010**, *132* (35), 12237–12239.

(115) Denneval, C.; Moldovan, O.; Baudequin, C.; Achelle, S.; Baldeck, P.; Plé, N.; Darabantu, M.; Ramondenc, Y. Synthesis and Photophysical Properties of Push-Pull Structures Incorporating Diazines as Attracting Part with a Fluorene Core. *European J. Org. Chem.* **2013**, No. 25, 5591–5602.

(116) Bukhanko, V.; Malfant, I.; Voitenko, Z.; Lacroix, P. G. Isoindole and Isomeric Heterocyclic Donating Substituents in Ruthenium(II) Nitrosyl Complexes with Large First Hyperpolarizabilities and Potential Two-Photon Absorption Capabilities: A Computational Approach. *Fr. Ukr. J. Chem.* **2017**, *5* (1), 8–23.

(117) Terenziani, F.; Katan, C.; Badaeva, E.; Tretiak, S.; Blanchara-Desce, M. *Enhanced Two-Photon Absorption of Organic Chromophores: Theoretical and Experimental Assessments*; 2008; Vol. 20.

(118) Oudar, J. L. Optical Nonlinearities of Conjugated Molecules. Stilbene Derivatives and Highly Polar Aromatic Compounds. *J. Chem. Phys.* **1977**, *67* (2), 446–457.

(119) Prasad, P. N.; Williams, D. J. *Introduction to NLO Effects in Molecules and Polymers*; John Wiley & Sons: New York, 1991.

(120) Kovtunenko, V. A.; Voitenko, Z. V.; Sheptun, V. L.; Tyltin, A. K.; Chernega, A. I.; Struchkov, Y. T.; Babichev, F. S. Comparative Analysis of The Electronic Structure of Positional Isomers: Indole-Isoindole. *Khimiya Geterociklicheskih Soedin.* **1984**, *11*, 1497–1503.

(121) Kovtunenko, V. A.; Voitenko, Z. V.; Sheptun, V. L.; Savranskiy, L. I.; Tyltin, A. K.; Babichev, F. S. The Electronic Structure of Azinoisoindoles with the Node Nitrogen Atom. *Ukr. Chim. J.* **1985**, *51*, 976–987.

(122) Morley, J. O.; D., P. Computational Evaluation of Second-Order Optical Nonlinearities. In *Nonlinear optics of organic molecules and polymers.*; Nalwa, H. S., Miyata, S., Eds.; CRC press Boca Raton, 1997; pp 29–56.

(123) Ducere, J. M.; Lepetit, C.; Lacroix, P. G.; Heully, J. L.; Chauvin, R.

Quadratic Hyperpolarizability of Carbomeric Structures. *Chem. Mater.* **2002**, *14* (8), 3332–3338.

(124) Shakibaei, G. I.; Bazgir, A. A Highly Efficient One-Pot Synthesis of Indenopyridine-Fused Spirocyclic Systems. *RSC Adv.* **2016**, *6* (27), 22306–22311.

(125) Pokholenko, A. A.; Voitenko, Z. V.; Kovtunenko, V. A. Pyrido- and Pyrimido-Isoindoles: Methods of Synthesis and Properties. *Russ. Chem. Rev.* **2004**, *73*, 771–784.

(126) Constable, E. C.; Ward, M. D. Synthesis and Co-Ordination Behaviour of 6',6''-Bis(2-Pyridyl)-2,2': 4,4'' : 2'', 2''' - Quaterpyridine; "Back-to-Back" 2'2' : 6',2''- Terpyridine. *J. Chem. Soc. Dalt. Trans.* **1990**, *0*, 1405–1409.

(127) Lin, C. P.; Florio, P.; Campi, E. M.; Zhang, C.; Fredericks, D. P.; Saito, K.; Jackson, W. R.; Hearn, M. T. W. Synthesis of Substituted Terpyridine Ligands for Use in Protein Purification. *Tetrahedron* **2014**, *70* (45), 8520–8531.

(128) Muro, M. L.; Castellano, F. N. Room Temperature Photoluminescence from [Pt(4'-Câ‰¡CR-tpy)Cl]+ Complexes. *Dalt. Trans.* **2007**, *9226* (41), 4659–4665.

(129) Nie, H. J.; Yao, J.; Zhong, Y. W. Synthesis of Vinyl-Substituted Polypyridyl Ligands through Suzuki-Miyaura Cross-Coupling of Potassium Vinyltrifluoroborate with Bromopolypyridines. *J. Org. Chem.* **2011**, *76* (11), 4771–4775.

(130) Zhang, W.; Cao, X. Y.; Zi, H.; Pei, J. Single-Molecule Nanosized Polycyclic Aromatics with Alternant Five- and Six-Membered Rings: Synthesis and Optical Properties. *Org. Lett.* **2005**, *7* (6), 959–962.

(131) Jeppesen, L.; Bury, P. S.; Mogensen, J. P.; Pettersson, I.; Sauerberg, P. Novel Vinyl N-(2-BenzoylPhenyl)-L-Tyrosine Derivatives and Their Use as AntiDiabetics Etc. WO 03/011814 A1, 2003.

(132) Treffert-Ziemelis, S. M.; Golus, J.; Strommen, D. P.; Kincaid, J. R. Resonance Raman and Time-Resolved Resonance Raman Studies of Tris(4-

Methyl-2,2′-bipyridine)ruthenium(II). Polarization of the Radical Fragment of the 3MLCT States. *Inorg. Chem.* **1993**, *32* (18), 3890–3894.

(133) Murahashi, S.-I.; Watanabe, T. Palladium Catalyzed Hydrolysis of Tertiary Amines with Water. *J. Am. Chem. Soc.* **1979**, *101* (24), 7429–7430.

(134) Kuo, P. L.; Chen, C. C. Generation of Gold Thread from Au(III) and Triethylamine. *Langmuir* **2006**, *22* (18), 7902–7906.

(135) Mccrindle, R.; Ferguson, G.; Arsenault, G. J.; Mcalees, A. J. Reaction of Tertiary Amines with Bis(benzonitri1e)dichloro- palladium(II). Formation and Crystal Structure Analysis of Di-μ-Chloro-dichlorobis[2-(N,N-Di-Isopropyliminio)ethyl-C]dipalladium (II) Robert. *J. Chem. Soc., Chem Commun.* **1983**, *30* (1), 571–572.

(136) Ling, Z.; Yun, L.; Liu, L.; Wu, B.; Fu, X. Aerobic Oxidative N-Dealkylation of Tertiary Amines in Aqueous Solution Catalyzed by Rhodium Porphyrins. *Chem. Commun.* **2013**, *49* (39), 4214–4216.

(137) Kucherak, O. A.; Didier, P.; Mèly, Y.; Klymchenko, A. S. Fluorene Analogues of Prodan with Superior Fluorescence Brightness and Solvatochromism. *J. Phys. Chem. Lett.* **2010**, *1* (3), 616–620.

(138) Jiang, X.; Wang, C.; Wei, Y.; Xue, D.; Liu, Z.; Xiao, J. A General Method for N-Methylation of Amines and Nitro Compounds with Dimethylsulfoxide. *Chem. - A Eur. J.* **2014**, *20* (1), 58–63.

(139) Atkinson, B. N.; Williams, J. M. J. Dimethylsulfoxide as an N-Methylation Reagent for Amines and Aromatic Nitro Compounds. *ChemCatChem* **2014**, *6* (7), 1860–1862.

(140) Wienhöfer, G.; Sorribes, I.; Boddien, A.; Westerhaus, F.; Junge, K.; Junge, H.; Llusar, R.; Beller, M. General and Selective Iron-Catalyzed Transfer Hydrogenation of Nitroarenes without Base. *J. Am. Chem. Soc.* **2011**, *133* (32), 12875–12879.

(141) Li, P.; Wang, H.; Qu, J. 1,n‑Rearrangement of Allylic Alcohols Promoted by Hot Water: Application to the Synthesis of Navenone B, a Polyene Natural Product. *J. Org. Chem.* **2014**, *79*, 3955–3962.

(142) Akl, J.; Billot, C.; Lacroix, P. G.; Sasaki, I.; Mallet-Ladeira, S.; Malfant, I.; Arcos-Ramos, R.; Romero, M.; Farfán, N. Molecular Materials for Switchable Nonlinear Optics in the Solid State, Based on Ruthenium-Nitrosyl Complexes. *New J. Chem.* **2013**, *37* (11), 3518–3527.

(143) Biner, M.; Buergi, H. B.; Ludi, A.; Roehr, C. Crystal and Molecular Structures of [Ru(bpy)3](PF6)3 and [Ru(bpy)3](PF6)2 at 105 K. *J. Am. Chem. Soc.* **1992**, *114* (13), 5197–5203.

(144) Garcia, J. S. Theoretical Study of New Nitrosyl Ruthenium Complexes: Mechanisms of Photoisomerization and Photorelease of NO, PhD Thesis, Toulouse III University - Paul Sabatier, 2016.

(145) Bukhanko, V.; Lacroix, P. G.; Sasaki, I.; Tassé, M.; Voitenko, Z.; Malfant, I. Mechanism and Oxidation State Involved in the Nitric Oxide (NO) Photorelease in a Terpyridine-Bipyridine-Based Ruthenium Nitrosyl Complex. *Inorganica Chim. Acta* **2018**, 10.1016/j.ica.2018.05.038 ICA.

(146) Akl, J.; Sasaki, I.; Lacroix, P. G.; Hugues, V.; Vicendo, P.; Bocé, M.; Mallet-ladeira, S.; Blanchard-desce, M. Trans- and Cis-(Cl,Cl)-[Ru(II)(FT)Cl2(NO)](PF6): Promising Candidates for NO Release in the NIR Region. *Photochem. Photobiol. Sci.* **2016**, *15*, 1484–1491.

(147) Pipes, D. W.; Meyer, T. J. Comparisons between Polypyridyl Nitrosyl Complexes of Osmium(II) and Ruthenium(II). *Inorg. Chem.* **1984**, *23* (16), 2466–2472.

(148) De, P.; Sarkar, B.; Maji, S.; Das, A. K.; Bulak, E.; Mobin, S. M.; Kaim, W.; Lahiri, G. K. Stabilization of {RuNO}6 and {RuNO}7 States in [RuII(trpy)(bik)(NO)]n+ {trpy = 2,2':6',2''-terpyridine, Bik = 2,2'-bis(1-Methylimidazolyl) Ketone} - Formation, Reactivity, and Photorelease of Metal-Bound Nitrosyl. *Eur. J. Inorg. Chem.* **2009**, No. 18, 2702–2710.

(149) Roose, M.; Sasaki, I.; Bukhanko, V.; Mallet-Ladeira, S.; Barba-Barba, R. M.; Ramos-Ortiz, G.; Enriquez-Cabrera, A.; Farfán, N.; Lacroix, P. G.; Malfant, I. Nitric Oxide Photo-Release from a Ruthenium Nitrosyl Complex with a 4,4-Bisfluorenyl-2,2-Bipyridine Ligand. *Polyhedron* **2018**, *151*, 101–

111.

(150) Rubbo, H.; Radi, R. Protein and Lipid Nitration: Role in Redox Signaling and Injury. *Biochim. Biophys. Acta - Gen. Subj.* **2008**, *1780* (11), 1318–1324.

(151) Radi, R. Protein Tyrosine Nitration: Biochemical Mechanisms and Structural Basis of Functional Effects. *Acc. Chem. Res.* **2013**, *46* (2), 550–559.

(152) Liu, J.; Duan, Q.; Wang, J.; Song, Z.; Qiao, X.; Wang, H. Photocontrolled Nitric Oxide Release from Two Nitrosylruthenium Isomer Complexes and Their Potential Biomedical Applications. *J. Biomed. Opt.* **2015**, *20* (1), 15004-1-015004–015007.

(153) Lavabre, D.; Pimienta, V. Program Sa3.3.

(154) Pimienta, V.; Frouté, C.; Deniel, M. H.; Lavabre, D.; Guglielmetti, R.; Micheau, J. C. Kinetic Modelling of the Photochromism and Photodegradation of a Spiro[indoline-Naphthoxazine]. *J. Photochem. Photobiol. A Chem.* **1999**, *122* (3), 199–204.

(155) SADABS. Bruker AXS Inc., Madison, Wisconsin, USA.

(156) Sheldrick, G. M. A Short History of SHELX. *Acta Crystallogr. Sect. A Found. Crystallogr.* **2008**, *64* (1), 112–122.

(157) Sheldrick, G. M. SHELXT - Integrated Space-Group and Crystal-Structure Determination. *Acta Crystallogr. Sect. A Found. Crystallogr.* **2015**, *71* (1), 3–8.

(158) Rose, M. J.; Mascharak, P. K. Photosensitization of Ruthenium Nitrosyls to Red Light with an Lsoelectronic Series of Heavy-Atom Chromophores: Experimental and Density Functional Theory Studies on the Effects of 0-, S- And Se-Substituted Coordinated Dyes. *Inorg. Chem.* **2009**, *48* (14), 6904–6917.

(159) Kleinman, D. A. Nonlinear Dielectric Polarization in Optical Media. *Phys. Rev.* **1962**, *126* (6), 1977–1979.

(160) Makarov, N. S.; Drobizhev, M.; Rebane, A. Two-Photon Absorption Standards in the 550-1600 Nm Excitation Wavelength Range. *Opt. Express*

2008, *16* (6), 4029–4047.

(161) Potts, K. T.; Konwar, D. Synthesis of 4′-Vinyl-2,2′:6′,2″-Terpyridine. *J. Org. Chem.* **1991**, *56* (15), 4815–4816.

(162) Gerstel, P.; Klumpp, S.; Hennrich, F.; Poschlad, A.; Meded, V.; Blasco, E.; Wenzel, W.; Kappes, M. M.; Barner-Kowollik, C. Highly Selective Dispersion of Single-Walled Carbon Nanotubes via Polymer Wrapping: A Combinatorial Study via Modular Conjugation. *ACS Macro Lett.* **2014**, *3* (1), 10–15.

Summary of thesis

The work “Two-photon induced photorelease of nitric oxide from ruthenium-nitrosyl complexes containing ligands with various push-pull capabilities” was devoted to the revealing of main factors that determine the efficiency of ruthenium-nitrosyl complexes in two-photon absorption (TPA) and to the improvement of TPA cross-section through modification of the ligands nature and their structure.

Starting from complexes previously obtained by the research group of Prof. I. Malfant we have modified their structure in several directions. It was shown that substitution of monodentate ligands by 2,2'-bipyridine in ruthenium complexes with nitrosyl ligand leads to a slight increase of their TPA cross-section, however this modification decreases the quantum yield of the nitric oxide photorelease.

Synthetic part of the work was mainly aimed at the modification of the ligand 4'-(9*H*-fluoren-2-yl)-2,2':6',2''-terpyridine. The elongation and flattening of the conjugation path could improve the polarizability of the ligand and the “push-pull” character of the complex. This subsequently results in an increased efficiency of the compounds in TPA that was confirmed in the current work. Insertion of double bond between two parts of the ligand leads to the enhancement of the TPA cross-section by 20%, whereas the triple bond appears better linker leading to 36% improved efficiency of complexes in TPA. Another parameter of compounds, sensitive to the structural modifications, is the difference in dipole moments between the ground and excited states of the molecules. It deserves particular attention whereas it enters the expression of the TPA efficiency as the criterion of “push-pull” character of the molecule. With the purpose of increasing this difference we put as a goal the synthesis of the complexes with ligands bearing donating dimethylamino-groups. Having optimized the methodology of ligands syntheses, we, however, found out that usual way of complex synthesis in this case has not resulted in the desired complex obtention. During the second step of the

ruthenium-nitrosyl compound synthesis an incorporated dimethylaminogroup undergoes the oxidation process with its subsequent demethylation.

However, having obtained a series of easier accessible complexes with groups displaying different donating abilities, we were able to discover some tendency. These complexes contain phenyl rings, carrying functional groups starting from withdrawing nitro- to donating metoxy- and dimethylaminogroups. It was shown that while accepting or neutral groups didn't show any significant influence on the TPA cross-sections of complexes, donating moieties increased it with the highest value of 154 GM observed for complex with 4'-(4-methoxyphenyl)-2,2':6',2''-terpyridine ligand. Thus the observation has confirmed the initial hypothesis that increasing of the difference in dipole moments between the ground and excited state would lead to an enhanced efficiency of complexes in TPA.

In the current work theoretical calculations on the basis of density functional theory (DFT) are widely involved. Apart from studying the ability of complexes to release NO under irradiation a theoretical investigation of their nonlinear optical properties was made. In order to improve the conjugation and the length of the π-conjugation system we have assessed the effect of the fluorenyl-fragment substitution by 22 different heterocyclic analogues having similar tricyclic skeleton and containing donating Nitrogen atom in the system. It was shown, that in spite of the fact that such modification doesn't lead to a desired improvement, such compounds could be indeed interesting as nonlinear optical materials.

The structure of the photoproduct and ruthenium oxidation states are discussed in details. In contrast to photoproducts previously observed, complexes having five pyridine rings in the coordination sphere of metal form Ru(II) products during the process of NO-photorelease, whereas the formation of NO-radical is confirmed by EPR-spectroscopy.

Résumé de these

Ce travail intitulé «Libération du monoxyde d'azote induite par deux photons à partir de complexes ruthénium-nitrosyle contenant des ligands de capacités push-pull différentes» a été consacré à l'étude des principaux facteurs qui déterminent l'efficacité des complexes ruthénium-nitrosyle (Ru(NO)) dans l'absorption à deux photons (ADP) et à l'amélioration de leur section efficace ADP par modification de la nature et de la structure de leurs ligands.

A partir de complexes précédemment obtenus dans le groupe de recherche du Prof. I. Malfant, nous avons effectué diverses modifications structurales. Il a été montré que la substitution des ligands monodentes par la 2,2'-bipyridine dans les complexes de Ru(NO) conduit à une légère augmentation de la section efficace, mais cette modification diminue le rendement quantique du relargage du monoxyde d'azote (NO).

La partie synthétique du travail a principalement porté sur la modification du ligand 4'-(9*H*-fluorène-2-yl)-2,2':6',2''-terpyridine. L'extension de la conjugaison doit améliorer la polarisabilité du ligand et le caractère «push-pull» du complexe. Cela entraîne une efficacité accrue des composés en ADP qui a été confirmée expérimentalement durant ce travail. L'insertion d'une double liaison au centre du système entre les fragments donneurs et accepteurs conduit à une augmentation de 20% de la section efficace, alors que la triple liaison apporte un gain de 36% et apparaît comme un meilleur transmetteur. La différence des moments dipolaires entre les états fondamentaux et excités des molécules est un paramètre additionnel particulièrement sensible aux modifications structurales des composés. Il mérite une attention particulière car il intervient dans l'expression de l'efficacité ADP en apportant une quantification de l'effet «push-pull». Pour augmenter sa valeur, nous nous sommes fixé comme objectif la synthèse de complexes possédant des ligands porteurs du substituent donneur diméthylamino. Après optimisation de la synthèse de ces ligands, l'obtention des complexes afférents par la méthode habituelle de synthèse des complexes Ru(NO) a été un échec. En effet, la deuxième étape de la

synthèse conduit à une oxydation progressive du groupement diméthyamino avec déméthylation.

L'étude d'une autre série de complexes plus accessibles avec des groupements donneurs de forces diverses a permis de mettre en évidence certaines tendances. Ces complexes contiennent des cycles phényles, portant des groupes fonctionnels accepteurs (nitro-) et donneurs comme métoxy- et diméthylamino-. Il a été montré que, si la présence de groupes accepteurs ou neutres a peu d'effet sur la section efficace, la présence de donneurs conduit à une amélioration des propriétés avec une valeur maximale de section efficace de 154 GM observée pour le complexe avec le ligand 4'-(4-méthoxyphényl)-2,2':6',2" – terpyridine. L'expérience confirme l'hypothèse initiale selon laquelle l'augmentation de la différence des moments dipolaires entre les états fondamentaux et excités des molécules conduirait à une efficacité ADP accrue dans ce type de molécules.

Une large part de ce travail a impliqué des calculs théoriques effectués à partie de la théorie de la fonctionnelle de la densité (DFT). En marge des effets liés à la photo-libération de NO, les propriétés optiques non linéaires des complexes de Ru(NO) ont été étudiées sur le plan théorique. L'effet de la substitution du fragment fluorényle par 22 analogues hétérocycliques différents ayant un squelette tricyclique similaire et contenant un atome d'azote donneur a été évalué afin d'améliorer la conjugaison et d'optimiser la longueur et la forme du système π-conjugué. Il a été montré que, bien qu'une telle modification ne conduise pas à une amélioration notable, de tels composés pourraient être intéressants en tant que matériaux pour l'optique non linéaire.

La structure du photoproduit et le degré d'oxydation du ruthénium sont discutés en détail. Contrairement au photoproduit précédemment étudié, les complexes possédant cinq cycles pyridine dans la sphère de coordination du métal conduisent à des complexes de Ruthénium(II) pendant le processus de photo-libération de NO, alors que la formation de radical NO est confirmée par spectroscopie RPE.

CONTENU PRINCIPAL

Dans **l'introduction** le contexte du travail est expliquée, le but et les objectifs de l'étude sont énoncés avec la signification des résultats obtenus.

Le **premier chapitre** de la thèse est consacré à la présentation de l'avancement de la recherche sur le sujet de la thèse. Une attention particulière est accordée aux types de donneurs d'oxyde nitrique connus aujourd'hui et à ceux mis en œuvre dans la pratique médicale, aux particularités de leur structure et aux conditions dans lesquelles le processus de libération de NO peut être observé. Les particularités de la structure des complexes ruthénium-nitrosyle sont examinées en détail. Les dernières avancées dans la chimie des complexes ruthénium-nitrosyle sont également mises en évidence. En particulier, les mécanismes théoriques par lesquels le processus de libération de NO peut se produire sont présentés en détail.

Le **second chapitre** du travail est principalement axé sur les effets sur les propriétés des complexes ruthénium-nitrosyle provoqués par la substitution de deux ligands monodentés dans la sphère de coordination du ruthénium, à savoir deux atomes de chlore, avec la molécule de 2,2'-bipyridine (bpy). Le ligand principal restant inchangé était le 4'-(9H-fluorén-2-yl)-2,2': 6', 2''- terpyridine (FT).

Ainsi, les objets de l'étude étaient *cis(Cl,Cl)*- $Ru^{II}(FT)Cl_2(NO)](PF_6)$ (**1a**), *trans*(Cl,Cl)-$Ru^{II}(FT)Cl_2(NO)](PF_6)$ (**1b**) et $[Ru^{II}(FT)(bpy)(NO)](PF_6)_3$ (**1c**) (Figure 1).

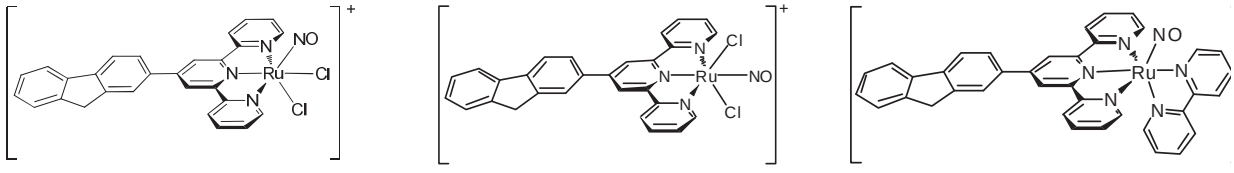

1a **1b** **1c**

Figure 1. La structure des cations des complexes *cis(Cl,Cl)*- $Ru^{II}(FT)Cl_2(NO)](PF_6)$ (**1a**), *trans*(Cl,Cl)-$Ru^{II}(FT)Cl_2(NO)](PF_6)$ (**1b**) et $[Ru^{II}(FT)(bpy)(NO)](PF_6)_3$ (**1c**).

Les spectres électroniques des solutions d'acétonitrile des trois composés sont présentés sur la figure 2. La bande d'absorption principale B est à la limite de la

région spectrale visible, mais pour le composé **1c**, on observe un décalage bathochrome de cette bande par rapport aux complexes contenant des ligands chloro. Dans ce cas, le coefficient d'extinction molaire de la bande B du composé **1c** est légèrement inférieur.

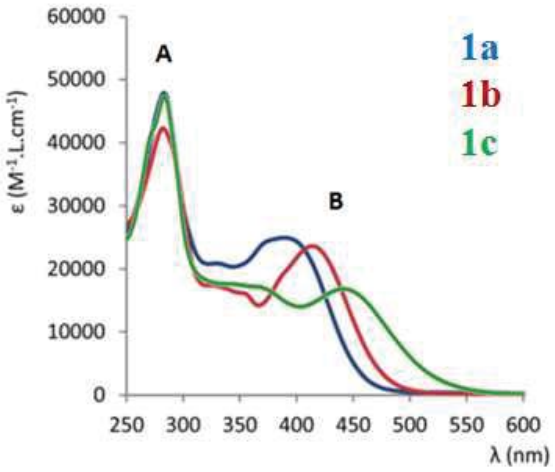

Figure 2. Spectres électroniques des solutions des complexes **1a**, **1b**, **1c** dans CH3CN.

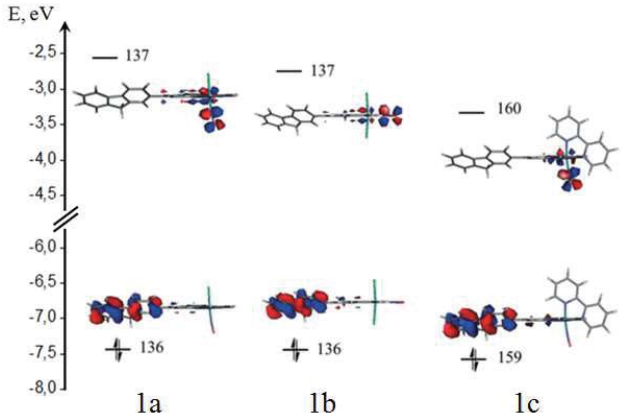

Figure 3. Visualisation de HOMO et LUMO pour les composés **1a**, **1b**, **1c**.

Une analyse détaillée des transitions électroniques responsables de l'apparition de la bande B dans les spectres montre que pour les trois composés les transitions les plus intenses sont essentiellement celles ayant la configuration HOMO-LUMO avec une certaine contribution de la transition HOMO-LUMO+2. La HOMO se concentre principalement sur le fragment fluorényle, qui est un substituant donneur dans les complexes, tandis que la principale contribution pour la LUMO est le fragment ruthénium-nitrosyle, dans lequel l'interaction d_{Ru}-π*(NO) a un caractère antiliant (figure 3). C'est pourquoi le transfert de densité électronique vers la LUMO entraîne une diminution de la constante de force de la liaison Ru-N et déclenche la libération de NO.

Les rendements quantiques de photolibération de l'oxyde nitrique des trois composés sous irradiation à une longueur d'onde de 405 nm donnent 0.31 (**1a**), 0.11 (**1b**) et 0.06 (**1c**). Le composé **1c** présente un rendement quantique légèrement inférieur par rapport au composé **1b**. Les rendements quantiques pour **1b** et **1c** sont

assez similaires et diffèrent donc significativement du rendement quantique du composé **1a**, bien que formellement, en termes de structure des composés, **1c** ressemble davantage à **1a**. Les valeurs des rendements quantiques de libération de NO dépendent de la nature du ligand en position *trans* par rapport au nitrosyle: la présence du cycle pyridine en *trans* du NO au lieu du ligand chloro entraîne une diminution du rendement quantique.

Les composés ont été étudiés pour leur capacité à absorber deux photons (ADP) par la méthode de z-scan. Dans cette approche pour la détemrination de la section efficace d'ADP (σ), une solubilité élevée des composés est requise. Cette condition a été remplie en introduisant des substituants n-hexyle en position 9 du fragment fluorényle. Les complexes résultants sont respectivement **1a'**, **1b'** et **1c'**. Des courbes de transmission typiques pour un rayonnement laser d'une longueur d'onde de 800 nm (utilisé pour activer les complexes de ruthénium-nitrosyle) pour des solutions de complexes d'acétonitrile sont présentées (Figure 4).

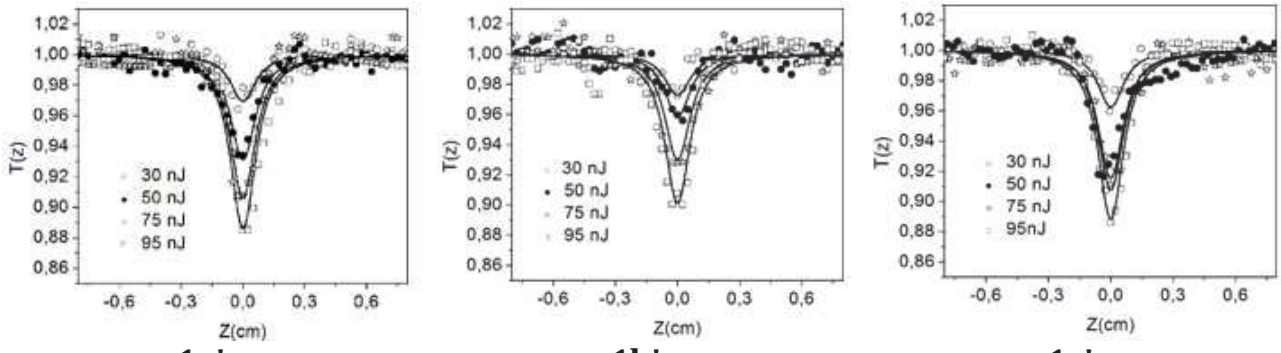

Figure 4. Courbes de transmission d'irradiation laser pour les composés **1a'**,**1b'**et **1c'**.

Les sections efficaces obtenues sont de 100 GM (**1a'**), 87 GM (**1b'**) et 108 GM (**1c'**). Compte tenu de l'erreur de mesure, on peut dire que les valeurs obtenues sont du même ordre et voisines de 100 GM, avec une tendance à l'augmentation de l'efficacité d'ADP dans la série **1a'**<**1b'**<**1c'**. Nous avons également effectué mesuré les propriétés d'ADP du composé **1c'** à la longueur

d'onde λ = 900 nm. Cependant, il n'y avait pas de changement significatif dans la valeur de σ. Lorsque l'on change la longueur d'onde à 900 nm, soit presque deux fois la longueur d'onde du maximum d'absorption pour le composé **1c**, la valeur de σ est de 89 ± 20 GM.

Le **troisième chapitre** de la thèse est consacré à l'étude théorique de l'effet de la substitution du fragment fluorényle par des analogues hétérocycliques, représentés par des systèmes condensés tricycliques, en particulier le pyrido[2,1-a]isoindole et hétérocycles isomères. Au total, 22 complexes ont été analysés ; leurs fragments hétérocycliques sont indiqués dans le tableau 1.

Les systèmes tricycliques contenant un atome d'azote ont été séparés du noyau de terpyridine par une double liaison afin de réduire la gêne stérique des atomes d'hydrogène des deux parties du ligand qui ont conduit à la conformation plane du ligand. Tous les complexes ont été classés selon l'emplacement du cycle à cinq atomes dans un hétérocycle: 6-6-5 (si le cycle à 5 atomes est situé sur le côté), 6-5-6 (si le cycle à 5 atomes est entre les deux cycles à 6 atomes). L'idée de remplacer le fragment fluorényle est liée au fait qu'une telle modification peut potentiellement conduire à des valeurs de sections efficaces plus élevées. On sait que le pyrido[2,1-a]isoindole est un hétérocycle donneur avec un système de conjugaison de 14 électrons π. Le fluorène est capable de fournir uniquement 10 électrons π. Le paramètre σ est un analogue du coefficient d'extinction molaire pour l'absorption à un photon et dépend des caractéristiques structurales de la molécule. Les principaux paramètres déterminant son ampleur sont notamment la longueur et l'efficacité de la conjugaison et la différence entre les moments dipolaires des états électroniques principal et excité des molécules.

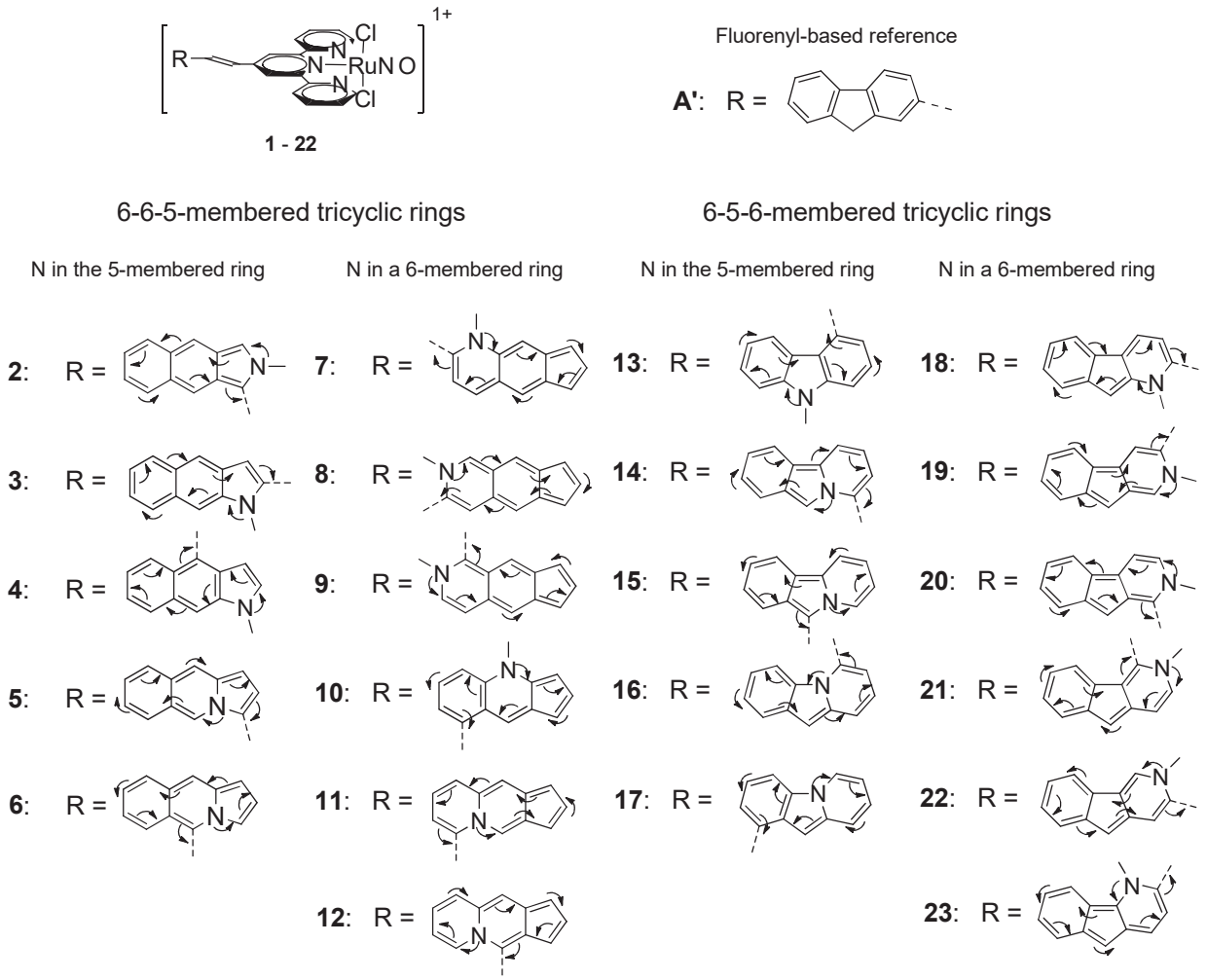

Tableau 1. Les complexes isomères ruthénium-nitrosyle avec des substituants tricycliques donneurs: 6-6-5 (**2-12**) et 6-5-6 (**13-23**) et le composé de référence A'.

Étant donné que le doublet non liant de l'atome d'azote dans la molécule de pyrido[2,1-a]isoindole est fortement conjugué au système π de la molécule, il est intéressant d'utiliser un tel hétérocycle en tant que fragment donneur dans le complexe. L'augmentation de la capacité donneur de l'hétérocycle augmentera l'efficacité du transfert de densité électronique au LUMO et conduira à une modification plus significative du moment dipolaire lors de l'irradiation.

Outre la capacité des complexes étudiés à participer au processus d'ADP, leur hyperpolarisabilité a également été analysée. Ceci est une caractéristique importante des matériaux optiques non linéaires.

Les valeurs calculées de l'hyperpolarisabilité (β) des composés varient largement - de $233 \cdot 10^{-30}$ à $2751 \cdot 10^{-30}$ $cm^5 \cdot esu^{-1}$. Les valeurs les plus élevées observées pour les composés **7** ($2710 \cdot 10^{-30}$ $cm^5 \cdot esu^{-1}$) et **9** ($2752 \cdot 10^{-30}$ $cm^5 \cdot esu^{-1}$)

dépassent les limites classiques rencontrées pour ces composés. Bien que ces valeurs soient théoriquement possibles, elles nécessitent des analyses et des recherches supplémentaires. L'explication possible des valeurs de β observées pourrait être la suivante: plus le chemin de conjugaison est court, plus l'hyperpolarisabilité est grande. En d'autres termes, les composés les plus efficaces sont ceux dans lesquels les 14 électrons π sont nécessairement impliqués dans la voie de la délocalisation. Ceci est illustré par la figure 5 pour les complexes **11** ($\beta = 1130 \cdot 10^{-30}$ $cm^5 \cdot esu^{-1}$) et **12** ($\beta = 732 \cdot 10^{-30}$ $cm^5 \cdot esu^{-1}$), qui contiennent le même substituant isomère R et le fragment accepteur (A), mais qui diffèrent par la position de la substitution. Alors que la seule voie de délocalisation implique les 14 électrons π dans **11**, une conjugaison plus courte apparaît dans **12** dans laquelle seuls 10 électrons π contribuent à la mésomérie (bas de la figure 5), sans impliquer de doubles liaisons du cycle pyridine latéral. Il est probable que la présence du chemin de conjugaison plus court explique la diminution de l'hyperpolarisabilité du composé.

L'augmentation de β devrait entraîner une augmentation de l'effet push-pull vers le fragment accepteur {Ru-NO}. En raison de cet effet, la densité électronique sur l'orbitale antiliante π* du ligand nitrosyle devrait augmenter, ce qui se traduirait par un affaiblissement de la constante de force de la liaison N-O et une diminution de sa fréquence de vibration de valence. La relation entre β et la fréquence de vibration de valence de NO est illustrée (Figure 6). Les valeurs calculées des fréquences ν(NO) sont très légèrement différentes des valeurs expérimentales pour ces composés et sont tout à fait fiables.

Cela devrait normalement conduire à une augmentation du transfert d'électrons vers une orbitale π* antiliante du ligand nitrosyle, avec pour conséquence une augmentation de la densité électronique (population de Mulliken) sur NO et une diminution de la fréquence d'étirement de ν (NO) (Figure 6).

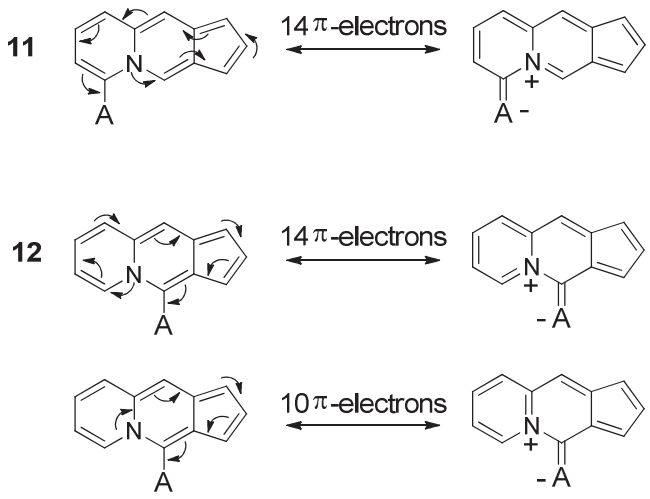

Figure 5. Structures de résonance du substituant hétérocyclique cyclopenta[b] quinolizine dans les complexes **11** et **12**, où le groupe de retrait A est situé respectivement aux positions 6 et 4

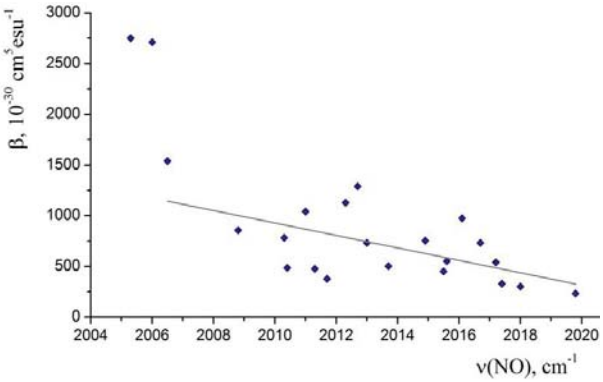

Figure 6. Les valeurs de l'hyperpolarisabilité en relation avec la fréquence des vibrations de valence ν(NO). Les valeurs pour les composés **7** et **9** sont exclues lors du calcul de la ligne de tendance.

Les propriétés d'ADP des complexes ont été évaluées à l'aide d'un modèle à deux niveaux, qui peut être appliqué à des systèmes présentant un fort caractère push-pull. L'analyse des résultats montre que, malgré l'augmentation du caractère donneur des substituants hétérocycliques, leur introduction dans les complexes ruthénium-nitrosyle n'augmente pas la capacité de cette dernière à absorber deux photons par rapport au complexe de référence A'.

Le quatrième chapitre de la thèse décrit les résultats des expériences menées dans le but d'accroître l'efficacité des composés en absorption à deux photons. L'augmentation de l'efficacité de la conjugaison et de la longueur de la chaîne de conjugaison π est l'un des moyens d'améliorer les propriétés d'ADP du composé. L'introduction d'une liaison multiple entre la terpyridine et les fragments fluorényle pourrait conférer une meilleure capacité de polarisation du système π du ligand, conduisant ainsi à des valeurs plus élevées de σ. Par conséquent, l'un des objectifs

du travail a été de synthétiser des ligands terpyridine avec des liaisons multiples et d'obtenir les complexes ruthénium-nitrosyle correspondants (Figure 7).

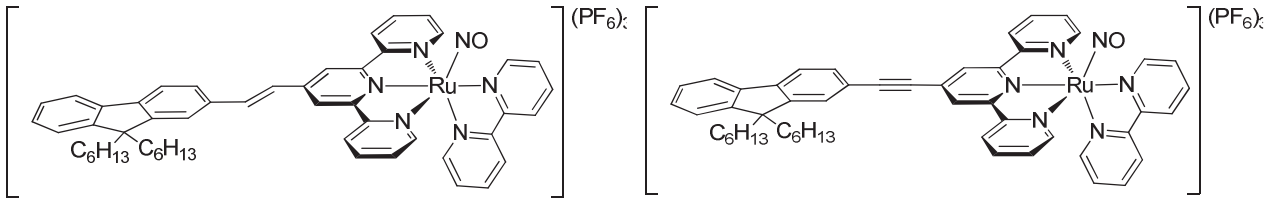

24a **24b**

Figure 7. Les structures des complexes $Ru(FCCT)(bpy)NO](PF_6)_3$ (**24a**) et $[Ru(FCC3T)(bpy)NO](PF_6)_3$ (**24b**).

Le ligand comprenant la double liaison FCCT a été obtenu par synthèse linéaire en 6 étapes avec un rendement total de 11% (schéma 1).

Le 1- (2-oxo-2- (pyridine-2-yl) éthyl)pyridine-1-iodure de sel de Krönke a été préparé par le procédé de réaction Ortoleva-King, selon lequel la 2-acétylpyridine interagit avec une solution d'iode en pyridine. (Schéma 2).

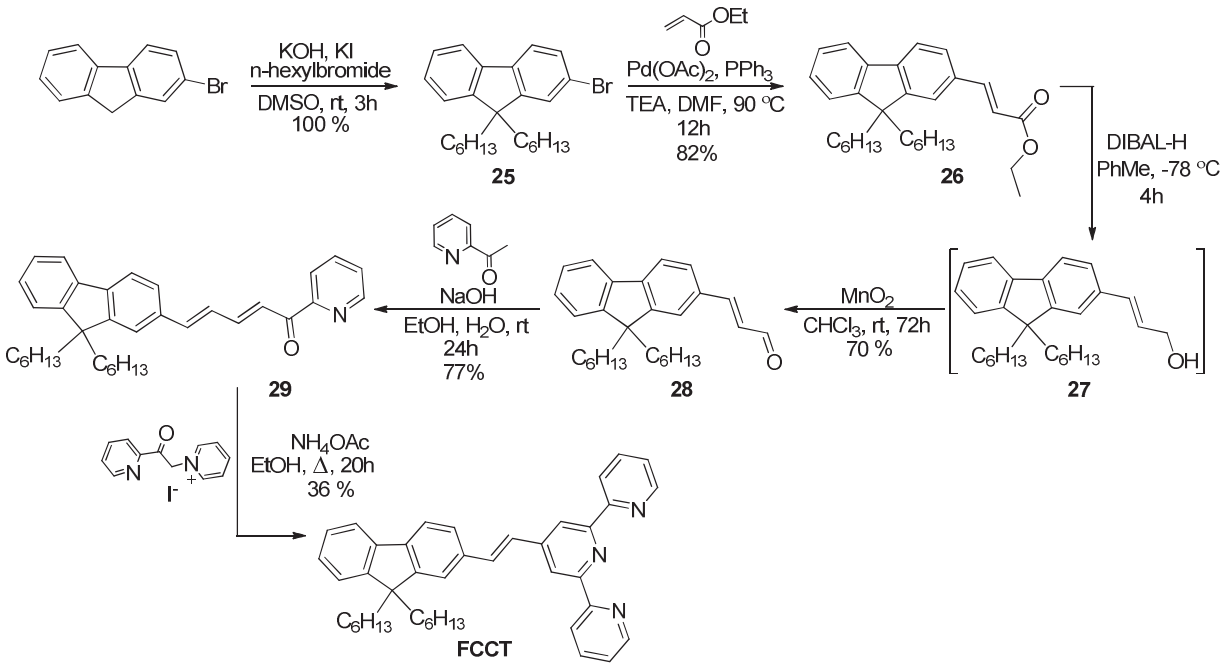

Schéma 1. La synthèse du ligand FCCT.

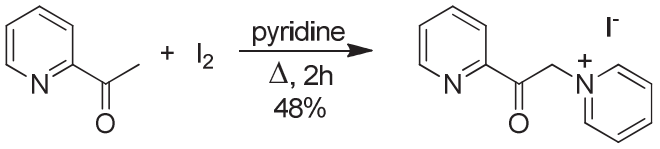

Schéma 2. La synthèse du 1-(2-oxo-2-(pyridin-2-yl) éthyl)pyridine-1-iodure.

Le ligand avec triple liaison FCC3T a été obtenu par synthèse convergente en 7 étapes. Le rendement total de synthèse était de 4.6%. Dans ce cas, la synthèse du noyau terpyridine a été effectuée séparément (Schéma 3).

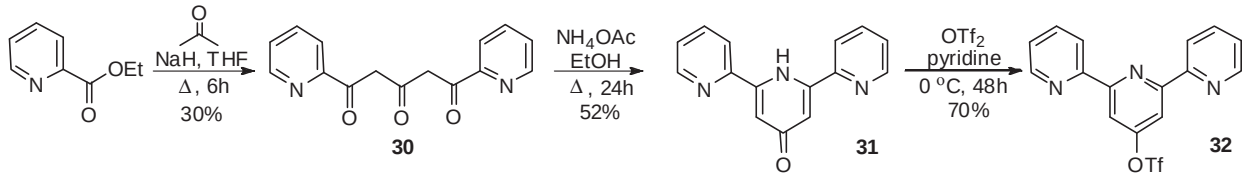

Schéma 3. Synthèse du trifluorométhanesulfonate de [2,2':6',2''-terpyridine]-4'-yle (**32**).

L'introduction de substituants n-hexyle en position 9 de fluorényle a été effectuée en utilisant comme agent d'alkylation n-$C_6H_{13}Br$, en présence de KOH solide dans DMSO. Dans ce cas, KI a joué un rôle de catalyseur. Le rendement d'alkylation est 100% (schéma 1 – la première étape de la synthèse).

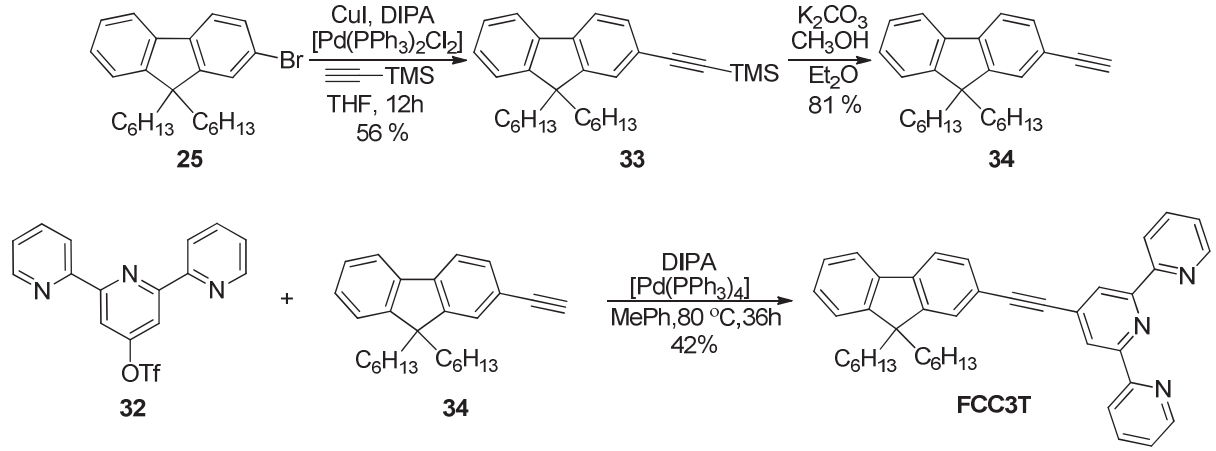

Schéma 4. La synthèse du ligand FCC3T.

La réaction de couplage de Sonogashira a été réalisée avec un rendement approprié de 42% dans une solution de toluène (Schéma 4).

La synthèse des complexes ruthénium-nitrosyle a été réalisée en 4 étapes selon le schéma 5.

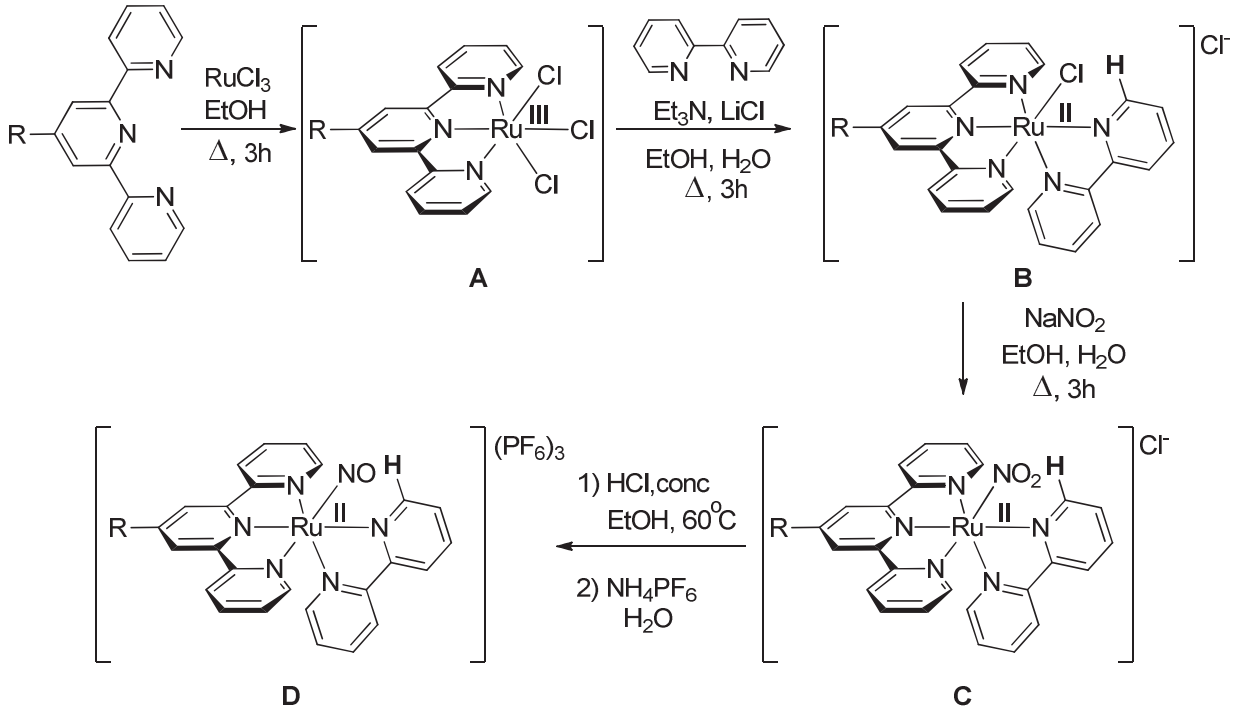

Schéma 5. Schéma général de synthèse de complexes ruthénium-nitrosyle avec des ligands de terpyridine et la molécule de ligand de 2,2'-bipyridine.

Une étude de la libération d'oxyde nitrique à partir des complexes résultants $[Ru(FCCT)(bpy)NO](PF_6)_3$ (**24a**) et $[Ru(FCC3T)(bpy)NO](PF_6)_3$ (**24b**) est apparue lorsque les composés ont été irradiés avec la lumière de longueur d'onde de 436 nm. La réaction a été contrôlée par spectroscopie électronique. Les changements des spectres électroniques des solutions d'acétonitrile de composés au cours de l'irradiation sont illustrés à la figure 8.

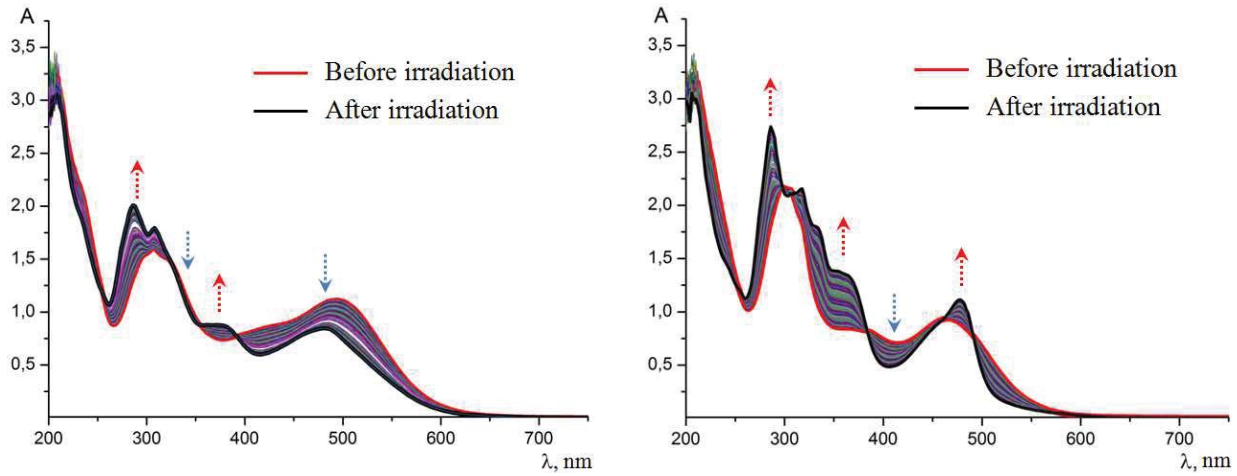

Figure 8. Evolutions des spectres électroniques des composés [Ru(FCCT)(bpy)(NO)]$(PF_6)_3$ (gauche) et [Ru(FCC3T)(bpy)(NO)]$(PF_6)_3$ (droite) dans l'acétonitrile λ = 436 nm.

Le rendement quantique de la réaction de libération d'oxyde nitrique est de 0.03 et est identique pour les deux composés. L'introduction d'une liaison multiple entre le groupe donneur et le fragment terpyridine-ruthénium-nitrosyle en retrait dans le ligand organique réduit la gêne stérique entre eux et aplatit le ligand. Cela entraîne une interaction plus efficace des systèmes π des deux parties du ligand et facilite le processus de transfert de charge intramoléculaire. Cet effet se retrouve dans le décalage bathochrome des transitions électroniques à faible énergie et dans l'augmentation de leur efficacité dans l'absorption à deux photons. Le composé **24a** (σ = 131 GM) a une capacité légèrement inférieure à absorber deux photons de longueur d'onde de 800 nm par rapport au complexe **24b**. L'introduction de la triple liaison entraîne en général une augmentation de la section efficace d'absorption de 40% (pour le composé **24b** σ = 150 GM), alors que la double liaison améliore σ de seulement 21%. Cette différence peut être expliquée par la configuration des transitions électroniques des deux composés, à savoir: aucune des transitions électroniques dans l'ion moléculaire $[Ru(FCCT)(bpy)(NO)]^{3+}$ par nature ne correspond au transfert de la densité électronique du fluorène vers le fragment {RuNO}, il n'y a donc aucune possibilité de transition intense avec un changement significatif du moment dipolaire de la molécule.

Etant donné la difficulté d'obtention des fluorényl-terpyridines substituées, nous avons synthétisé une série de complexes ruthénium-nitrosyle contenant des phénylterpyridines en tant que ligands. Dans ces composés, la position 4 du cycle benzénique est substituée par divers groupes: $-NO_2$, -H, -Br, -OMe, $-NEt_2$. Ces complexes sont analogues aux composés **1a** et **1b**.

Il a été montré que l'introduction de substituants donneurs (en particulier le méthoxyle et le diméthylamino) augmente l'efficacité des composés dans l'absorption à deux photons, tandis que des groupes accepteurs n'entraînent pas une telle amélioration. La plus grande valeur a été observée pour le complexe trans (Cl,Cl)-$[Ru(MeOPh\text{-}tpy)Cl_2NO]PF_6$, où MeOPh-tpy – 4'-(4-méthoxyphényl)-2,2':6',2''-terpyridine.

Dans **le cinquième chapitre**, certains aspects de la libération d'oxyde nitrique à partir de complexes ruthénium-nitrosyle avec leur activation à un photon sont examinés en détails. Il a été montré que l'irradiation des complexes ruthénium-nitrosyle à des longueurs d'onde correspondant, selon les calculs de chimie quantique, à l'énergie de transfert le plus efficace de la densité électronique du donneur au fragment ruthénium-nitrosyle (généralement la transition HOMO-LUMO) conduit à la libération de monoxyde d'azote avec un rendement quantique inférieur à celui obtenu par un processus de photoactivation aux énergies supérieures. Cela contredit l'idée précédente selon laquelle une augmentation du caractère donneur des substituants dans les ligands de la terpyridine devrait conduire à une augmentation des rendements quantiques de la libération de NO en raison de la population plus efficace de l'orbitale antiliante située sur la liaison Ru-N.

Une attention particulière est également accordée à la question de l'état d'oxydation du ruthénium dans les photoproduits. L'atome de ruthénium du photoproduit, contrairement à l'état d'oxydation habituel +3, se trouve dans l'état d'oxydation +2 à la suite de la libération de NO des complexes, dans lesquels les ligands sont représentés par la terpyridine et la 2,2'-bipyridine. La confirmation de ce résultat a été faite par plusieurs observations. Premièrement, l'évolution de la

photoréaction suivie par RMN, a montré que la solution de photoproduit ne contient pas d'espèces paramagnétiques. Deuxièmement, l'étude par diffraction des rayons X de monocristaux du complexe photoproduit a été réalisée. Deux anions de nitrate ont joué un rôle de contre-ion dans ce cas. Les structures du complexe ruthénium-nitrosyle initial et du photoproduit sont présentées à la figure 9.

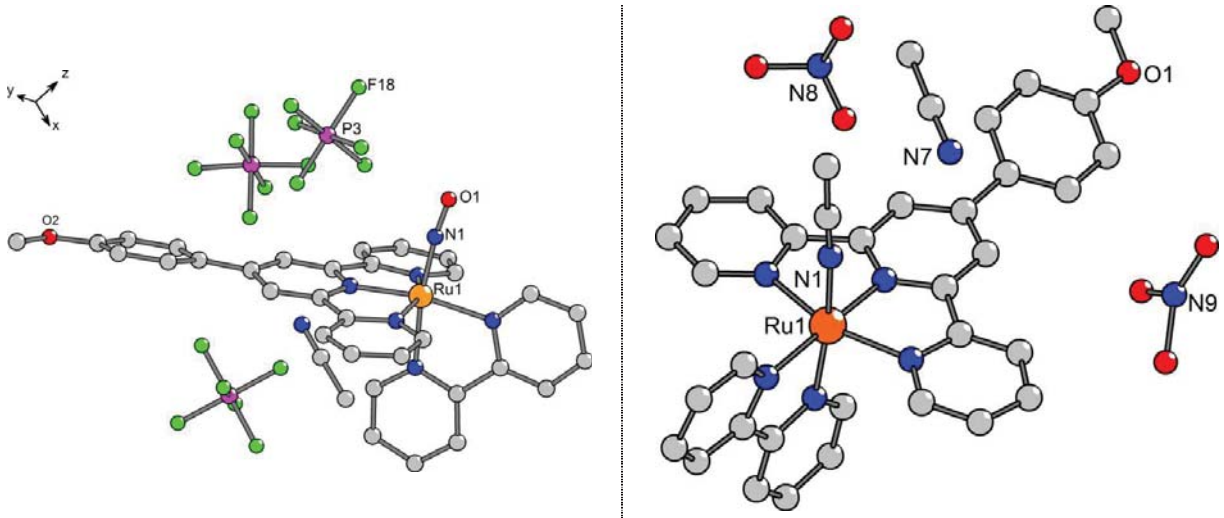

а б

Figure 9. Les structures du complexe initial $[Ru^{II}(MeO\text{-}Phtpy)(bpy)(NO)](PF_6)_3$ (a) et du photoproduit correspondant $[Ru^{II}(MeO\text{-}Phtpy)(bpy)(CH_3CN)](NO_3)_2$ (b).

La seule source possible d'anions nitrate dans le complexe peut être l'oxyde nitrique libéré. La présence de ces deux ions dans la structure cristalline du composé indique que pendant ou après la réaction, le monoxyde d'azote libéré est oxydé par l'oxygène ou par le complexe de ruthénium(III) qui est rapidement réduit en ruthénium(II). L'oxydation du monoxyde d'azote s'accompagne de la formation d'autres espèces contenant de l'azote à des états d'oxydation plus élevés qui, en présence d'eau (dans une solution non déshydratée), augmentent l'acidité de la solution. Un tel effet peut être observé dans une série de spectres RMN obtenus lors de l'étude de la libération de NO par le complexe initial. Le pic correspondant aux protons d'eau (δ = 2,13 ppm, 0 min) est décalé vers le champ faible lorsque

NO est libéré (δ = 6,85 ppm, 155 min), ce qui se traduit par une diminution du pH de la solution (Figure 10).

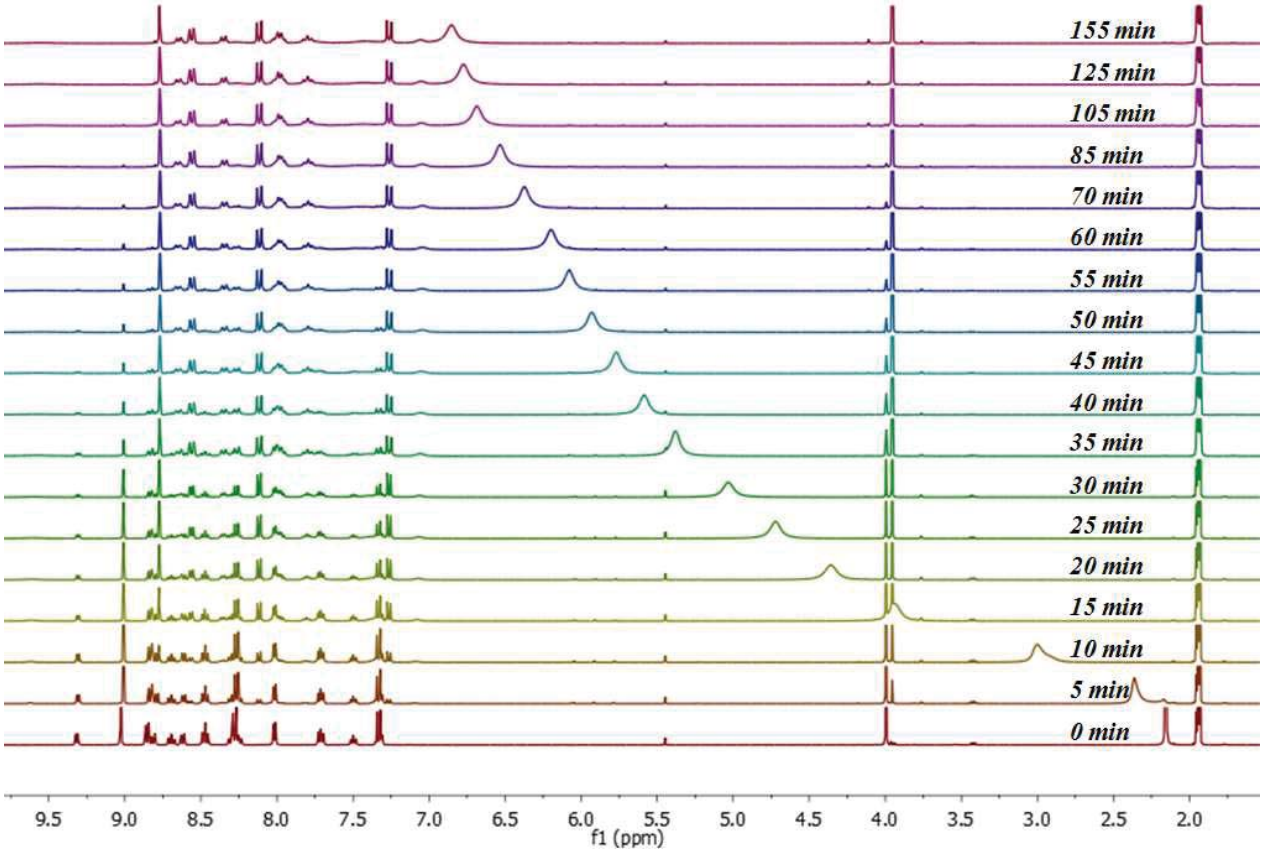

Figure 10. Suivi RMN de la libération de NO· par [Ru^{II}(MeO-Phtpy)(bpy)(NO)]$(PF_6)_3$ irradié avec une lumière continue dans la plage de 350-450 nm, dans CD_3CN.

CONCLUSIONS

1. Il a été montré que l'introduction de la 2,2'-bipyridine en tant que ligand dans la structure des complexes ruthénium-nitrosyle à la place des deux ligands chloro entraîne une diminution du rendement quantique de la photolibération de l'oxyde nitrique de 0.11 (trans Cl,Cl)-[Ru^{II}(FT)Cl_2(NO)](PF_6)) à 0.06. Cependant, cela entraîne une augmentation de la section efficace d'ADP de 90 à 100 GM à 108 GM.
2. Par des calculs de chimie quantique, il a été démontré que l'introduction de systèmes azahétérotricycliques avec un système de conjugaison des électrons 14π dans la structure du ligand terpyridine dans le complexe ruthénium-nitrosyle peut contribuer à une faible augmentation de l'efficacité du composé en absorption à deux photons (la section efficace maximale d'ADP obtenue pour le composé 1-méthyl-1H -benzo[f]indole (composé **4**) est seulement supérieure de 1% à celle du composé de référence trans1, pour lequel la section efficace est de 87 GM. Cependant, le remplacement du fluorène par de tels analogues hétérocycliques modifie sensiblement l'aptitude des composés à l'hyperpolarisation, dont la valeur varie en fonction de l'hétérocycle de $233.1 \cdot 10^{-30}$ $cm^5 \cdot esu^{-1}$ (composé **13**) à $2751,7 \cdot 10^{-30}$ $cm^5 \cdot esu^{-1}$ (composé **9**).
3. Des méthodes de préparation pour la synthèse de complexes ruthénium-nitrosyle avec des ligands contenant différents types de d'espaceur entre le fluorényle donneur et des fragments de terpyridine ont été développées – [Ru(FCCT)(bpy)NO](PF_6)$_3$, [Ru(FCC3T)(bpy)NO](PF_6)$_3$.
4. Il a été montré que l'augmentation de la conjugaison et l'amélioration de son efficacité par la diminution de l'angle de torsion entre les fragments donneurs et accepteurs du complexe améliorent les propriétés d'absorption à deux photons du complexe (une augmentation de la section efficace d'ADP observée est de 20 à 40%).

5. Il a été démontré sur les séries de complexes ruthénium-nitrosyle avec des phényl-terpiridines substituées que les substituants donneurs d'électrons augmentent l'efficacité des composés en absorption à deux photons, tandis que les groupes accepteurs ne permettent pas une telle amélioration. La valeur maximale de la section efficace d'ADP est observée pour le complexe contenant le ligand 4'-(4-méthoxyphényl)-2,2':6',2''-terpyridine – trans(Cl,Cl)-[Ru(MeOPh-tpy)Cl_2(NO)]PF_6 - 154 GM.
6. La structure du photoproduit formé lors de la libération d'oxyde nitrique du complexe ruthénium-nitrosyle contenant du 4'-(4-méthoxyphényl)-2,2':6',2''-terpyridine et de la 2,2'-bipyridine a été établie. Il a été prouvé que contrairement aux complexes avec des chloro-ligands au lieu de la 2,2'-bipyridine, l'état d'oxydation du ruthénium chez eux est +2. Il a également été confirmé au moyen de la spectroscopie RPE en utilisant un piège à spin que NO est libéré sous forme de radical.
7. Il a été établi que, contrairement aux idées précédentes, l'irradiation de composés à des énergies permettant le transfert de densité électronique d'un fragment donneur à un fragment ruthénium-nitrosyle ne joue pas un rôle décisif dans l'efficacité de la photolibération de NO par le composé. Une irradiation à des énergies plus élevées pourrait entraîner une photolibération avec des rendements quantiques plus élevés.